THE UNIVERSITY *of* EDINBURGH

Extension and Practical Evaluation of the Spatial Modulation Concept

Nikola Serafimovski

A thesis submitted for the degree of Doctor of Philosophy.
The University of Edinburgh.
April 20, 2013

Abstract

The spatial modulation (SM) concept combines, in a novel fashion, digital modulation and multiple antenna transmission for low complexity and spectrally efficient data transmission. The idea considers the transmit antenna array as a spatial constellation diagram with the transmit antennas as the constellation points. To this extent, SM maps a sequence of bits onto a signal constellation point and onto a spatial constellation point. The information is conveyed by detecting the transmitting antenna (the spatial constellation point) in addition to the signal constellation point. In this manner, inter-channel interference is avoided entirely since transmission is restricted to a single antenna at any transmission instance. However, encoding binary information in the spatial domain means that the number of transmit antennas must be a power of two. To address this constraint, fractional bit encoded spatial modulation (FBE—SM) is proposed. FBE–SM uses the theory of modulus conversion to facilitate fractional bit rates over time. In particular, it allows each transmitter to use an arbitrary number of transmit antennas.

Furthermore, the application of SM in a multi-user, interference limited scenario has never been considered. To this extent, the average bit error rate (ABER) of SM is characterised in the interference limited scenario. The ABER performance is first analysed for the interference-unaware detector. An interference-aware detector is then proposed and compared with the cost and complexity equivalent detector for a single–input multiple–output (SIMO) system. The application of SM with an interference-aware detector results in coding gains for the system.

Another area of interest involves using SM for relaying systems. The aptitude of SM to replace or supplement traditional relaying networks is analysed and its performance is compared with present solutions. The application of SM to a fixed relaying system, termed dual-hop spatial modulation (Dh-SM), is shown to have an advantage in terms of the source to destination ABER when compared to the classical decode and forward (DF) relaying scheme. In addition, the application of SM to a relaying system employing distributed relaying nodes is considered and its performance relative to Dh-SM is presented.

While significant theoretical work has been done in analysing the performance of SM, the implementation of SM in a practical system has never been shown. In this thesis, the performance evaluation of SM in a practical testbed scenario is presented for the first time. To this extent, the empirical results validate the theoretical work presented in the literature.

Declaration of originality

I hereby declare that the research recorded in this thesis and the thesis itself was composed and originated entirely by myself in the School of Engineering at The University of Edinburgh.

The exceptions to the above are as follows:

- The MATLAB code used for the digital signal processing of the experimental data was developed jointly with Abdelhamid Younis and Dr. Raed Mesleh as part of the Beyond 4G, UK-China Bridges project.
- The data used to obtain the channel statistics was collected by Dr. Pat Chambers as part of the Beyond 4G, UK-China Bridges project.

Nikola Serafimovski

Acknowledgements

I would like to extent my endless gratitude to my supervisor and mentor, Prof. Harald Haas. His enthusiasm for new ideas has inspired me even in the hardest of hours. His eye for detail and relentless pursuit for perfection have challenge me to grow as a person. Above all, however, I am most grateful for his loyalty. Loyalty and responsibility are rare qualities. It is reassuring to know that they still exist. It is his loyalty that has often been the difference between success and failure. Thank you Professor, I shall never forget.

I would like to express my deepest gratitude to Dr. Sinan Sinanović. My co-author in arms who has been by my side through thick and thin! You have been instrumental to both my professional and personal development. I thank you from the bottom of my heart i nek je Bog uvek sa tobom. My sincerest thanks goes to all of my friends for the support and understanding. Our friendships are always cherished. As they say, birds of a feather, flock together...so let us fly together. A special note of appreciation goes to Harald Burchardt and Stefan Videv, boys, we made it!

Acknowledgement also goes to the Engineering and Physical Sciences Research Council (EPSRC) along with the UK-China Science Bridges, “(B)4G Wireless Mobile Communications (UC4G)” which provided the funding for this work.

Finally, this thesis is dedicated to my family. No matter how complicated, how hard or how large a problem may appear, hard work and persistence will always yield results. To give up is easy. To persevere is hard and rewarding. My parents thought me this as a child. My unutterable appreciation goes to them for their unfailing love, understanding and unending support. Thank You. You have been and still are an unwavering pillar of support and the wind under my wings.

Mama i tato, Vie ste isvorot na mojot uspeh. Vie ste vetarot pod moite krilja. Vie ste, i sekogash ke bidete, moite roditeli. Se gordeam so Vas!

Contents

List of figures

List of tables

Acronyms and abbreviations

3GPP	3^{rd} Generation Partnership Project
4G	fourth generation
ABER	average bit error ratio
AF	amplify and forward
ARQ	automatic repeat request
ASER	average symbol error ratio
AWGN	additive white Gaussian noise
BER	bit error ratio
BPSK	binary phase shift keying
CDF	cumulative density function
CDMA	code division multiple access
CSI	channel state information
D-BLAST	diagonal Bell Laboratories layered space-time architecture
DDF	dynamic decode and forward
DF	decode and forward
Dh-SM	dual-hop spatial modulation
DSM	distributed spatial modulation
DSP–Rx	digital signal processing algorithm at the receiver
DSP–Tx	digital signal processing algorithm at the transmitter
ESPAR	electronically steerable parasitic array receptor
FBE	fractional bit encoding
FBE–SM	fractional bit encoded spatial modulation

FDMA	frequency division multiple access
FIR	finite impulse response
GSM	generalised spatial modulation
GSMC	Global System for Mobile Communications
IAI	inter–antenna interference
ICI	inter–channel interference
IF	intermediate frequency
IGCH	information guided channel hopping
ITU	International Telecommunications Union
LoS	line of sight
LTE-A	Long-Term Evolution Advanced
MA	multiple active
MGF	moment generating function
MIMO	multiple–input multiple–output
ML	maximum likelihood
MMSE	minimum mean-squared error
MPPI	Moore-Penrose pseudo-inverse
MRC	maximum ratio combining
NI	National Instruments
OFCOM	Office of Communications
OFDM	orthogonal frequency division multiplexing
OFDMA	orthogonal frequency division multiple access
PAM	pulse amplitude modulation
PEP	pairwise error probability
PI	power imbalance
PSK	phase shift keying

PXIe–Rx	hardware receiver that detects and processes the RF signal
PXIe–Tx	hardware transmitter that processes the matlab vectors and broadcasts an RF signal
QAM	quadrature amplitude modulation
QPSK	quadrature phase shift keying
RAM	random access memory
RF	radio frequency
RRC	root raised cosine
SD	sphere decoding
SDM	spatial division multiplexing
SER	symbol error ratio
SIC	successive interference cancellation
SIMO	single–input multiple–output
SINR	signal-to-interference-plus-noise-ratio
SISO	single–input single–output
SM	spatial modulation
SNR	signal-to-noise-ratio
SSK	space shift keying
STBC	space-time block codes
SULB	single user lower bound
SVD	singular value decomposition
TAS	transmit antenna selection
TDMA	time division multiple access
TOSD-SM	time-orthogonal signal design assisted spatial modulation
TOSD-SSK	time-orthogonal signal design assisted space shift keying
V-BLAST	vertical Bell Laboratories layered space-time architecture
WiMAX	IEEE 802.16 wireless access standard

ZF zero-forcing

Nomenclature

$\mathbf{w}_{n_t}$	Weight vector for zero-forced nulling
$\mathcal{B}, \mathcal{C}, \mathcal{Q}, \mathcal{R}$	Complex valued matricies that are used in derivations
D_1	Distance to the nearest transmitter
D_2	Distance to the second nearest transmitter
$\mathrm{D}_2/\mathrm{D}_1$	Interference distance ratio
N_t	Number of transmit antennas in a point-to-point communication system
N_r	Number of available antennas at the receiver
M	Number of possible constellation points in a signal modulation for a point-to-point communication system
$(\cdot)^*$	Complex conjugate
$(\cdot)^+$	Moore-Penrose pseudo-inverse
n, p, q, S	Arbitrary integer numbers
τ	Number of bits
ϖ	Fractional bit rate
$\widetilde{\varpi}$	Best rational approximation of ϖ
$\lfloor \cdot \rfloor$	Largest previous integer value
L	Modulus base
$(\cdot)_L$	Base-L representation of a number
n_t, $\hat{n}_t$	Transmit antenna index
$\upsilon_{n_t,\hat{n}_t}$	Spatial cross correlation coefficient between n_t and $\hat{n}_t$
υ	Spatial correlation decay coefficient
$\mathbf{h}_{n_t}$	Channel vector from transmit antenna n_t to all receive antennas
$\exp(\cdot)$	Exponential function
$\mathrm{tr}(\cdot)$	Trace of a matrix
$\mathcal{R}_{\mathrm{tx}}$	Correlation matrix for the transmitter
$\mathcal{R}_{\mathrm{rx}}$	Correlation matrix for the receiver
$\mathcal{H}$	Channel matrix

$\mathcal{H}^{\text{corr}}$	Correlated channel matrix
λ	Antenna spacing in terms of the carrier wavelength in radians
$J_0(\lambda)$	Bessel function of the first kind of order zero
t_i	Time instance i
x_i	Signal symbol i
N_u	Number of nodes/users broadcasting simultaneously
ξ	Node of interest
r	Index of the receive antenna
y_r	Received signal at antenna r
E_m	Transmit energy per symbol
$n_t^{(u)}$	Index of the active transmit antenna on node u
$N_t^{(u)}$	Number of available transmit antenna on node u
$\alpha_{(u)}$	Channel attenuation coefficient for all channels between transmitting node u and the receiver
$\alpha_{(n_t,r)}$	Channel attenuation coefficient from antenna n_t to antenna r
$h_{(n_t^{(u)},r)}$	Fast fading channel coefficient for the channel between n_t on node u and the receiving antenna r
$x^{(u)}$	Signal constellation symbol transmitted form node u
$\mathcal{X}^{(u)}$	Set of signal constellation points for node u
$\mathcal{CN}(0, N_o)$	Complex normal distribution with zero mean and variance N_o
$\mathcal{N}(\mu, \sigma^2)$	Normal distribution with mean μ and variance σ^2
η_r	AWGN at receiving antenna r
$\mathbf{y}$	Received vector
m	Index of a generic constellation point
ω_m	Generic constellation point m
$d(\cdot, \hat{\cdot})$	Hamming distance between any two constellation points coming from the same set
$R_{\hat{m}}$	Decision region of the symbol $\omega_{\hat{m}}$
$P_{\omega_m \mid \omega_{\hat{m}}}$	Probability that the received signal lies in the decision region $R_{\hat{m}}$ if ω_m was transmitted

$\varrho(\cdot)$	Conditional probability density function defined by a two dimensional Gaussian distribution
σ_m^2	Variance of the Gaussian distribution centred at the point ω_m
$\Re\{\cdot\}$	Real part of a complex variable
$\Im\{\cdot\}$	Imaginary part of a complex variable
$\Pr(\mathbf{h}_{n_t} x \neq \mathbf{h}_{\hat{n}_t} \hat{x})$	PEP between signal x, emitted from antenna n_t, to signal $\hat{x}$, emitted from antenna $\hat{n}_t$
x_{est}	Estimated constellation symbol
$n_t^{(\xi)}$	Active transmit antenna index on node ξ
$N_t^{(\xi)}$	Number of available transmit antennas on node ξ
$\|\| \cdot \|\|_{\text{F}}$	Frobenius norm
$\mathcal{X}^{(\xi)}$	Signal symbol constellation on node ξ
$M^{(\xi)}$	Cardinality of $\mathcal{X}^{(\xi)}$
$\text{E}_{\mathcal{H}}[\cdot]$	Expectation across the fast fading generic channel $\mathcal{H}$
$Q(\cdot)$	Q-function
$\sum_{x^{(\xi)}, n_t^{(\xi)}, \hat{x}^{(\xi)}, \hat{n}_t^{(\xi)}}^{M^{(\xi)} N_t^{(\xi)}}$	Four fold summation, two for all $x^{(\xi)}$, $\hat{x}^{(\xi)} \in \mathcal{X}^{(\xi)}$ and two for the indices $n_t^{(\xi)}$, $\hat{n}_t^{(\xi)} \in \left\{1, \ldots, N_t^{(\xi)}\right\}$
$\gamma_{\mathbf{I}}$	Signal-to-interference-plus-noise-ratio between node ξ and the receiver, divided by two
σ_z^2	Variance per receive antenna of SM using a variable amplitude modulation scheme
$\sigma_{z^{\text{PSK}}}^2$	Variance per receive antenna of SM using a constant amplitude modulation scheme
$\tilde{\rho}_K(\kappa)$	Central Chi-squared distribution with $2N_r$ degrees of freedom
$(\cdot)!$	Factorial function
$\arg(\cdot)$	Phase of a complex symbol
$\gamma = \frac{E_m}{N_0}$	Signal-to-noise-ratio
Ω	Set of all possible spatial and signal constellation points in a multi-user environment

$\mathcal{H}^{(\Omega)}$	Channel from every transmit antenna to every receive antenna in a multi-user environment
PEP $\left(x^{(\Omega)}, n_t^{(\Omega)}, \hat{x}^{(\Omega)}, \hat{n}_t^{(\Omega)}\right)$	PEP between the symbols $x^{(\Omega)}$ emitted from antennas $n_t^{(\Omega)}$ being detected as symbols $\hat{x}^{(\Omega)}$ emitted by antennas $\hat{n}_t^{(\Omega)}$
$\vartheta^2_{(u)}$	Variance per receive antenna of SM using a variable amplitude modulation scheme for node u
g_{QAM}	Normalising factor for a QAM constellation
k	Transmitting node, which may be the source (s) or relay (r) node
ℓ	Receiving node, which may be the relay (r) or destination (d) node
$\gamma_{(k\ell)}$	SNR on the link between nodes k and ℓ
$N_t^{(k)}$	Number of transmit antennas on node k
$N_r^{(\ell)}$	Number of receive antennas on node ℓ
$P_{(k\ell)}$	ABER of the link between nodes k and ℓ
$\mathbf{u} = <\widetilde{\alpha}, \widetilde{\varepsilon}>$	Unit vector
$\widetilde{\alpha}, \widetilde{\varepsilon}$	Non-negative coefficients defining the direction of the derivative
$\nabla_{\mathbf{u}}$	Directional derivative with respect to $\mathbf{u}$
$\mathcal{M}_\gamma(s)$	Moment generating function of the fading channel
P_C	Probability of correct detection by both relays
P_W	Probability of wrong detection by both relays
P_B	Probability of both relays activating
$P_{B\|0}$	Probability of both relays activating when a '0' was sent from the source
$P_{B\|1}$	Probability of both relays activating when a '1' was sent from the source
P_N	Probability of no relays activating
γ_0	SNR between the source and relay R_0
γ_1	SNR between the source and relay R_1
$\gamma_{0\mathrm{D}}$	SNR between relay R_0 and the destination
$\gamma_{1\mathrm{D}}$	SNR between relay R_1 and the destination

$\mathrm{BER}_{\mathrm{sd}}$	Source to destination BER for DSM
$\mathrm{BER}_{\mathrm{0D/1D}}$	Probability of detecting '1' at the destination when '0' was transmitted from the source and both relays are active
$\mathrm{BER}_{\mathrm{1D/0D}}$	Probability of detecting '1' at the destination when '0' was transmitted from the source and both relays are active
$\mathcal{H}_0$	Channel matrix between the source to relay R_0
$\mathcal{H}_1$	Channel matrix between the source to relay R_1
$\mathcal{H}_{\mathrm{0D}}$	Channel matrix between relay R_0 to the destination
$\mathcal{H}_{\mathrm{1D}}$	Channel matrix between relay R_1 to the destination
ζ	Ratio of the ABER on the link between relay R_0 to the destination relative to the ABER on the link between relay R_1 to the destination
K	Ratio of the coherent power component, usually the direct path, to the non-coherent power components, usually the scattered paths
ϑ	Phase angle of the coherent power component

Chapter 1
Introduction

The number of wireless devices has steadily increased since the first mobile phones in the early 1980s. In turn, the original function of a mobile phone has changed radically. Today, mobile devices are everywhere. To this extent, the expectations from the wireless devices of today are vastly different. Indeed, they are used as much for telephone conversations as for browsing the internet, making banking transactions, locating tourist attractions, identifying the best restaurants, social networking, remotely controlling the cooling, lighting and security in a home, and many other situations where an endless host of applications is limited only by the human imagination and the available resources. These wireless devices (smart phones or sensors) have changed the way humanity functions. They have become the foundations of a larger, smarter, more technologically advanced society, which aims to be connected, mobile and increasingly energy efficient.

The increasing role of these devices has led to their refinement and the requirement for more bandwidth. Higher data rates, longer battery life and greater portability have become expected. Yet for all the engineering marvel that goes into the creation of a single smart phone or sensor, the achievable data rates depend as much on an intelligent design, as on the available spectrum. Indeed, the spreading use of mobile devices has led to an exponential growth in wireless data traffic. The global demand for data to and from mobile devices has more than doubled over the last several years and this trend is expected to continue, as shown in Fig. 1.1 [1]. However, the fundamental limit to the achievable data rate for a communication system was established by Claude Shannon. He introduced the relation between the available bandwidth, the signal-to-noise-ratio (SNR) and the data rate of the system in [2]. In short, Shannon proves that the data rate increases linearly with the available bandwidth and logarithmically with an increasing SNR.

The physical resources, therefore, place a fundamental limit on the achievable data rates, irrespective of the growing demand. Indeed, the frequency spectrum is a limited resource which is highly regulated, crowded and expensive [3]. In particular, detailed technical information about

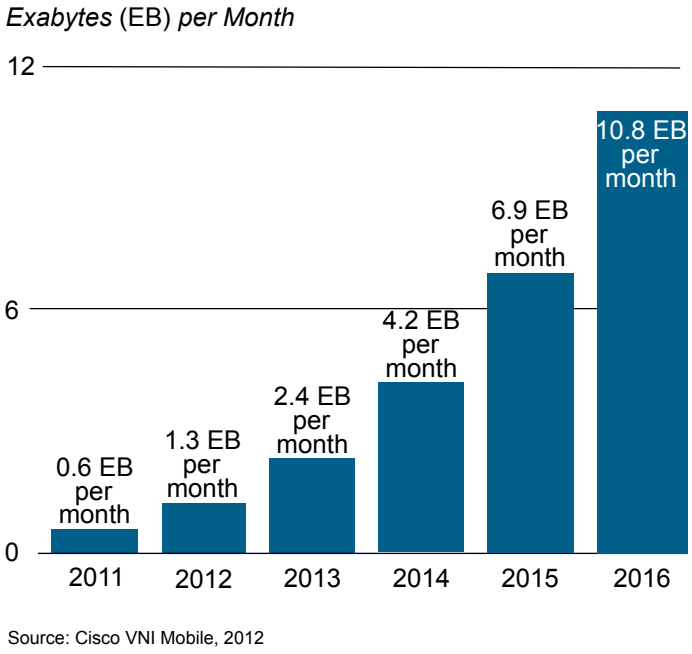

Figure 1.1: *Global demand for mobile data per month as predicted by Cisco [1].*

the UK spectrum allocations is provided in [4, 5] and the usage rights for each entity are defined in [6]. Therefore, to use the frequency spectrum more efficiently, the combination of multiple wireless devices operating in the same frequency band has become more widespread. To this extent, various interference cancellation algorithms are developed to facilitate as many users as possible. In addition, cognitive radio aims to locate unused spectrum slots and establish communication links while avoiding any interference. Yet despite the best efforts of researchers, the achievable data rates are limited.

In an attempt to increase the spectral efficiency, and thereby increase the available data rate, researchers ventured into the new, and largely unexplored, spatial domain. To this extent, the idea of multiple channels between two users is considered in [7] and the application of spatial multiplexing to a wireless network is first proposed in [8]. The idea behind spatial multiplexing is that a high-rate source signal is split into several low-rate signals. Each low-rate signal is then transmitted from a different transmitter. In addition, all transmitters transmit simultaneously on the same time-frequency resource block. Each receiver then uses multiple antennas to detect the co-channel signals. For successful reception, a rich scattering environment is assumed and the receiver uses the different channel signatures of each co-channel signal to differentiate among them. The separated signals are then demodulated and recombined to recover the original source signal. In fact, the work by Foschini in [9] provides a basis for approaches that employ

multiple transmit antennas and multiple receive antennas in a system. The general principle is termed multiple–input multiple–output (MIMO). One implementation of the MIMO concept is known as Vertical Bell Laboratories Layered Space-Time Architecture (V-BLAST) [10]. Indeed, Bell Labs was the first to demonstrate a laboratory prototype where spatial multiplexing was used as a principal technology to improve the performance in a communication system by employing V-BLAST [11].

Spatial multiplexing systems offer a linear increase of the spectral efficiency with respect to the number of transmit antennas. This increase, however, comes at a cost. Spatial multiplexing systems and MIMO systems in general, rely on a rich scattering environment to provide unique channel signatures between each transmit and each receive antenna since detection is performed using the eigenmodes of the channel. Therefore, optimal detection using V-BLAST is possible when the channel has at least the same number of receive antennas as there are transmitting antennas, otherwise the channel matrix is underdefined at the receiver. Nonetheless, if maximum likelihood (ML) detection is used at the receiver, then the number of receive antennas only determines the receive diversity of the system and all spatial streams are detected. In addition, inter–antenna synchronisation is required and may cause inter–antenna interference (IAI) if it is not well implemented. Indeed, spatial multiplexing MIMO systems suffer from inter–channel interference (ICI) which requires interference cancellation. However, interference cancellation algorithms suffer from error propagation and successive interference cancellation (SIC), in particular, results in detection algorithms with a high computational complexity, such the one used in V-BLAST. High computational complexity, in turn, increases the power consumption and decreases the battery life of a mobile device. Most importantly, to facilitate MIMO, multiple radio frequency (RF) chains must be active simultaneously. The most energy consuming part of a wireless base station, however, are the power amplifiers and the RF chains associated with each transmitter [12]. In fact, the power requirements of a base station are shown to increase linearly with the number of RF chains added [13]. Thus, while MIMO systems increase the spectral efficiency of a system linearly with the number of transmit antennas, the presented drawbacks limit their practical deployment.

To address some of the disadvantages of MIMO, the idea of spatial modulation (SM) is proposed in [14]. The aim is to retain as many of the advantages of classical MIMO systems, while avoiding many of the disadvantages. The basic idea of SM is to map blocks of information bits onto two information carrying units [15]: i) a signal symbol, chosen from a complex

signal constellation diagram, and ii) a unique transmit antenna, chosen from the set of antennas in an antenna array at the transmitter, *i.e.*, the spatial constellation. Jointly, the spatial and signal constellation symbols form a single SM constellation symbol. For example, if a total of four bits/s/Hz are transmitted using SM with four available transmit antennas, then the first two bits define the spatial constellation point identifying the active antenna, while the remaining two bits determine which signal constellation point is transmitted. An illustration of the constellation diagram for SM is shown in Fig. 1.2.

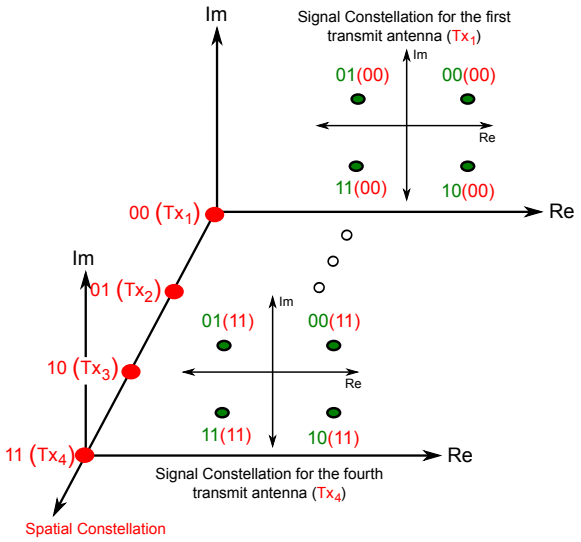

Figure 1.2: *The SM constellation diagram for a spectral efficiency of* $4\,\mathrm{bits/s/Hz}$ *with* 4 *signal constellation points and* 4 *available transmit antennas,* $\mathrm{Tx}_{n_t \in \{1,\ldots,N_t\}}$. Re *and* Im *denote the real and imaginary axis of the signal constellation diagram, respectively. The first two bits, from right to left, define the spatial constellation point which identifies the active antenna, while the remaining two bits determine the signal constellation point that is transmitted.*

In contrast to classical MIMO, SM places no constraint on the number of receive antennas, achieves spatial multiplexing gains even for a single receive antenna and requires no synchronisation between the transmit antennas. In addition, SM avoids ICI entirely by activating a single antenna at any transmission instance and the SM detection algorithm does not suffer from error propagation. Furthermore, the lower detection complexity for SM reduces the power usage of the mobile terminal and prolongs battery life [16]. Indeed, SM requires only a single RF chain at the transmitter, regardless of the number of transmit antenna elements. Additionally, SM is shown to outperform a MIMO system using V-BLAST in terms of the average bit error ratio (ABER) [15]. Lastly, SM is shown as more robust to channel estimation errors and to channel correlation when compared to V-BLAST [17, 18]. SM is therefore, a more optimal

system for exploiting the advantages of multiple transmit antennas while maintaining a single RF chain for green communications.

Nonetheless, SM is a young concept and it is still being developed. To this extent, encoding binary data in the spatial domain requires that the number of transmitter antenna elements is a power of two. However, doubling the number of antenna elements at the transmitter for every extra bit sent in the spatial domain may not be feasible due to space and cost constraints. In addition, the performance of SM in the interference limited scenario has never been considered, nor has the aptitude of SM to replace or supplement traditional relaying networks, ever been discussed. Finally, V-BLAST has been implemented in a practical scenario. Until now, SM has remained a purely theoretical concept.

Thesis layout and contributions

An overview of the history of wireless communications is presented in Chapter 2. The nature of the wireless channel and its application in MIMO and SM is considered. A detailed explanation of the operating principles behind spatial multiplexing systems and SM is followed by the strengths and perceived weaknesses. The main drawbacks identified in each system are discussed and the state-of-the-art advances for SM are explored. Lastly, the motivation and the research goals for the thesis are presented.

A novel method called fractional bit encoded spatial modulation (FBE–SM), which permits the transmitter to be equipped with an arbitrary number of transmit antennas, is presented in Chapter 3. FBE–SM uses the theory of modulus conversion to facilitate fractional bit rates over time. To this extent, the theory of modulus conversion is first explained. Its application to SM is discussed and an algorithm for an optimised implementation of FBE–SM is provided. The ABER performance of the system is then analysed in both the correlated and uncorrelated scenarios. Lastly, state-of-the-art alternatives to FBE–SM are discussed. While FBE–SM removes a fundamental limitation for the practical application of SM, most real world systems are interference, and not noise, limited.

The performance of a SM system in the interference limited environment is discussed in Chapter 4. The ABER performance of SM using the interference-unaware detector is then modelled. The asymptotic behaviour of the system is then discussed and compared to the *cost and complexity* equivalent SIMO system. In addition, a ML, interference-aware detector is proposed along with a closed form solution for the upper bound of the system in a Rayleigh fading envi-

ronment. Lastly, numerical analysis shows that the system employing SM performs better than the complexity and cost equivalent multi-user MIMO system.

Another area of interest involves using SM in relaying systems. The ABER performance of SM in the relaying scenario with both fixed and distributed relaying nodes is discussed in Chapter 5. In particular, the system model and an analytical upper bound for the source to destination ABER of the system using SM are presented. Furthermore, the application of SM with a fixed relaying node, termed dual-hop spatial modulation (Dh-SM), is shown to have a significant advantage in terms of the source to destination ABER when compared to the classical decode and forward (DF) relaying scheme. The application of SM to a relaying system employing distributed relaying nodes, termed distributed spatial modulation (DSM), is then considered. In particular, a closed form solution for the ABER of a system with two distributed relay nodes is presented and the performance of DSM is compared to Dh-SM in terms of the source to destination ABER.

Along with other theoretical work done in the field, SM is shown as a viable candidate for future wireless networks. However, despite the generated interest in SM, there is no practical implementation to prove that SM behaves as predicted in the literature. To this extent, the performance evaluation of SM in a practical testbed scenario is presented for *the first time* in Chapter 6. In particular, the digital signal processing for the transmitter and receiver is discussed. In addition, the equipment and the hardware constraints are then presented along with an analytical upper bound for the ABER performance of the system. Finally, the experimental data is compared to analytical and numerical results.

Lastly, Chapter 7 highlights the contributions made in the thesis. The limitations of the presented work are considered and potential avenues of research are proposed.

A list of publications that are related to the presented work in this thesis can be found in Appendix C. Furthermore, published works that related to the scope of this thesis and extend the SM concept, are attached in Appendix D.

Chapter 2
Background

In this chapter, a brief overview of the history and evolution of wireless communications is provided in Section 2.1. The properties of the wireless channel and their relevance for enabling multiple–input multiple–output (MIMO) and spatial modulation (SM) are then discussed in Section 2.2. In addition, the operating principles of MIMO systems, along with their advantages and perceived disadvantages, are deliberated in Section 2.3. Furthermore, a possible solution to the problems that plague MIMO systems is then proposed in the form of the SM concept in Section 2.4. In particular, the motivation for the extensions of the SM concept are presented in Section 2.5. Lastly, the chapter is summarised in Section 2.6.

2.1 Evolution of Wireless Communications

As with any scientific field, the initial research of the modern wireless communication systems was cumbersome, expensive and not practical. Yet with time and more work, the field changes. It grows, as new work builds on past knowledge and the open questions are addressed. The understanding of the electromagnetic force is a founding pillar of the modern world. There could be no wireless communications without this understanding.

The idea of wireless communications is grounded on work done by James Clerk Maxwell. His equations form the basis of computational electromagnetics and are the foundation of wireless technology. Indeed, the first known experiment in wireless communications was performed by Samuel Morse when he established a wireless telegraph connection in water. He laid two electrodes across 24 m of water and changed the number of galvanic elements. Later on, a breakthrough came when Heinrich Hertz verified the prediction made by Maxwell's equations with his 1887 discovery of electromagnetic radiation at ultra high frequencies. Despite the ground breaking nature of these experiments, however, they were impractical. In 1893, Nikola Tesla described, in detail, the principles of radio communication [19]. He was the first to apply the mechanism of electrical conduction to wireless practise. Tesla was also the first to

use sensitive electromagnetic receivers. These principles were later widely publicised. Yet Guglielmo Marconi was the first scientist to achieve successful radio transmission in 1895. Later, in 1897, he was awarded a patent with the British Patent Office which became the initial patent on radio [20].

It was not until the work of Claude Shannon, however, that the potential of wireless communications was unlocked. In 1948, Shannon provided information theory that characterised the limits of reliable communication [2]. He showed that there is a maximal channel capacity (achievable data rate) for which the error probability could be as low as desired. In particular, communicating at higher data rates demands either more bandwidth or greater signal-to-noise-ratio (SNR) [21]. Indeed, it was Shannon who established the limits of all modern communication systems. Since then, significant research has gone into achieving the information theoretic channel capacity predicted in his work.

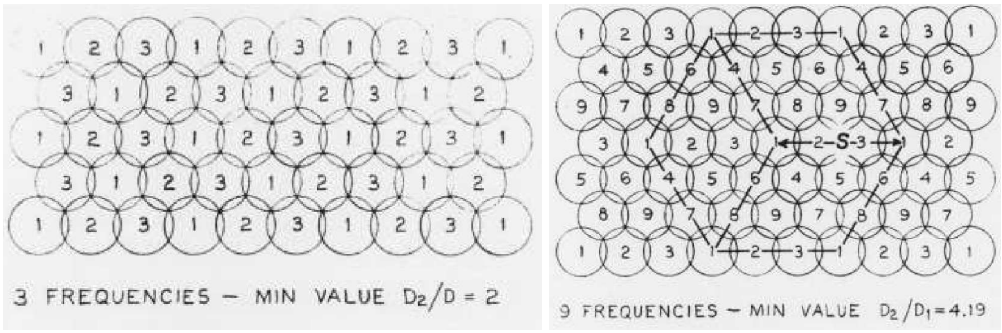

(a) Frequency reuse factor of 3. (b) Frequency reuse factor of 9.

Figure 2.1: *The first proposed use of frequency reuse for a mobile cellular system where* D_1 *is the distance from the receiver to the nearest base station,* D_2 *is the distance from the receiver to the second nearest base station and* $\mathrm{D}_2/\mathrm{D}_1$ *is the interference distance ratio. The interference is minimised by maximising the physical distance between two base stations transmitting on the same frequency [22].*

Although Shannon established the capacity bounds for any communication system, he did not provide guidelines how to achieve this capacity. Nonetheless, his work ascertained that to maximise the achievable data rate, the SNR and the available bandwidth must be maximised. On the one hand, all nodes could be active on the entire frequency spectrum but the SNR of each would become limited by the interference emitted from its neighbours. On the other hand, the frequency spectrum could be divided such that the interference from the neighbouring nodes is minimised but only a portion of the available spectrum is used at any node. The latter approach resulted in the frequency reuse idea.

Some of earliest reported efforts to establish a mobile communication system came from Bell Telephone Laboratories (Bell Labs) [22]. At the time, the frequency spectrum was barren and a strong SNR was necessary. To this extent, the notion of fractional frequency reuse, which became the backbone for the later deployment of the Global System for Mobile Communications (GSMC) in 1982, was first proposed in [22]. The idea is to minimise interference from neighbouring cells by using a different transmit frequency in each cell, as shown in Fig. 2.1. As the distance between the antennas that are active on the same frequency is increased, the interference on that frequency is minimised. To this extent, a more comprehensive wireless communication system was presented in [23]. To permit mobility between cells, a control cen-

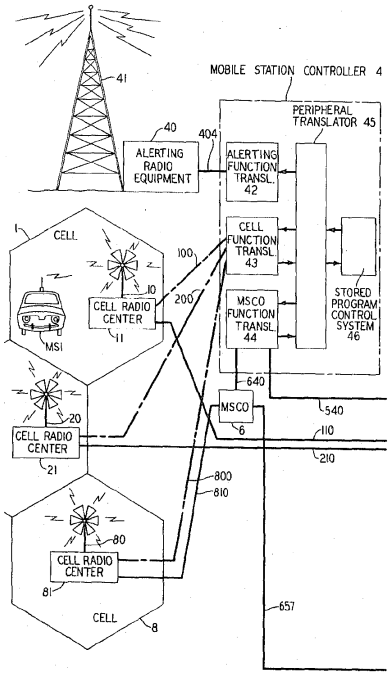

Figure 2.2: *The first patent description of a mobile cellular system where a central base station communicates with a mobile terminal. A central processing station controls the hand-over of users between different base stations. The base stations in different cells transmit on different frequencies and interference is minimised [23].*

tre determines the location of the mobile station and enables a switching centre to regulate the transfer of the mobile station from the currently occupied cell to a new cell. A basic overview of the elements necessary for the implementation of the early cellular concept is presented in Fig. 2.2.

From these beginnings, the evolution of mobile communication systems through the years is discussed in [24]. In contrast to the first generation wireless systems, which were separated

by national borders with incompatible control systems, the second generation systems were developed in a collaborative spirit. In particular, GSMC became a robust, interoperable and widely-accepted standard that combined the expertise from various entities under the guidance of the European Telecommunications Standards Institute. GSMC gained such momentum that it was quickly addopted by many contries around the globe. The digital nature of the GSMC systems enabled data services to be incorporated. Indeed, packet data services were introduced in the second half of the 1990s. These services provided a glimpse to the possible applications of wireless systems despite the low data rates. The interoperability of GSMC, along with its digital nature, provided a ubiquitous availability of mobile communications around the world and motivated the need for further, global, amalgamation of services and technologies.

As the second generation wireless systems were being deployed across the world, research into the third generation networks was on the way. Indeed, the International Telecommunications Union (ITU) had started work on the evolution of the GSMC standard in the 1980s. The rapidly growing demand for data services meant that the 14.4 kb/s download speed of the GSMC systems was insufficient. To this extent, research in the third generation systems aimed at providing data rates of at least 2000 kb/s. To facilitate this tremendous technological advance, the 3^{rd} Generation Partnership Project (3GPP) was established. Its aim is to coordinate research activity across the world. 3GPP is an international consortium consisting of several international standardisation bodies from Europe, U.S.A., Japan, China and South Korea. Where second generation systems used time division multiple access (TDMA) or frequency division multiple access (FDMA) to facilitate multiple users, the third generation systems were designed to use code division multiple access (CDMA). CDMA would support ultra wide bandwidth and would facilitate a large number of users, while remaining immune to interference [25]. Unfortunately, practical implementations could not achieve the theoretical predictions [26]. Nonetheless, the third generation systems have progressed throughout their deployment. The immediate demand for higher data rates has driven research forward and new releases have facilitated the evolution of third generation systems [24].

The spreading application of mobile devices has led to an exponential growth in the wireless data requirements, with the global demand for mobile data more than doubling over the last several years and expected to continue, as shown in Fig. 1.1. Yet the physical resources, the available spectrum and transmit power, place fundamental limits on the achievable data rates. Indeed, Shannon proved that to increase the achievable data rate, the bandwidth of a system or

the SNR must be increased.

In an attempt to increase the spectral efficiency without more bandwidth or a greater SNR, researchers began to exploit the spatial domain. The idea of multiple spatial channels between two users is first considered in [7] where each channel is envisioned to operate with the same data rate. As a result, the overall data rate would increase linearly with the number of parallel connections between the transmitter and receiver. This new idea became known as a MIMO system and is distinct from the earlier work on space-division multiple access (beam forming) which is aimed at improving the performance of a system against the effects of multipath fading [27–29]. An example of a MIMO setup is shown in Fig. 2.3 where the receiver detects multiple versions of the transmitted signal from reflections in the wireless environment.

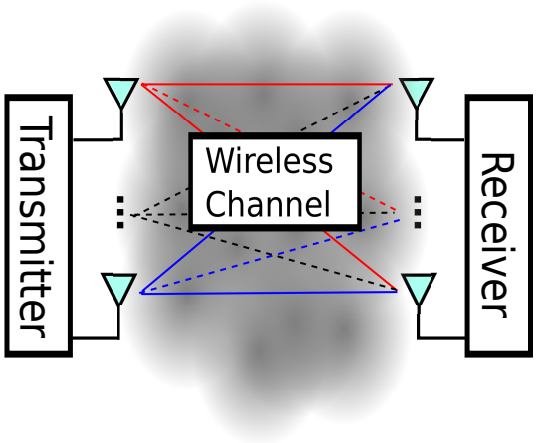

Figure 2.3: *The MIMO system setup. The MIMO channel depends on the deployment scenario and can experience small scale fading. The signal transmitted from each transmit antenna is detected by all receiving antennas.*

To keep pace with the data rate demands, the new research direction was incorporated for the first time in Release 7 of the 3GPP evolution and has remained an integral part [24]. Indeed, MIMO systems, along with orthogonal frequency division multiplexing (OFDM), are pegged as the backbone of the forth generation wireless technologies led by the Long-Term Evolution Advanced (LTE-A) initiative where peak data rates of 1 Gbit/s in the downlink and 450 Mbits/s in the uplink are expected. In particular, the employed technology is designed to be competitive for the next decade [30]. Aside from LTE-A, the IEEE 802.16 wireless access standard, often referred to as WiMAX, also incorporates the use of MIMO systems [31]. In addition, MIMO systems are already part of the latest IEEE 802.11n standard for wireless local area networks and most modern wireless network cards are manufactured with the IEEE 802.11n standard in

mind [32].

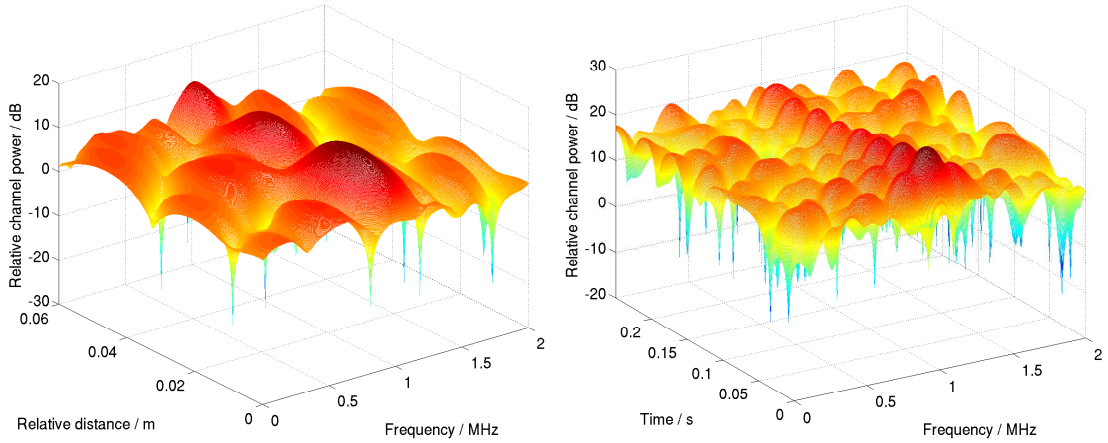

(a) Changes over a distance equivalent to 6 wavelengths (b) Changes over time as the receiver is moving at $6\,\mathrm{km/h}$

Figure 2.4: *Baseband illustration of the changes in the wireless channel environment when a carrier frequency of* $3\,\mathrm{GHz}$ *is used and a bandwidth of* $2\,\mathrm{MHz}$ *is available in an indoor environment.*

2.2 Wireless Channel Environment

The understanding of the wireless channel environment is a key factor to the development and deployment of MIMO systems. To this extent, the time and frequency behaviour of the wireless channel is addressed in [33–35]. The presence of reflectors in the environment creates multiple paths and, as a result, the receiver detects superimposed copies of the original signal. Depending on the scattering environment, therefore, the statistics of the channel change and can amplify or attenuate the received signal. The wireless channel is principally described through large scale fading and small scale fading. On the one hand, large scale fading refers to the mean signal strength at the receiver and is most used in estimating the coverage area of a transmitter. On the other hand, small scale fading refers to the rapid fluctuations of the channel envelope which depend on the momentary interactions of the signals coming from various reflections in the environment. Small scale fading is principally described by slow and fast fading, along with flat and frequency-selective fading. A brief explanation of each follows.

- *Slow fading* characterises the event when the coherence time of the channel is large relative to the signal symbol duration. The coherence time is the interval within which the phase of the signal is, on average, predictable. To this extent, the power and phase changes in the channel are a result of shadowing or movement since the channel is corre-

lated from one signal symbol to the next. Slow fading can be illustrated by the relatively slow channel variations across the frequency range for any symbol duration of less than 0.01 s in Fig. 2.4(b).

- *Fast fading* characterises the event when the coherence time of the channel is small relative to the signal symbol duration. The power and phase changes in the channel arise from random reflections and, as a result, the channel is decorrelated from one signal symbol to the next. Fast fading can be illustrated by the relatively rapid channel variations across the frequency range for a symbol duration of 0.05 s in Fig. 2.4(b). The fast fading makes the channel distinct from one transmission instance to the next. In particular, it provides the unique channel signature which facilitates MIMO and SM. Indeed, throughout this thesis, the channel is assumed to be slow fading for only a single symbol, unless otherwise stated. Therefore, the channel coefficients used are said to be the fast fading coefficients. Common models used to define the statistical behaviour of the amplitude in fast fading channels include Rayleigh, Rician and Nakagami-*m* distributions.

- *Flat fading* and *frequency-selective fading* characterises the spectral components of the transmitted signal. The coherence bandwidth is the approximate bandwidth over which two frequencies of a signal experience correlated amplitude fading. Flat or narrowband fading assumes that the bandwidth of the transmitted signal is much smaller than the coherence bandwidth of the channel, therefore all frequency components of the signal experience the same magnitude and phase. Frequency-selective fading occurs when the bandwidth of the transmitted signal is larger than the coherence bandwidth of the channel, therefore different frequency components of the signal experience decorrelated fading. In particular, Fig. 2.4(a) and Fig. 2.4(b) have different coherence frequencies. As a result of the larger coherence frequency, the channel presented in Fig. 2.4(a) varies much less across its spectrum than the one presented in Fig. 2.4(b). To this extent, a narrowband channel is assumed throughout this thesis.

With the time and frequency characteristics of the wireless channel presented, Fig. 2.4(a) shows that channel fading is also unique with respect to the physical location of the transmitter and receiver, just as it is unique across time and frequency in Fig. 2.4(b). In particular, the empirical statistics of a MIMO channel in different environments are presented in [36]. It is the varying nature of the channel that gives each detected signal at the receiver a unique signature, a channel fingerprint, and facilitates both MIMO and SM. The advantages and perceived disadvantages

of MIMO are now analysed.

2.3 MIMO algorithms and operation

Multiple-antenna systems are fast becoming a key technology for modern wireless systems. They offer improved error performance and higher data rates, at the expense of increased complexity and power consumption [37]. To this extent, the application of spatial multiplexing to a wireless network is first proposed in [8]. The idea behind spatial multiplexing is that a high-rate source stream is split into several low-rate sub-streams. Each sub-stream is then transmitted from a separated transmitter. All transmitters are active on the same time-frequency resource block and each receiver uses multiple antennas to detect the multiple co-channel signals. To facilitate detection, a rich scattering environment is required. In particular, the receiver exploits the different channel fingerprints of each co-channel signal to differentiate among them. The sub-streams are then demodulated and recombined to obtain the original source signal. Indeed, the work by Foschini provided a basis for approaches that employ multiple transmit antennas and multiple receive antennas in a system [9].

In addition to spatial multiplexing, multiple transmit antennas may be used to increase the transmit-diversity of a system or provide a combination of spatial multiplexing and transmit-diversity. The notion of using the multiple antennas for transmit-diversity is known as space-time coding [38–40]. A notable method that successfully achieves both spatial multiplexing and transmit-diversity for two transmit antennas was presented by Alamouti in [41]. Aside from the scheme presented by Alamouti, all other systems must trade-off spatial multiplexing with transmit-diversity [35, 40].

An efficient technique for spatial multiplexing that breaks information data streams into sub-streams is termed Diagonal Bell Laboratories Layered Space-Time Architecture (D-BLAST) and is defined in [9]. D-BLAST uses antenna arrays at both the transmitter and receiver along with a diagonally-layered coding structure where code blocks are dispersed across *diagonals* in space-time. This leads to theoretical rates which grow linearly with the number of transmit and receive antennas in rich scattering environments. Indeed, D-BLAST is shown to achieve up to 90% of the Shannon capacity [9].

Another approach, termed Vertical Bell Laboratories Layered Space-Time Architecture (V-BLAST), is proposed in [10]. The vector encoding process is the fundamental difference be-

tween V-BLAST and D-BLAST, where a vector is defined as the vector-valued transmitter (a collection of the transmit antenna sub-streams). On the one hand, in D-BLAST, vector encoding is introduced through the use of inter-sub-stream block coding such that the block codes are organised along diagonals in space-time. On the other hand, in V-BLAST, the vector encoding is simply a demultiplexing operation of the original data stream, followed by independent bit-to-symbol mapping of each sub-stream. In particular, no inter-sub-stream coding is required. The sub-stream coding structure in D-BLAST and V-BLAST is illustrated in Fig. 2.5(a) and Fig. 2.5(b), respectively, where the sub-streams from the same high-rate source stream are denoted by the same colour.

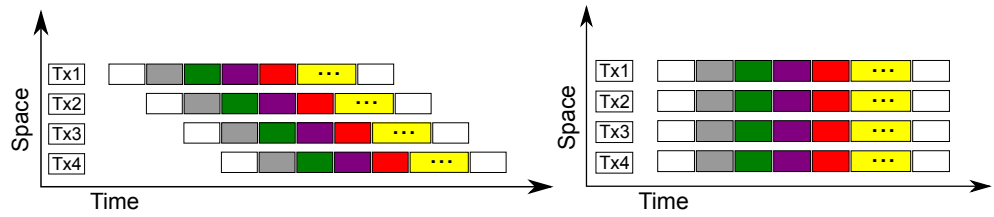

(a) D-BLAST. (b) V-BLAST.

Figure 2.5: *Sub-stream coding for D-BLAST and V-BLAST given four transmit antennas where sub-streams from the same high-rate source stream are denoted with the same colour. The sub-streams in D-BLAST have been coded along diagonals in space-time while the sub-streams in V-BLAST are the result of a simple demultiplexing operation.*

Despite enabling higher spectral efficiency, the deployment of D-BLAST is hindered by its complexity. To this extent, V-BLAST has emerged as the dominant MIMO technique in the pursuit for higher data rates [10]. The V-BLAST receiver decodes the sub-streams using nulling, optimum ordering, and successive interference cancellation (SIC). A brief explanation of each detection step is presented.

- *Nulling* - is defined as the process of removing the detected n_{i-1} sub-streams from a received vector $\mathbf{y}$. The n^{th} sub-stream is detected by removing the effects from all other sub-streams. While there are different methods to detect a sub-stream in the presence of interference [42], nulling is performed by linearly weighting the received signals to satisfy a criteria such as minimum mean-squared error (MMSE) or zero-forcing (ZF). ZF nulling can be performed by choosing weight vectors, $\mathbf{w}_{n_t}$, such that

$$\mathbf{w}_{n_t}^{\text{T}} \, \mathbf{h}_{\hat{n}_t} = \delta_{(n_t,\hat{n}_t)}, \tag{2.1}$$

where $(\cdot)^T$ is the transpose of a vector or a matrix, n_t, $\hat{n}_t \in \{1, \ldots, N_t\}$, N_t is the number of transmit antennas, $\mathbf{h}_{\hat{n}_t}$ is the channel vector from transmit antenna $\hat{n}_t$ to all receiving antennas, and $\delta_{(n_t,\hat{n}_t)}$ is the Kronecker delta. In MMSE, the problem of estimating a random vector $\mathbf{w}_{n_t}$ on the basis of the received signal $\mathbf{y}$, is equivalent to choosing a matrix $\mathcal{H} = [\mathbf{h}_1, \ldots, \mathbf{h}_{N_t}]^T$, that minimises the mean square error [42]. All bold symbols throughout the thesis denote vectors. While linear nulling is sufficient, non-linear techniques exploit the timing synchronisation in the system model of V-BLAST for faster detection. Timing synchronisation can be exploited if the transmitters are co-located and transmit antenna synchronisation is implemented. This enables both symbol cancellation and linear nulling to be used in the detection process [10].

If non-linear nulling techniques are used, they result in a gradually increasing diversity gain for the sub-stream with the weaker signal-to-interference-plus-noise-ratio (SINR). In effect, the weakest sub-stream in terms of the SINR is detected last with the greatest diversity [42]. Therefore, to obtain a better performance and minimal error propagation, the receiver should decode the strongest sub-stream first.

- *Optimal Ordering* - is achieved by selecting the sub-stream with the strongest SINR. It is shown that this greedy approach leads to a globally optimal ordering in the maximin sense. In addition, establishing an optimal ordering reduces error propagation [10]. To this extent, the optimal ordering is determined by the eigenvalues of the channel matrix.

- *SIC* - is the process of selecting the strongest sub-stream, in terms of SINR, nulling its effects from the received vector and repeating the process for the next strongest sub-stream [10]. An example of a MIMO system using SIC is considered in Fig. 2.6. To this extent, four distinct sub-streams are assumed where each one is sent from a different transmit antenna and the summation of all co-channel signals is detected at the receiver. Although every transmit antenna is transmitting with the same power, the wireless channel environment creates a power imbalance between the individual sub-streams. The thickness of the blocks in Fig. 2.6 illustrate the relative power imbalances. In this regard, the sub-stream that passes through $\mathbf{h}_1$ has the strongest SINR, while the sub-stream that passes through $\mathbf{h}_4$ has the weakest SINR. The receiver first determines the sub-stream with the strongest SINR by looking at the eigenvalues of the channel matrix. By applying SIC, the receiver then decodes and removes the effects of the sub-stream arriving through $\mathbf{h}_1$. On the next step, it removes the effects of the sub-stream arriving through $\mathbf{h}_2$ from the aggregate signal and so on. However, error propagation can occur if the optimal ordering

is not maintained, *i.e.*, if a sub-stream with a weaker SINR is decoded prior to one with a stronger SINR.

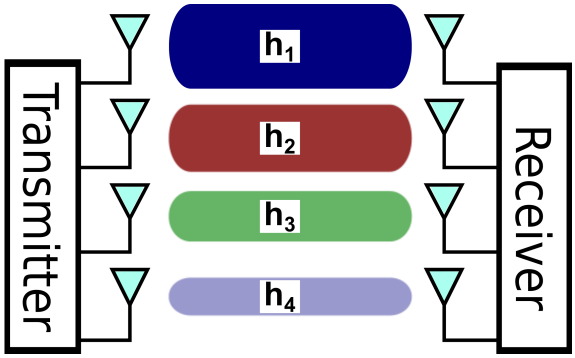

Figure 2.6: *A 4×4 MIMO system setup. The relative power of each sub-stream at the receiver is denoted by the thickness of the channel block. Although all transmit antennas use the same transmit power, the channel environment changes the relative power of the sub-streams at the receiver.*

Since the eigenvalues of the channel matrix define the optimal ordering, the number of antennas at the receiver must be greater or equal to the number of antennas at the transmitter for V-BLAST to function. In particular, a V-BLAST system requires a full rank channel matrix which is only achieved in rich scattering environments [42]. In addition, the detection algorithm for V-BLAST requires the computation of the Moore-Penrose pseudo-inverse (MPPI), which implies that either a sigular value decomposition (SVD) or a QR decomposition of the channel matrix must be obtained. The MPPI is required to determine the eigenvalues of the channel matrix, along with the nulling vector used in V-BLAST detection [10]. Indeed, the diagonalised matrix from the SVD decomposition results in the ranked channel weights needed for the optimal ordering and nulling.

The bottleneck in the V-BLAST decoding algorithm is, therefore, the need to repeatedly calculate the MPPI of the channel matrix. To address this problem, an $N_r \times N_t$ channel matrix $\mathcal{H}$ is assumed, with rank n where N_r is the number of receive antennas, then its MPPI is defined as

$$\mathcal{H}^{+} = \mathcal{C}^{*} \left(\mathcal{C}\mathcal{C}^{*}\right)^{-1} \left(\mathcal{B}^{*}\mathcal{B}\right)^{-1} \mathcal{B}^{*}, \tag{2.2}$$

where $(\cdot)^{+}$ is the MPPI, $(\cdot)^{*}$ is the complex conjugate of a matrix or a vector, $\mathcal{B}$ is an $N_r \times n$ matrix and $\mathcal{C}$ is an $n \times N_t$ matrix. Provided that $\mathcal{H}$ has full row rank $(N_r = n)$, then $\mathcal{B}$ can be chosen as the identity matrix and the formula reduces to $\mathcal{H}^{+} = \mathcal{H}^{*} \left(\mathcal{H}\mathcal{H}^{*}\right)^{-1}$. Instead, if $\mathcal{H}$ has full column rank $(N_t = n)$, then $\mathcal{H}^{+} = \left(\mathcal{H}^{*}\mathcal{H}\right)^{-1} \mathcal{H}^{*}$. In both instances, however, $\mathcal{H}\mathcal{H}^{*}$

or $\mathcal{H}^*\mathcal{H}$ must be computed along with the inverse. This can be done by using the Cholesky decomposition. Given that $\mathcal{H}$ is of full row rank $(N_r \geq N_t)$, then

$$\mathcal{H}\mathcal{H}^* = \mathcal{R}\mathcal{R}^*, \tag{2.3}$$

where $\mathcal{R}$ is an upper triangular matrix. To obtain this factorisation, QR decomposition can be applied which results in

$$\mathcal{H}\mathcal{H}^* = (\mathcal{Q}\mathcal{R})(\mathcal{Q}\mathcal{R})^* = \mathcal{R}\mathcal{Q}\mathcal{Q}^*\mathcal{R}^* = \mathcal{R}\mathcal{I}\mathcal{R}^* = \mathcal{R}\mathcal{R}^*, \tag{2.4}$$

where $\mathcal{Q}$ is a unitary matrix, and $\mathcal{I}$ is the identity matrix. The resulting $\mathcal{R}$ is the Cholesky factor of $\mathcal{H}\mathcal{H}^*$ [43]. This method is used in most current approaches to the problem, where QR decomposition of the channel matrix reduces the computational complexity in the implementation [44]. A key requirement, however, is that the channel matrix $\mathcal{H}$ must be either full row rank or be overdetermined. If this is not the case, *i.e.*, when the number of transmit antennas is greater than the number of receive antennas, the decoding algorithm loses the $(N_t - N_r)$ sub-streams with the weakest SINRs and a maximum diversity gains of N_r is achieved.

Aside from requiring that $N_r \geq N_t$, the detection algorithm for V-BLAST requires that all symbols are transmitted simultaneously. Antenna synchronisation is therefore necessary. The requirement for timing synchronisation is particularly important if any of the non-linear nulling techniques are used in the detection. As discussed earlier, this synchronisation facilitates symbol cancellation [10]. As an example, the Agilent Technologies equipment used for MIMO testing must synchronise the input and output trigger signals to ensure proper functioning [45]. If this is not the case, the received sub-streams will not align in time to reconstruct the original signal. In particular, the lack of timing synchronisation can lead to a serious degradation of the system performance in terms of the average bit error ratio (ABER) as discussed in [46, 47].

In addition to timing synchronisation, inter–channel interference (ICI) is an integral part of a spatial multiplexing system. Although interference cancellation algorithms have been developed to address ICI, they increase the receiver complexity and are prone to error propagation. In addition, any increase in the receiver complexity consumes more power and is detrimental to the battery life of a mobile terminal. Indeed, interference cancellation algorithms also effect the transmit power of a terminal. In particular, different interference cancellation algorithms suppress noise differently. The two methods for establishing the weighting factors, MMSE

and ZF, result in different transmit power requirements. When conventional block decoding interference cancellation is used at the receiver, the transmitter uses less power if MMSE is employed. Similarly, SIC using MMSE requires even less transmit power. However, if the need for interference cancellation is removed altogether, both the transmitter and receiver use less power and the overall power consumption of the system is significantly reduced [48].

V-BLAST, along with other spatial multiplexing systems, is shown to offer a linear increase of the spectral efficiency with respect to $\min\{N_r, N_t\}$. To this extent, a rich scattering environment is necessary to provide unique channel signatures between each transmit and each receive antenna since detection is performed using the eigenmodes of the channel. This increase, however, comes at a cost. Inter–antenna synchronisation is required, otherwise timing synchronisation problems may arise along with inter–antenna interference (IAI), if it is not well implemented. In particular, MIMO systems suffer from ICI and require SIC. However, interference cancellation results in detection algorithms with a high computational complexity that impact the energy efficiency of a system [48]. Most importantly, multiple radio frequency (RF) chains must be active simultaneously which further increase the required power and are expensive to manufacture. Indeed, the most energy consuming part of a wireless base station are the power amplifiers and the RF chains associated with each transmitter [12]. In addition, the power requirements of a base station are shown to increase linearly with the number of RF chains added [13]. Thus, while MIMO systems increase the spectral efficiency of a system linearly with the number of transmit and receive antennas, the presented drawbacks limit their practical deployment.

2.4 Spatial Modulation

2.4.1 Operating Principle

As an alternative to standard MIMO systems, the idea of SM is proposed in [14]. The aim is to retain as many of the advantages of standard MIMO systems, while removing many of the disadvantages. The basic idea of SM is to map blocks of information bits onto two information carrying units [15]: i) a signal symbol, chosen from a complex signal constellation diagram, and ii) a unique transmit antenna, chosen from the set of transmit antennas in an antenna array, *i.e.*, the spatial constellation. Jointly, the spatial and signal constellation symbols form a single SM constellation symbol. To this extent, SM offers spatial multiplexing gains by using the

transmit antenna index as an information carrying unit. In fact, the active antenna selection distinguishes SM from transmit-antenna selection (TAS) or spatial division multiplexing (SDM), where the differences in the channel signatures are exploited to facilitate multiple access and not data modulation [15, 37]. Due to the different spatial positions occupied by the transmitting antennas, the transmitted signal from each antenna experiences a unique channel. Indeed, the varying nature of the wireless channel with respect to the spatial location of the transmit or receive antennas is illustrated in Fig. 2.4(a) and is discussed in [36]. It is this channel fingerprint that is used as a "modulation unit". In particular, it is the Euclidean distance between the different channel signatures that directly affects the ABER performance of a SM system.

The SM constellation is exemplified in Fig. 1.2. In general, the spectral efficiency of a system employing SM is given as $\log_2(MN_t)$, where M is the cardinality of the signal constellation. Unlike MIMO systems, the number of transmit antennas is independent from the number of receiver antennas and spatial multiplexing gains are achieved even for a single receive antenna. In addition, the need for transmit antenna synchronisation is completely removed. By activating only a single antenna at any transmitting instances, SM avoids the need for interference cancellation algorithms entirely and does not suffer from error propagation. In fact, SM requires only a single RF chain at the transmitter which reduces the manufacturing costs and consumes less power. The single RF chain is a key advantage of SM for improving the energy efficiency of future wireless networks. Indeed, the outage and ergodic capacity for SM over Rayleigh fading channels are computed and SM is shown to offer capacity gains with respect to other systems employing space-time block codes (STBC) when the number of transmit antennas is greater than two [49]. The latest advances of the SM concept are now considered.

2.4.2 State-of-the-Art

SM offers an intrinsic flexibility to trade off the number of transmit antennas with the modulation order in the signal domain to achieve the desired data rate and ABER. Although, the concept of using the channel signature for data transmission was first discussed in [50], the proposed method required multiple active transmit antennas. By contrast, the first use of the channel signature as a "modulation unit" to provide multiplexing gains is reported in [14]. The use of the spatial domain to attain multiplexing gains, means that a greater number of transmit antennas and a lower order signal modulation can be used, which result in a better ABER performance at low SNR. This behaviour is characteristic of SM since the detection of the spatial

constellation point is influenced by the channel environment and the ability of the detector to distinguish the various transmit antennas [51].

To this extent, the signal symbol is the main source of error at low SNR, while the error probability of the spatial constellation point depends on the channel environment. In particular, the ABER performance of SM degrates in the presence of severe channel imperfections such as spatial correlation and mutual antenna coupling. These imperfections reduce the Euclidean distance between the different spatial constellation points and result in an increased ABER [15]. On the one hand, SM is shown to outperform a MIMO system using V-BLAST in terms of the ABER primarily because it avoids ICI. On the other hand, the main advantage of SM over the Alamouti scheme stems from the flexibility in the spatial constellation which may be increased to reduce the signal constellation [15]. These results are obtained despite SM being used with a sub-optimal maximum ratio combining (MRC) receiver structure in [15]. An optimum detector is presented in [52] that demonstrates even better system performance in terms of the ABER with respect to both V-BLAST and SM using iterative MRC. In particular, the optimum detector is simply a maximum likelihood (ML) receiver with respect to the entire SM symbol, *i.e.*, it decodes the spatial and signal constellation points jointly.

A generalised framework for analysing the ABER of SM is proposed in [53]. To this extent, an analytical upper bound for the ABER and the average symbol error ratio (ASER) of SM for any channel environment with an arbitrary signal modulation scheme is derived. However, the ML receiver proposed in [52] and analysed in [53] requires full channel state information (CSI). Although this is not a practical assumption, if slow fading is assumed, CSI can be obtained via quick channel estimation at the receiver. In some mobile scenarios, however, the channel fading may vary so rapidly such that practical channel estimation becomes impossible. To this extent, the optimal detector for SM with partial CSI is developed in [17]. Partial CSI at the receiver inevitably leads to a sub-optimal receiver design but a more practical system. However, partial CSI also results in a substantial performance loss because the receiver cannot use the phase information for ML detection. The loss of the phase information translates to an unrecoverable rotation of the signal constellation and a higher ABER. In addition, the effects of channel estimation errors along with an asymptotically tight upper bound for the ABER of SM over a Rayleigh fading channel are analysed in [54]. Nonetheless, in all publications thus far, SM is shown as more robust to the negative effects of the channel estimation errors and is shown to perform better than V-BLAST for the same spectral efficiency.

One of the more comprehensive analysis of SM is presented in [55]. The ABER performance of SM is characterised over generic fading channels for any MIMO setup, arbitrary spatial correlation and arbitrary signal modulation schemes. The authors report simple formulae for the optimal choice of a signal modulation scheme in an identical and independently distributed (i.i.d.) Rayleigh fading environment. The exact role of the bit mapping in the spatial and signal constellation diagrams is also highlighted. To this extent, the authors show that there is an optimal allocation of the information bits between the spatial and signal constellation diagrams depending on the fading environment. Indeed, the fading environment is demonstrated to play a key role in the ABER performance of SM as it directly effects the diversity gain of the system. In particular, the ABER performance gains over other SIMO systems are shown to increase in less sever fading and are shown to decrease for more sever fading, where sever channel fading is classified by the small separability of the channel signatures. Therefore, for the same spectral efficiency, encoding more bits in the spatial domain is recommended in less sever fading environments, while encoding more bits in the signal domain is recommended in more sever fading environments. In addition, the effects of both transmit and receive side spatial correlation are considered. A discussion on the effects of spatial correlation on the ABER performance of SM follows in Section 3.6.2.

To improve the detection of the spatial constellation symbols, trellis coded spatial modulation is proposed in [56, 57]. In particular, a $1/2$-rate trellis modulation is used to encode the bits defining the transmit antenna. To this extent, the spatial domain symbols are grouped into sub-sets of equal sizes such that the Hamming distance is maximised among the elements of a sub-set. The transmit antennas are chosen such that the larger the Hamming distance between two spatial symbols is, the larger their physical separation is. This minimises the spatial correlation between the transmitting antennas belonging to the same sub-set and results in a better ABER. As with all coding schemes, however, the reduced error probability comes at the cost of reduced system throughput, since more bits are sent, yet fewer information bits are decoded. Nonetheless, the proposed system shows an improvement over the original SM system at the same spectral efficiency. Furthermore, a new trellis code design is proposed in [58]. At the receiver, a soft decision Viterbi decoder is used, which is fed with the soft information supplied by the ML SM decoder. The newly presented system achieves better performance in terms of the ABER when compared to the system proposed in [56, 57] as well as the coded V-BLAST system at the same spectral efficiency.

All work presented thus far, considers the application of ML decoding for the detection of SM symbols. The ML detector, however, results in a high computational complexity. To this extent, a novel detection algorithm for SM based on the sphere decoding (SD) tree search idea is analysed in [59]. In particular, the proposed detector reduces the detection complexity of SM by as much as 85% with a nearly optimal ABER performance. In addition, the idea of using SD for SM is further refined in [16] where a number of different SD algorithms, which offer the same ABER performance as ML detection, are discussed. The authors conclude that the best SD to use, depends on the deployment scenario. More importantly, the detector complexity for one of the proposed SD algorithms is shown to be independent of the number of transmit antennas. This permits any SM system to employ large antenna arrays at the transmitter with no negative effects for the computational cost at the receiver. These findings are particularly important for SM since the spectral efficiency of the system increases logarithmically with the number of transmit antennas.

The ABER performance of SM, when applied in an orthogonal frequency division multiple access (OFDMA) system, is shown in [51, 60]. The idea is that multiple RF chains are active but on different resource blocks. In this manner, ICI is avoided along with the need for antenna synchronisation. SM is again shown to outperform V-BLAST in terms of the ABER in a Rician fading environment by as much as 7 dB, despite spatial correlation and mutual antenna coupling. More recently, a soft decision ML detector for SM is presented in [61]. The performance of the new detector exhibits a better ABER when compared to the narrowband SM system by as much as 3 dB. These gains are also seen when the new detector is applied in an OFDMA system in conjunction with SM.

It is the ability of SM to use the channel signature between the transmitter and receiver as a "modulation unit" that distinguishes SM from other MIMO schemes. To this extent, a single pulse sent from any transmit antenna is sufficient to identity the channel between the transmitter and receiver. The system in which only a pulse signal is sent, is termed space shift keying (SSK). The SSK concept is first introduced in [62, 63]. Since then, a number of publications address various aspects of SSK modulation; from determining the optimal detector with partial CSI and imperfect channel knowledge [64, 65], to establishing a general framework for the performance analysis in a correlated Nakagami fading environment [66], to deriving the secrecy capacity with two transmit antennas [67]. Notably, SSK is shown to offer better performance in the presence of power imbalances between the transmit antennas. Indeed, an optimised power

allocation for various transmit antennas is addressed in [68].

Furthermore, time-orthogonal signal design assisted space shift keying (TOSD-SSK) is introduced as a novel SSK scheme in [69]. It uses multiple active antennas and offers transmit-diversity gains by designing the transmitted pulse to have an auto-correlation function such that ICI is avoided. Due to the transmit signal design, TOSD-SSK is shown to have an intrinsic robustness to spatial correlation and is shown to have a better ABER performance relative to standard SSK. Additional work on TOSD-SSK is presented in [70], where the authors develop a general closed form analytical framework to compute the ABER for an arbitrary system with varying fading distributions, spatial correlation and pilot training sequences. To this extent, TOSD-SSK is shown to be more robust to channel estimation errors than the Alamouti scheme and both transmit and receive side diversity are maintained even with imperfect channel knowledge. Furthermore, a generalised architecture for space-time shift keying is proposed and analysed in [71, 72]. In addition, a scheme enabling transmit-diversity for SSK along with a number of other algorithms aimed at achieving transmit-diversity gains are discussed in [73].

More recently the idea of SM has also been applied to optical communication systems. In particular, the ABER of an indoor optical wireless communication using SM is discussed in [74, 75]. Comprehensive work on applying SM to an optical wireless system is presented in [76]. The optical MIMO channel impulse response is obtained via Monte Carlo simulations by applying ray tracing techniques. The authors show that the power efficiency of the system can be improved by increasing the receive side diversity or introducing hard and soft channel coding techniques. However, if the transmit and receive units are aligned, then the ABER of the system decreases such that it performs better than on-off keying, pulse position modulation, and pulse amplitude modulation. In addition, the relevance of SM as applied to an optical wireless system, is further demonstrated in terms of the ABER and the energy efficiency of the system in [77]. Lastly, experimental results demonstrate the practical aspects of applying SM in the optical wireless communications system [78].

A summary of the current research efforts along with possible avenues for further research are also presented in [79].

2.5 Motivation

Over the recent years, the SM concept has attracted growing research interest as its performance benefits compared to other MIMO schemes are established. SM imposes no limit on the number of receive antennas and achieves spatial multiplexing gains even for a single receive antenna. In addition, SM requires no timing synchronisation for the transmit antennas and avoids ICI as well as IAI. In particular, the lower detection complexity for SM reduces the power consumption of the mobile terminal thus enabling a longer battery life [16]. It also offers better robustness to channel estimation errors and channel correlation when compared to V-BLAST [17, 18]. Lastly, SM requires only a single RF chain at the transmitter, regardless of the number of transmit antenna elements. SM is therefore, a more optimal system for exploiting the advantages of multiple transmit antennas while maintaining a single RF chain for green communications. These advantages make SM a viable candidate for future wireless networks.

Nonetheless, SM is still a relatively new concept. As such, there are many aspects to be considered before it is deployed in a real world system. To this extent, encoding binary data in the spatial domain means that the number of transmit antennas doubles for every extra bit added in the spatial domain. This might pose practical limits on the achievable data rates by small–scale mobile terminals. Indeed, the cost and physical space limitations are most prominent for such small-scale devices. Placing eight transmit antennas on such a device might not be feasible, while five or six antennas may be possible. In such a scenario, however, SM would only use four. A method for overcoming the limitation on the number of transmit antennas is proposed in Chapter 3. In addition, more recent alternatives to the proposed method are discussed in Section 3.7.

Thus far, the application of SM has been considered strictly in a point-to-point communication system, *i.e.*, a noise limited scenario. Most practical systems, however, are interference limited. To this extent, work in Chapter 4 aims to characterise the behaviour of SM in the multi-user, interference limited scenario and compare it to the *complexity and cost equivalent* multi-user MIMO system.

Another area of interest involves using SM in relaying systems. It is well established that the ABER between the source and the destination in a dual-hop relaying system depends on the ABER between the source to relay and the relay to destination links. To this extent, the focus is on orthogonal amplify and forward (AF) and decode and forward (DF) protocols.

Outage probabilities, mutual information calculations and transmit diversity bounds for AF and DF relaying are derived in [80] with the end-to-end ABER performance considered in [81]. Considering the above relaying protocols, the use of SM is proposed to provide additional power and capacity gains over the non-cooperative AF and DF systems in Chapter 5.

Numerical simulations and theoretical analysis often provide a reliable measure for the expected performance of new transmission technologies. However, only practical implementations of the theoretical concepts can provided definitive proof of the ABER performance of a system [11, 78]. To this extent, the first practical implementation of the SM concept is presented in Chapter 6 and the experimental results are discussed.

2.6 Summary

In this chapter, the evolution of wireless communication systems was presented and the initial radio experiments were discussed. In addition, the implications of the capacity derivation for all communication systems by Shannon were considered. Furthermore, the development and current deployment of MIMO systems was reviewed. The properties and impact of the wireless channel on a MIMO communications system, along with the working principles for MIMO communications, were presented and elaborated. To this extent, the advantages and perceived disadvantages of MIMO were reviewed and a solution in terms of the SM concept was proposed. The relative advantages of SM compared to other MIMO systems were discussed and its limitations were considered. To support the claims made, an overview of the latest research in SM was presented. Finally, the motivation for the extensions of the SM concept and the need for its practical implementation was presented. This sets the context for the work that follows.

Chapter 3

Fractional Bit Encoded Spatial Modulation

3.1 Introduction

In this chapter a method for overcoming the limitation on the number of transmit antennas in spatial modulation (SM) is proposed. The aim is to equip the transmitter with an arbitrary number of antennas. Traditionally, the number of bits sent in the spatial domain has been limited to an integer number, which constrained the number of transmit antennas to be a power of two. A solution to this limitation in SM is proposed which increases the granularity of the data encoding process in the spatial domain. The novel method is called fractional bit encoded spatial modulation (FBE–SM) and uses fractional bit encoding (FBE).

FBE–SM relies on encoding each point in the spatial domain (the antenna index) with a non–integer number of bits, while the encoding process in the signal domain is left unchanged. This results in a more versatile system design, allowing a wider range of spectral efficiencies given restrictions on space and power consumption [15]. By using FBE–SM, a system can achieve otherwise unavailable data rates. For example, it may not be possible to install eight antennas in a small-scale portable device, while five or six might be feasible. In such a case, however, SM would use only four antennas [15]. FBE–SM is designed to address exactly this problem.

The concept behind FBE is not new in modern communication systems. For instance, the application of FBE to a pulse amplitude modulation (PAM) communication system is reported in [82]. The idea has been used for communication systems with data rate throttling through a selection of different signal constellations depending on the signal energy. In addition, block modulus coding systems and methods for block coding with non-binary modulus also use FBE. To the best of the authors' knowledge, however, this principle has never been applied to SM.

Two general methods for fractional bit transmission exist. The first approach is called *constellation switching* which alternates between the transmission of τ and $\tau + 1$ bits per symbol to

achieve FBE over time [82]. A notable downside of this approach is the inherent bit shift that results from incorrectly decoded symbols, making it prone to error propagation. The second approach is called *modulus conversion* and is designed to minimise the error propagation effect that afflicts the performance of the constellation switching method [83]. In this chapter, modulus conversion is applied to SM and a system that can offer satisfactory performance for an arbitrary number of antennas at the transmitter is proposed. Throughout this thesis the coding gain is defined as the difference between the signal-to-noise-ratio (SNR) levels of two systems that is required to reach the same average bit error ratio (ABER).

In the remainder of this chapter, the modulus conversion is briefly summarised in Section 3.2. The novel FBE–SM scheme is then introduced in Section 3.3. Furthermore, the analytical performance for the average symbol error ratio (ASER) is presented in Section 3.4. In addition, the ASER and ABER performance of FBE–SM is analysed via simulations and is compared with the performance of conventional SM in the uncorrelated scenario in Section 3.5. The performance of the system in a spatially correlated environment is then addressed in Section 3.6. The latest alternates to FBE–SM and their perceived weaknesses are finally discussed in Section 3.7. Lastly, a summary of the chapter is presented in Section 3.8.

3.2 Modulus Conversion

Modulus conversion achieves fractional bit rates by converting the incoming bit stream to numbers in an arithmetic base, or modulus, that is not a power of two [83]. In particular, the modulus converter operates as follows: i) blocks of S by ϖ bits are extracted from the incoming bit stream, where S is a positive integer and ϖ is the desired fractional bit rate; ii) each block is then converted to S numbers of base L. The modulus is defined as the smallest integer number, L, such that $L \geq 2^{\varpi}$.

In general, one may use modulus conversion to achieve an arbitrary fractional bit rate, *i.e.*, ϖ could be a real number. This is particularly relevant when applying this method to SM, as will be discussed in Section 3.3. However, since both L and S are positive integer numbers, it follows that the modulus converter can only handle rational bit rates. This problem can be circumvented by approximating any ϖ, with $\widetilde{\varpi}$ given as the ratio of two positive and relatively prime integers p and q. In other words, the problem can be stated as finding the best rational approximation, $\widetilde{\varpi} = p/q$, to a real number ϖ. A simple way of achieving this, is to exploit the

following inequality

$$0 \leq n\varpi - \lfloor n\varpi \rfloor \leq 1 \Rightarrow 0 \leq \varpi - \frac{\lfloor n\varpi \rfloor}{n} \leq \frac{1}{n}, \tag{3.1}$$

where $\lfloor \cdot \rfloor$ denotes the floor function and n is an arbitrary and positive integer number.

From (3.1), it follows that $S\varpi \cong S\widetilde{\varpi} = S\left(\lfloor n\varpi \rfloor / n\right)$, which according to modulus conversion, must be a positive integer. It is worth mentioning that, in general, $S \neq n$. In particular, although n and S could be arbitrarily chosen, the following guidelines should be considered for their optimal setting:

1. The larger n is, the smaller the approximation error $\varpi - \widetilde{\varpi}$ is, which follows from (3.1).

2. The larger S is, the longer the decoding delay is, which follows from the operating principle of modulus conversion. It allows the receiver to decode the data only after receiving S, base–L numbers.

3. The larger S is, the greater the vulnerability to error propagation within each block of bits is (see Section 3.5).

Accordingly, for any given ϖ, and provided that $S\left(\lfloor n\varpi \rfloor / n\right)$ is a positive integer, n and S should be chosen to be as large and as small as possible, respectively.

3.2.1 Example of FBE–SM

Consider a simple example with $L = 5$ with no signal modulation, equivalent to space shift keying (SSK) modulation [63], such that $\varpi = 2.3219$. In particular, $\widetilde{\varpi} = 2.25$ is obtained if $(S, n) = (4, 4)$. This approaches ϖ and is greater than the spatial multiplexing gain offered by a system with $N_t = 4$. Indeed, if the block of $S\widetilde{\varpi}$ bits is equal to $(110001011)_2$, then the modulus converter will return an $(S\widetilde{\varpi})_{N_t}$ block equal to $(3040)_5$, where $(\cdot)_L$ denotes the base–L representation. The output of the modulus converter is then mapped to a spatial constellation point. First, the antenna with index 3 transmits an energy signal, then the antenna with index 0 transmits the same signal, etc. The receiver will estimate each transmit antenna index by using the detection algorithm in [52]. After decoding the S antenna indexes, ideally with no errors, it will recover the original data stream as: $(3040)_5 = (110001011)_2$.

To understand the effect of error propagation, consider that an error has occurred in the detection of the second antenna index. The decoded block is then given as $(3140)_5$. In this case, the decoded bit stream will be $(3140)_5 = (110\mathbf{1}10\mathbf{0100})_2$ with 5 out of 9 bits in error. Indeed, the error propagation effect is evident in the last 4 digits. This example highlights the important role played by S to limit the error propagation effect in the decoded bit stream for each incorrectly decoded base–N_t number. In particular, an error that occurs in the last digits of the base–N_t sequence results in fewer erroneous bits than an error that occurs in the first digit of the same sequence. To address this problem, unequal error protection can be employed [84]. Some of the work done in the field establishes exponential error bounds and provides some fundamental limits and optimal strategies for problems of unequal error protection [85]. However, all work in this field is based on the coding level. To the best of the authors' knowledge, there is no way of applying unequal error protection at the physical layer without losing spectral efficiency. To this extent, numerical results in Section 3.5 quantify the system performance with respect to the ASER and ABER where the effects of the error propagation are discussed further.

3.3 Application of Modulus Conversion to Spatial Modulation

Modulus conversion is now applied to SM and the FBE–SM method is introduced. As mentioned in Section 3.1, the motivation for the proposed scheme is to avoid fundamental constraints on the number of transmit antennas employed by SM systems. In particular, the proposed method applies only to bit encoding in the spatial domain, while the encoding process in the signal domain is left unchanged. In fact, FBE–SM reduces to conventional SM if the number of transmit antennas is a power of two.

3.3.1 Step–by–Step Description of FBE–SM

The working principle of FBE–SM can be summarised in the following subsequent steps:

1. Determine the available number of transmit antennas, N_t, according to the system constraints, such as the data rate, cost, available space, etc.

2. Set the modulus L in Section 3.2 equal to N_t, *i.e.*, $L = N_t$.

3. Compute the maximum spatial multiplexing gain of the system as $\varpi = \log_2(N_t)$.

4. Choose the pair (S, n) such that $S\ (\lfloor n\varpi \rfloor / n)$ is a positive integer number and follows the design guidelines described in Section 3.2. In particular:
   - Optimise $\widetilde{\varpi} = (\lfloor n\varpi \rfloor / n)$ to be as close as possible to ϖ. This allows the system to approach the maximum spatial multiplexing gain offered by the N_t transmit antennas. In general, this is achieved for larger values of n.
   - Optimise S to be as small as possible. This reduces the decoding delay and, more importantly, minimises error propagation in the decoded bit stream.
5. Map each of the S base–N_t encoded numbers in the transmission block to a transmit antenna index, in the range $[0,\ N_t - 1]$.

The receiver will perform the reverse operation to recover the encoded data:

1. For each signalling interval, the maximum likelihood (ML) algorithm in [52] is applied to detect the spatial and signal constellation points jointly.
2. The spatial constellation points (the base–N_t encoded numbers) are grouped into blocks of S points each.
3. Each block is converted to the equivalent base–2 bit stream of $S\,(\lfloor n\varpi \rfloor / n)$ bits.

These are merely guidelines to achieve a balance between the best approximation of ϖ and minimising the error propagation effects. In particular, the best rational approximation for any real number is obtained using continuous fractions given the restriction on the available block size [86]. The simple continued fraction for a real number generates its best rational approximations. In addition, the monotonic increase in the denominators of continued fractions as terms are added, permits an algorithm to impose a limit on either the size of denominator or the tightness of the approximation. Therefore, the proposed algorithm can impose a limit on either the closeness of approximating ϖ, or the number of the blocks, S.

3.4 Analytical Modelling

The jointly optimal ML detector used for the symbol detection in SM and FBE–SM is presented in [52]. In particular, the analytical bound for the ASER of SM in an arbitrary channel environment using an arbitrary signal constellation, is presented in [53]. This bound is derived

using the union bound approach. To this extent, a brief overview of the need and application of the union bound is followed by the analytical treatment of the ASER.

3.4.1 Union Bound Approach

The main result and derivation of the exact ABER for an arbitrary modulation system can be found in [87]. In particular, it means that the ABER for a generic modulation scheme with M possible constellation points, $\omega_{m\in\{1,\ldots,M\}}$, can be computed as

$$\text{ABER} = \frac{1}{M}\sum_{m=1}^{M}\left\{\frac{1}{\log_2(M)}\sum_{\hat{m}=1}^{M}\left[d\left(\omega_m,\omega_{\hat{m}}\right)P_{\omega_{\hat{m}}|\omega_m}\right]\right\}, \tag{3.2}$$

where $d\left(\omega_m,\omega_{\hat{m}}\right)$ is the Hamming distance between the bit assignments of the two constellation points ω_m and $\omega_{\hat{m}}$. $P_{\omega_{\hat{m}}|\omega_m} = \Pr\left\{\omega \in R_{\hat{m}}|\omega_m\right\}$ is the probability that the received signal ω lies in the decision region, $R_{\hat{m}}$, of the symbol $\omega_{\hat{m}}$, when ω_m was transmitted. Provided that $P_{\omega_{\hat{m}}|\omega_m}$ can be computed as a closed form solution, the ABER of the system will also be a closed form solution.

Strictly speaking, this approach can describe the true error performance of any system employing any detection technique. To this extent, to obtain the true error for an arbitrary received point ω, a contour around each constellation point which exactly defines the decision region, $R_{\hat{m}}$, must be considered. To obtain $R_{\hat{m}}$, the conditional probability density of the distribution around the constellation point $\omega_{\hat{m}}$ must be integrated along its decision boundaries. Since the received point ω belongs to the set of complex numbers, the probability distribution around any constellation point ω_m is continuous. Therefore, the conditional probability density function for a signal constellation is defined by a two dimensional Gaussian distribution,

$$\varrho(\omega|\omega_m) = \frac{1}{2\pi\sigma_m^2}\exp\left(\frac{-(\Re\{\omega\}-\Re\{\omega_m\})^2-(\Im\{\omega\}-\Im\{\omega_m\})^2}{2\sigma_m^2}\right), \tag{3.3}$$

where σ_m^2 is the variance of the Gaussian distribution centred at the point ω_m, and $\Re\{\cdot\}$ and $\Im\{\cdot\}$ are the real and imaginary parts of the variable, respectively. In general, $R_{\hat{m}}$ is defined on the complex plane and may not have a closed form solution. As a consequence, the bit and symbol error probabilities cannot be obtained as closed form expressions for an arbitrary modulation system, *i.e.*, union bound based approaches are the most analytically tractable alternative [88, Ch.5].

The most common approach is to assume that any particular decision boundary of the decision region, $R_{\hat{m}}$, is defined by the pairwise error probability (PEP),

$$P_{\hat{m}|m} \leq \Pr\left(\omega_m \neq \omega_{\hat{m}}\right), \tag{3.4}$$

where $\Pr\left(\omega_m \neq \omega_{\hat{m}}\right)$ is the PEP of the emitted signal ω_m being detected as $\omega_{\hat{m}}$. In particular, the union of the PEPs results in an asymptotically tight approximation in the high SNR region because the mass of the Gaussian distribution around ω_m is focused around the mean of the distribution at high SNRs. This approach has previously been used to describe the behaviour of SM in the literature for the single user scenario [52, 53, 89].

3.4.2 Analytical Symbol Error Ratio

A ML detector is considered. It computes the Euclidean distance between the received signal, $\mathbf{y}$, and the set of all possible received signals, selecting the closest one [52],

$$(x_{\text{est}}, n_t) = \underset{x\,,\,\mathbf{h}_{n_t}}{\arg\min} \left\{ ||\mathbf{y} - \mathbf{h}_{n_t} x||^2 \right\}, \tag{3.5}$$

such that

$$x \in \mathcal{X}, \qquad n_t \in \{1, \ldots, N_t\},$$

where the pair (x_{est}, n_t) is formed from the estimated symbol x_{est}, emitted from antenna n_t and x is the current symbol being evaluated from the set of possible signal constellation points $\mathcal{X}$ with cardinality M.

The ASER of SM, using the optimal detector, can now be obtained using the union bound approach and is given as

$$\text{ASER} \leq \sum_{x \in \mathcal{X}} \sum_{\hat{x} \neq x \in \mathcal{X}} \sum_{n_t=1}^{N_t} \sum_{\hat{n}_t \neq n_t = 1}^{N_t} \frac{\mathrm{E}_{\mathcal{H}}\left[\text{PEP}\left(x,\, n_t,\, \hat{x},\, \hat{n}_t\right)\right]}{M N_t}. \tag{3.6}$$

such that $\text{PEP}\left(x,\, n_t,\, \hat{x},\, \hat{n}_t\right) = \Pr\{\mathbf{h}_{n_t} x \neq \mathbf{h}_{\hat{n}_t} \hat{x}\}$ is the PEP where the symbol x, emitted from antenna n_t, is detected as symbol $\hat{x}$, emitted from antenna $\hat{n}_t$ and $\mathrm{E}_{\mathcal{H}}[\cdot]$ is the expectation of the system with respect to the channel, $\mathcal{H}$. The PEP is obtained in [53] as

$$\text{PEP}\left(x,\, n_t,\, \hat{x},\, \hat{n}_t\right) = Q\left(\sqrt{\frac{\gamma}{2} ||\mathbf{h}_{n_t} x - \mathbf{h}_{\hat{n}_t} \hat{x}||^2}\right). \tag{3.7}$$

where γ is the SNR and $Q(\omega) = \frac{1}{\sqrt{2\pi}} \int_{\omega}^{\infty} \exp\left(-\frac{t^2}{2}\right) \mathrm{dt}$ defines the Q-function. In particular, (3.6) is valid for any SM or FBE–SM constellation in any fading environment where the expectation across the fast fading channel coefficients may be performed either analytically or numerically. However, the ABER of FBE–SM is more difficult to obtain because of the error propagation effects resulting from the FBE process. As such, the analytical ABER of FBE–SM has not been treated in this thesis. Nonetheless, (3.6) is used to validate the simulation results for the ASER in Section 3.5 and Section 3.6.1.

3.5 Numerical Analysis in an Uncorrelated Scenario

In the simulations, each transmit antenna broadcasts a 4-quadrature amplitude modulation (QAM) signal. In addition, the channel is assumed to be Rayleigh fading with identical and independently distributed (i.i.d.) wireless links. It is slow fading for the duration of a transmission block, *i.e.*, the coherence time of the channel is longer than the duration of the transmission block. Furthermore, the receiver is equipped with 4 antennas and additive white Gaussian noise (AWGN) is assumed at each receive antenna. Lastly, a ML detector is used to jointly decode the spatial and signal constellation points [52]. In particular, the performance of the system is quantified based on the ASER and the ABER. To this extent, working with bit streams is essential to highlight the effect of error propagation introduced by the FBE process. In addition, the spectral efficiency is compared by considering only the number of transmit antennas since the modulation scheme in the signal domain remains the same.

Fig. 3.1 shows the ABER of FBE–SM for various combinations of (S, n) where $N_t = 5$. It aims to substantiate the claims in Section 3.2 and Section 3.3. Indeed, the ABER gets progressively worse for increasing values of S due to the error propagation effect previously discussed. In particular, the ABER of the system with $(S, n) = (4, 4)$ worsens by approximately 1.5 dB at an ABER of 10^{-3} when compared to the ABER of the system with $(S, n) = (16, 16)$. However, this performance drop is compensated by a small increase in the spectral efficiency, from 2.25 bits/s/Hz to 2.3125 bits/s/Hz; an increase of less than 3%. To this extent, Fig. 3.1 demonstrates the effects of error propagation. It shows that $S = 4$ and $\widetilde{\varpi} = 2.25$ is a better choice than $S = 16$ and $\widetilde{\varpi} = 2.3125$; a combination resulting from jointly optimising the steps in Section 3.3.1.

Furthermore, Fig. 3.5 shows the ASER and ABER of FBE–SM for various numbers of transmit

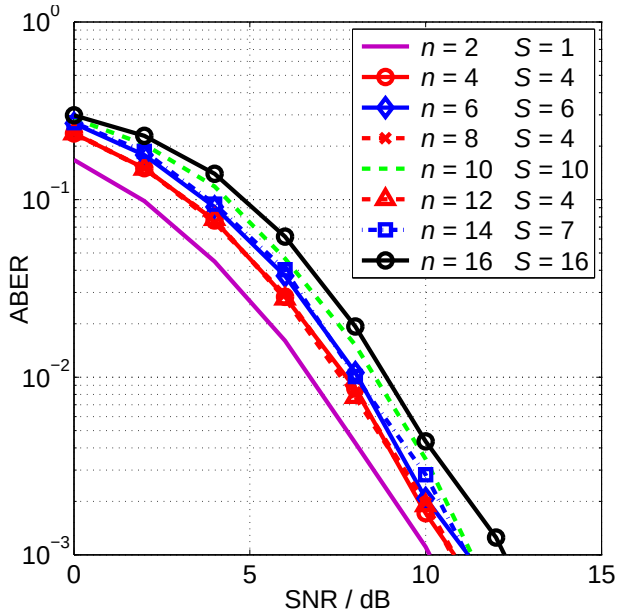

Figure 3.1: *ABER of FBE–SM. Parametric study for different values of* (S, n)*. Setup:* $N_t = 5$ *and* $\varpi = 2.3219\,\mathrm{bits/s/Hz}$.

antennas, respectively. If $N_t = \{2,\ 4,\ 8\}$, then the system reduces to conventional SM. For the sake of clarity, only two of the analytical upper bounds are presented. In particular, the upper bounds for the systems with $N_t = 2$ and $N_t = 8$ are shown in Fig. 3.2(a) where the ASER is shown to worsen monotonically for increasing values of N_t. This is expected as it translates to an increase in the spatial spectral efficiency from 1 bit/s/Hz for $N_t = 2$, to 3 bits/s/Hz for $N_t = 8$. When looking at Fig. 3.2(b), however, the ABER does not worsen monotonically for increasing N_t. For example, the system setups with $N_t = \{5, 6, 7\}$ offer a worse ABER and a lower spectral efficiency than the setup with $N_t = 8$. This is due to the error propagation effect of the FBE process. However, the performance difference between the setups with $N_t = \{5, 6\}$ and the setup with $N_t = 8$ reduces for high SNRs. In fact, the 1.7 dB difference seen at an ABER of 10^{-1} between $N_t = 6$ and $N_t = 8$, reduces to only 0.9 dB at an ABER of 10^{-4}, as shown on Fig. 3.2(b). Even though SM with $N_t = 8$ offers a better data rate, this solution may not be practical due to cost and space constraints. In such scenarios, the proposed FBE–SM scheme with $N_t = \{5, 6\}$ may be an effective solution for trading–off spectral efficiency for performance. In this context, the results for a large number of transmit antennas are over–optimistic since no channel correlation is assumed. In particular, if more antennas are placed in a limited space, mutual antenna coupling and spatial correlation increase, which hinder the performance of the system.

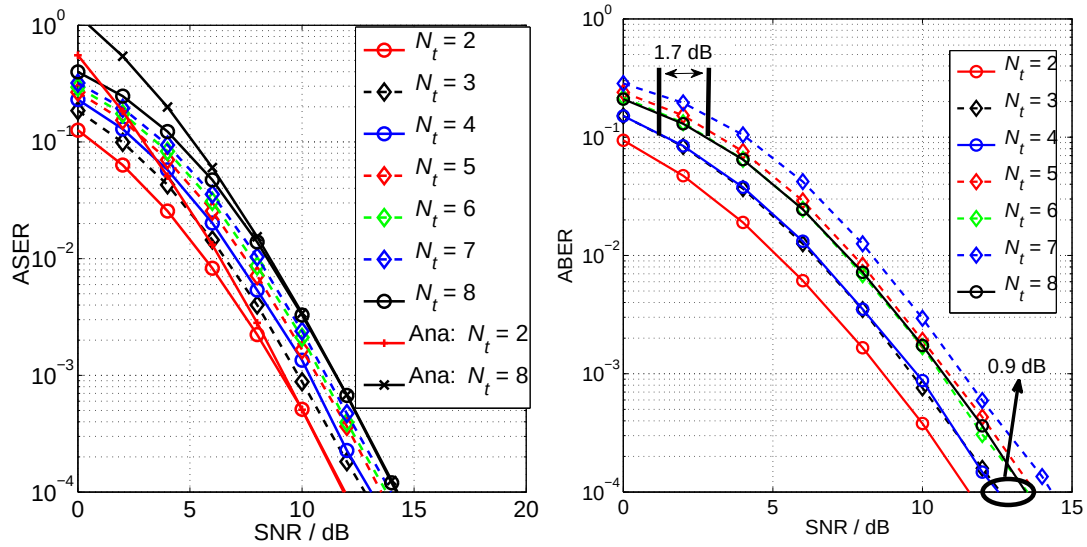

(a) ASER (b) ABER

Figure 3.2: *ASER and ABER of FBE–SM when there is no spatial correlation. The analytical upper bound is denoted as* Ana*. Parametric study for different values of transmit antennas,* N_t*. Setup: i)* $S = 4$*, and ii)* $n = 4$*.*

3.6 FBE–SM in a Correlated Scenario

From the analysis in Section 3.5, the deployment of FBE–SM in a practical scenario is shown to be directly related to the space and cost limitations of the portable device. Indeed, classical SM performs better than FBE–SM when there is no correlation between the transmit or receive antennas. Therefore, to determine the practicality of FBE–SM, the performance of the system under a correlated scenario must be assessed.

The channel correlation experienced by a communication system is a function of both the environment and the antenna element spacing. Given that the transmitter and receiver are far apart relative to the scattering environment between them, then the correlation they experience is independent of each other, *i.e.*, Rayleigh fading is assumed, as in Section 3.5. To this extent, the well established Kronecker model with an exponential correlation profile for both the transmitter and receiver correlation matrices is used [90–92].

The cross correlation, $\upsilon_{n_t,\hat{n}_t}$, between any two transmit antennas $(n_t, \hat{n}_t)$ can be calculated as

$$\upsilon_{n_t,\hat{n}_t} = \mathrm{E}_{\mathcal{H}}\left[\mathbf{h}_{n_t}\mathbf{h}_{\hat{n}_t}^{H}\right], \tag{3.8}$$

where $(\cdot)^H$ is the Hermitian of a vector or a matrix, $\mathbf{h}_{n_t}$ and $\mathbf{h}_{\hat{n}_t}$ are channel vectors from

transmit antennas n_t and $\hat{n}_t$ to all receive antennas, respectively. These correlation coefficients are the elements of the transmit correlation matrix. However, since the exponential decay model is used, then the cross correlation coefficients, *i.e.*, the elements of the correlation matrix $\mathcal{R}_{\mathrm{tx}}$, may be obtained element-vise as

$$\mathcal{R}_{\mathrm{tx}}^{(n_t,\hat{n}_t)} = \exp\left(\left(n_t - \hat{n}_t\right)\upsilon\right), \tag{3.9}$$

where υ is the correlation decay coefficient and $\exp(\cdot)$ is the exponential function. Similarly, by compiling the correlation coefficients from every receive antenna to all transmit antennas or by applying the exponential decay model, the correlation matrix at the receiver, $\mathcal{R}_{\mathrm{rx}}$, can also be obtained. The correlated channel matrix can then be represented as

$$\mathcal{H}^{\mathrm{corr}} = \frac{1}{\sqrt{\mathrm{tr}\left(\mathcal{R}_{\mathrm{rx}}\right)}}\mathcal{R}_{\mathrm{rx}}^{1/2}\,\mathcal{H}\,\mathcal{R}_{\mathrm{tx}}^{1/2}, \tag{3.10}$$

where $\mathrm{tr}(\cdot)$ denotes the trace of a matrix and $\mathcal{H}^{\mathrm{corr}}$ is the correlated channel matrix [57].

The correlation matrices, $\mathcal{R}_{\mathrm{tx}}$ and $\mathcal{R}_{\mathrm{rx}}$, can also be computed based on the power azimuth spectrum distribution and array geometry [91]. Indeed, the Fast-R model, as it is termed in [91], is used in many cluster channel model such as the IEEE 802.11n Technical Group [93] and the 3GPP Technical Specification Group [94] under the condition that angular spread is less than 15^{o}. In this work, the angular spread is set to 0^{o} and the channel coefficients follow a Rayleigh distribution.

3.6.1 Numerical Analysis

In this section, the behaviour of FBE–SM in a correlated scenario is analysed via simulations and a carrier frequency of 3 GHz is assumed for use with the correlation model. In particular, the relation between the correlation decay coefficient and the relative distance between the transmit antennas is given as $\upsilon = J_0\left(\lambda\right)$, where $J_0(\cdot)$ is a Bessel function of the first kind of order zero and λ is the antenna spacing in terms of the carrier wavelength in radians [95]. In addition, a linear array of antenna elements is assumed at the transmitter, *i.e.*, all transmit antennas must fit within the available space. With this assumption, the decay correlation coefficients for an available space of 10 cm, 9 cm and 8 cm are given in Table 3.1, *i.e.*, there is at most one wavelength separation between the furthest transmit antennas. Furthermore, if the antenna separation is greater than one half of the carrier wavelength, then the correlation coefficient can be

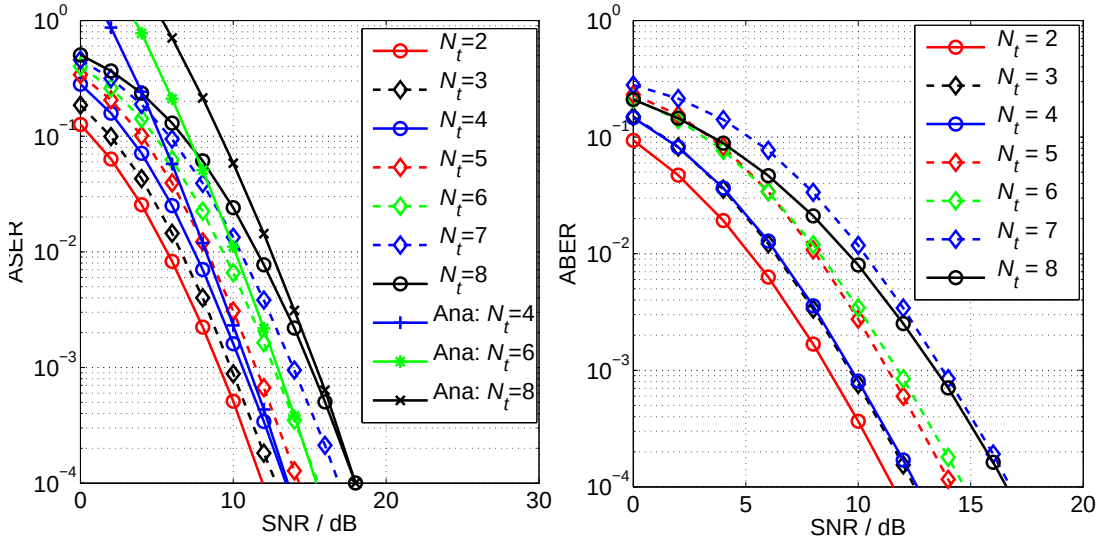

(a) ASER (b) ABER

Figure 3.3: *ASER and ABER of FBE–SM under spatial correlation when the transmitter has at most* $10\,\mathrm{cm}$ *of available space. The analytical upper bound is denoted as* Ana *and the decay coefficients are given in the first column of Table 3.1. Parametric study for different values of transmit antennas,* N_t*. Setup: i)* $S = 4$*, and ii)* $n = 4$*.*

considered to be zero [96]. In addition, since FBE–SM is only applicable at the transmitter side, no spatial correlation is assumed at the receiver. In particular, the impact of the receiver side correlation is discussed in Section 3.6.2. As in Section 3.5, four receive antennas are assumed.

Available Space:	10 cm	9 cm	8 cm
$N_t = 2$	0	0	0
$N_t = 3$	0	0.05	0.09
$N_t = 4$	0.17	0.29	0.41
$N_t = 5$	0.47	0.56	0.64
$N_t = 6$	0.64	0.70	0.76
$N_t = 7$	0.74	0.79	0.83
$N_t = 8$	0.81	0.84	0.88

Table 3.1: *Correlation decay coefficients,* υ*.*

A gradual worsening of the ASER in the systems which experience spatial correlation, *i.e.*, when $N_t \geq 4$, is visible in Fig. 3.2(a), 3.3(a) and 3.4(a). This is expected since correlation makes the channels less distinct by reducing the Euclidean distance between the spatial constellation points and results in a larger ASER. Indeed, as antennas are placed in a more limited space at the transmitter, the performance of the system worsens. In particular, the ASER in-

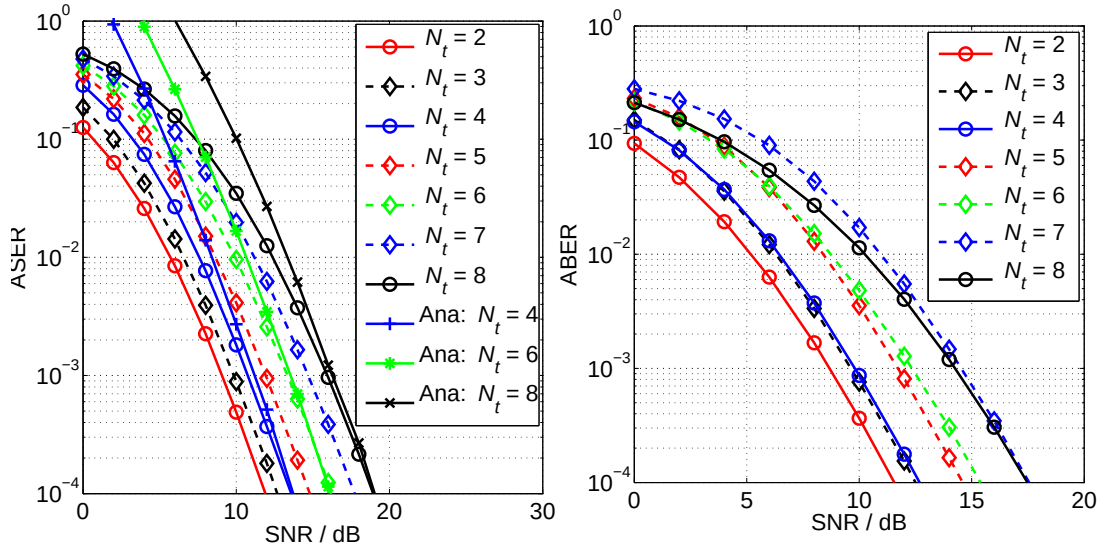

(a) ASER (b) ABER

Figure 3.4: *ASER and ABER of FBE–SM under spatial correlation when the transmitter has at most* $9\,\mathrm{cm}$ *of of space available. The analytical upper bound is denoted as* Ana *and the decay coefficients are given in the second column of Table 3.1. Parametric study for different values of transmit antennas* N_t*. Setup: i)* $S = 4$*, and ii)* $n = 4$*.*

creases from around 14.5 dB for $N_t = 8$ in Fig. 3.2(a), to around 16 dB in Fig. 3.3(a), to around 17.5 dB in Fig. 3.4(a), where the available space is reduced in 1 cm steps from one figure to the next. In addition, the upper bound for the ASER presented in (3.6), is shown in Fig. 3.3(a) and Fig. 3.4(a) for $N_t = \{4, 6, 8\}$, where the expectation across the wireless channel is performed numerically. The upper bound in (3.6) serves to validate the simulation results.

Looking at the ABER in Fig. 3.2(b) through Fig. 3.5, however, FBE–SM starts performing better than classical SM in a constrained environment. In particular, Fig. 3.3(b) shows that FBE–SM with $N_t = \{5, 6\}$ performs marginally better than SM with $N_t = 8$ at an ABER of 10^{-4}. The system with $N_t = 7$, however, still exhibits a much worse ABER. If the available space is reduced by 1 cm, however, then FBE–SM with $N_t = \{5, 6\}$ performs as much as 3 dB better relative to SM with $N_t = 8$, as shown in Fig. 3.4(b). Furthermore, Fig. 3.5 shows how reducing the available space by another 1 cm worsens the ABER of all systems and further increases the coding difference between FBE–SM with $N_t = \{5, 6\}$ and SM with $N_t = 8$.

It is the wavelength separation between the neighbouring antenna elements that determines the channel correlation in the system. Future wireless networks, however, are well below the 3 GHz carrier frequency assumed here [24]. Therefore, correlation must be considered in the

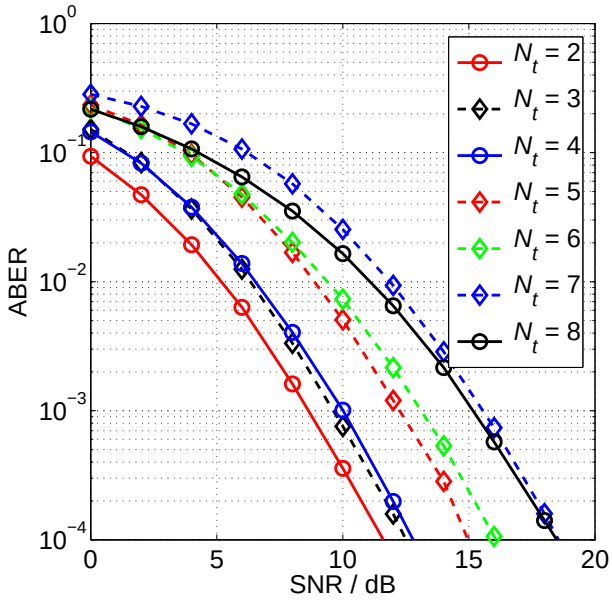

Figure 3.5: *ABER of FBE–SM under spatial correlation when the transmitter has at most* $8\,\mathrm{cm}$ *of space available. The decay coefficients are given in the third column of Table 3.1. Parametric study for different values of transmit antennas,* N_t*. Setup: i)* $S = 4$*, and ii)* $n = 4$*.*

deployment of any future multiple–input multiple–output (MIMO) system. Indeed, the larger wavelengths at lower frequencies, make FBE–SM a viable candidate for any real world application of SM, even though classical SM performs better in the uncorrelated scenario.

3.6.2 Spatial Modulation with Spatial Correlation

A number of publications exist that aim to classify the performance of SM in a spatially correlated scenario [57], [69]. Most recently, however, a more in-depth performance analysis is presented in [55]. The authors analyse the effects of transmit and receive side correlation in a Nakagami fading environment. In particular, the impact of correlation on the ABER is shown to increase with N_t when the spatial correlation coefficient is kept constant, *i.e.*, the more transmit antennas there are, the more difficult it becomes to distinguish them. Furthermore, the authors demonstrate that the better the fading environment in terms of the channel separability, the stronger the impact of transmit side correlation. Similarly, the poorer the fading environment, the weaker the impact. Correlation at the receiver, however, is shown to have the same impact regardless of the fading environment. In addition, increasing the number of transmit antennas is suggested as a means of combating the effects of the receive side correlation. On the one hand, in the case of high transmit side correlation, the error associated with the spatial constellation

point detection is shown to govern the ABER. On the other hand, in the case of high receive side correlation, the error associated with the signal constellation point detection is shown to govern the ABER. It is therefore a trade–off between the size of the signal, and the size of the spatial constellation diagrams, that results in the best performance for SM and FBE–SM alike.

3.7 Alternatives to FBE–SM

Since the publication of the FBE–SM concept, a number of papers have emerged that attempt to address the limitation placed on the number of transmit antennas for SM and increase its spectral efficiency.

In one example, the authors first introduce their understanding of the SM principle and term it information guided channel hopping (IGCH) [97]. Since FBE–SM suffers from error propagation, the authors introduce a new approach to the problem and term it bit-padded IGCH. Based on the bit padding technique, this approach supposedly offers better performance than FBE–SM, while having lower computational complexity. To achieve this, a symbol mapping sequence is proposed when the number of transmit antennas is not a power of two. The interested reader is encouraged to look at [97] for a detailed description of the algorithm. In brief, the approach is to create a unique bit-to-symbol mapping where some transmit antennas convey an extra bit compared to others. To this extent, bit-padding the antennas that carry fewer bits is suggested to provide a consistent bit length per symbol at the receiver. An example of a possible bit-to-symbol allocation is given in Table I from [97] and is given here for convenience as Table 3.2. The idea is that every symbol decoded individually will always result in the same number of bits, hence stopping error propagation.

n_t	$N_t = 3$	$N_t = 4$	$N_t = 5$	$N_t = 6$	$N_t = 7$	$N_t = 8$
1	0**0**	00	00**0**	00**0**	00**0**	000
2	10	01	01**0**	01**0**	010	001
3	11	10	10**0**	100	011	010
4		11	110	101	100	011
5			111	110	101	100
6				111	110	101
7					111	110
8						111

Table 3.2: *Mapping in Bit-Padded–IGCH systems. Numbers in bold denote the padded zeros.*

Furthermore, the authors in [97] provide capacity calculations for their proposed scheme along with a numerical comparison between bit-padded IGCH and FBE–SM in terms of the ABER. Unfortunately, the proposed scheme is limited by a key conceptual aspect which can be illustrated by an example.

A bit stream, given as $0001\ 11010\ 1011$, and a system that has 5 available transmit antennas and uses 4-QAM for the signal symbol modulation is assumed. According to the bit-padded IGCH principles, the bit stream will be broken up into three blocks, each to be transmitted at a single time interval. Given the bit-to-symbol mapping for the transmit antennas from Table 3.2, at time instance t_1, antenna 1 would transmit symbol x_1, at t_2, antenna 4 would transmit symbol x_2 and at t_3, antenna 3 would transmit symbol x_3, where $x_{i,i\in\{0,1,2,3\}}$ is a symbol chosen from the 4-QAM constellation. For antenna 1 and antenna 3 an additional '0' would be added at the end of the sequence (reading it left to right) as per Table 3.2. A ML detector is then applied at the receiver.

An error event, such that antenna 4 and symbol x_1 are detected at time t_1, is assumed and all remaining SM constellation points are assumed to be correct. In this event, $\mathbf{11}0001\ 11010\ 1011$ is obtained when the newly detected sequence is decoded, as per Table 3.2. There are now more information bits decoded than were originally sent. Indeed, it is the principles behind bit-padding IGCH that create an off-by-one decoding error, *i.e.*, a single error in the entire bit stream will result in all other bits being wrongly detected. When dealing with uncoded physical layer bit streams at the receiver, it is inherently impossible to know which symbol is correct, which is wrong and how to properly decode the performed bit-padding. This simple example clearly shows that bit-padded IGCH suffers from the same problems as other *constellation switching* algorithms and performs worse in terms of ABER than FBE–SM, despite the claims in [97].

A second approach, aimed at easing the constraint on the number of transmit antennas, is called generalised spatial modulation (GSM). The concept is originally introduced in [98]. In particular, the idea is to activate multiple antennas simultaneously to broadcast the same signal constellation symbol. In general, SM requires that the channel signatures for each spatial symbol (transmit antenna) are discernible. However, unique channel signatures can also be obtained by activating different combinations of the available transmit antennas. By taking this approach, a SM system is free to have any number of transmit antennas greater than or equal to two. Indeed, a power of two number of distinct channels between the transmitter and the receiver is the only

requirement, regardless of how each channel is obtained. To this extent, GSM is shown to result in a similar system performance with respect to the ABER when compared with classical SM systems [98].

Recently, work has also gone into combining SM with more traditional space-time block codes (STBC) [99]. The resulting system, termed STBC–SM, benefits from transmit side diversity and an increased set of distinct channels. The interested reader is encouraged to look at [99] for a detailed description of the algorithm used to maximise the coding gain difference between various codebooks. In brief, the authors propose the use of standard STBC with a specific selection of transmit antennas. They define that a non-interfering codeword group is one where the active transmit antennas of a single codeword (which may last two or more time intervals) are strictly inactive for any other codeword in the same codeword group. To this extent, an algorithm to obtain an optimised STBC–SM transmission scheme is provided in [99, Section II.A]. Step 4 of the algorithm establishes two key aspects that must be considered when designing the STBC–SM scheme:

- "every codebook must contain non-interfering codewords chosen from pairwise combinations of the available transmit antennas,"
- "each codebook must be composed of codewords with antenna combinations that were never used in the construction of a previous codebook."

In effect, the signal symbols being transmitted from the active antennas over the duration of a single codeword should not be used for any other codeword in the same codeword group. Similarly, the active antenna group used for a single codeword group should not be used in another codeword group, *i.e.*, the used signal symbols distinguish the various codewords while the used active antennas distinguish the various codeword groups.

To maintain separability between the transmitted codebooks, the authors propose the use of a rotational angle. The rotational angle must be optimised for a given modulation format to ensure maximum diversity and coding gain. If the rotational angle is not considered, however, overlapping active transmit antennas used in different codeword groups would reduce the transmit diversity order to one. In particular, an analytical method for determining the optimal rotational angle needed to maximise the transmit side diversity when using binary phase shift keying (BPSK) and 4-QAM is presented. However, the optimal rotational angles must be determined by an exhaustive numerical search for a signal constellation of 16-QAM or 64-QAM.

Indeed, it is the rotational angles that help the diversity of the system when multiple transmit antennas must be active.

On the one hand, increasing the number of transmit antennas results in an increasing number of antenna combinations and an increasing spectral efficiency at the expense of optimising a greater number of angles. On the other hand, lowering the spectral efficiency for a greater number of transmit antennas, means fewer rotational angles must be optimised thus aiding detection. In addition, a demodulator combining a ML algorithm along with the linear STBC decoder is shown to be optimal at the receiver. Similarly to FBE–SM, STBC–SM is also shown to result in fractional data rates over time.

More recently the authors of [100] have also considered GSM. The interested reader is encouraged to refer to [100] for further details. In brief, unlike GSM where all active antennas transmit the same symbol, the authors propose activating several transmit antennas, each carrying different signal symbols during each time slot, similar to STBC–SM. This improves the spatial multiplexing of the system and removes the constraint on the number of transmit antennas. To this extent, the effects of codeword groups sharing the same active antennas are shown in [100, Section III]. In short, overlapping antenna indices between different groups lead to an increase of the linear dependence probability of the channel space (the channel matrix) and result in an increase of the ABER. Effectively, similar to [99], the authors aim to optimise the three dimensional SM constellation space. Whereas in classical SM the third dimension is strictly the channel signature of a single active antenna, both multiple active (MA)–SM and STBC–SM seek to create the most unique channel signatures by activating multiple transmit antennas and changing the rotation of the signal symbol constellations.

In addition, the MA–SM scheme is proposed in conjunction with a near-optimal decoder with linear complexity. In essence, it seeks to emulate successive interference cancellation (SIC) by projecting each received stream to a space orthogonal from the common channel plain. After finding a suitable projection, the decoder applies it to the received vector and performs matched filtering in the new space. Since both the projection and matched filtering are linear operations, the decoder can be viewed as a linear filter that maximises the output SNR, provided that the filter eliminates the interference coming from all other data streams. Effectively, this detection method means that the antenna index and signal detection are decoupled while still resulting in a nearly optimal performance. Furthermore, the complexity of the proposed decoder is unrelated to the size of the signal constellation which means that as higher constellation sizes are used,

the computational complexity benefits of MA–SM over STBC–SM and GSM grow.

However, in both STBC–SM and MA–SM, the number of active antennas cannot be more than the number of receiver antennas to ensure successful detection [101]. This is not the case with GSM since there is no need for separability of the spatial streams. Nonetheless, in all scenarios and transmission schemes, a trade-off must be considered between the capacity and ABER performance of the system.

Despite the multiplexing and diversity gains offered by multiple active antennas, however, the problems that plague MIMO systems such as timing synchronisation, inter–antenna interference (IAI), inter–channel interference (ICI) and multiple radio frequency (RF) chains are all associated with each technique using multiple active antennas. In addition to the power consumption, multiple RF chains also imply higher manufacturing costs. Indeed, FBE–SM could be implemented by using an electronically steerable parasitic array receptor (ESPAR). ESPAR may be used to generate unique channel signatures between the transmitter and receiver, thereby mimicking the effect of multiple transmit antennas. Parasitic antenna technology uses a single RF chain to transmit and receive data and the parasitic elements require mutual coupling to the active antenna, which makes this technology well suited for deployment on small scale devices, [102] and references therein. FBE–SM is therefore the most optimal system for using a non-power of two number of transmit antennas while maintaining a single RF chain for green communications.

3.8 Summary

In this chapter, a novel and more versatile SM scheme called FBE–SM was introduced. The method relied on the application of modulus conversion to achieve fractional bit rates over time. It allowed any SM system to use an arbitrary number of antennas at the transmitter. To this extent, guidelines were presented for the optimal selection of the FBE–SM parameters.

On the one hand, numerical results showed that classic SM performed better in terms of the ABER in uncorrelated scenarios since it avoided the error propagation problem that plagues FBE–SM. Indeed, classical SM was shown to have a better ABER and a higher spectral efficiency relative to FBE–SM in an uncorrelated Rayleigh fading environment. On the other hand, when spatial correlation was introduced, FBE–SM showed performance gains of as much as 3 dB relative to classic SM systems. To this extent, the standard Kronecker model was used to emulate the spatial correlation in a system with exponential fading of the correlation decay coefficient.

In addition, various alternative techniques to FBE–SM were discussed, including GSM, STBC–SM, and MA–SM. Each activated more than one transmit antenna to obtain a unique channel signature. Both STBC–SM and MA–SM were shown to improve the diversity of SM but required at least as many receive as there were activate transmit antennas. GSM did not have this limitation but neither did it offer an increase in the transmit diversity of the system. The activation of multiple transmit antennas, however, required the use of multiple RF chains. Taking this into consideration, FBE–SM was shown as a viable candidate for the design of compact mobile devices using SM with a single transmit RF chain. It offered an additional degree of freedom for trading–off performance, spectral efficiency, power efficiency and cost.

By employing FBE–SM, one of the fundamental challenges to the practical deployment of SM was removed while retaining the essential advantages over other MIMO systems such as no ICI, no IAI and a single RF chain. To effectively deploy any system in the real world, however, its performance in both the noise and interference limited scenarios must be analysed. The performance of SM in an interference limited scenario is discussed in Chapter 4.

Chapter 4

Interference Limited Spatial Modulation

4.1 Introduction

The aim of this chapter is to characterise the behaviour of spatial modulation (SM) in an interference limited scenario. To this extent, a maximum likelihood (ML) detector for SM is proposed and its performance in terms of the average bit error ratio (ABER) is analysed. In addition, if only the spatial constellation of SM is used to transmit information, SM reduces to space shift keying (SSK) [63]. Therefore, all presented work can be extended to SSK without loss of generality.

Most contributions thus far have addressed aspects of SM in point-to-point communication systems, *i.e.*, the single-user noise limited scenario. These include the application of SM in traditional, multiple access systems such as frequency division multiple access (FDMA), time division multiple access (TDMA) or orthogonal frequency division multiple access (OFDMA) where multi-user interference is managed by ensuring orthogonal transmissions by all users in the system. Notable exceptions are given in [103] and [104], where the authors focus their analysis on the performance of SSK in an interference limited scenario. However, the signal symbol sent in SM distinguishes SM from SSK. To this extent, the influence of the signal symbol must be considered to characterise the performance of the SM system in the interference limited scenario.

In addition, the ABER of SM should be compared to the *complexity and cost equivalent* multi-user multiple–input multiple–output (MIMO) system to assess the suitability of SM for practical deployment. Since only one antenna is active at any transmission instance, SM requires only a single radio frequency (RF) chain at the transmitter. To this extent, a single RF chain at the transmitter means that multi-user SM is not comparable in terms of energy efficiency or cost to the more complicated spatial-multiplexing multi-user systems analysed in [105–108].

The aggregate power usage in a system employing SM is significantly lower than a system employing classical MIMO due to the fewer RF chains. In addition to higher power consumption, multiple RF chains imply higher manufacturing costs and inter-antenna synchronisation problems. To this extent, SM is a more optimal system for taking advantage of multiple transmit antennas while still maintaining a single RF chain. Furthermore, the lower detection complexity for SM reduces mobile station power usage, enabling a longer battery life for the mobile terminal [16].

In this chapter, the performance of a single-user detector as applied in an interference limited scenario is first characterised, *i.e.*, a ML interference-unaware optimal receiver is analysed. A ML detector which can successfully decode incoming data in the multi-user scenario and is not interference limited is then proposed, *i.e.*, an interference-aware detector which can successfully decode data from several users/nodes. To this extent, an analytical framework to support simulation results is developed for each detector which is applicable to any channel environment. In addition, closed form solutions are provided to compute the upper bound for the ABER over identical and independently distributed (i.i.d.) Rayleigh fading channels.

The remainder of this chapter is organised as follows. The system model is introduced in Section 4.2. The performance of SM in the interference limited scenario is characterised and the analytical modelling for the multi-user detectors is proposed in Section 4.3. Numerical results, which substantiate the accuracy of the developed analytical framework, are presented in Section 4.4. Lastly, the chapter is summarised in Section 4.5 .

4.2 System Model

Multiple nodes/users, as shown in Fig. 4.1, are assumed in this chapter. A total of N_u transmit nodes, denoted as $\{1, \ldots, \xi, \ldots, N_u\}$, broadcast simultaneously on the same time-frequency slot to a single receiver. Each node broadcasts a signal constellation symbol, $x^{(u)}$, from one of its available antennas.

The received signal at antenna r is given by

$$y_r = \sum_{u=1}^{N_u} \left[\sqrt{E_m \alpha_{(u)}^2}\, h_{(n_t^{(u)},r)} x^{(u)} \right] + \eta_r, \tag{4.1}$$

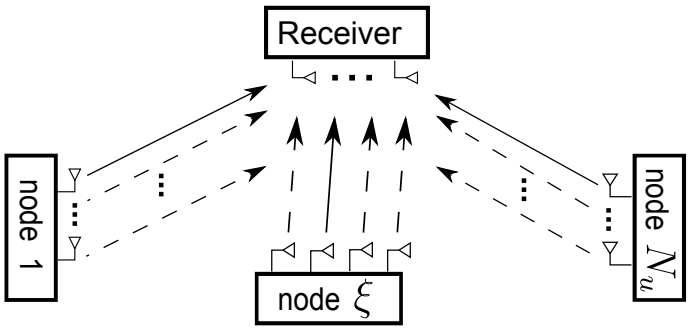

Figure 4.1: *Multi-user SM system setup. Nodes* $1, \ldots, \xi, \ldots, N_u$ *send information simultaneously to the receiver on the same time-frequency resource block. Each solid line represents the active transmit antenna from each node to every receiving antenna. Each dashed line represents the inactive channel from every transmit antenna at a particular node to a receiving antenna.*

where:

- E_m is the average transmit energy per symbol,
- $n_t^{(u)}$ is the index of the active transmit antenna from a total of $N_t^{(u)}$ available on node u,
- r is the index of the receive antenna from a total of N_r available on the receiving node,
- $\alpha_{(u)}^2$ is the power of the channel attenuation coefficients between all receive antennas and all transmit antennas on the link between node u and the receiver,
- $h_{(n_t^{(u)},r)}$ is the fast fading channel coefficient between the active transmit antenna n_t on node u and the receiving antenna r,
- $x^{(u)}$ is the signal constellation symbol transmitted from the set of all possible signal constellation points, $\mathcal{X}^{(u)}$, for node u, and
- η_r, is additive white Gaussian noise (AWGN), defined as a complex normal random variable with zero mean and variance N_o, *i.e.*, $\eta_r \sim \mathcal{CN}(0, N_o)$.

Throughout the thesis, the average power in the signal constellation is normalised to one, *i.e.*, $\mathrm{E}_{\mathcal{X}}\left[|x|^2\right] = 1$. To avoid repetitive definitions, symbols denoted with $\hat{\cdot}$ are simply an element of the same set as the symbol without $\hat{\cdot}$, *i.e.*, $\hat{x}$ comes from the same set as x. If the signal constellation is replaced by a single tone and N_t is chosen such that $\log_2(N_t)$ equals the spectral efficiency, then all presented work can be directly applied to any system employing SSK by replacing $x^{(u)} = 1$.

4.3 Analytical Modelling and Receiver Design

In this section, the ML detectors used in the interference limited scenario are analysed. The detectors computes the Euclidean distance between the received vector signal, $\mathbf{y}$, and the set of all possible received signals, selecting the closest one.

4.3.1 Interference-Unaware Detection

Starting from the system model presented in Section 4.2, the decoded pair $(x_{\text{est}}, n_t)^{(\xi)}$, formed by the estimated symbol x_{est}, emitted from antenna n_t, on node ξ, is given by

$$(x_{\text{est}}, n_t)^{(\xi)} = \underset{x^{(\xi)}, \mathbf{h}_{n_t^{(\xi)}}}{\arg\min} \left\{ \left|\left| \mathbf{y} - \sqrt{E_m \alpha^2_{(\xi)}}\, x^{(\xi)} \mathbf{h}_{n_t^{(\xi)}} \right|\right|^2 \right\}, \tag{4.2}$$

$$x_{\text{est}}^{(\xi)} \in \mathcal{X}^{(\xi)}, \qquad n_t^{(\xi)} \in \{1, \ldots, N_t^{(\xi)}\}, \qquad \mathbf{h}_{n_t^{(\xi)}} = \left[h_{(n_t^{(\xi)},1)}, \ldots, h_{(n_t^{(\xi)},N_r)} \right]^T,$$

where $N_t^{(\xi)}$ is the number of available transmit antennas at node ξ, $||\cdot||_{\text{F}}$ is the Frobenius norm and $\mathcal{X}^{(\xi)}$ has a total of $M^{(\xi)}$ constellation points. Note that u represents the index of a general node in the system, and ξ is the index of the desired node whose data stream is being decoded.

The union bound approach can be used to describe the behaviour of the interference-unaware SM detector in the high signal-to-noise-ratio (SNR) regions. In particular, the behaviour of the interference-unaware detector can be characterised by defining

$$\begin{aligned} \mathbf{A} &= \sqrt{E_m \alpha^2_{(\xi)}}\, \mathbf{h}_{n_t^{(\xi)}} x^{(\xi)}, \\ \mathbf{B} &= \sum_{\substack{u=1 \\ u \neq \xi}}^{N_u} \sqrt{E_m \alpha^2_{(u)}}\, \mathbf{h}_{n_t^{(u)}} x^{(u)}, \end{aligned} \tag{4.3}$$

such that

$$\begin{aligned} A_r &= \sqrt{E_m \alpha^2_{(\xi)}}\, h_{(n_t^{(\xi)},r)} x^{(\xi)}, \quad \text{and} \\ B_r &= \sum_{\substack{u=1 \\ u \neq \xi}}^{N_u} \sqrt{E_m \alpha^2_{(u)}}\, h_{(n_t^{(u)},r)} x^{(u)}, \end{aligned}$$

define the symbols at the receive antenna r. In this notation $\mathbf{y} = \mathbf{A} + \mathbf{B} + \boldsymbol{\eta}$, where $\mathbf{A}$ is the desired signal, $\mathbf{B}$ is the interference signal and $\boldsymbol{\eta}$ is the AWGN. The pairwise error probability

(PEP) can now be derived as

$$\begin{aligned}
&\Pr\{\mathbf{A} \neq \hat{\mathbf{A}}|\mathbf{B}\} = \Pr\left\{ ||\mathbf{y}-\mathbf{A}||^2 > \left|\left|\mathbf{y}-\hat{\mathbf{A}}\right|\right|^2 \middle| \mathbf{B} \right\} \\
&= \Pr\left\{ \sum_{r=1}^{N_r} \left[|y_r - A_r|^2 \right] > \sum_{r=1}^{N_r} \left[\left| y_r - \hat{A}_r \right|^2 \right] \middle| \mathbf{B} \right\} \\
&= \Pr\left\{ \sum_{r=1}^{N_r} \left[2\Re\left\{ \left(\hat{A}_r - A_r\right)(B_r+\eta_r)^* \right\} \right] > \sum_{r=1}^{N_r} \left[\left| A_r - \hat{A}_r \right|^2 \right] \right\}, \\
&\Rightarrow \eta_r^{\text{new}} \sim \mathcal{N}\left(\sum_{r=1}^{N_r} \left[2\Re\left\{ (\hat{A}_r - A_r) B_r^* \right\} \right], \sum_{r=1}^{N_r} \left[2N_o |\hat{A}_r - A_r|^2 \right] \right),
\end{aligned} \tag{4.4}$$

where $(\cdot)^*$ represents the complex conjugate, $\Re\{\cdot\}$ represents the real part of a complex number, η_r^{new} is the distribution of the PEP defined by $\mathcal{N}(\mu, \sigma^2)$ which is the normal distribution with mean μ and variance σ^2. Knowing that η_r^{new} is the only remaining random variable with a normal distribution, means that the PEP in (4.4) is defined by the Q-function. Considering η_r^{new} and (4.4), the PEP can be defined as

$$\Pr\{\mathbf{A} \neq \hat{\mathbf{A}}|\mathbf{B}\} = Q\left(\frac{\sum_{r=1}^{N_r} \left[\left| A_r - \hat{A}_r \right|^2 - 2\Re\left\{ \left(\hat{A}_r - A_r\right) B_r^* \right\} \right]}{\sqrt{\sum_{r=1}^{N_r} \left[2N_o \left| A_r - \hat{A}_r \right|^2 \right]}} \right), \tag{4.5}$$

where $Q(\omega) = \frac{1}{\sqrt{2\pi}} \int_{\omega}^{\infty} \exp\left(-\frac{t^2}{2}\right) \mathrm{dt}$ defines the Q-function. It should be noted that this PEP is valid for all channel fading statistics. To simplify it further, the fast fading channel statistics of each element of $\mathbf{B}$ can be assumed to follow a Rayleigh distribution, *i.e.*, $h_{(n_t^{(u)},r)} \sim \mathcal{CN}(0,1)$. To simplify the notation in the derivation,

$$\Omega_P = \left|\left|\mathbf{A} - \hat{\mathbf{A}}\right|\right|_{\mathrm{F}}^2, \qquad \Omega_I = 2\Re\left\{ (\hat{\mathbf{A}} - \mathbf{A})\mathbf{B}^* \right\}, \qquad \Omega_N = \sqrt{2N_o\Omega_P}, \tag{4.6}$$

where

$$\Omega_I \sim \mathcal{N}\left(0, 2E_m |x_{\mathbf{B}}|^2 \Omega_P\right), \tag{4.7}$$

such that $|x_{\mathbf{B}}|^2 = \sum_{u \neq \xi = 1}^{N_u} \alpha_{(u)}^2 |x^{(u)}|^2$ and $\sigma_I^2 = 2E_m|x_{\mathbf{B}}|^2\Omega_P$. In particular, Ω_I is the distribution of the interfering signal with zero mean and variance σ_I^2, Ω_P is the Euclidean distance of the two hypothesis vectors and Ω_N is the noise. The channel effects of $\mathbf{B}$ can be removed by taking the expectation of (4.5) across the fading channel $\mathcal{H}_B$, such that

$$\begin{aligned} \Pr\{\mathbf{A} \neq \hat{\mathbf{A}}\} &= \mathrm{E}_{\mathcal{H}_\mathbf{B}}\left[\Pr\{\mathbf{A} \neq \hat{\mathbf{A}}|\mathbf{h_B}\}\right], \\ \Pr\{\mathbf{A} \neq \hat{\mathbf{A}}\} &\approx \mathrm{E}_{\mathcal{H}_\mathbf{B}}\left[Q\left(\tfrac{\Omega_P - \Omega_I}{\Omega_N}\right)\right], \\ &\approx \mathrm{E}_{\mathcal{H}_\mathbf{B}}\left[Q\left(\tfrac{\Omega_P}{\Omega_N} - \tfrac{\sigma_I}{\Omega_N}\hat{\Omega}_I\right)\right], \end{aligned} \tag{4.8}$$

where $\hat{\Omega}_I \sim \mathcal{N}(0,1)$ and $\mathrm{E}_{\mathcal{H}_B}[\cdot]$ represents the expectation of the system with respect to the fast fading channel $\mathcal{H}_B$. From here, appling [109, eq. 3.66] results in

$$\Pr\{\mathbf{A} \neq \hat{\mathbf{A}}\} = Q\left(\frac{\Omega_P}{\sqrt{\Omega_N^2 + \sigma_I^2}}\right). \tag{4.9}$$

After replacing Ω_P, Ω_N, and σ_I ,

$$\Pr\{\mathbf{A} \neq \hat{\mathbf{A}}\} \approx Q\left(\sqrt{\gamma_\mathbf{I}\left|\left|\mathbf{h}_{n_t^{(\xi)}}x^{(\xi)} - \mathbf{h}_{\hat{n}_t^{(\xi)}}\hat{x}^{(\xi)}\right|\right|_\mathrm{F}^2}\right), \tag{4.10}$$

where

$$\gamma_\mathbf{I} = \frac{1}{2}\frac{E_m\alpha_{(\xi)}^2}{N_o + E_m\sum\limits_{u\neq\xi=1}^{N_u}\alpha_{(u)}^2\left|x^{(u)}\right|^2}, \tag{4.11}$$

represents half of the signal-to-interference-plus-noise-ratio (SINR) between node ξ and the receiver. Throughout the work, averaging is performed only across the fast fading channel statistics. As (4.11) shows, $\gamma_\mathbf{I}$ is still dependent on the magnitude of the modulated signal symbols of the interfering nodes, $|x^{(u)}|$. This means that all expressions using $\gamma_\mathbf{I}$ maintain their dependence on the signal symbols of the interfering nodes.

Given this formulation, the ABER of the single-user detector using the union bound approach in the presence of interference, can be defined as

$$\mathrm{ABER}_\xi^{(\textbf{inter})} \leq \sum_{\substack{x^{(\xi)},\, n_t^{(\xi)},\\ \hat{x}^{(\xi)},\, \hat{n}_t^{(\xi)}}}^{M^{(\xi)}N_t^{(\xi)}} \underbrace{\sum\sum\cdots\sum}_{(N_u-1)\text{ summations}} \frac{d_\xi(x, n_t, \hat{x}, \hat{n}_t)}{\log_2\left(M^{(\xi)}N_t^{(\xi)}\right)} \frac{\mathrm{E}_{\mathcal{H}_A}\left[\Pr\{\mathbf{A} \neq \hat{\mathbf{A}}\}\right]}{M^{(\xi)}N_t^{(\xi)}} \left[\prod_{u\neq\xi=1}^{N_u}\frac{1}{M^{(u)}}\right], \tag{4.12}$$

where the u^{th} summation from the $(N_u - 1)$ summations above is defined for all $x^{(u)} \in \mathcal{X}^{(u)}$

and $u \neq \xi$ with $M^{(\xi)}$ being the cardinality of $\mathcal{X}^{(\xi)}$. The symbol $\sum_{\substack{x^{(\xi)}, n_t^{(\xi)}, \\ \hat{x}^{(\xi)}, \hat{n}_t^{(\xi)}}}^{M^{(\xi)} N_t^{(\xi)}}$ is defined as a four fold summation, two for all $x^{(\xi)}$, $\hat{x}^{(\xi)} \in \mathcal{X}^{(\xi)}$ and two for the indices $n_t^{(\xi)}$, $\hat{n}_t^{(\xi)} \in \left\{1, \ldots, N_t^{(\xi)}\right\}$. Additionally, $d_\xi(x, n_t, \hat{x}, \hat{n}_t) = d_\xi(n_t - 1, \hat{n}_t - 1) + d_\xi(x, \hat{x})$, where $d_\xi(\cdot, \hat{\cdot})$ denotes the Hamming distance between the binary representations any two symbols coming from the same set for node ξ.

As with the interfering nodes, the fast fading of the desired node is assumed to follow a Rayleigh distribution. To obtain the average PEP, $z_r = h_{(n_t^{(\xi)}, r)} x^{(\xi)} - h_{(\hat{n}_t^{(\xi)}, r)} \hat{x}^{(\xi)}$ is defined with a variance of

$$\sigma_z^2 = \begin{cases} \left(|x^{(\xi)}|^2 + |\hat{x}^{(\xi)}|^2\right) & n_t^{(\xi)} \neq \hat{n}_t^{(\xi)}, \\ \left(|x^{(\xi)} - \hat{x}^{(\xi)}|^2\right) & n_t^{(\xi)} = \hat{n}_t^{(\xi)}, \\ 0 & n_t^{(\xi)} = \hat{n}_t^{(\xi)} \text{ and } x^{(\xi)} = \hat{x}^{(\xi)}, \end{cases} \tag{4.13}$$

where σ_z^2 is the variance of a SM hypothesis test per receive antenna, z_r, using a variable amplitude modulation scheme. In particular, it is the variance per receive antenna of the argument inside the Q-function in (4.10). Furthermore, the random variable

$$\kappa = \frac{||\mathbf{z}||_{\mathrm{F}}^2}{\gamma_{\mathbf{I}} \sigma_z^2 / 2} = \sum_{r=1}^{N_r} \left| \frac{z_r}{\gamma_{\mathbf{I}} \sigma_z / \sqrt{2}} \right|^2, \tag{4.14}$$

is defined, which has a central Chi-squared distribution with $2N_r$ degrees of freedom given as

$$\tilde{\rho}_K(\kappa) = \frac{1}{2^{N_r}(N_r - 1)!} \kappa^{N_r - 1} e^{-\kappa/2} \tag{4.15}$$

where $(\cdot)!$ represents the factorial function. Finally,

$$\mathrm{E}_{\mathcal{H}_A}\left[\Pr\{\mathbf{A} \neq \hat{\mathbf{A}}\}\right] = \frac{(1/2)^{N_r}}{(N_r - 1)!} \int_0^\infty e^{-\kappa/2} \kappa^{N_r - 1} Q\left(\sqrt{\frac{\gamma_{\mathbf{I}} \sigma_z^2}{2}} \kappa\right) \mathrm{d}\kappa, \tag{4.16}$$

can be posed. By direct inspection, the solution to [110, eq. 62] can be applied to obtain

$$\mathrm{E}_{\mathcal{H}_A}\left[\Pr\{\mathbf{A} \neq \hat{\mathbf{A}}\}\right] = f(\beta)^{N_r} \sum_{r=0}^{N_r - 1} \binom{N_r - 1 + r}{r} (1 - f(\beta))^r, \tag{4.17}$$

where

$$f(\beta) = \frac{1}{2}\left(1 - \sqrt{\frac{\beta}{1+\beta}}\right), \tag{4.18}$$

and

$$\beta = \frac{\gamma_{\mathbf{I}}\sigma_z^2}{2}. \tag{4.19}$$

The analytical upper bound for a SM system employing quadrature amplitude modulation (QAM) in an arbitrary channel environment and an interference limited scenario is given by (4.12). Although, the average power of any signal symbol constellation in (4.12) is one, a variable amplitude modulation scheme means that the instantaneous SINR changes. In particular, the instantaneous SINR must be strictly defined to study the asymptotic behaviour of the system. This is necessary because the instantaneous SINR is an argument of the PEP which is defined using the Q-function. To obtain the ABER, however, the PEP must be averaged across all channel realisations and all signal symbol constellations. Therefore, a closed-form expression for the asymptotic behaviour of (4.12) and (4.13) is difficult to obtain. If a constant-amplitude modulation such as phase shift keying (PSK) is used, then for a fixed channel realisation

$$z_r^{\text{PSK}} = |a|e^{j\arg(a)}|b|e^{j\arg(b)} - |\hat{a}|\, e^{j\arg(\hat{a})}|\hat{b}|e^{j\arg(\hat{b})}, \tag{4.20}$$

can be posed, where $a = h_{(n_t^{(\xi)},r)}$, $b = x^{(\xi)}$ are used to shorten the notation and $\arg(\cdot)$ represents the phase of a complex symbol. Since the amplitude of all signal constellation points is unity,

$$z_r^{\text{PSK}} = |a|e^{j(\arg(a)+\arg(b))} - |\hat{a}|e^{j\left(\arg(\hat{a})+\arg(\hat{b})\right)}. \tag{4.21}$$

From the definition of z_r^{PSK}, it is clear that its variance is defined as

$$\sigma^2_{z^{\text{PSK}}} = \begin{cases} 2 & \text{if } n_t^{(\xi)} \neq \hat{n}_t^{(\xi)} \text{ or } \arg\left(x^{(\xi)}\right) \neq \arg\left(\hat{x}^{(\xi)}\right), \\ 0 & \text{if } n_t^{(\xi)} = \hat{n}_t^{(\xi)} \text{ and } \arg\left(x^{(\xi)}\right) = \arg\left(\hat{x}^{(\xi)}\right). \end{cases} \tag{4.22}$$

In this case, (4.12) reduces to

$$\text{ABER}_{\xi}^{\text{(PSK-inter)}} \leq \sum_{n_t=1}^{N_t^{(\xi)}} \sum_{\hat{n}_t=1}^{N_t^{(\xi)}} \frac{d_{\xi}(x, n_t, \hat{x}, \hat{n}_t)}{\log_2\left(M^{(\xi)}N_t^{(\xi)}\right)} \frac{\text{E}_{\mathcal{H}_A}^{\text{PSK}}\left[\Pr\{\mathbf{A} \neq \hat{\mathbf{A}}\}\right]}{M^{(\xi)}N_t^{(\xi)}}, \tag{4.23}$$

where

$$\mathrm{E}_{\mathcal{H}_A}^{\text{PSK}}\left[\Pr\{\mathbf{A}\neq\hat{\mathbf{A}}\}\right]=f\left(\beta^{\text{PSK}}\right)^{N_r}\sum_{r=0}^{N_r-1}\binom{N_r-1+r}{r}\left(1-f\left(\beta^{\text{PSK}}\right)\right)^{r},\tag{4.24}$$

such that

$$\beta^{\text{PSK}}=\gamma_{\mathbf{I}}^{\text{PSK}}=\frac{1}{2}\frac{E_m\alpha_{(\xi)}^2}{N_o+2E_m\sum\limits_{u\neq\xi=1}^{N_u}\alpha_{(u)}^2}.\tag{4.25}$$

It should be noted that (4.22) and (4.23) are special cases of (4.12) and (4.13) which enable a simpler theoretical analysis of the asymptotic behaviour of the system in the interference limited scenario as the SINR grows to infinity. In particular, simulation results in Section 4.4 show that the asymptotic bounds derived for SM using a constant amplitude modulation scheme in the interference limited scenario are also valid for SM using 4-QAM in the same environment. To this extent, the asymptotic behaviour of the system using the interference-unaware detector is now analysed in both the noise and interference limited scenarios.

4.3.2 Asymptotic Analysis of the Interference-Unaware Detector

In this section, some asymptotic cases are investigated to highlight trends in the ABER of SM at high SINR. Simulations in Section 4.4 show that the presented results are asymptotically tight in the high SINR region. $\text{SNR}_\xi=E_m\alpha_{(\xi)}^2/N_o$ and $\text{SIR}_\xi=\frac{\alpha_{(\xi)}^2}{\sum_{u\neq\xi=1}^{N_u}\alpha_{(u)}^2|x^{(u)}|^2}$ are defined for use in the noise and interference limited scenarios, respectively. When considering these definitions, the asymptotic performance of SM and SIMO in the noise limited scenario and the asymptotic performance of SM in the interference limited scenario are analysed.

1) $\text{SNR}_\xi\gg 1$ and $\text{SINR}\approx\text{SNR}$ (noise limited scenario)
This is the classic single user scenario where co-channel interference can be neglected, and high-SNR analysis for the probe link can be performed. The expression in (4.12) is considered such that $\gamma_{\mathbf{I}}\approx\gamma=E_m\alpha_{(\xi)}^2/N_o$ in the limit. Since interference can be neglected,

$$\lim_{\gamma\to\infty}\text{ABER}_{\xi}^{(\textbf{inter})}=\lim_{\gamma\to\infty}\sum_{\substack{x^{(\xi)},n_t^{(\xi)},\\ \hat{x}^{(\xi)},\hat{n}_t^{(\xi)}}}^{M^{(\xi)}N_t^{(\xi)}}\frac{d_\xi(x,n_t,\hat{x},\hat{n}_t)}{\log_2\left(M^{(\xi)}N_t^{(\xi)}\right)}\frac{\mathrm{E}_{\mathcal{H}_A}\left[\Pr\{\mathbf{A}\neq\hat{\mathbf{A}}\}\right]}{M^{(\xi)}N_t^{(\xi)}}.\tag{4.26}$$

To simplify (4.26), the limit in (4.17) and (4.24), can be tackled by considering a Taylor expan-

sion with two terms of (4.18) such that

$$\begin{aligned} f(\beta) &= \frac{1}{2}\left(1 - \sqrt{\frac{\beta}{1+\beta}}\right) \Rightarrow \text{Taylor expansion} \\ f(\beta) &\approx \frac{1}{2}\left(\frac{1}{2(\beta+1)}\right) = 2^{-2}(\beta+1)^{-1}. \end{aligned} \tag{4.27}$$

The average symbol error ratio (ASER) for SM is defined similar to the ABER and can be posed as

$$\text{ASER}_{\xi}^{(\textbf{inter})} \leq \sum_{\substack{x^{(\xi)}, n_t^{(\xi)}, \\ \hat{x}^{(\xi)}, \hat{n}_t^{(\xi)}}}^{M^{(\xi)} N_t^{(\xi)}} \frac{\text{E}_{\mathcal{H}_A}\left[\Pr\{\mathbf{A} \neq \hat{\mathbf{A}}\}\right]}{M^{(\xi)} N_t^{(\xi)}}. \tag{4.28}$$

Indeed, the ABER can be upper bounded as one half of the ASER. The random SM constellation diagram at the receiver, along with the joint detection of the signal and spatial constellation points, mean that any benefits from advanced bit-to-symbol mappings such as Gray coding can be neglected. Nonetheless, the detector will create a long binary sequence which has at most 50% bit-errors within the erroneous symbol sequence, *i.e.*, the ABER is bounded to be at most $1/2$ of the ASER. The tightness of this bound can be seen in Section 4.4. This step eliminates the dependence on the Hamming distance between the various SM symbols, which means

$$\lim_{\gamma\to\infty} \frac{\text{ABER}_{\xi}^{(\textbf{inter})}}{\gamma^{-N_r}} = \lim_{\gamma\to\infty} \binom{2N_r - 1}{N_r} 2^{-2N_r} \frac{M^{(\xi)} N_t^{(\xi)}}{2} \text{E}_{x, n_t, \hat{x}, \hat{n}_t}\left[\left(\frac{\sigma_z^2}{2}\right)^{-N_r}\right], \tag{4.29}$$

can be posed, where

$$\text{E}_{x, n_t, \hat{x}, \hat{n}_t}\left[\left(\frac{\sigma_z^2}{2}\right)^{-N_r}\right], \tag{4.30}$$

is the expectation of $\left(\frac{\sigma_z^2}{2}\right)^{-N_r}$ across the various possibilities of σ_z^2 for $x, n_t, \hat{x}$ and $\hat{n}_t$. However, the authors are not aware of a closed form solution to the generic expression for (4.30) given a variable-amplitude modulation. To this extent, (4.30) can be upper bounded by setting $\sigma_z^2 = \min\left(\sigma_z^2, 2\right)$. In particular, the general form of σ_z^2 is defined by the underlying SM signal-symbol constellation size, $M^{(\xi)}$ and expressions for σ_z^2 are defined using the upper bound for square QAM constellation sizes. A summary of the derivation of (4.32) is provided in Ap-

pendix A.1. Nonetheless, when $M^{(\xi)} = 4$, then

$$\Psi = \mathrm{E}_{n_t,x,\hat{n}_t,\hat{x}}\left[\left(\frac{\sigma_z^2}{2}\right)^{-N_r}\right] \leq \frac{4N_t^{(\xi)} + \left(2^{-N_r} - 2\right)}{4N_t^{(\xi)}}. \tag{4.31}$$

When $M^{(\xi)} = 16$, then

$$\Psi = \mathrm{E}_{n_t,x,\hat{n}_t,\hat{x}}\left[\left(\frac{\sigma_z^2}{2}\right)^{-N_r}\right] \leq \frac{\psi_1 + \psi_2}{\left(16N_t^{(\xi)}\right)^2}, \tag{4.32}$$

where

$$\begin{aligned}\psi_1 &= \left(16(0.2)^{-N_r} + 32(0.6)^{-N_r} + 208\right)\left(N_t^{(\xi)}\right)^2, \\ \psi_2 &= \left(32(0.2)^{-N_r} + 36(0.4)^{-N_r} - 32(0.6)^{-N_r} + 32(0.8)^{-N_r} - 84\right)N_t^{(\xi)}.\end{aligned} \tag{4.33}$$

With this in mind, the closed form of the limit is defined as

$$\lim_{\gamma\to\infty}\frac{\mathrm{ABER}_{\xi}^{(\textbf{inter})}}{\gamma^{-N_r}} = M^{(\xi)}N_t^{(\xi)}\binom{2N_r-1}{N_r}2^{-(2N_r+1)}\Psi. \tag{4.34}$$

At this point, the work can be simplified by considering a constant-amplitude modulation scheme for the node of interest, such as PSK where $\sigma^2_{z^{\mathrm{PSK}}}$ is either 2 or 0 as shown in (4.22). The expression in (4.30) is then unity which simplifies further analysis. In such a scenario, the authors in [18] demonstrate that there is a crossing point where the ABER of SM using PSK improves over SM using QAM. Nonetheless, there are two conclusions that can be drawn from (4.34): i) the system error increases with the product of the spatial constellation size, $N_t^{(\xi)}$, and symbol constellation size, $M^{(\xi)}$, ii) the system error decreases exponentially with the addition of each received antenna, *i.e.*, the diversity order is equal to N_r. Additionally, the coding gain with respect to the number of receive antennas is quantified as $\binom{2N_r-1}{N_r}2^{-(2N_r+1)}$. This is apparent when considering

$$\binom{2N_r-1}{N_r} < \binom{2N_r}{N_r} \ll \sum_{r=0}^{2N_r}\binom{2N_r}{r} = 2^{2N_r} < 2^{2N_r+1}. \tag{4.35}$$

In general, it can be shown that as $N_r \to \infty$, the inverse of (4.35) tends to zero and is always less than one. Since the inverse of (4.35) is always less than one, the addition of an extra receive antenna implies a smaller ratio, which means a lower ABER and hence coding gains for the system.

2) SIMO system using QAM (noise-limited scenario):

To quantify the SNR difference between SM and SIMO using QAM, the ABER performance of a SIMO system using QAM must be analysed in at the asymptote. In particular, a closed form solution for the ASER of a SIMO system using QAM with i.i.d. inputs is provided in [111, eq. 9.23], *i.e.*, no correlation is assumed in the system . To begin the asymptotic analysis, [111, eq. 9.23] is tightly upper bounded by

$$\mathrm{ASER}_{\mathrm{QAM}} \leq 4\left(1-\frac{1}{\sqrt{\widetilde{M}}}\right) f(\gamma_{\mathrm{QAM}})^{N_r} \sum_{r=0}^{N_r-1} \binom{N_r-1+r}{r} \left(1-f(\gamma_{\mathrm{QAM}})\right)^r, \quad (4.36)$$

where $\gamma_{\mathrm{QAM}} = \frac{3}{2(\widetilde{M}-1)}\gamma$. The interested reader is invited to look at work in [111] for more details in obtaining (4.36). If Gray mapping is used, then $\mathrm{ASER}_{\mathrm{QAM}}/\log_2(\widetilde{M}) \approx \mathrm{ABER}_{\mathrm{QAM}}$ can be posed, where $\widetilde{M} = M^{(\xi)}N_t^{(\xi)}$ [111, eq. 8.7].

If (4.36) is evaluated in the limit as γ tends to infinity by using (4.27), then it reduces to

$$\lim_{\gamma\to\infty} \frac{\mathrm{ABER}_{\mathrm{QAM}}}{\gamma^{-(N_r)}} \leq \frac{4}{\log_2(\widetilde{M})}\left(1-\frac{1}{\sqrt{\widetilde{M}}}\right)\left(\frac{3}{2(\widetilde{M}-1)}\right)^{-N_r}\binom{2N_r-1}{N_r}2^{-(2N_r)}. \quad (4.37)$$

After some analytical manipulations shown in Appendix A.2, the ratio of (4.34) with (4.31) to (4.37) can be posed as

$$\lim_{\gamma\to\infty} \frac{\mathrm{ABER}_{\xi}^{(\mathbf{inter})}/\gamma^{-N_r}}{\mathrm{ABER}_{\mathrm{QAM}}/\gamma^{-N_r}} = \frac{\left(2N_t^{(\xi)}+2^{-N_r-1}-1\right)}{\left(\frac{2\left(4N_t^{(\xi)}-1\right)}{3}\right)^{N_r}\frac{4}{\log_2\left(4N_t^{(\xi)}\right)}\left(1-\frac{1}{\sqrt{4N_t^{(\xi)}}}\right)}, \quad (4.38)$$

for $M^{(\xi)} = 4$. If the right hand side of (4.38) is set to one, however, then the expression cannot be solved in closed form. Nonetheless, since N_r and $N_t^{(\xi)}$ are natural numbers, (4.38) can be evaluated numerically. On the one hand, if the result of evaluating (4.38) is greater than one, then SIMO transmission using only QAM is better than using SM. On the other hand, if the result is less than one, then transmission using SM performs better than transmission using only QAM. In particular, the results for $N_t^{(\xi)} = 2^q$ where $q \in \{1,\ldots,6\}$ and $N_r \in \{1,2,3\}$ are presented in Table 4.1. The results show that SM is always better if $N_r \geq 2$. Additionally, the ratio of the two, as shown in Table 4.1, quantifies the coding gain of SM relative to QAM for the same spectral efficiency of $\log_2\left(M^{(\xi)}N_t^{(\xi)}\right)$ at the asymptote in a noise limited scenario, given $M^{(\xi)} = 4$.

Proceeding in a similar manner as for (4.38), the general ratio of the relative coding gains achieved by SM using a variable-amplitude modulation, over a SIMO system using QAM is given as

$$\lim_{\gamma\to\infty}\frac{\mathrm{ABER}_{\xi}^{(\mathbf{inter})}/\gamma^{-(N_r)}}{\mathrm{ABER}_{\mathrm{QAM}}/\gamma^{-(N_r)}}=\frac{\widetilde{M}\Psi}{\left(\frac{2\left(\widetilde{M}-1\right)}{3}\right)^{N_r}\frac{2}{\log_2\left(\widetilde{M}\right)}\left(1-\frac{1}{\sqrt{\widetilde{M}}}\right)}, \tag{4.39}$$

where Ψ must be defined for the desired SM signal constellation size, $M^{(\xi)}$. The exact ratios, as given in Table 4.1, will vary depending on $M^{(\xi)}$. However, the trend (SM outperforming SIMO) will remain, as can be seen in Table 4.2 for $M^{(\xi)}=16$ where the values in the last two rows of the tables are smaller than one.

N_r	$N_t^{(\xi)}=2^1$	$N_t^{(\xi)}=2^2$	$N_t^{(\xi)}=2^3$	$N_t^{(\xi)}=2^4$	$N_t^{(\xi)}=2^5$	$N_t^{(\xi)}=2^6$
1	1.6	1.9	2.3	2.6	2.9	3.2
2	0.67	0.38	0.22	0.12	0.068	0.038
3	0.28	0.075	0.021	0.0057	0.0016	$4.4(10^{-4})$

Table 4.1: *Relative coding gains of SM using* 4-QAM *compared to SIMO using* $\widetilde{M}$-QAM.

N_r	$N_t^{(\xi)}=2^1$	$N_t^{(\xi)}=2^2$	$N_t^{(\xi)}=2^3$	$N_t^{(\xi)}=2^4$	$N_t^{(\xi)}=2^5$	$N_t^{(\xi)}=2^6$
1	3.8359	3.8724	4.0859	4.4031	4.7832	5.2024
2	0.2551	0.1121	0.0542	0.0278	0.0147	0.0079
3	0.0245	0.0050	0.0011	0.0003	0.0001	$2.0\left(10^{-5}\right)$

Table 4.2: *Relative coding gains of SM using* 16-QAM *compared to SIMO using* $\widetilde{M}$-QAM.

If a constant-amplitude modulation scheme such as PSK is used, then Ψ in (4.39) will be unity. Implementing this change means that a single table of values for (4.39), can be obtained and is shown in Table 4.3.

N_r	$\widetilde{M}=2^2$	$\widetilde{M}=2^3$	$\widetilde{M}=2^4$	$\widetilde{M}=2^5$	$\widetilde{M}=2^6$	$\widetilde{M}=2^7$
1	2	1.9889	2.1333	2.3511	2.6122	2.9022
2	0.5000	0.2131	0.1067	0.0569	0.0311	0.0171
3	0.1250	0.0228	0.0053	0.0014	$3.7\left(10^{-4}\right)$	$1.0\left(10^{-4}\right)$

Table 4.3: *Relative coding gains of SM using PSK compared to SIMO using* $\widetilde{M}$-QAM.

Table 4.1, 4.2 and 4.3 demonstrate that a single-input single-output (SISO) system using QAM performs better than SM using QAM or PSK, *i.e.*, the values in the first row of each table are greater than one. However, SM exhibits increasing coding gains as either N_t or N_r are

increased, for any system with $N_r \geq 2$.

3) $\text{SIR}_\xi \gg 1$ and $\text{SINR} \approx \text{SIR}_\xi$ (interference limited scenario):
In this case, the AWGN in the channel can be neglected since the SIR_ξ is the dominant term dictating the ABER performance of the system. To this extent, $\gamma_{\mathbf{I}}$ is a function of the signal symbol amplitude for all nodes as well as their respective channel attenuations and governs the SIR_ξ. Therefore, $\gamma_{\mathbf{I}}$ cannot be separated from (4.34). In particular, in the expression for $\gamma_{\mathbf{I}}$ in (4.11), $\left|x_{(u)}\right|$ may be greater than one, which could change the interference from the remaining users. Due to the complexity of the expressions, further asymptotic study of the interference limited scenario for SM is constrained to using a constant-amplitude modulation scheme such as PSK. For SM using PSK,

$$\gamma_{\mathbf{I}}^{\text{PSK}} \approx \frac{\alpha_{(\xi)}^2}{2\sum_{u\neq\xi=1}^{N_u} \alpha_{(u)}^2}, \tag{4.40}$$

in the interference limited scenario. In particular, as $\gamma_{\mathbf{I}}$ approaches infinity, the limit of the ABER tends to (4.34) with a slight, but very important distinction: the system reaches an error floor. This is expected when the receiver is interference-unaware. Indeed, there are three consequences that should be considered similar to the noise limited scenario analysed above: i) the system error performance worsens as more SM constellation points are added, as either $N_t^{(\xi)}$ or $M^{(\xi)}$ is increased, ii) the system error performance improves when more receive antennas are added at the receiver, and iii) the detector will fail to decode any data emitted from a node whose desired signal is weaker than the interfering signal. Although analytical work for SM using QAM becomes intractable, numerical results demonstrate that SM using a variable-amplitude modulation performs in a similar fashion to SM using PSK in the interference limited environment and leads to the same conclusions. In the remainder of this work, co-channel interference is completely mitigated by applying a jointly-optimal ML detector for SM in an interference limited scenario. In other words, all incoming streams can be decoded and the error in the system tends to zero as the AWGN approaches zero, despite any interference.

4.3.3 Interference-Aware Detection

Starting from the system model presented in Section 4.2, the decoded pair $(x_{\text{est}}, n_t)^{(\xi)}$, formed from the estimated symbol x_{est}, emitted from antenna n_t, on node ξ, is given by jointly detecting the entire transmitted signal from all active nodes in the system as

$$\left\{\begin{array}{c}(x_{\text{est}}, n_t)^{(1)},\\ \vdots\\ (x_{\text{est}}, n_t)^{(\xi)},\\ \vdots\\ (x_{\text{est}}, n_t)^{(N_u)},\end{array}\right\} = \underset{x^{(u)},\, \mathbf{h}_{n_t^{(u)}}}{\arg\min} \left\{ \left|\left| \mathbf{y} - \sum_{u=1}^{N_u} x^{(u)} \mathbf{h}_{n_t^{(u)}} \right|\right|^2 \right\}, \tag{4.41}$$

$$x^{(u)} \in \mathcal{X}^{(u)} \qquad \text{and} \qquad n_t^{(u)} \in \{1, \ldots, N_t^{(u)}\}.$$

Similar to the work in Section 4.3.1, the union bound approach is used to describe the behaviour of the interference-aware SM detector in the high SNR region. The main difference between the two detectors comes from the computation of the PEP between the possible received symbols. The union bound for the interference-aware SM detector, which estimates the ABER for node ξ, can be expressed as

$$\text{ABER}_\xi \leq \sum_{\substack{x^{(1)}, n_t^{(1)},\\ \hat{x}^{(1)}, \hat{n}_t^{(1)}}}^{M^{(1)} N_t^{(1)}} \cdots \sum_{\substack{x^{(N_u)}, n_t^{(N_u)},\\ \hat{x}^{(N_u)}, \hat{n}_t^{(N_u)}}}^{M^{(N_u)} N_t^{(N_u)}} \frac{d_\xi(x, n_t, \hat{x}, \hat{n}_t)}{\log_2\left(M^{(\xi)} N_t^{(\xi)}\right)} \frac{\text{E}_{\mathcal{H}^{(\Omega)}}\left[\text{PEP}\left(x^{(\Omega)},\, n_t^{(\Omega)},\, \hat{x}^{(\Omega)},\, \hat{n}_t^{(\Omega)}\right)\right]}{\prod_{u=1}^{N_u} M^{(u)} N_t^{(u)}}, \tag{4.42}$$

where $\text{E}_{\mathcal{H}^{(\Omega)}}[\cdot]$ is the expectation across the fast fading statistics of every channel is the system. To this extent, the pairs, $\left(x^{(\Omega)}, n_t^{(\Omega)}\right)$ and $\left(\hat{x}^{(\Omega)}, \hat{n}_t^{(\Omega)}\right)$, come from the set of all possible symbol-antenna pairings for all nodes, *i.e.*, they independently take values from the set of all possible spatial and signal constellation points, Ω. $\text{PEP}\left(x^{(\Omega)},\, n_t^{(\Omega)},\, \hat{x}^{(\Omega)},\, \hat{n}_t^{(\Omega)}\right)$ is the PEP between the symbols $x^{(\Omega)}$, emitted from antennas $n_t^{(\Omega)}$, being detected as symbols $\hat{x}^{(\Omega)}$, emitted by antennas $\hat{n}_t^{(\Omega)}$.

Similar to the analytical derivation of (4.4) in Section 4.3.1, the ABER for node ξ is shown in (4.42), where the PEP is given as

$$\text{PEP}\left(x^{(\Omega)},\, n_t^{(\Omega)},\, \hat{x}^{(\Omega)},\, \hat{n}_t^{(\Omega)}\right) = Q\left(\sqrt{\frac{E_m}{2N_o}\left|\left|\sum_{u=1}^{N_u}\alpha_{(u)}\left(\mathbf{h}_{n_t^{(u)}}x^{(u)} - \mathbf{h}_{\hat{n}_t^{(u)}}\hat{x}^{(u)}\right)\right|\right|^2}\right). \tag{4.43}$$

A more detailed derivation of (4.43) is given in Appendix A.3. Thus far, no assumptions have been made as to the channel distribution. However, if Rayleigh fading is assumed for all links in the system, then the closed form solution for $\text{E}_{\mathcal{H}}\left[\text{PEP}\left(\cdot\right)\right]$ in (4.42) can be derived in the same manner as shown in Section 4.3.1 with (4.16) and (4.17) such that

$$\beta = \frac{E_m}{4N_o}\sum_{u=1}^{N_u}\alpha_{(u)}^2\vartheta_{(u)} \tag{4.44}$$

and

$$\vartheta_{(u)} = \begin{cases} \left(|x^{(u)}|^2 + |\hat{x}^{(u)}|^2\right) & n_t^{(u)} \neq \hat{n}_t^{(u)}, \\ \left(|x^{(u)} - \hat{x}^{(u)}|^2\right) & n_t^{(u)} = \hat{n}_t^{(u)}, \\ 0 & n_t^{(u)} = \hat{n}_t^{(u)} \text{ and } x^{(u)} = \hat{x}^{(u)}. \end{cases} \tag{4.45}$$

Note that (4.42) presents an analytical treatment of the most general case of SM using variable amplitude modulation for the signal symbol.

By using the interference-aware detector, the system behaves similarly to the noise limited system, in that for an arbitrarily high SNR, each user can achieve an arbitrarily low ABER. However, due to the simultaneous detection process, the users with the best SNR will not be able to achieve their single-user-lower-bound (SULB) defined as the performance of the system in the noise limited scenario. The exact effect of the additional nodes/users is further discussed in Section 4.4.

4.4 Numerical Analysis

In this section the aim is to show the performance of the interference-unaware and interference-aware detectors proposed in (4.2) and (4.41). In particular, (4.41) is shown to successfully decode the incoming streams for all nodes. In addition, numerical results demonstrate that (4.12) and (4.42) provide tight upper bounds for the ABER of the detectors at high SNR in the interference limited scenario. Furthermore, the interference-aware detector for SM demonstrates better ABER performance than the interference-aware ML detector for a multi-user SIMO sys-

tem using QAM.

The proposed interference-aware detector is jointly optimal for all nodes but requires full channel state information (CSI) from all possible transmitting antennas to each receiving antenna. Additionally, finding the optimal solution is an exponentially complex problem. If each node is assumed to have the same number of transmit antennas, N_t, and uses the same signal constellation with M points, then the proposed interference-aware ML detector has $\mathcal{O}\left((MN_t)^{N_u}\right)$ computational complexity which is proven to be an NP-complete problem [112].

The $\mathcal{O}(\cdot)$ complexity can be justified by realising that the signal and spatial domain symbols combine to form a single SM symbol. To this extent, the constellation size, *i.e.*, the spectral efficiency of any SM system, depends on the multiplication of the number of available transmit antennas and the signal symbol constellation used, MN_t. This is in contrast to other MIMO systems where each spatial branch is used to increase the diversity or multiplexing gains. In such a system, if each transmit antenna is used for multiplexing gains, the system has a maximum spectral efficiency of $\log_2\left(M^{N_t}\right)$. From here, the detection complexity of a single user SM system is given by $\mathcal{O}\left(MN_t\right)$, while the detection complexity of a single user MIMO system used for multiplexing gains is given by $\mathcal{O}\left(M^{N_t}\right)$. In this case, the two systems have different spectral efficiencies.

Even if the two systems operate at the same spectral efficiency and their complexities will be of the same $\mathcal{O}(\cdot)$ order, the cost, in terms of RF chains and power consumption, would not be. The aim of this work is to characterise the behaviour of SM in the multi-user, interference limited scenario and compare it to the *complexity and cost equivalent* multi-user MIMO system. As discussed in Section 4.1 and given the complexity expressions for the single user MIMO system and the single user SM system, the only valid *complexity and cost equivalent* comparison is to analyse multi-user SM with respect to multi-user SIMO. The optimal ML detector for the interference-aware SIMO system also has $\mathcal{O}\left(\left(\widetilde{M}\right)^{N_u}\right)$ computational complexity, where $\widetilde{M} = MN_t$. This makes it comparable to the interference-aware SM detector. Despite the generality of the analytical results, however, the simulation results consider only two and three node scenarios for the sake of conciseness.

4.4.1 Simulation Setup

A frequency-flat Rayleigh fading channel with no correlation between the transmitting antennas and AWGN is assumed. In addition, perfect CSI is assumed at the receiving node, with no CSI at the transmitter. Furthermore, only one of the available transmit antennas for each node is active at any transmitting instance. In theory, each node independently decides the number of transmit antennas and the signal symbol modulation it uses. In the simulations, however, each node has the same number of transmit antennas as well as the same spectral efficiency target. To this extent, three sets of results are presented in each figure: i) the simulation results for the multi-user detector for each node, denoted by $\texttt{Sim}(\mathrm{N}_{(\xi)})$, ii) the theoretical results from (4.12) or (4.42) for the node of interest, and iii) the SULB, denoted by $\texttt{SULB}(\mathrm{N}_{(\xi)})$.

The asymptotically tight SULB is defined as the system performance in a noise limited scenario given in (4.26) which is governed purely by its SNR, defined as E_m/N_o. Furthermore, the ABER in the noise limited scenario, as defined in (4.26), and the ASER in the noise limited scenario divided by two, as defined in (4.28), are shown to overlap in Fig. 4.2-4.3(b). The dot-dashed lines denote (4.26) while (4.28) divided by two is denoted by the triangular markers. For the sake of clarity, both are denoted as $\texttt{SULB}(\mathrm{N}_{(\xi)})$ in the legend. This justifies the use of (4.28) in the asymptotic analysis in Section 4.3.2. Additionally, (4.26) is based on the union bound approach and $\texttt{SULB}(\mathrm{N}_{(\xi)})$ can be above 1, which is impossible for a real system. In this regard, the SULB is a lower bound on the analytical performance of each system only at low ABER. Furthermore, to help illustrate the difference in the behaviour of the two detectors, the channel attenuations, $\alpha^2_{(u)}$, are set in 10 dB intervals. In general, however, $\alpha^2_{(u)}$ may be any real number. Throughout the results, QAM modulation is used for the signal symbol modulation in SM with the notable exception of Fig. 4.2, where quadrature phase shift keying (QPSK) modulation is used to illustrate the accuracy of work done in Section 4.3.2.

4.4.2 Results for Interference-Unaware Detection

The asymptotic results in Section 4.3.2, in particular (4.34) using QPSK for the signal symbol modulation, are verified in Fig. 4.2. In this case, Ψ is strictly defined by (4.22). Indeed, the horizontal lines in Fig. 4.2 represent (4.34) for varying values of $\alpha^2_{(u)}$ using QPSK modulation. In addition, the accuracy of the analytical work is shown in Fig. 4.3(a)-4.4 where QAM is used for the signal-symbol modulation. In fact, by moving from Fig. 4.2 to Fig. 4.3(a), where an additional receive antenna is added, the analytical model presented in (4.12) proves a tight

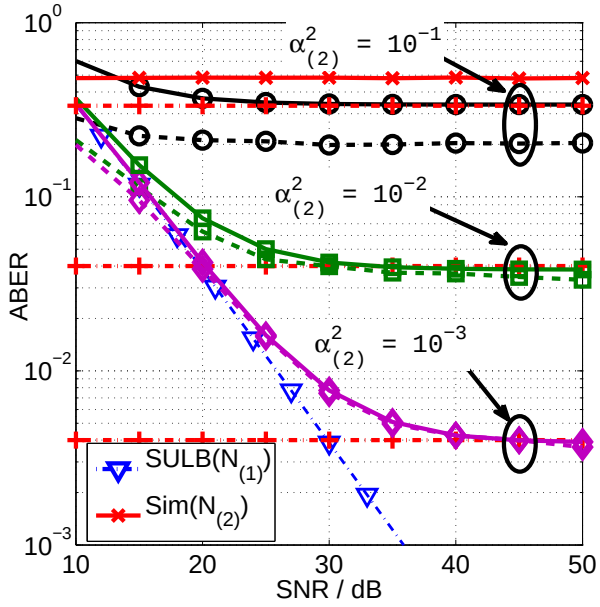

Figure 4.2: $N_t = 4$, $N_r = 1$ *and a spectral efficiency of* $4\,\mathrm{bits/s/Hz}$. *ABER for node* 1 *using the interference-unaware detector with* $\alpha^2_{(1)} = 1$ *and a varying* $\alpha^2_{(2)}$. *Dashed lines denote simulation results for node* 1, *while solid lines denote the analytical upper bound. Since the analytical bound is asymptotically tight at low ABER, the dashed and solid lines overlap. Each constant value dashed-dot line with '+' markers corresponds to the asymptote derived in* (4.34) *using* (4.40) *for node* 1 *and the indicated values for* $\alpha^2_{(2)}$.

upper bound on the system in the high SINR region. Furthermore, as the channel attenuations for the interfering nodes increase, the detector approaches the SULB. Similar to the effects observed in Fig. 4.2 and Fig. 4.3(a), Fig. 4.3(b) shows how the tightness of the bound improves as the number of receive antennas increases. To this extent, the presented results show that (4.34) tightens as the system approaches its ideal transmission and the mass of the complex Gaussian distributions around each SM constellation point concentrates around the mean. This is achieved by decreasing the interference in the system or by increasing the number of receive antennas. Nonetheless, in all instances where the interference-unaware detector is used, the node with the strongest SINR dominates the detection. In particular, the bit streams of all other nodes are not decoded since all other nodes remain below the effective noise floor at the receiver. This is apparent by looking at the simulation results for $N_{(2)}$ and $N_{(3)}$ in Fig. 4.2 through Fig. 4.3(b).

Fig. 4.3(b) shows that the increase in diversity resulting from the addition of only a single receive antenna significantly influences the system performance. Indeed, the addition of a receive

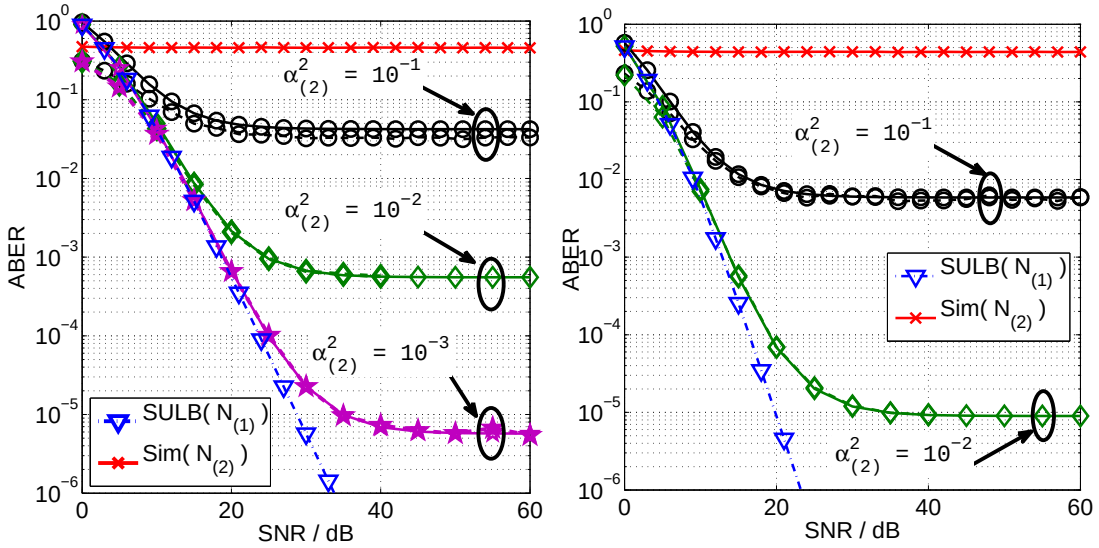

(a) $N_r = 2$ (b) $N_r = 3$

Figure 4.3: *ABER for node* 1*, using the interference-unaware detector with* $\alpha^2_{(1)} = 1$ *and a varying* $\alpha^2_{(2)}$*.* $N_t = 4$ *and a spectral efficiency of* $4\,\mathrm{bits/s/Hz}$*. Dashed lines denote simulation results for node* 1 *while solid lines denote the analytical upper bound. Since the analytical bound is asymptotically tight, the dashed and solid lines overlap at low ABER.*

antenna increases the Euclidean distance between the received and incorrect hypothesis vectors, which results in a lower ABER. To this extent, the addition of a single receive antenna is equivalent to lowering the interference, $\alpha^2_{(u)}$, by more than 10 dB. This can be seen when comparing Fig. 4.2 with Fig. 4.3(a) and similarly, Fig. 4.3(a) with Fig. 4.3(b), where the number of receive antennas is increased in each figure. In fact, the effect of each receive antenna is more pronounced as the imbalance between the desired and interfering links increases. This is apparent when the results for $\alpha^2_{(2)} = 10^{-2}$ in Fig. 4.2, the results for $\alpha^2_{(2)} = 10^{-2}$ in Fig. 4.3(a), and the results for $\alpha^2_{(2)} = 10^{-2}$ in Fig. 4.3(b) at an SNR of 40 dB are considered. The ABER of the simulation and analytical prediction move from 2×10^{-1} in Fig. 4.2, to 4×10^{-3} in Fig. 4.3(a), to 9×10^{-5} in Fig. 4.3(b). In particular, the decrease in the ABER shows how the number of receive antennas dominates the performance of SM in general, and particularly in an interference limited scenario. In addition, Fig. 4.4 demonstrates that the findings can be extended even in the presence of multiple interfering nodes.

The presented results show that when the interference-unaware detector is used, the system ABER plateaus at the derived limits, irrespective of the transmit power being used. Nonetheless, the ABER improves when the number of receive antennas is increased as the system

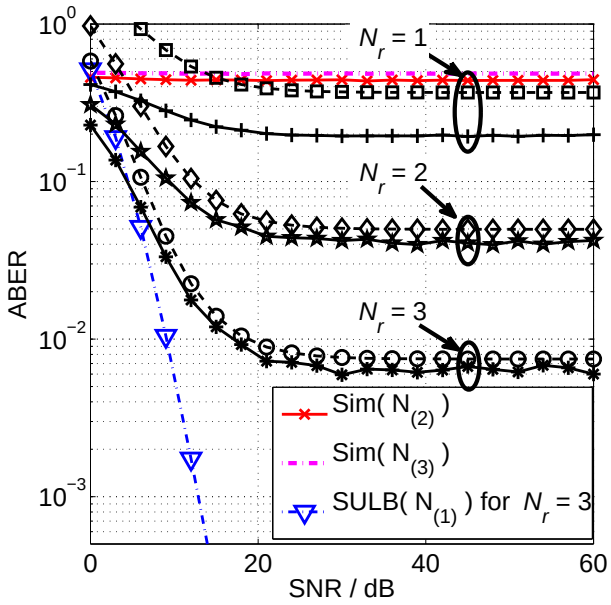

Figure 4.4: $N_t = 4$, *a varying* N_r *and a spectral efficiency of* $4\,\mathrm{bits/s/Hz}$. *ABER for node* 1 *using the interference-unaware detector with* $\alpha^2_{(1)} = 1$, $\alpha^2_{(2)} = 0.1$ *and* $\alpha^2_{(3)} = 0.01$. *All presented curves are for node* 1, *unless otherwise stated in the legend. Dashed lines denote simulation results for node* 1 *while solid lines denote the analytical upper bound. The addition of more receive antennas reduces the ABER and hence closes the gap between the analytical and simulation results.*

achieves both coding and diversity gains, as discussed in Section 4.3.1.

4.4.3 Results for Interference-Aware Detection

The performance of the jointly optimal interference-aware ML detector for a two user scenario is illustrated in Fig. 4.5(a). To this extent, Fig. 4.5(a) demonstrates that the analytical model presented in (4.42) represents an asymptotically tight upper bound for the system in the high SNR region where the node with the worse channel attenuation performs close to its SULB. However, this is not the case for the node with the better channel.

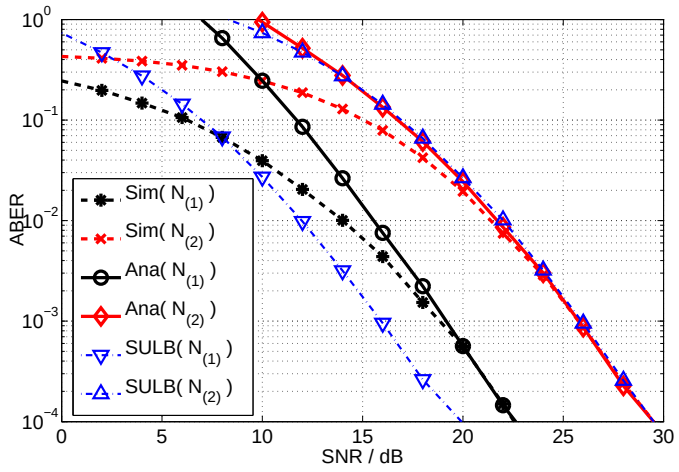

(a) $N_t = 2$

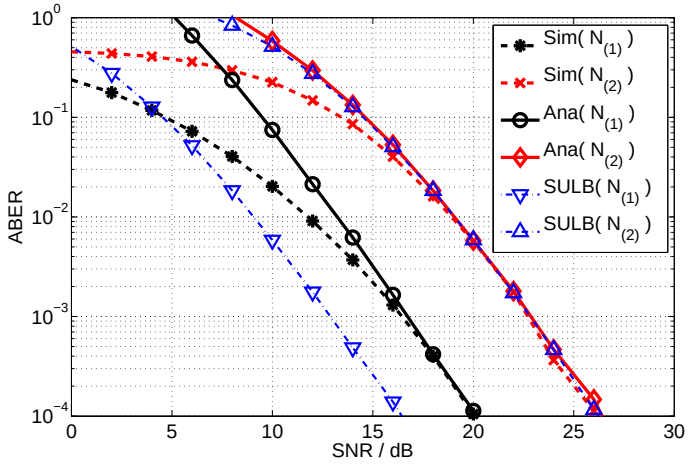

(b) $N_t = 4$

Figure 4.5: $N_r = 3$ *and a spectral efficiency of* $4\,\text{bits/s/Hz}$. *ABER using the interference-aware detector for node* 1 *with* $\alpha^2_{(1)} = 1$ *and for node* 2 *with* $\alpha^2_{(2)} = 0.1$.
Ana($\text{N}_{(u)}$ *) denotes the analytical upper bound for node* u. *Since the analytical bound is asymptotically tight, the dashed and solid lines overlap at low ABER.*

To understand this, one can think of the multi-user ML detector as employing interference cancellation for the node with the worse channel attenuation. If the interfering user is sufficiently powerful, then the primary source of errors for the weakest node is the background AWGN rather than the randomness caused by the interfering signal [109]. To this extent, all users that have good channel conditions can be considered as strong interferers, so when they are removed, the weakest nodes obtain performance closer to their SULB, *i.e.*, the interference-aware detector is akin to strong interference cancellation for the weakest node. On the contrary, for the nodes with better channel conditions, the primary source of errors is the randomness caused

by the interfering signal rather than the background AWGN. This is why the nodes with better channel conditions can never perform near their SULB.

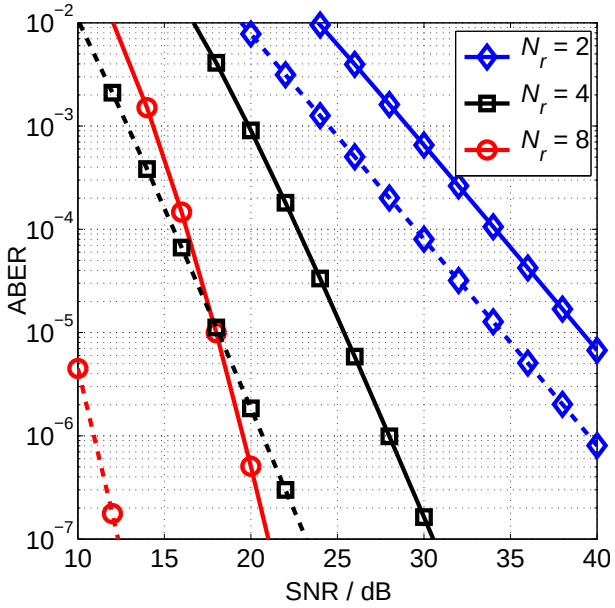

Figure 4.6: $N_t = 4$, *a varying* N_r *and a spectral efficiency of* $4\,\mathrm{bits/s/Hz}$. *Analytical ABER using the interference-aware detector for node* 1 *with* $\alpha^2_{(1)} = 1$ *and for node* 2 *with* $\alpha^2_{(2)} = 0.1$. *Dashed lines denote the analytical performance of node* 1, *while the solid lines denote the analytical performance of node* 2 *with a varying number of receive antennas.*

As discussed earlier, the addition of more transmit antennas at each of the nodes results in coding gains for each node, as can be seen when Fig. 4.5(a) and Fig. 4.5(b) are compared. In particular, the reduction in the ABER as the number of transmit antennas increases is explained by a corresponding increase of the average variance σ_z^2. Indeed, as σ_z^2 increases, it leads to a larger Euclidean distance in (4.10) and (4.43). The Euclidean distance is increased because there are more cases where the variance is the summation of the individual symbol constellation points, rather than the difference, *i.e.*, $n_t^{(\xi)} = \hat{n}_t^{(\xi)}$ occurs less frequently. Effectively, more transmit antennas mean that the transmit vectors are spread in a larger Euclidean space. This effect can only be observed when the same spectral efficiency is maintained. In particular, a 2 dB coding gain is apparent when comparing Fig. 4.5(b) to Fig. 4.5(a) at an ABER of 10^{-4}. However, increasing the number of transmit antennas does not change the relative behaviour of the system, *i.e.*, the SNR difference between the ABER curves of the two nodes remains constant. This behaviour is expected when considering that (4.17) is independent of N_t and influenced only by N_r.

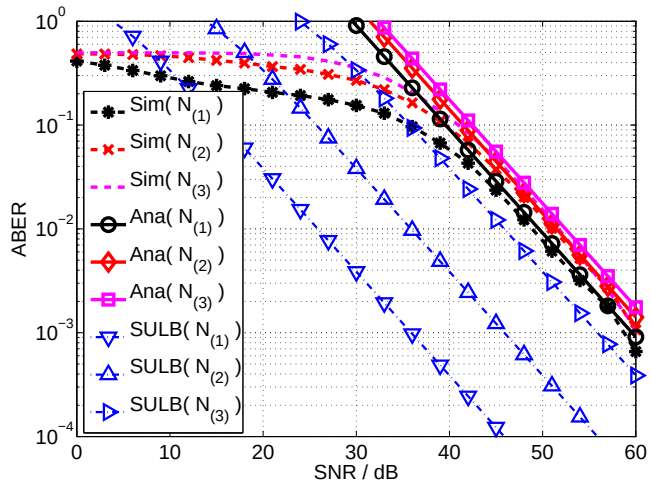

(a) $N_r = 1$

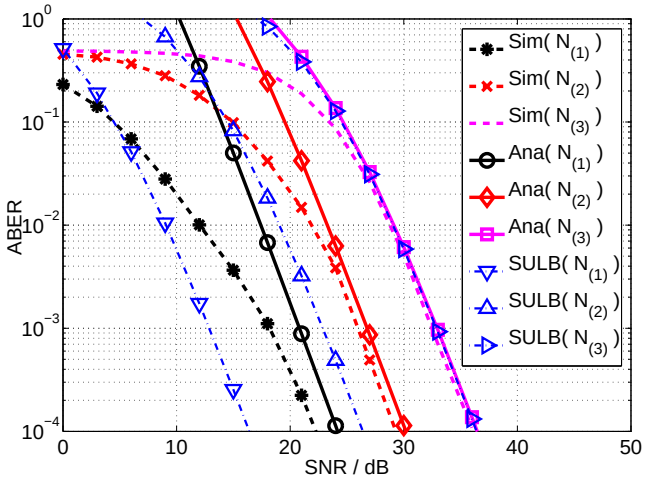

(b) $N_r = 3$

Figure 4.7: $N_t = 4$ *and a spectral efficiency of* $4\,\mathrm{bits/s/Hz}$. *ABER for node* 1 *with* $\alpha^2_{(1)} = 1$, *for node* 2 *with* $\alpha^2_{(2)} = 0.1$ *and for node* 3 *with* $\alpha^2_{(3)} = 0.01$.
Ana($\mathrm{N}_{(u)}$ *) denotes the analytical upper bound for node* u. *The analytical bound is again shown to be asymptotically tight at low ABER.*

Fig. 4.6 shows the performance of the system when the number of receive antennas is increased. On the one hand, Fig. 4.6 shows that for a fixed spectral efficiency and a fixed number of transmit antennas, the addition of more receive antennas results in an increasing gap between the analytical ABER curves of the two nodes. In particular, a gap of 4 dB between the performance of node 1 and node 2 with $N_r = 2$ is increased to around 7 dB when $N_r = 4$ and further increased to 9 dB for $N_r = 8$. On the other hand, given that the two nodes experience a channel gain difference of 10 dB, the interference-aware detector cannot reach the performance of

independent detection and the SULB for the node with the better channel attenuation. Nonetheless, the gap between their respective ABER curves tends toward the difference between their respective channel attenuation as N_r grows.

These trends can also be observed by looking at the progression of the ABER curves in Fig. 4.7(a) and Fig. 4.7(b). Fig. 4.7(a) and Fig. 4.7(b) illustrate the system performance with three nodes/users and varying N_r. In particular, similar to the two user scenario, each user performs better as N_r is increased and the gap to its SULB is reduced. As expected, the addition of more nodes increases the interference and pushes the performance of each node further from its SULB, noticeable when comparing Fig. 4.5(b) and Fig. 4.7(b) for node 2.

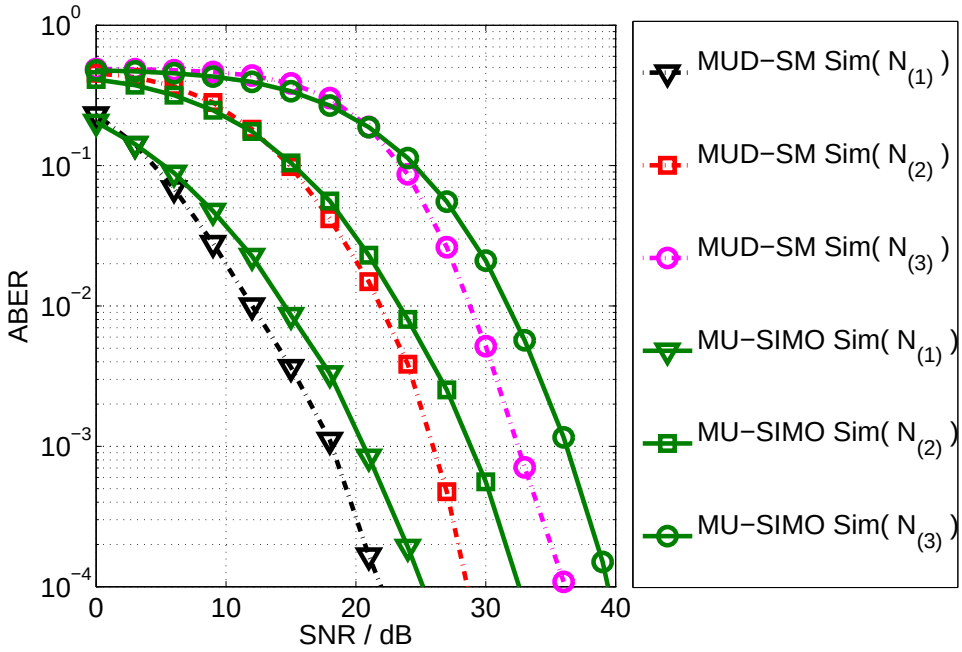

Figure 4.8: $N_t = 4, N_r = 3$ *and a spectral efficiency of* $4\,\mathrm{bits/s/Hz}$. *The ABER of multi-user SM and multi-user SIMO using interference-aware detectors with channel attenuation of* $\alpha^2_{(1)} = 1$, $\alpha^2_{(2)} = 0.1$ *and* $\alpha^2_{(3)} = 0.01$. *Solid lines represent simulation results for the ML interference-aware SIMO detector for node* $N_{(u)}$. *Dashed lines represent simulation results for the ML interference-aware SM detector for node* $N_{(u)}$ *and* $u \in \{1, 2, 3\}$.

Lastly, Fig. 4.8 demonstrates that SM performs better than the complexity and cost equivalent ML detector for the multi-user SIMO system in the interference limited scenario. Specifically, the system employing SM exhibits an approximately 3 dB better performance in terms of the SNR at an ABER of 10^{-4} for each user. Indeed, the relatively constant coding gain is the result of the similar detection used for both systems. While multi-user SM and multi-user SIMO

may be comparable in terms of detector complexity and the number of transmit and receive RF chains required, each SM node requires multiple transmit antenna elements. Therefore, by using the spatial domain, the SM constellation points are spread in a larger Euclidean space and have a lower error probability.

4.5 Summary

In this chapter, the performance of SM in the multiple access, interference limited scenario was investigated. Two ML detectors for use with SM were discussed.

The interference-unaware detector was defined and studied in the limit as the SNR approached infinity. Its performance over uncorrelated Rayleigh fading channels was studied and a closed form solution for the upper bound of the system was provided. In addition, it was shown that this detector inevitably reaches an error floor which was dependent on the SINR in the system. In particular, the exact level was defined and concrete examples were provided. To this extent, it was shown that the increase in the number of receive antennas has a greater impact on the asymptotic performance of the system compared to reducing the interference in the system. Indeed, the addition of a single receive antenna resulted in greater coding gains than reducing the interference by more than 10 dB at high SNR. This indicated that the number of receive antennas dominated the performance of SM in general, and particularly in an interference limited scenario.

The interference-aware ML detector for SM was proposed. As with the interference-unaware detector, its performance over uncorrelated Rayleigh fading channels was studied and a closed form solution for the upper bound of the system was provided. In addition to avoiding the error floor present in the interference-unaware detector, the jointly optimal detector mimicked a noise limited scenario for the detection of all transmitted streams, *i.e.*, an arbitrarily small ABER could be obtained by any node for a sufficiently high SNR. On the one hand, for the same spectral efficiency, increasing the number of transmit antennas at each of the nodes from two to four resulted in coding gains of around 2 dB. This measure did not, however, have any effect on the coding gain difference between the ABER curves. On the other hand, increasing the number of receive antennas increased the diversity of the system and provided additional coding gains. Effectively, this increased the coding gain difference between the ABER curves of the nodes because the receiver could distinguish the channels more easily and better mitigate

interference. To this extent, the impact on the diversity and coding gains demonstrated the importance of the number of receive antennas in any SM system. A limiting factor, as with all ML detectors, was the complexity. In addition, the receiver must have full channel knowledge. Nonetheless, the interference-aware detector enabled SM to perform better in terms of ABER than the complexity and cost equivalent multi-user SIMO system in an interference limited environment.

The presented work demonstrated that in order to apply SM in an interference limited scenario effectively, the number of receive antennas should be maximised. Although more computationally complex than the interference-unaware detector, the interference-aware detector can guarantee that the system does not reach an error floor. Having analysed the performance of SM in an interference limited scenario, the performance of a relaying system employing the SM principles is now considered in Chapter 5.

Chapter 5
Dual–hop Spatial Modulation

5.1 Introduction

In this chapter, the application of spatial modulation (SM) in a relaying scenario is proposed. As discussed in Section 2.2, the power of a transmitted wireless signal diminishes as the distance between the transmitter and receiver increases. As the power of the signal decreases, the signal-to-noise-ratio (SNR) at the receiver also decreases. Therefore, a direct communication link between the source node and the intended destination node may not be established if the signal power falls below a certain minimum threshold. One proposed solution to this problem is to introduce a relaying node between the source and destination nodes.

There are several detection methods that are used in the context of relaying communications which include direct, non-cooperative, cooperative and adaptive detection. Non-cooperative detection relies solely on information recovered by the destination from the relay. Cooperative detection uses the signal received from both direct and relaying transmissions and adaptive detection chooses the best of the three presented strategies [80]. Loosely speaking, cooperative decode and forward (DF) demonstrates the highest achievable rates when the source to relay channel quality is very good. Aside from these, *observation* encoding, in which a relay encodes only quantised versions of the received signal using ideas from source coding, demonstrates higher spectral efficiency when the relay to destination channel quality is better than the source to relay channel quality [80].

When considering cooperative detection, the destination node combines the two signals received from the source and relay nodes which results in a diversity gain. In addition, adaptive detection [113] and incremental relaying [80], address the selection of the optimal transmission in a given cooperative situation. In particular, incremental relaying, as presented in [80], defines relaying protocols that exploit limited feedback from the destination terminal to dramatically improve the spectral efficiency of the classical amplify and forward (AF) and DF protocols. Incremental relaying can be viewed as an extension of incremental redundancy, or automatic repeat request (ARQ), to relaying scenarios.

Further improvements come in [114], where Azarian defines a cooperative scheme which achieves the upper bound of the diversity-multiplexing trade-off for a single source-relay-destination system, called dynamic decode and forward (DDF). In it, the outage probabilities and diversity vs. multiplexing trade-off characteristics are addressed and the system is compared with several state-of-the-art solutions including the non-orthogonal AF protocol. The optimality of the ARQ–DDF protocol is again addressed in [115] where the performance of the protocol is characterised in terms of the diversity multiplexing tradeoff of the channel. In fact, the ARQ–DDF protocol is shown to achieve the upper bound of the diversity multiplexing tradeoff when the source nodes do not cooperate initially. This protocol, however, operates on the packet layer and relies on whatever modulation technique is available at the transmitter for communications. Indeed, if the transmission between the nodes can be improved, then the source to destination performance in terms of the average bit error ratio (ABER) will improve.

The aim of this work is to analyse the performance of SM in a relaying scenario and determine its potential to either alleviate the multihop burden or improve the source to destination ABER. To this extent, the focus is on orthogonal AF and DF protocols. On the one hand, orthogonal AF uses the relay antenna as a simple amplifier. Any signal received by the relay at time instance t_1, is amplified and retransmitted at instance t_2, forming a non-regenerative system. On the other hand, the orthogonal DF algorithm decodes the received signal at the relay, then re-encodes and retransmits this information, establishing a regenerative system. Outage probabilities, mutual information calculations and transmit diversity bounds for AF and DF relaying are derived in [80] with the source to destination performance being considered in [81]. Taking into consideration the above relaying protocols, the use of SM is proposed to provide additional power and capacity gains over the non-cooperative AF and DF systems.

In orthogonal AF and DF, two time slots are needed for the relevant information to reach the destination node, effectively halving the source to relay spectral efficiency. To this extent, dual-hop spatial modulation (Dh-SM) can partially mitigate this effect. Dh-SM can use the spatial domain to transmit additional information bits, while maintaining a fixed signal constellation. Since the receiver decodes the channel used for the transmission, it can determine the transmitting antenna and decode the bits used to activate that particular antenna. This serves to increase the source to destination spectral efficiency and alleviate the multihop burden, as will be explained in Section 5.2. Alternatively, a lower order modulation scheme can be used for the signal domain transmission which leads to a lower transmit power requirement. In fact, this

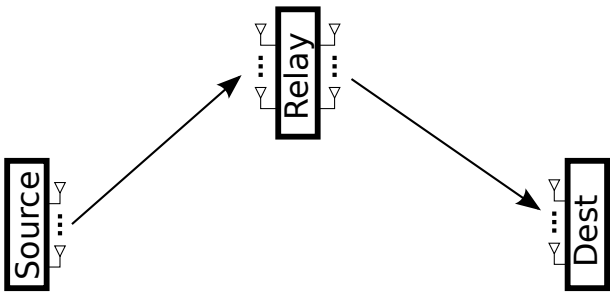

Figure 5.1: *System setup for Dual-hop Spatial Modulation where 'Dest' is the destination.*

is a unique advantage that Dh-SM has when compared to all other relaying systems resulting in a better ABER at the destination for the same transmit power, *i.e.*, Dh-SM can increase the coding gain of the system. It is the application of SM to a standard DF relaying system that is termed Dh-SM and is shown in Fig. 5.1. SM, however, requires multiple transmit antenna elements which may not be feasible when dealing with simpler nodes.

SM is also applied to a system with distributed relaying nodes, termed distributed spatial modulation (DSM). In a realistic scenario, the distributed nodes in a DSM system would be simple relays which have only a single antenna used for both transmission and reception. However, if each node has at most one receive antenna, then a system employing the SM principle will perform worse in terms of the ABER when compared to a classical single-input single-output (SISO) system, as is shown in Section 4.3.2.2. Therefore, each node in DSM is assumed to have multiple receive antennas. On the one hand, multiple receive antennas are necessary in any system employing the SM principle since it is the number of receive antennas that significantly influences the performance of SM relative to other SIMO systems, as is shown in Section 4.3.2. On the other hand, the multiple receive antenna elements may also be used as transmit antennas. However, having distributed nodes with multiple transmit antennas means that Dh-SM would become the backbone for analysing the DSM system, which is not the purpose of introducing the distributed scenario. In particular, the idea behind DSM is to examine the performance of SM in a distributed scenario, where the combination of the relay nodes forms a virtual antenna array and no relay node has multiple transmit antennas available. Therefore, only a single transmit antenna per relay node is assumed. Fig. 5.2 shows an example of a DSM system where, according to the SM principle, only a single relay node is active at any transmission instance.

In the remainder of this chapter, the system model for Dh-SM is introduced in Section 5.2, the theoretical framework is provided in Section 5.3 and the numerical results for Dh-SM are

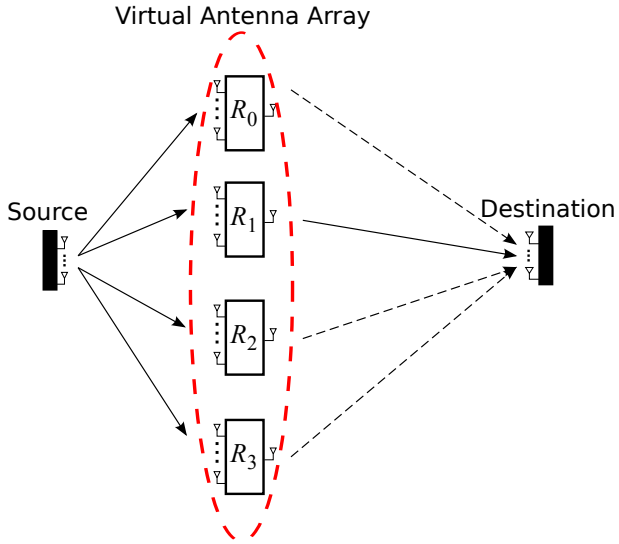

Figure 5.2: *An example of Distributed Spatial Modulation, with four relay nodes, $R_{i\in\{0,1,2,3\}}$, each having multiple receive antennas and only a single transmit antenna. No relay nodes cooperate with each other and, given that the information from the source is decoded correctly at each relay, form a virtual antenna array. The solid line between the relays and the destination denotes the activate link, while the dashed lines denote potential links.*

discussed in Section 5.4. The system model and the ABER of DSM are then analysed in Section 5.5. The performance of Dh-SM is finally compared to that of DSM in Section 5.6. Lastly, the chapter is summarised in Section 5.7.

5.2 System Model

A three node scenario, as shown in Fig. 5.1, is assumed. Even though AF, DF and Dh-SM use only a single antenna at any transmission instance and have a single radio frequency (RF) chain, Dh-SM requires the transmitter to have multiple transmit antennas available. In particular, the aim of this chapter is to characterise the ABER performance of a system using Dh-SM. As such, its ABER is compared to that of a system employing non-cooperative DF. Given that the source broadcasts a signal constellation symbol, x, then the received signal is given by $y_r = h_{(n_t,r)}x + \eta_r$, where n_t is the index of the transmit and r is the index of the receive antenna, $h_{(n_t,r)}$ is the fast fading channel coefficient of the link between the active antenna n_t and the receiving antenna r. η_r is the additive white Gaussian noise (AWGN) and is described by $\mathcal{CN}\left(0,\sigma^2\right)$ with $\sigma^2 = 1/\gamma$ where γ is the average SNR of the link. The estimated symbol

at each receiving node in the DF system using maximum ratio combining (MRC) is given by

$$x_{\text{est}}^{(\ell)} = \frac{\left(\mathbf{h}_{n_t}^{(k\ell)}\right)^* \mathbf{y}_{(k\ell)}}{\left(\mathbf{h}_{n_t}^{(k\ell)}\right)^* \mathbf{h}_{n_t}^{(k\ell)}}, \tag{5.1}$$

where $(\cdot)^*$ denotes the complex conjugate and $\mathbf{h}_{n_t}^{(k\ell)} = \left[h_{(n_t,1)}, \ldots, h_{\left(n_t,N_r^{(\ell)}\right)}\right]^T$ is a vector composed of the single tap channel coefficients from antenna n_t on the transmitting node k to the receiving node ℓ which has $N_r^{(\ell)}$ number of receive antennas. In addition, the transmitting node is either the source (s), or the relay (r), while the receiving node is either the relay or the destination (d), *i.e.*, $k \in \{\text{s}, \text{r}\}$ and $\ell \in \{\text{r}, \text{d}\}$. Furthermore, the received vector, $\mathbf{y}_{(k\ell)}$, is comprised of the symbols at each receive antenna on node ℓ. Finally, $x_{\text{est}}^{(\ell)}$ is passed through a maximum likelihood (ML) detector, at both the relay and destination nodes, to recover the original bit sequence, *i.e.*, a hard decision is also made at the relay.

A ML decoder is considered for detection in Dh-SM. It computes the Euclidean distance between the received signal, $\mathbf{y}_{(k\ell)}$, and the set of all possible received signals, selecting the closest one [52],

$$(x_{\text{est}}, n_t)^{(k)} = \underset{x\,,\,\mathbf{h}_{n_t}^{(k\ell)}}{\arg\min} \left\{ \left|\left| \mathbf{y}_{(k\ell)} - \mathbf{h}_{n_t}^{(k\ell)} x \right|\right|^2 \right\}, \tag{5.2}$$

$$x \in \mathcal{X}, \qquad n_t \in \{1, \ldots, N_t^{(k)}\},$$

where the pair $(x_{\text{est}}, n_t)^{(k)}$ is formed from the estimated symbol x_{est}, emitted from antenna n_t, on node k, x is the current symbol being evaluated from the set of possible constellation points $\mathcal{X}$, and $N_t^{(k)}$ is the number of available transmit antennas on node k.

Example:

A basic relaying system is assumed, as shown in Fig. 5.1. Transmissions are carried out at 2 bits/s/Hz in the signal domain and only a single transmit antenna is active at the source and relay nodes. On the one hand, orthogonal AF and DF require two time slots for the relevant information to reach the destination node. This results in a source to destination spectral efficiency of 1 bit/s/Hz. On the other hand, if the system in Fig. 5.1 is considered with a single transmit antenna at the source and four transmit antennas at the relay, 2 bits can be sent in the signal domain and 2 more in the spatial domain on the relay to destination link. In fact, the use of SM on the relay to destination link enables the system to operate at 4 bits/s/Hz on that link. In particular, the source can transmit to the relay in the first two time slots a total of 4 bits since

the system remains unchanged in the source to relay link. In turn, the relay can then transmit those 4 bits to the destination in the third slot by making use of the spatial domain. To this extent, the use of Dh-SM results in 4 bits going from the source to the destination in three time slots and an end-to-end (source to destination) average spectral efficiency of 1.33 bits/s/Hz; a 33% improvement over standard AF and DF.

Alternatively, Dh-SM can be used to improve the ABER of the system by transmitting a lower order modulation signal symbol. In particular, the coding gains of Dh-SM are quantified in Section 5.4.2.

5.3 Analytical Modelling

The scenario presented in Fig. 5.1 represents a well-known orthogonal relaying system. A major distinction is the use of multiple transmit and receive antennas. To this extent, the end-to-end performance of a two-hop wireless communication system with non-regenerative (AF) and regenerative (DF) relays over a Rayleigh-fading channel is presented in [81]. The authors develop a closed form expression for the ABER of AF given in terms of the moment generating function (MGF) of the system. Furthermore, the system performance in terms of outage probability and ABER demonstrate that DF systems perform better than AF systems at both low and high average SNRs in a Rayleigh fading environment. For this reason, the ABER performance of Dh-SM is only compared to that of DF. The aim is to show that the use of SM in a fixed relaying system can provide coding gains.

Starting from the system model presented in Section 5.2, the signal undergoes two stages of decoding [116]. To this extent, the ABER, for all dual–hop regenerative systems over independent channels, can readily be expressed as

$$P_{(\mathrm{sd})} = P_{(\mathrm{sr})} + P_{(\mathrm{rd})} - 2P_{(\mathrm{sr})}P_{(\mathrm{rd})}. \tag{5.3}$$

$P_{(k\ell)}$ is the ABER of the link between nodes k and ℓ with an average SNR of $\gamma_{(k\ell)}$. In a regenerative system, the overall ABER is a function of the individual links. This means that if a system performs better in terms of ABER on the individual links, it will also perform better for the dual–hop. To prove this claim, the directional derivative of $P_{(\mathrm{sd})}$ with respect to $P_{(\mathrm{sr})}$ and $P_{(\mathrm{rd})}$ is considered, given that both $P_{(\mathrm{sr})}$ and $P_{(\mathrm{rd})}$ must be less than $1/2$. A unit vector

$\mathbf{u} = <\widetilde{\alpha}, \widetilde{\varepsilon}>$ is defined where $\widetilde{\alpha}$ and $\widetilde{\varepsilon}$ are non-negative coefficients defining the direction of the derivative. The directional derivative, $\nabla_{\mathbf{u}}$, of $P_{(\mathrm{sd})}$ is then given by

$$\nabla_{\mathbf{u}} P_{(\mathrm{sd})} = \widetilde{\alpha}\left(1 - 2P_{(\mathrm{rd})}\right) + \widetilde{\varepsilon}\left(1 - 2P_{(\mathrm{sr})}\right). \tag{5.4}$$

Looking at (5.4), it is clear that the directional derivative is monotonically increasing with respect to the individual error probabilities since $\{P_{(\mathrm{sr})},\, P_{(\mathrm{rd})}\} \in [0,\, 1/2]$. The expressions for these error probabilities are now analysed. Since the overall system error depends solely on the error of the individual links, it is sufficient to analyse the error expressions for the arbitrary single-hop k to ℓ link.

The ABER of a SIMO system using $\widetilde{M}$-quadrature amplitude modulation (QAM) across multiple fading channels is given in (5.5). To this extent, the generalised expression for the ABER of a single-hop link between nodes k and ℓ using QAM and Gray coding is given in [111] such that

$$P_{(k\ell)}^{\mathrm{SIMO}} \cong 4\left(\frac{\sqrt{\widetilde{M}}-1}{\sqrt{\widetilde{M}}\log_2(\widetilde{M})}\right)\sum_{m=1}^{\sqrt{\widetilde{M}}/2}\frac{1}{\pi}\int_0^{\pi/2}\mathcal{M}_{\gamma_{(k\ell)}}\left(\frac{c}{2\sin^2(\theta)}\right)^{N_r^{(\ell)}} d\theta, \tag{5.5}$$

where

$$c = -\frac{3\log_2(\widetilde{M})(2m-1)^2}{\widetilde{M}-1},$$

and $\mathcal{M}_\gamma(s)$ is the moment generating function of the fading channel. The moment generating functions for different channel fading models can be found in [111]. In particular, the MGF for a Rayleigh fading channel is given by

$$\mathcal{M}_\gamma(s) = \frac{1}{1+s\gamma}.$$

Dh-SM is, in principle, a DF system and its ABER can be represented by (5.3), where the individual error probabilities are those of the individual SM links.

The ABER of SM using the optimal detector can be obtained using the union bound approach presented in Section 3.4.1, and is given as

$$P_{(k\ell)}^{\mathrm{SM}} \leq \sum_{\substack{x,\, n_t,\\ \hat{x},\, \hat{n}_t}}^{MN_t} \frac{d_{(k\ell)}(x, n_t, \hat{x}, \hat{n}_t)}{\log_2(MN_t)} \frac{\mathrm{E}_{\mathcal{H}}\left[\mathrm{PEP}_{(k\ell)}\left(x,\, n_t,\, \hat{x},\, \hat{n}_t\right)\right]}{MN_t}. \tag{5.6}$$

such that $d_{(k\ell)}(x, n_t, \hat{x}, \hat{n}_t) = d(n_t - 1, \hat{n}_t - 1) + d(x, \hat{x})$, where $d(\cdot, \hat{\cdot})$ is the Hamming distance between the binary represention of two symbol coming from the same set and
$Q(\omega) = \frac{1}{\sqrt{2\pi}} \int_{\omega}^{\infty} \exp\left(-\frac{t^2}{2}\right) \mathrm{dt}$ defines the Q-function.
$\mathrm{PEP}_{(k\ell)}\left(x,\, n_t,\, \hat{x},\, \hat{n}_t\right) = \Pr\{\mathbf{h}_{n_t}^{(k\ell)} x \neq \mathbf{h}_{\hat{n}_t}^{(k\ell)} \hat{x}\}$ is the pairwise error probability (PEP) on the link between node k and node ℓ where the symbol x, emitted from antenna n_t, is detected as symbol $\hat{x}$, emitted from antenna $\hat{n}_t$ and $\mathrm{E}_{\mathcal{H}}[\cdot]$ represents the expectation of the system with respect to the channel $\mathcal{H}$. Using similar analytical steps as for (4.4), the PEP between the nodes k and ℓ can be obtained as

$$\mathrm{PEP}_{(k\ell)}\left(x,\, n_t,\, \hat{x},\, \hat{n}_t\right) = Q\left(\sqrt{\frac{\gamma_{(k\ell)}}{2}\left|\left|\mathbf{h}_{n_t}^{(k\ell)} x - \mathbf{h}_{\hat{n}_t}^{(k\ell)} \hat{x}\right|\right|^2}\right). \tag{5.7}$$

Given this analytical modelling, the ABER performance of Dh-SM and DF is now analysed.

5.4 Numerical Analysis

The aim of this section is to compare the performance of Dh-SM with that of DF under the same spectral efficiency in a variety of conditions. In particular, the presented results depict the different behaviour of the system when: i) $N_t^{(\mathrm{s})}$ is changed, ii) $N_t^{(\mathrm{r})}$ is changed, iii) $N_r^{(\mathrm{r})}$ is changed, iv) $N_r^{(\mathrm{d})}$ is changed and, v) $\gamma_{(k\ell)}$ is varied. The work begins by analysing the most constrained Dh-SM system where $N_t^{(\mathrm{s})} = 2, N_r^{(\mathrm{r})} = 2, N_t^{(\mathrm{r})} = 2$ and $N_r^{(\mathrm{d})} = 2$. Each parameter is then adjusted to see the effect it has on the system.

5.4.1 Simulation Setup

A frequency-flat Rayleigh fading channel with no correlation between the transmitting antennas and AWGN is assumed. In addition, MRC in combination with ML detection is used in the DF system, with the ML detector in (5.2) being used for Dh-SM. Furthermore, perfect channel state information (CSI) is assumed at the receiving node, with no CSI at the transmitter. Since part of the data is encoded in the spatial domain, Dh-SM uses a lower order modulation symbol. Nonetheless, the energy per symbol is equivalent to that in the DF system.

5.4.2 Results

In the legend on each figure, `An` represents the analytical ABER on the link, while `Sim` is the simulation result. The analytical expression in (5.5) describes the behaviour of DF, whereas (5.6) bounds the behaviour of Dh-SM.

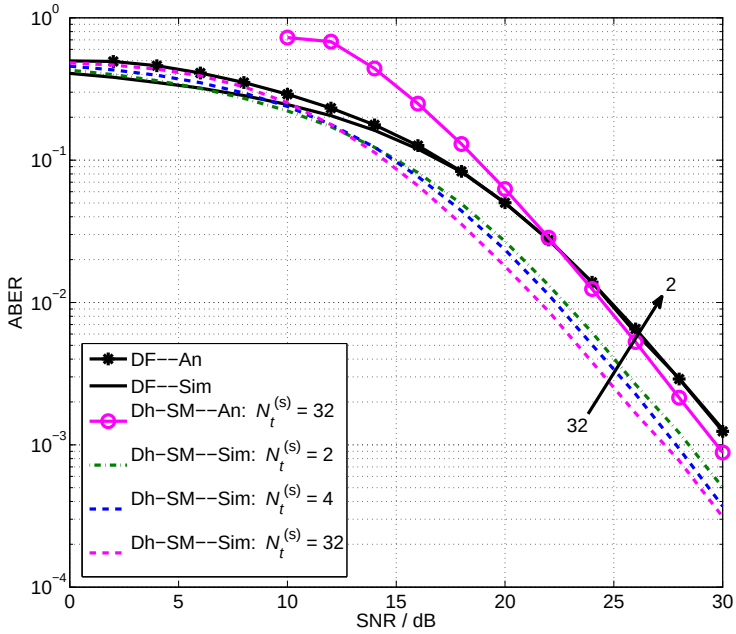

Figure 5.3: *ABER between the source and destination when $\gamma_{(\mathrm{sr})} = \gamma_{(\mathrm{rd})}$ and the number of transmit antennas at the source is varied. $N_r^{(\mathrm{r})} = N_r^{(\mathrm{d})} = 2$, $N_t^{(\mathrm{r})} = 2$ and the average source to destination spectral efficiency is $3.5\,\mathrm{bits/s/Hz}$. The arrow on the figure indicates the progression of the curves going from $N_t^{(\mathrm{s})} = 32$ as the leftmost dashed curve to $N_t^{(\mathrm{s})} = 2$ as the rightmost dashed curve. To improve the legibility of the figure, the analytical results for $N_t^{(\mathrm{s})} = 2$ and $N_t^{(\mathrm{s})} = 4$ are not presented.*

The effects of additional transmit antennas are now analysed. In Fig. 5.3, when the source to relay and relay to destination channel conditions are comparable, Dh-SM exhibits over a 2 dB coding gain relative to DF as the signal constellation used in Dh-SM is reduced. However, as any DF system, Dh-SM is susceptible to bottlenecks. In particular, Fig. 5.3 shows that the relay to destination link constraints the performance of Dh-SM and the addition of more transmit antennas at the source results in marginal gains. Indeed, having 4 transmit antennas at the source increases the coding gains of Dh-SM to 2.4 dB and transmission using 32 transmit antennas results in coding gains of only 3.5 dB, despite using only binary phase shift keying (BPSK) as the signal constellation. In addition, Fig. 5.3 shows that the high ABER on the

relay to destination link also affects the analytical results. As discussed in Section 3.4.1, the union bound approach leads to asymptotically tight analytical results, as the mass of the two-dimensional Gaussian distribution around each SM constellation point becomes concentrated around its mean. The same principle is true for Dh-SM, however, if one of the links exhibits a high ABER, then the overall analytical expression will need longer to converge to its asymptote. Nonetheless, the coding gain between the simulation and analytical curves is decreasing as the ABER of the system decreases, which is expected when using the union bound approach.

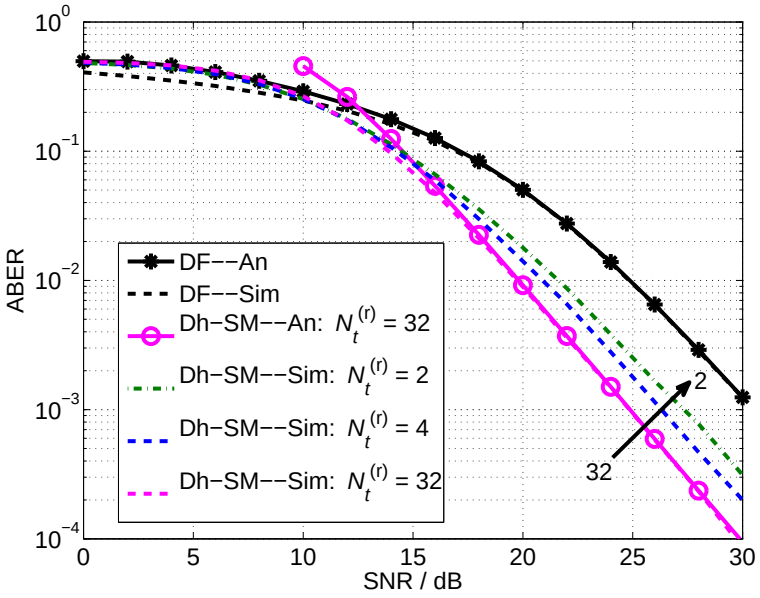

Figure 5.4: *ABER between the source and destination when $\gamma_{(\mathrm{sr})} = \gamma_{(\mathrm{rd})}$ and the number of transmit antennas at the relay is varied. $N_r^{(\mathrm{r})} = N_r^{(\mathrm{d})} = 2$, $N_t^{(\mathrm{r})} = 32$ and the average source to destination spectral efficiency is equal to $3.5\,\mathrm{bits/s/Hz}$. The arrow on the figure indicates the progression of the curves going from $N_t^{(\mathrm{r})} = 32$ as the leftmost dashed curve to $N_t^{(\mathrm{r})} = 2$ as the rightmost dashed curve. To improve the legibility of the figure, the analytical results for $N_t^{(\mathrm{r})} = 2$ and $N_t^{(\mathrm{r})} = 4$ are not presented.*

As a next step, the bottleneck on the source to relay link is removed by setting $N_t^{(\mathrm{s})} = 32$ and the effects of the number of transmit antennas at the relay is analysed. To this extent, coding gains of 3.5 dB relative to DF are achieved with only 2 transmit antennas at the relay, as illustrated in Fig. 5.4. This advantage is increased to about 4 dB with 4 transmit antennas and reaches 5 dB when using 32 transmit antennas at the relay. In general, systems with more available transmit antennas exhibit better performance in terms of the ABER as the SM symbols are spread in a larger Euclidean space for every additional antenna at the transmitter, although the coding gains achieved are diminishing. In addition, as the ABER on each link is reduced, applying (5.6) for

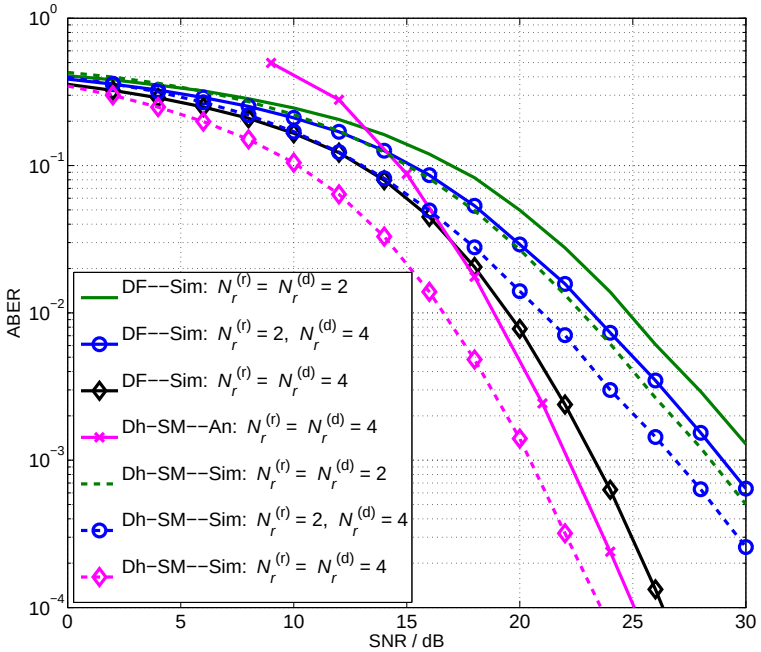

Figure 5.5: *ABER between the source and destination when* $\gamma_{(\mathrm{sr})} = \gamma_{(\mathrm{rd})}$ *and the number of receive antennas at the relay and destination is varied.* $N_t^{(\mathrm{s})} = N_t^{(\mathrm{r})} = 2$ *and the average source to destination spectral efficiency is equal to* $3.5\,\mathrm{bits/s/Hz}$.

each term in (5.3) provides an asymptotically tight upper bound for the source to destination ABER, as shown in Fig. 5.4. Furthermore, while having 32 transmit antennas on a single node may not be realistic, this work provides a basis for the expected performance of a distributed relaying scenario employing SM where multiple transmit antennas would be available. Indeed, Section 5.5 looks at the ABER of a system employing distributed relaying nodes as compared to the system employing fixed relaying nodes. In particular, Dh-SM is compared to DSM in Section 5.6. In addition, multiple transmit antennas for SM do not mean multiple RF chains. In fact, multiple transmit antennas can be obtained by simply having more antenna elements.

The behaviour of Dh-SM with respect to the number of receive antennas is now investigated. As Fig. 5.5 shows, Dh-SM performs better as more receive antennas are added to the system, irrespective of which node they are added to. Despite the coding gains observed, the system is still limited by its worse performing link in terms of the ABER since the diversity of the overall system is $\min\left\{N_r^{(\mathrm{r})},\ N_r^{(\mathrm{d})}\right\}$. In particular, this is evident if the slopes of the different curves in Fig. 5.5 are compared in the high SNR region. Indeed, Fig. 5.5 shows that Dh-SM has about 2.2 dB coding gain with respect to DF when there are 2 receive antennas at both the relay and the destination. However, when there are 2 and 4 receive antennas at the relay and destination

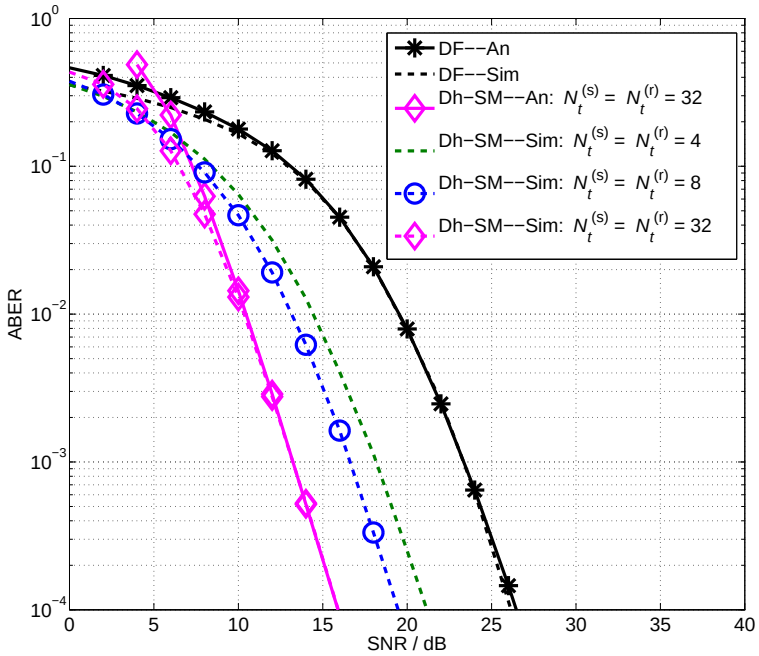

Figure 5.6: *ABER between the source and destination when* $\gamma_{(\mathrm{sr})} = \gamma_{(\mathrm{rd})}$ *and the number of transmit antennas at the source and relay is varied.* $N_r^{(\mathrm{r})} = N_r^{(\mathrm{d})} = 4$ *and the average source to destination spectral efficiency is equal to* $3.5\,\mathrm{bits/s/Hz}$.

nodes, respectively, Dh-SM has a 2.6 dB coding gain with respect to DF, *i.e.*, the performance of Dh-SM improves by 0.4 dB with the addition of 2 receive antennas at the destination. Again, the small increase in the coding gain as the number of receive antennas at the destination is increased, is the result of a bottleneck created by the 2 receive antennas at the relay. However, when there are 4 receive antennas at each of the nodes, Dh-SM exhibits about 3.3 dB better performance compared to DF. Furthermore, the coding gains in Dh-SM are in addition to the diversity gains experienced by both DF and Dh-SM, a result of increasing the number of receive antennas.

With the separate effects of the number of transmit and receive antennas analysed, Fig. 5.6 shows that Dh-SM can exhibit between 5 dB and 10 dB gains compared to DF when the number of receive antennas at both the relay and the destination is increased to 4 and $N_t^{(\mathrm{s})} = N_t^{(\mathrm{r})}$. In particular, these gains are larger than those presented in Fig. 5.3 and Fig. 5.4 since both links have more receive antennas. The greater number of receive antennas provides an increase in spatial diversity for both DF and Dh-SM with further coding gains for Dh-SM. Indeed, the coding gains exhibited by Dh-SM are partially a result of the lower order signal–constellation symbols used in SM transmission and are discussed in Section 4.3.2 for a single link.

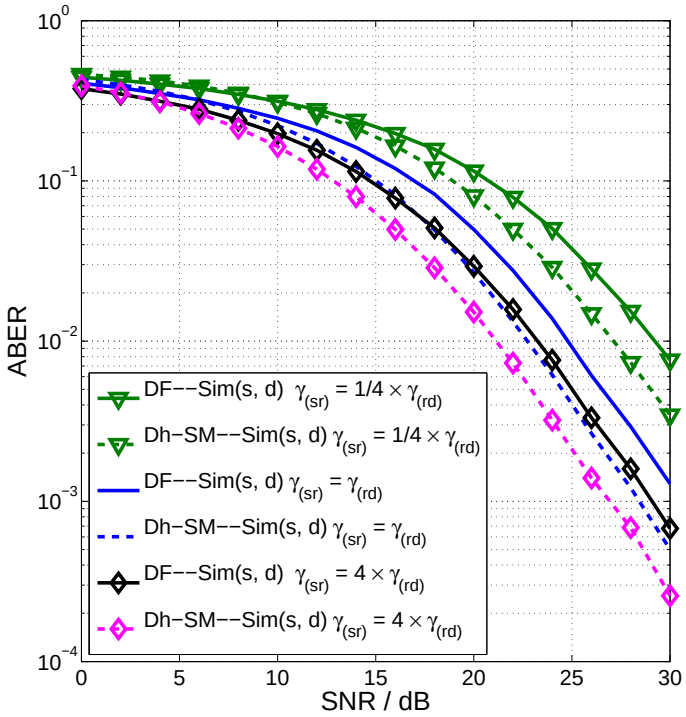

Figure 5.7: *ABER between the source and the destination for* $N_r^{(\mathrm{r})} = N_r^{(\mathrm{d})} = 2$, $N_t^{(\mathrm{s})} = N_t^{(\mathrm{r})} = 2$, *and the average source to destination spectral efficiency is equal to* $3.5\,\mathrm{bits/s/Hz}$. *The channel gains are varied.*

With the effect of the number of antennas analysed, Fig. 5.7 shows the effects of varying the link SNRs, *i.e.*, $\gamma_{(\mathrm{sr})} \neq \gamma_{(\mathrm{rd})}$. Both DF and Dh-SM, exhibit better performance when the average SNR on the source to relay link is greater than the average SNR on the relay to destination link, as shown in Fig. 5.7. Nonetheless, the performance difference between the two systems remains unchanged regardless of the ratio between $\gamma_{(\mathrm{sr})}$ and $\gamma_{(\mathrm{rd})}$. This means that the effects discussed above extend to arbitrary channel gain conditions and system geometry.

5.5 Distributed Spatial Modulation

Applying SM in the relaying scenario is shown to result in significant coding gains for a system with a fixed relaying node. Next, the aim is to analyse the behaviour of a system employing the SM principles in a distributed scenario. In particular, the ABER of a system with two relaying nodes that make independent decisions on data forwarding is characterised.

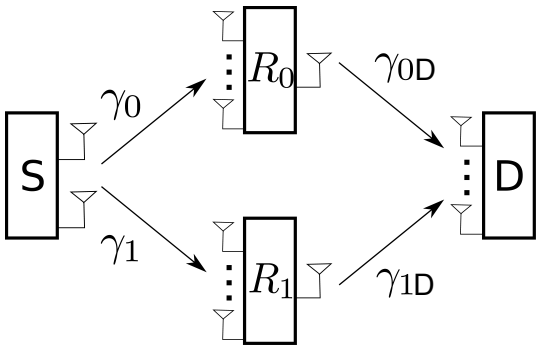

Figure 5.8: *Distributed Spatial Modulation: The source node,* S*, broadcasts a message at* $1\,\mathrm{bit/s/Hz}$ *using SSK. The relay nodes,* R_0 *and* R_1*, have the same number of receive antennas as the destination node,* D*, and decode the message independently.* R_0 *only transmits a signal when it sees a '0' in its decoded message. Similarly,* R_1 *only transmits a signal when it sees a '1' in its decoded message.*

5.5.1 System Model

The system shown in Fig. 5.8 is assumed. All analytical derivations are applicable only if the spectral efficiency of the system is $\log_2(N_u)$ where N_u is the number of relay nodes. In particular, the analytical result is only valid when the probability of incorrectly activating a relay is the same as the probability of error for a given symbol.

To this extent, the simplest system transmitting at 1 bit/s/Hz using space shift keying (SSK) is considered. The source is assumed to have 2 transmit antennas and all receiving nodes (the two relays and the destination) have N_r number of receive antennas. In particular, the two relays aim to operate as a virtual antenna array where the array transmits using SSK principles, *i.e.*, relays R_0 or R_1 activate only when a '0' or a '1' is detected, respectively. Furthermore, γ_0 is the SNR between the source and R_0, γ_1 is the SNR between the source and R_1, $\gamma_{0\mathrm{D}}$ is the SNR between R_0 and the destination, and $\gamma_{1\mathrm{D}}$ is the SNR between R_1 and the destination. Additionally, a strictly two-hop system is assumed with no direct communication between the source and destination nodes. Before proceeding with further work, the ABER for a point-to-point SSK system must be determined. In particular, the ABER of a 2-by-N_r SSK system.

5.5.2 Derivation of the ABER for SSK

The general detector for SM can be reduced to an SSK detector assuming $x = 1$ for all events. In this case, the optimal detector for SSK is given as

$$n_t = \underset{n_t \in \{1,2,\ldots,N_t\}}{\arg\min} \left\{ ||\mathbf{y} - \mathbf{h}_{\hat{n}_t}||_{\mathrm{F}}^2 \right\}. \tag{5.8}$$

In particular, the ABER of any point-to-point SSK system can be posed by using a union bound approach and is given as

$$\mathrm{ABER}_{\mathrm{SSK}} \leq \sum_{n_t}^{N_t} \sum_{\hat{n}_t}^{N_t} \frac{d(n_t - 1, \hat{n}_t - 1)}{\log_2(N_t)} \frac{\mathrm{E}_{\mathcal{H}}\left[\Pr\left(\mathbf{h}_{n_t} \neq \mathbf{h}_{\hat{n}_t}\right)\right]}{N_t}. \tag{5.9}$$

After some analytical manipulations, similar to (4.4), the PEP is given as

$$\Pr\left(\mathbf{h}_{n_t} \neq \mathbf{h}_{\hat{n}_t}\right) = Q\left(\sqrt{\frac{E_m}{2N_o} ||\mathbf{h}_{n_t} - \mathbf{h}_{\hat{n}_t}||_{\mathrm{F}}^2}\right). \tag{5.10}$$

It should be noted that this PEP is valid for all channel fading statistics and is equal to the instantaneous symbol error ratio (SER), *i.e.*,

$$\mathrm{SER}(\gamma) = Q\left(\sqrt{\frac{\gamma}{2} ||\mathbf{h}_{n_t} - \mathbf{h}_{\hat{n}_t}||_{\mathrm{F}}^2}\right)$$

where $\gamma = \frac{E_m}{N_o}$ is the instantaneous SNR.

If a Rayleigh fading channel is considered, the closed form solution for $\mathrm{E}_{\mathcal{H}}\left[\Pr\left(\mathbf{h}_{n_t} \neq \mathbf{h}_{\hat{n}_t}\right)\right]$ in (5.9) can be derived by employing the solution to [110, eq. 62]. By assuming a Rayleigh fading channel, the argument within (5.10) can be represented as the summation of $2N_r$ squared Gaussian random variables, with zero mean and variance equal to 1. This means they can be described by a central Chi-squared distribution with $2N_r$ degrees of freedom and a probability density function given in (4.15). The result for $\mathrm{E}_{\mathcal{H}}\left[\Pr\left(\mathbf{h}_{n_t} \neq \mathbf{h}_{\hat{n}_t}\right)\right]$ is given as

$$\mathrm{E}_{\mathcal{H}}\left[\Pr\left(\mathbf{h}_{n_t} \neq \mathbf{h}_{\hat{n}_t}\right)\right] = f(\beta)^{N_r} \sum_{r=0}^{N_r-1} \binom{N_r - 1 + r}{r} \left(1 - f(\beta)\right)^r, \tag{5.11}$$

such that $f(\beta)$ is given in (4.18) and $\beta = \frac{E_m}{2N_o}$.

In general, (5.9) is a union bound to the ABER of any SSK system in a Rayleigh fading environment. In particular, this is an exact closed form for the ABER of a 2-by-N_r system since the PEP exactly defines all error events. In addition, the ABER is the same as the average symbol error ratio (ASER) since the Hamming distance is either 1 or 0 for the 2-by-N_r SSK system

which also means that the instantaneous bit error ratio (BER) is equal to the instantaneous SER. The source to destination ABER for DSM is now considered.

5.5.2.1 Analytical Source to Destination ABER for DSM

The source to destination instantaneous BER can be defined as

$$\mathrm{BER}_{\mathrm{sd}} = \frac{1}{2}\left[\mathrm{BER}_{\mathrm{sd}|0} + \mathrm{BER}_{\mathrm{sd}|1}\right] \tag{5.12}$$

where $\mathrm{BER}_{\mathrm{sd}|0}$ and $\mathrm{BER}_{\mathrm{sd}|1}$ are the source to destination BER given a '0' or a '1' was transmitted by the source, respectively. Both of the relays, as well as the destination, use a ML receiver. After some analytical manipulations shown in Appendix B.1, (5.13) is obtained.

P_C is the probability of correct detection by both nodes, while P_W is the probability of incorrect detection by both nodes. In addition, $P_{B|0}$ is the probability of both nodes activating when only R_0 was intended and $P_{B|1}$ is the probability of both nodes activating when only R_1 was intended. To this extent, the expressions governing P_C, P_W, $P_{B|0}$ and $P_{B|1}$ in terms of the BER as a function of the respective SNRs, are given in Appendix B.1. The full source to destination BER can now be posed as

$$\begin{aligned}
\mathrm{BER}_{\mathrm{sd}} &= \tfrac{1}{2}\mathrm{BER}_{\mathrm{sd}|0} + \tfrac{1}{2}\mathrm{BER}_{\mathrm{sd}|1} \\
&= \tfrac{1}{2}\left[P_C\left(\mathrm{BER}(\gamma_{0\mathrm{D}}) + \mathrm{BER}(\gamma_{1\mathrm{D}})\right)\right] \\
&+ \tfrac{1}{2}\left[P_W\left(1 - \mathrm{BER}(\gamma_{0\mathrm{D}}) + 1 - \mathrm{BER}(\gamma_{1\mathrm{D}})\right)\right] \\
&+ \tfrac{1}{2}\left[P_{B|0}\ \mathrm{BER}_{0\mathrm{D}/1\mathrm{D}}\right] \\
&+ \tfrac{1}{2}\left[P_{B|1}\ \mathrm{BER}_{1\mathrm{D}/0\mathrm{D}}\right].
\end{aligned} \tag{5.13}$$

In particular, $\mathrm{BER}_{0\mathrm{D}/1\mathrm{D}}$ is the probability of detecting '1' at the destination when '0' was transmitted from the source and both relays are active. Similarly, $\mathrm{BER}_{1\mathrm{D}/0\mathrm{D}}$ is the probability of detecting '0' at the destination when '1' was transmitted from the source and both relays are active. In addition, the probability of error is governed by the strongest SNR when both relay nodes are active, *i.e.*, given a constant transmit power of E_m, it is governed by the channel attenuations. Specifically, if both relay nodes are active, then the destination will detect an interference limited signal. Analytical work for the performance of the system in an interference limited scenario is shown in Section 4.3.1. In this scenario, the 'correctly' decoded symbol will be the one detected on the better link, *i.e.*, the link with the weakest channel attenuation.

Therefore, if $\gamma_{0\mathrm{D}} < \gamma_{1\mathrm{D}}$, then the event of detecting a '0' when a '1' was sent from the source constitutes an error and is governed by $\mathrm{BER}(\gamma_{1\mathrm{D}}/\gamma_{0\mathrm{D}})$. However, the event of detecting a '1' when a '1' was sent from the source is correct and is given as $1-\mathrm{BER}(\gamma_{1\mathrm{D}}/\gamma_{0\mathrm{D}})$. This means that if $\gamma_{0\mathrm{D}} < \gamma_{1\mathrm{D}}$, then $\mathrm{BER}_{0\mathrm{D}/1\mathrm{D}} = 1-\mathrm{BER}(\gamma_{1\mathrm{D}}/\gamma_{0\mathrm{D}})$. Similarly, if $\gamma_{1\mathrm{D}} < \gamma_{0\mathrm{D}}$, then $\mathrm{BER}_{1\mathrm{D}/0\mathrm{D}} = 1-\mathrm{BER}(\gamma_{0\mathrm{D}}/\gamma_{1\mathrm{D}})$.

At this point, to move from the instantaneous BER to the ABER, the expectation of (5.10) with respect to the fast fading channel coefficients must be obtained. To this extent, the expectation with respect to the channel for all multiplicative BER terms that compose it must be considered for each term in (5.13). The ABER of two multiplicative BER terms, assuming that the channels are identical and independently distributed (i.i.d.), is given as

$$\mathrm{E}_{\mathcal{H}_0,\mathcal{H}_{0\mathrm{D}}}\left[\mathrm{BER}(\gamma_0)\mathrm{BER}(\gamma_{0\mathrm{D}})\right] = \mathrm{E}_{\mathcal{H}_0}\left[\mathrm{BER}(\gamma_0)\right]\mathrm{E}_{\mathcal{H}_{0\mathrm{D}}}\left[\mathrm{BER}(\gamma_{0\mathrm{D}})\right], \tag{5.14}$$

where $\mathcal{H}_0$ and $\mathcal{H}_{0\mathrm{D}}$ are the channel matrices between the source to R_0 and R_0 to the destination, respectively. Given this independence, after some mathematical manipulations and realising that $\mathrm{BER}(0) = 0.5$, the closed form for the source to destination ABER for the system presented in Fig. 5.8 can be derived. For the sake of conciseness,

$$P_0 = \mathrm{E}_{\mathcal{H}_0}\left[\mathrm{BER}(\gamma_0)\right];\ P_{0\mathrm{D}} = \mathrm{E}_{\mathcal{H}_{0\mathrm{D}}}\left[\mathrm{BER}(\gamma_{0\mathrm{D}})\right];\ P_{0\mathrm{D}/1\mathrm{D}} = \mathrm{E}_{\mathcal{H}_{0\mathrm{D}}}\left[\mathrm{BER}(\gamma_{0\mathrm{D}}/\gamma_{1\mathrm{D}})\right]$$

and

$$P_1 = \mathrm{E}_{\mathcal{H}_1}\left[\mathrm{BER}(\gamma_1)\right];\ P_{1\mathrm{D}} = \mathrm{E}_{\mathcal{H}_{1\mathrm{D}}}\left[\mathrm{BER}(\gamma_{1\mathrm{D}})\right];\ P_{1\mathrm{D}/0\mathrm{D}} = \mathrm{E}_{\mathcal{H}_{1\mathrm{D}}}\left[\mathrm{BER}(\gamma_{1\mathrm{D}}/\gamma_{0\mathrm{D}})\right].$$

From here, the source to destination ABER for the distributed case using SSK can be defined.

$$\begin{aligned} &\mathrm{If}\,\gamma_{0\mathrm{D}} = \gamma_{1\mathrm{D}}, \mathrm{then} \\ &\qquad \mathrm{ABER}_{(\mathrm{sd})} = \tfrac{1}{2}\left[P_0 + P_1 + P_{0\mathrm{D}} + P_{1\mathrm{D}} - (P_0+P_1)(P_{1\mathrm{D}}+P_{0\mathrm{D}})\right]. \end{aligned} \tag{5.15}$$

$$\begin{aligned} &\mathrm{If}\,\gamma_{0\mathrm{D}} > \gamma_{1\mathrm{D}}, \mathrm{then} \\ &\qquad \mathrm{ABER}_{(\mathrm{sd})} = \tfrac{1}{2}\left[1.5\,P_0 + 0.5\,P_1 + P_{0\mathrm{D}} + P_{1\mathrm{D}} - (P_0+P_1)(P_{0\mathrm{D}}+P_{1\mathrm{D}})\right] \\ &\qquad\qquad - \tfrac{1}{2}\left[P_0\,P_1\,(P_{0\mathrm{D}}+P_{1\mathrm{D}}) + P_{0\mathrm{D}/1\mathrm{D}}\,(P_1 - P_0)\right]. \end{aligned} \tag{5.16}$$

$$\text{If} \gamma_{0\text{D}} < \gamma_{1\text{D}}, \text{then}$$

$$\begin{aligned} \text{ABER}_{(\text{sd})} &= \tfrac{1}{2}\left[0.5\,P_0 + 1.5\,P_1 + P_{0\text{D}} + P_{1\text{D}} - (P_0 + P_1)\,(P_{0\text{D}} + P_{1\text{D}})\right] \\ &- \tfrac{1}{2}\left[P_0\,P_1\,(P_{0\text{D}} + P_{1\text{D}}) + P_{1\text{D}/0\text{D}}\,(P_0 - P_1)\right]. \end{aligned} \tag{5.17}$$

The accuracy of the analytical expressions vs. the simulations in the high ABER is shown in Fig. 5.9. The ABER performance of DSM can now be compared to that of Dh-SM.

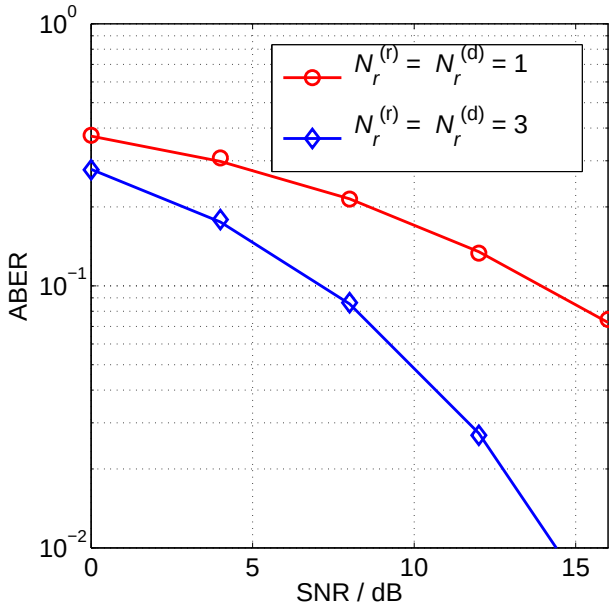

Figure 5.9: *Simulation vs. analytic prediction for DSM.* $N_t^{(s)} = 2$, $N_t^{(r)} = 1$, $N_u = 2$ *and a varying number of receive antennas. The markers denote the simulation results while the solid lines are the analytical predictions. The source to* R_0 *link experiences a* $10\,\text{dB}$ *weaker channel than the presented SNR. The source to* R_1 *link experiences a* $3\,\text{dB}$ *stronger channel than the presented SNR.* R_0 *to the destination link experiences a* $10\,\text{dB}$ *stronger channel than the presented SNR.* R_0 *to the destination link experiences the presented SNR.*

5.6 Comparing Dh-SM and DSM

The aim is to compare the performance of Dh-SM relative to that of DSM. In particular, to define the ratio between the distributed relaying system employing SSK and a fixed node relaying system using SSK. To this extent, Section 5.4 shows that the worst performing link in a relaying scenario becomes the bottleneck for all other communications. Therefore, to ensure a fair comparison between the two systems, the same SNR level at the relay nodes is set, *i.e.*,

$P_{(\mathrm{sr})} = P_0 = P_1$. Furthermore, the probability of error between relay R_0 and the destination in DSM, is assumed equal to the probability of error between the relay and the destination in Dh-SM, *i.e.*, a factor, ζ, such that $P_{(\mathrm{rd})} = P_{0\mathrm{D}} = \zeta P_{1\mathrm{D}}$ is established. With these assumptions,

$$\mathrm{ABER}_{\mathrm{DhSM}} = P_0 + \zeta P_{1\mathrm{D}} - 2\zeta P_0 P_{1\mathrm{D}}, \tag{5.18}$$

and

$$\mathrm{ABER}_{\mathrm{DSM}} = P_0 + \frac{1+\zeta}{2} P_{1\mathrm{D}} - \frac{1+\zeta}{2} P_0 P_{1\mathrm{D}} - \frac{1+\zeta}{2} P_0^2 P_{1\mathrm{D}}. \tag{5.19}$$

In particular, P_0 and $P_{1\mathrm{D}}$ are the ABER of two, point-to-point, SSK systems. In a Rayleigh fading environment, the closed form for each is given by (5.11). In addition, $\zeta = P_{0\mathrm{D}} \,/\, P_{1\mathrm{D}}$ is the ratio of the ABER on the link between relay R_0 to the destination relative to the ABER on the link between relay R_1 to the destination. In effect, ζ is proportional to the ratio of the SNRs on those links, *i.e.*, $\zeta \propto \frac{\gamma_{0\mathrm{D}}}{\gamma_{1\mathrm{D}}}$. This means that ζ is monotonically increasing as either value is varied.

The ratio of $\mathrm{ABER}_{\mathrm{DhSM}}$ relative to $\mathrm{ABER}_{\mathrm{DSM}}$ is given in Fig. 5.10. In particular, the ratio of the ABERs is one for $\zeta > 1$. This proves that Dh-SM performs better than DSM when all relay to destination links in the system experience the same SNR, *i.e.*, $P_{\mathrm{rd}} = P_{0\mathrm{D}} = P_{1\mathrm{D}}$. Indeed, if $\zeta = 1$ in (5.19), it follows that $\mathrm{ABER}_{\mathrm{DhSM}} < \mathrm{ABER}_{\mathrm{DSM}}$. In addition, as ζ increases, a monotonic increase in the performance difference between the two systems can be seen.

The worse performance of DSM can be explained by looking at the error terms that compose its ABER. Indeed, the distributed nodes mean that an incorrectly detected symbol by any node has a greater effect on the overall ABER. In particular, there are conditions which permit either both relay nodes to activate simultaneously or none. When all transmit antennas are on the same node, however, the activation of only a single antenna at any transmitting instance is guaranteed. In addition, the performance difference between the two systems depends on the relative SNRs on the relay to destination links. This means that the applicability of DSM depends on the deployment scenario. On the one hand, DSM lends itself to the creation of self–organising virtual antenna arrays. On the other hand, it performs worse in terms of ABER than Dh-SM.

DSM also requires the use of more RF chains, since every relay node must be capable of broadcasting and every node must have the same number of receive antennas. To this extent, if one node has fewer receive antennas than the rest, it will have a negative influence on the ABER

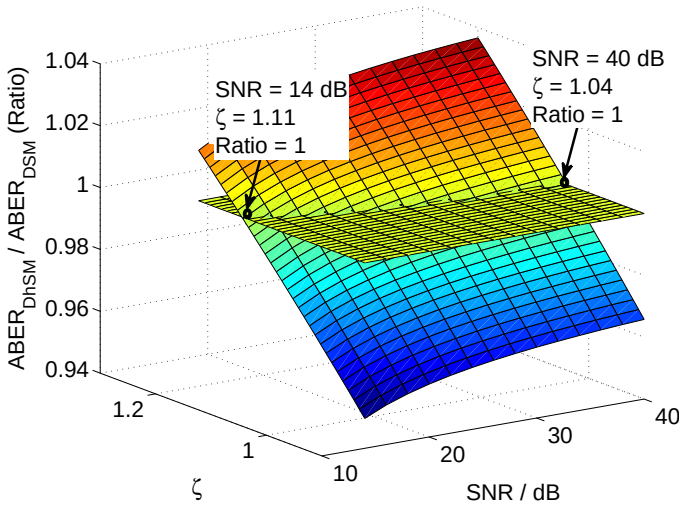

Figure 5.10: *Numerical analysis of the ratio between Dh-SM and DSM, i.e.,* $\mathrm{ABER}_{\mathrm{DhSM}} / \mathrm{ABER}_{\mathrm{DSM}}$, *when* $N_t^{(s)} = 2,\ N_t^{(r)} = 1,\ N_u = 2$ *and* $N_r^{(r)} = N_r^{(d)} = 1$. γ_0 *is the SNR presented. The horizontal plane defines the decision boundary below which the* $\mathrm{ABER}_{\mathrm{DSM}}$ *is smaller than the* $\mathrm{ABER}_{\mathrm{DhSM}}$. *However, this only occurs for* $\zeta > 1$ *which proves that Dh-SM performs better than DSM when all relay to destination links in the system experience the same SNR.*

of DSM. In particular, work in Section 4.4 and Section 5.4, shows that the number of receive antennas plays a key role in determining the ABER performance of any system employing SM by providing both coding and diversity gains. Indeed, the overall system diversity is limited by the minimum number of receive antennas at any receiving node, whether it is a relay or the destination. The influence of the number of receive antennas is also apparent when considering that each term in (5.18) and (5.19) is the ABER of a single link. In addition, by having a single relay node, Dh-SM can better exploit the multiplexing and energy efficient benefits of SM by employing a single transmit RF chain at the relay.

5.7 Summary

In this chapter the application of SM in a dual-hop, non-cooperative scenario was considered. In particular, the spatial domain of Dh-SM was used to transmit extra information bits which help alleviate the multihop burden. Dh-SM was also shown to provide coding gains by lowering the number of bits sent in the signal domain. In addition, the union bound method was used to bound the ABER behaviour of SM and provided an estimate for the potential performance of Dh-SM.

It was demonstrated that the application of SM in a relaying scenario results in better end–to–end system performance when compared to non-cooperative DF. To this extent, the coding gain improved as the number of transmit antennas increased at either the source or relay nodes. The coding gain was also improved when more receive antennas were added at either the relay or destination nodes.

A closed form for the ABER of a two relay node DSM system was derived and verified through simulations. It was shown that the ABER of DSM was governed by the ABER on the weakest link in terms of the SNR. To this extent, its performance was influenced by the number of receive antennas at each relay. In particular, the number of receive antennas at each node should have been the same to allow the system to take full advantage of SM. If this was not the case, then the system experienced a bottleneck as the worst performing link dominated the source to destination ABERby limiting the overall diversity in the system.

Furthermore, DSM was shown to perform worse in terms of the ABER when compared to Dh-SM. In fact, Dh-SM exhibited a better ABER performance than DSM if the same source to relay SNR was assumed. In particular, a single relay node removed two erroneous events which were possible in DSM and improved the source to destination ABER of Dh-SM. In addition, the energy consumption and cost of employing a single RF chain for transmission make Dh-SM a more suitable candidate for relaying systems.

Having analysed the application and performance of SM in the relaying scenario, the practical implementation of a SM system is now considered in Chapter 6.

Chapter 6

Practical Implementation of Spatial Modulation

6.1 Introduction

The performance of spatial modulation (SM) has been analysed in a variety of scenarios thus far. In Chapter 3, a novel method that permits the transmitter to be equipped with an arbitrary number of transmit antennas is proposed. In Chapter 4, SM is deployed in the multi-user, interference limited, environment. In particular, a maximum likelihood (ML) detector is proposed and the system employing SM is shown to perform better than the *cost and complexity* equivalent SIMO system. In Chapter 5, the average bit error ratio (ABER) of SM in the relaying scenario with both fixed and distributed relaying nodes is discussed. Along with other theoretical work done in the field and discussed in Section 2.4.2, SM is shown as a viable candidate for future wireless networks. Despite the generated interest in SM, however, there is no practical implementation to prove that SM behaves as predicted in the literature.

This work is part of a larger project that aims to demonstrate SM as a candidate fourth generation (4G) transmission technique capable of providing energy efficient high speed data transfer. To this extent, parts of the digital signal processing algorithms were developed jointly with Dr. Read Mesleh and Mr. Abdelhamid Younis. In addition, the data used to obtain the channel statistics was collected by Dr. Pat Chambers as part of the Beyond 4G, UK-China Bridges project. In this chapter, the performance of SM in an experimental environment is presented for the first time in the world.

The remainder of this chapter is organised as follows. The system set-up, equipment, digital signal processing and channel characteristics are presented in Section 6.2. The equipment constraints are then considered in Section 6.3 while the analytical modelling is discussed in Section 6.4. The performance of SM is then characterised in the experimental and simulation environments in Section 6.5. Lastly, the chapter is summarised in Section 6.6.

6.2 System Set-up and Transmission

The system set-up and transmission chain, from the generation of the binary information to its recovery, are explained in this section. Fig. 6.1 shows the data encoding and decoding chain.

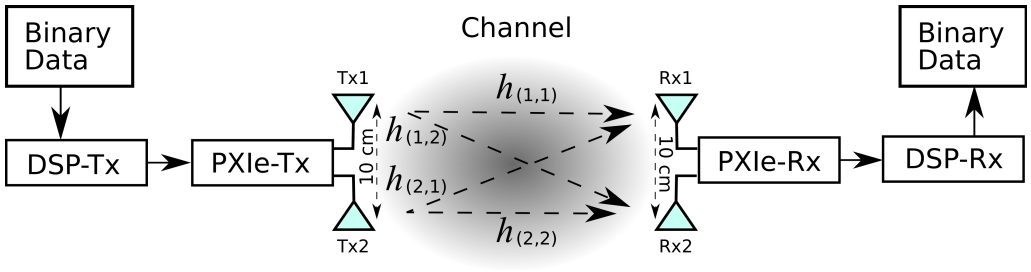

Figure 6.1: *Block sequence of the main steps in the experiment, from the generation of the binary data to its recovery.*

The binary data to be broadcast is first passed through the digital signal processing algorithm at the transmitter, (DSP–Tx). The processed data is then passed to the physical transmitter on the National Instruments (NI)-PXIe chassis, (PXIe–Tx). Each of the transmit antennas ('Tx1' and 'Tx2') are then activated according to the SM principles at a carrier frequency of 2.3 GHz. The

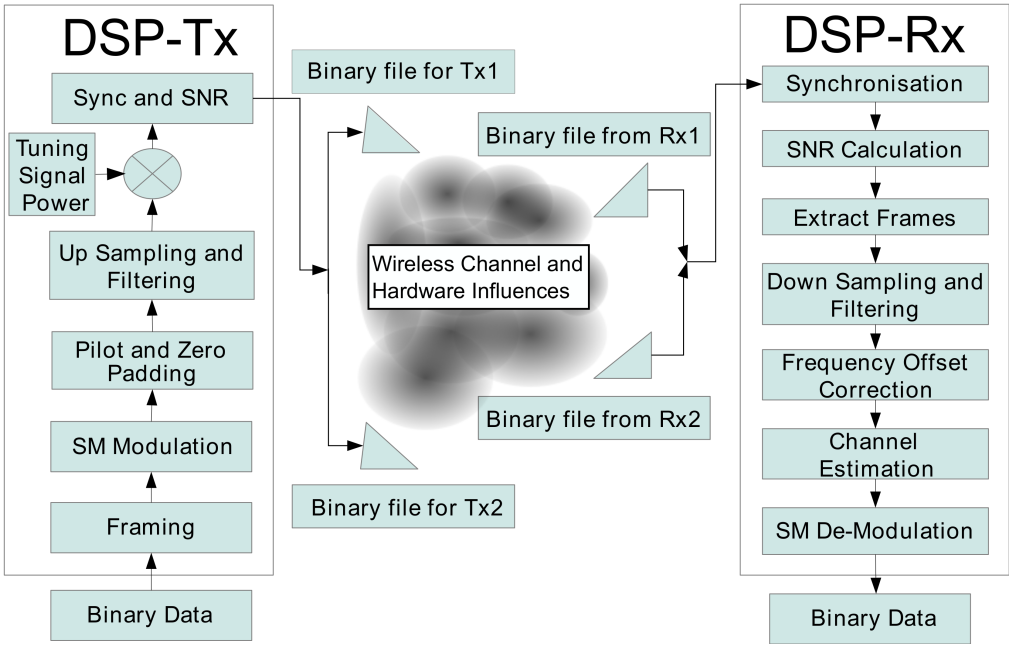

Figure 6.2: *Binary data encoder (DSP–Tx) and decoder (DSP–Rx) algorithms for SM.*

data is received after passing through the channel. In particular, $h_{(n_t,r)}$ is the fast fading channel coefficient on the link between transmit antenna, n_t, and receive antenna, r. The receiver then

detects and processes the radio frequency (RF) signal in PXIe–Rx. Lastly, the receive side digital signal processing algorithm (DSP–Rx) recovers the original data stream. To this extent, Fig. 6.2 is a more detailed layout of the DSP–Tx and DSP–Rx algorithms where the relevant information is labelled as 'Binary Data'. The experiment is performed in a room environment with a line of sight (LoS) between the transmit and receive antennas. Fig. 6.3 shows the exact geometry of the experiment in terms of the relative antenna spacing.

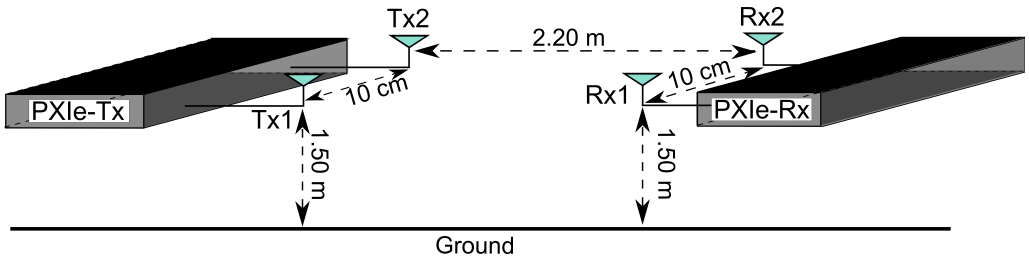

Figure 6.3: *Physical experimental layout: A pair of receive and a pair of transmit antennas are set* $2.2\,\mathrm{m}$ *apart from each other with a direct line of sight. Each pair of antennas is* $1.5\,\mathrm{m}$ *from the ground and there is a* $10\,\mathrm{cm}$ *spacing between the antennas in a pair corresponding to* 0.77 *times the wavelength at* $2.3\ \mathrm{GHz}$*. All antennas are omnidirectional.*

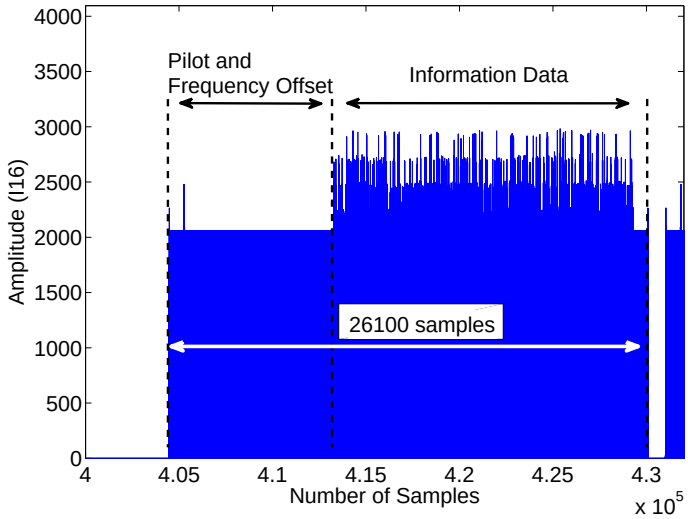

Figure 6.4: *The absolute value representation of a single frame from the vector being transmitted by* $\mathrm{Tx1}$ *in the* $\mathrm{I16}$ *data format which is a signed* 15 *bit representation of an integer number. Each frame is composed of the pilot and frequency offset estimation along with the information data section. Each frame has at most* 26100 *samples.*

6.2.1 Digital Signal Processing for Transmission (DSP–Tx)

As seen in Fig. 6.2, the binary data is first split into information segments of the appropriate size. The information data in each segment is then modulated using SM. A pilot signal used for channel estimation is then added, along with a frequency offset estimation section. In addition, zero-padding is performed which permits up-sampling of the data while maintaining the same signal power. The up-sampling ratio is set to four and the up-sampled data is then passed through a root raised cosine (RRC) finite impulse response (FIR) filter with 40 taps and a roll-off factor of 0.75. A large roll-off factor and a long tap-delay are necessary to ensure that the power is focused in a short time, *i.e.*, ensure that only a single RF chain is active. In addition,

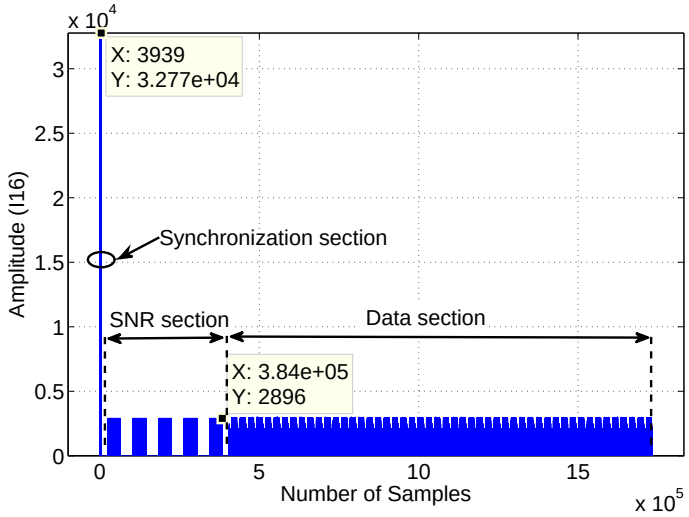

Figure 6.5: *The absolute value representation of the transmission vector being sent to* $\mathrm{Tx1}$. *The synchronisation, SNR estimation and data sections are shown. The value of the peak must equal* 2^{15} *since the digitiser operates using an* $\mathrm{I16}$ *format before tuning the data signal power. The highest value in the SNR section is the same as the highest value in the information data section. There is approximately a* $21.1\,\mathrm{dB}$ *difference between the peak power in the synchronisation section and the peak power in the SNR estimation and data sections. This is apparent when looking at the two data points shown in the figure.*

the resulting vector is multiplied with a factor labelled 'Tuning Signal Power' in Fig. 6.2 to obtain the desired transmit power for the information sequence.

Frames are created such that the frame length multiplied by the sampling rate is less than the coherence time of the channel which is typically $\approx 7\ \mathrm{ms}$ for a stationary indoor environment [36]. This ensures that all channel estimations at the receiver are valid for the frame duration. A frame includes the frequency offset estimation sequence, the pilot and up-sampled data se-

quences, as shown in Fig. 6.4 where the vertical scale shows the I16 symbol amplitude versus the sample number. To this extent, the 'Data section' in Fig. 6.5 is formed from a series of concatenated frames from Fig. 6.4. In particular, the differences between the amplitude of the 'Pilot and Frequency Offset' estimation section and the amplitude of the 'Information Data' section in Fig. 6.4, can be seen in the fine structure of the 'Data section' in Fig. 6.5. Furthermore, sequences of power and no power are then added to the start of the transmission vector, labelled 'SNR section' in Fig. 6.5. Lastly, a transmitter-receiver synchronisation section is added. The synchronisation sequence is formed by a series of maximum power peaks and is labelled as 'Synchronisation section' in Fig. 6.5. To this extent, Fig. 6.5 shows the absolute value representation of the vector that is sent to Tx1. The two transmit vectors are written to binary files that are then broadcast from antennas Tx1 and Tx2 in Fig. 6.3. The methods used to obtain and verify the SNR at the receiver are discussed in Section 6.3.1.

6.2.2 Description of the Transmission Hardware (PXIe–Tx)

The NI-PXIe-1075 chassis is used, which has an on-board Intel-i7 processor operating at 1.8 GHz with $4\,\mathrm{GB}$ of RAM and is shown in Fig. 6.6(a). In addition, the following NI-PXIe modules are used:

- NI-PXIe-5450 I/Q Signal Generator,
  - 400 Mega samples (Ms)/s, 16-Bit I/Q Signal Generator,
  - Dual-channel, differential I/Q signal generation; 512 MB of deep on-board memory, 16-bit resolution, 400 Ms/s sampling rate per channel,
  - ± 0.15 dB flatness to 120 MHz with digital flatness correction; 140 dBc/Hz phase noise density ,
  - -160 dBm/Hz average noise density; 25 ps channel-to-channel skew,
- NI-PXIe-5652 RF Signal Generator,
  - -110 dBc/Hz phase noise at 1 GHz and 10 kHz offset typical,
  - 500 kHz to 6.6 GHz frequency range,
  - Typically less than 2 ms frequency sweep tuning speed,
- NI-PXIe-5611 intermediate frequency (IF) to carrier RF up-converter.

Initially, the NI-PXIe-5450 is fed the transmit vector from the binary file generated in Matlab by the encoding DSP–Tx algorithm. An example of the transmit vector is illustrated in Fig. 6.5. In particular, the NI-PXIe-5450 performs a linear mapping of the signed 16-bit range to the output power and polarisation, *i.e.*, peak voltage amplitude is assigned to any value equal to 2^{15} and a linear scale of the voltage amplitude down to zero. The output from NI-PXIe-5450 then goes to NI-PXIe-5652 which is connected to the NI-PXIe-5611 card. NI-PXIe-5611 outputs the analogue waveform corresponding to the binary data at a carrier frequency of 2.3 GHz. This completes a single RF chain. Each antenna at the transmitter and receiver contains two quarter–wave dipoles, and one half–wave dipole placed in the middle. All three dipoles are vertically polarised. In addition, each antenna has a peak gain of 7 dBi in the azimuth plane, with an omnidirectional radiation pattern. The 10 cm inter-antenna separation is sufficient to guarantee very low, if any, spatial correlation when broadcasting at 2.3 GHz with a 2.2 m separation between the transmitter and receiver [96].

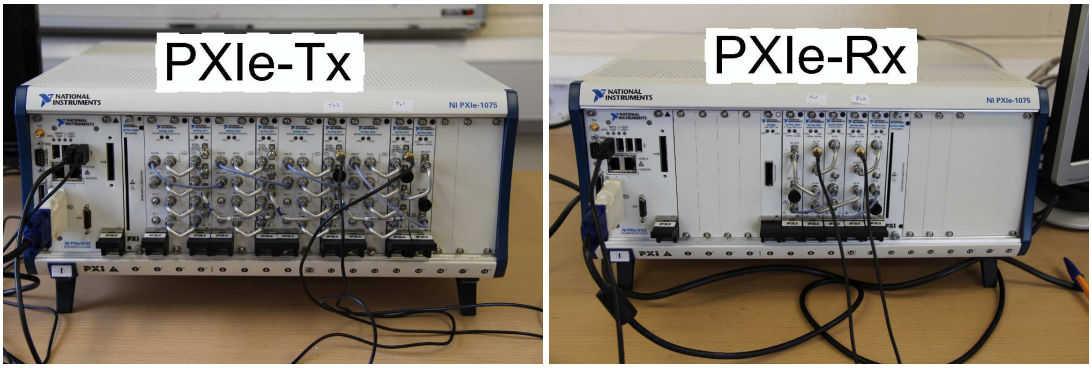

(a) PXIe–Tx (b) PXIe–Rx

Figure 6.6: *NI-PXIe-1075 chassis with the on-board modules used at the transmitter (PXIe–Tx) and at the receiver (PXIe–Rx).*

6.2.3 Propagation Environment (Channel)

The physical layout of the experimental set-up is shown in Fig. 6.7 and the relative antenna spacing is provided in Fig. 6.3. In particular, the two transmit and two receive antennas are identical and are placed directly across each other. As such, the channel between the transmitter and receiver has a strong LoS component. Therefore, the transmitter to receiver channel is defined as a Rician fading channel with a large K-factor due to the distance between the transmit and receive antennas where K is the ratio between the power in the direct path and the power in all other, scattered, paths. In addition, the omnidirectional transmit antennas broad-

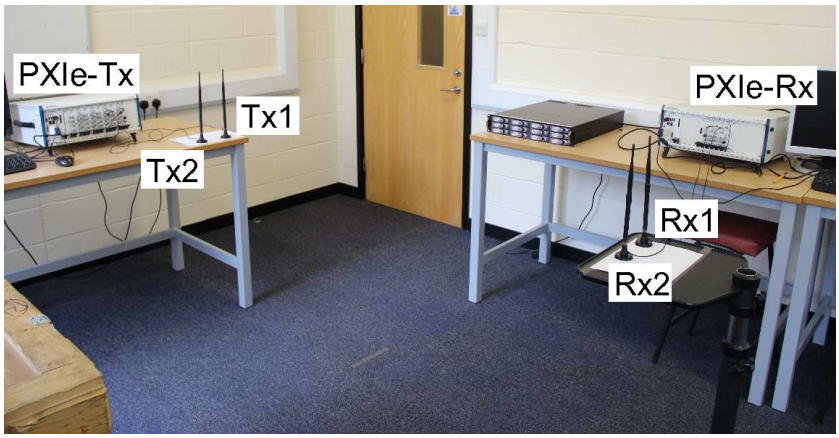

Figure 6.7: *Experimental setup in the laboratory.*

cast on a frequency of 2.3 GHz at 10 Ms/s. It takes 2.61 ms to send 26100 samples at this transmission rate. This duration is much less than the coherence time of a stationary channel in a Rician indoor environment as shown in [36, Section 6.3]. Furthermore, the transmit antennas broadcast at peak voltage amplitude for any value equal to 2^{15} in the transmission vector and a linear scaling of the voltage amplitude down to zero follows.

Several methods for frame synchronisation were tested. In general, these methods are based on using a sequence whose autocorrelation function has a distinct peak marking the sequence [117–119]. However, determining the peak in this fashion is influenced by the channel. The calculated location is typically accurate to within a couple of samples but is not exact, often resulting in off-by-one errors. At present, peak detection is used for synchronisation to avoid the off-by-one errors. To this extent, a large power difference between the synchronisation section and remaining data is necessary. In particular, Fig. 6.5 shows a 21.1 dB power difference between the peak power in the synchronisation sequence and the peak power in the SNR and data sequences. The large power difference is justified when considering that the instantaneous channel power may fluctuate by as much as 20 dB [36, Section 3.5.4]. To guarantee successful peak detection, the power difference between the synchronisation section and the remaining sections must be larger than the maximum channel variation. If this is not the case, no peak may be detected at the receiver and all further decoding would be erroneous.

6.2.4 Description of the Receiver Hardware (PXIe–Rx)

The RF signal at Rx1 and Rx2 in Fig. 6.3 is now received. The NI-PXIe-1075 chassis is again used with an on-board Intel-i7 processor operating at 1.8 GHz with 4 GB of RAM and is shown in Fig. 6.6(b).

The following NI-PXIe modules are used:

- NI-PXIe-5652 on-board reference clock,
- NI-PXIe-5622 16-Bit Digitiser (I16),
  - 150 Ms/s real-time sampling,
  - 3 to 250 MHz band in direct path mode, or 50 MHz bandwidth centred at 187.5 MHz,
- NI-PXIe-5601 RF downconverter.

The receiving antennas are the same as those used for transmission. In particular, the NI-PXIe-5601 is used to detect the analogue RF signal from the antennas. The signal is then sent to the NI-PXIe-5622 IF digitiser. The NI-PXIe-5622 applies its own bandpass filter with a real flat bandwidth equal to $0.4 \times \mathrm{SampleRate}$ [120]. The sampling rate in the experiment is 10 Ms/s which results in a real flat bandwidth of 4 MHz. To this extent, the large bandwidth may result in frequency-selective fading. However, this constraint is not considered since the transmitter and receiver are close enough such that no delayed copies of the transmitted symbol are received, *i.e.*, the channel does not have multiple taps. In addition, detection in SM relies on decoding the spatial and signal symbols jointly since a SM symbol is created by the effects of the channel on the signal symbol. Therefore, if equalisation is applied to a SM symbol, it would remove the channel effects and would effectively result in a step by step detection process which is shown to be sub-optimal [52]. Furthermore, the NI-PXIe-5622 is synchronised with the NI-PXIe-5652 on-board reference clock and writes the received binary files. Indeed, the PXIe–Rx has two RF chains and the described sequence defines a single RF chain. To this extent, the multiple processing cores and multiple NI-PXIe modules enable the simultaneous recording of the two signals coming from Rx1 and Rx2. The recorded binary files are then processed according to 'DSP–Rx' in Fig. 6.2.

6.2.5 Digital Signal Processing for Reception (DSP–Rx)

The binary files recorded by the NI-PXIe-5622 on the PXIe–Rx are converted to Matlab vectors. In particular, a sample received vector detected by PXIe–Rx on Rx1 at an SNR of 30 dB is shown in Fig. 6.8(a). The vectors are then combined to form a received matrix. Furthermore, the DSP–Rx algorithm is applied to each received vector. To this extent, the detector first finds the beginning of the transmitted sequence by using the synchronisation sequence. The SNR is then calculated using the 'SNR section' in Fig. 6.5. After the SNR for that vector has been determined, each vector is decomposed into its underlying frames. Each frame is then down-sampled and passed through the RRC filter which completes the matched-filtering. In addition, frequency offset estimation, timing recovery and correction of each frame follows and is performed according to [121]. The pilot signal is then used for channel estimation. The remaining data, along with the estimated channels, is finally used to recover an estimated binary sequence.

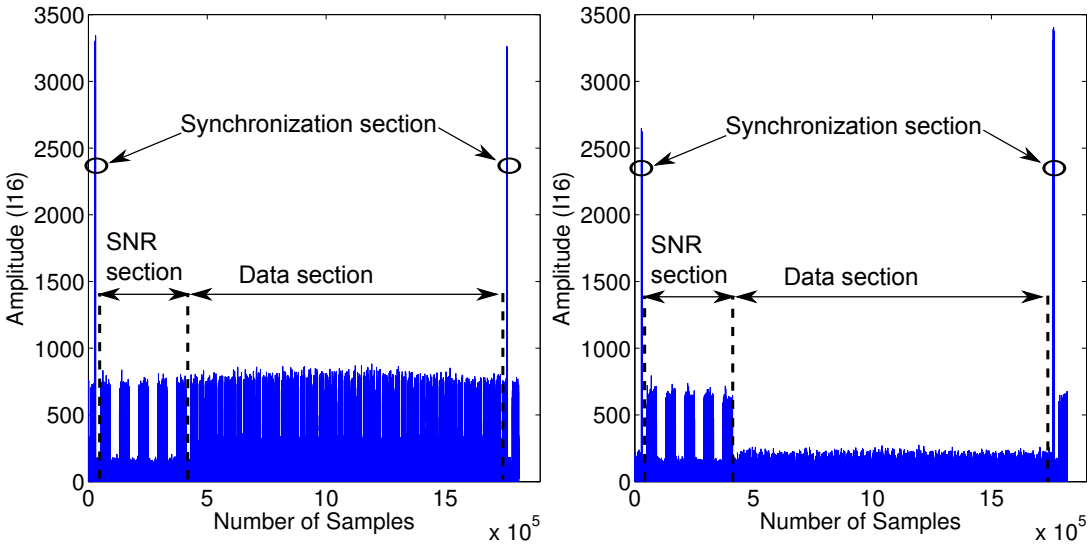

(a) $\mathrm{SNR} = 30\,\mathrm{dB}$ (b) $\mathrm{SNR} = 14\,\mathrm{dB}$

Figure 6.8: *The absolute value representation of the received vector from PXIe–Rx on* $\mathrm{Rx1}$ *at varying SNRs.*

6.3 Equipment Constraints

Starting from the system model in Section 6.2, the equipment constraints are considered.

6.3.1 Verification of the SNR

Obtaining the correct SNR for each received vector, is the first step to validating the experimental results. In particular, an SNR estimation section is added before the information data frames since a practical system has multiple sources of noise. These could be additive white Gaussian noise (AWGN) at the receive antennas, AWGN at the digitiser and filter, rounding errors caused by conversion to and from the I16 format which is the signed 15 bit representation of an integer number, and others. To this extent, incorporating an estimation sequence in the received vector permits a more exact verification of the SNR. Indeed, calculating the average SNR in this manner permits the use of the 'Tuning Signal Power' constant in Fig. 6.2. With this, the amplitude of the information data is changed such that the desired SNR is obtained. In addition, Fig. 6.8(b) shows the absolute value representation of the received vector from PXIe–Rx on Rx1 at an average SNR of 14 dB. The difference in the amplitude of the data section is evident when comparing Fig. 6.8(a) with Fig. 6.8(b). In particular, the 'Tuning Signal Power' constant does not effect the power of the sequence used for SNR estimation or the power of the synchronisation sequence. To this extent, the stationary environment means that the estimated average SNR is valid for the duration of the following data vector transmission.

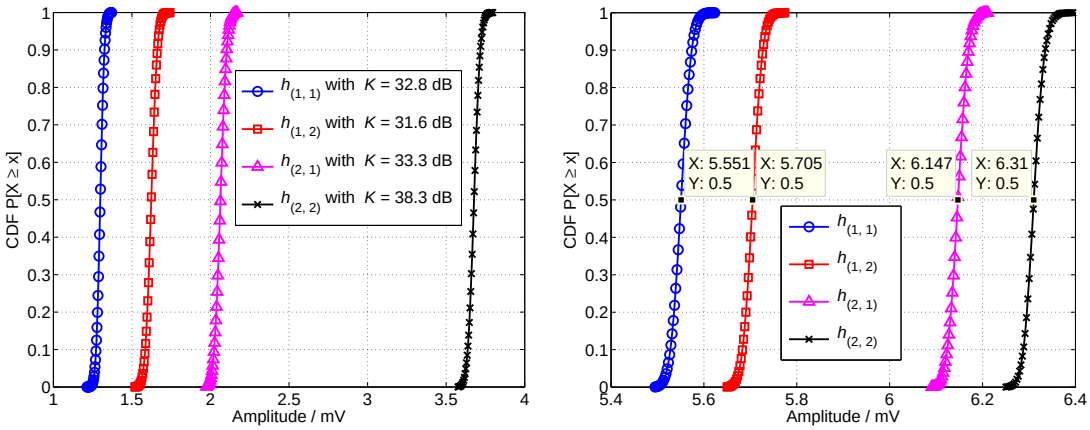

(a) The wireless channel is measured between the transmit and receive antennas.

(b) A coaxial cable with a loss of 10 dB is connected between the transmit and receive antennas.

Figure 6.9: *CDFs for each of the fast fading coefficients, $h_{(n_t,r)}$, of the four channels in the experiment. Each is defined by a Rician distribution with a unique K-factor. The markers denote the measurement points while the lines denote the best fit approximation. Note that the wireless channel mean values fall in the range of* 1.3 mV *to* 3.6 mV, *while the direct connections are in the reduced range of* 5.5 mV *to* 6.3 mV.

6.3.2 Wireless Channel

The Rician fading environment between the transmit and receive antennas is described in Section 6.2.3. To this extent, channel measurements were collected to verify this claim. In particular, the transmitter is broadcasting pulses at 10 Ms/s on a carrier frequency of 2.3 GHz at 4 dBm peak power. Each pulse includes a frequency offset estimation section and a total of 10^5 pulse samples were collected. A best fit approximation is then calculated for the collected data. In particular, a maximum likelihood estimation is fitted to the collected data. A Chi-squared goodness-of-fit test is then performed to ascertain that the distribution resulting from the maximum likelihood estimation fits at least 95% of the data. To this extent, the empirical CDF for each link is presented in Fig. 6.9(a). Indeed, the different K-factors on the links between the transmit and receive antennas could be explained by the room geometry, the antenna positioning and the overall propagation environment. However, note that each of the CDFs has a different mean.

6.3.3 Wireline Channel

If the transmitter RF chains are identical to each other and the receiver RF chains are identical to each other, there should be no differences between the means of the CDFs. In particular, any difference in the means should be due to the propagation environment. To verify this claim, a coaxial cable with a 10 dB pathloss is connected from each transmit to each receive antenna. The transmitter is again broadcasting at 10 Ms/s on a carrier frequency of 2.3 GHz at 4 dBm peak power. However, Fig. 6.9(b) shows that each channel still exhibits a unique mean, even though the same coaxial cable is connected between the transmit and receive antennas. This empirical result shows that the RF chains are not identical. Indeed, each component used in the manufacture of a single RF chain has variations and tolerances depending on the operating characteristics such as the operating temperature, frequency range, power range, etc. These tolerances effect the performance of the RF chain and make each one unique.

6.4 Analytical Modeling

An analytical model for the ABER performance of the experimental system is developed by considering the system model presented in Section 6.2 and the system constraints in Section 6.3. In particular, (6.1) characterises the performance of SM over a single link in a noise-limited

scenario where (6.2) defines the pairwise error probability (PEP) for an arbitrary channel distribution and an arbitrary signal symbol constellation [53].

$$\text{ABER} \leq \sum_{\substack{x, n_t, \\ \hat{x}, \hat{n}_t}}^{MN_t} \frac{d(x, n_t, \hat{x}, \hat{n}_t)}{\log_2(MN_t)} \frac{\text{E}_{\mathcal{H}}\left[\text{PEP}\left(x,\, n_t,\, \hat{x},\, \hat{n}_t\right)\right]}{MN_t}, \tag{6.1}$$

where $d(x, n_t, \hat{x}, \hat{n}_t) = d(n_t, \hat{n}_t) + d(x, \hat{x})$, where $d(\cdot, \hat{\cdot})$ is the Hamming distance between the binary represention of two symbol coming from the same set and

$$\text{PEP}\left(x,\, n_t,\, \hat{x},\, \hat{n}_t\right) = Q\left(\sqrt{\gamma_{\text{ex}} \left|\left|\mathbf{h}_{n_t} x - \mathbf{h}_{\hat{n}_t}\hat{x}\right|\right|^2}\right) \quad \text{where} \quad \gamma_{\text{ex}} = \frac{E_m}{2N_0}, \tag{6.2}$$

such that γ_{ex} represents half of the SNR between the transmitter and receiver. In addition, $\text{E}_{\mathcal{H}}[\cdot]$ is the expectation across the channel $\mathcal{H}$ and $Q(\omega) = \frac{1}{\sqrt{2\pi}} \int_{\omega}^{\infty} \exp\left(-\frac{t^2}{2}\right) \text{dt}$ defines the Q-function. As Fig. 6.3 indicates, the transmit and receive antennas in the experiment experience a very strong LoS environment. Accordingly, the channel between each transmit to receive antenna pair is characterised by Rician fading as discussed in Section 6.3.2. A generic Rician channel is defined as

$$h_{(n_t,r)} = \sqrt{\frac{K}{1+K}} \exp(-j\vartheta 2\pi) + \sqrt{\frac{1}{1+K}} \widetilde{h}_{(n_t,r)}, \tag{6.3}$$

where K is the ratio of the coherent power component, usually the direct path, to the non-coherent power components, usually scattered paths, $\widetilde{h}_{(n_t,r)} \sim \mathcal{CN}(0,1)$ is a complex normal, circular symmetric random variable with zero mean and unit variance, ϑ is the phase angle of the coherent power component, $n_t \in \{1, 2\}$ is the index of the transmit antenna and $r \in \{1, 2\}$ is the index of the receive antenna.

SM relies on the ability of the receiver to distinguish the channels from each of the transmit antennas. To this extent, a strong LoS environment is detrimental to the performance of SM if all link pairs experience the same pathloss. However, the channel $h_{(n_t,r)}$ is not defined purely by the physical environment. In fact, $h_{(n_t,r)}$ is the channel from the moment the binary file is read by NI-PXIe-5450, to the moment the received binary file is written by NI-PXIe-5622. This means there may be a power imbalance (PI) between the various link pairs in the channel matrix $\mathcal{H}$ coming from connector losses, differences in the RF chains, different phase responses, attenuations and similar. Some of these effects are demonstrated in Fig. 6.9(b)

and are discussed in Section 6.3.3. To account for these imbalances, the fast fading channel coefficients are redefined as

$$h_{(n_t,r)} = \sqrt{\alpha_{(n_t,r)}} \left[\sqrt{\frac{K}{1+K}} + \sqrt{\frac{1}{1+K}} \widetilde{h}_{(n_t,r)} \right], \tag{6.4}$$

where $\alpha_{(n_t,r)}$ is the channel attenuation coefficient from antenna n_t to antenna r. To this extent, the relative PIs between the various channels can be approximated by looking at the relative means of the CDFs presented in Fig. 6.9(b). Indeed, taking the SNR on $h_{(1,1)}$ as the basis, the different $\alpha_{(n_t,r)}$ factors can be calculated by using the voltage values shown in Fig. 6.9(b). In particular, the PI factors are given as

$$\alpha_{(1,1)} = 0\,\text{dB}, \qquad \alpha_{(1,2)} = 0.25\,\text{dB}, \qquad \alpha_{(2,1)} = 0.88\,\text{dB}, \qquad \alpha_{(2,2)} = 1.1\,\text{dB}. \tag{6.5}$$

The experimental and simulation results are now discussed.

6.5 Experimental Results and Numerical Analysis

A stream of 10^5 information bits is sent per transmission to obtain the experimental results. The information data is put in 50, 2000 bit frames as shown by the fine detail in the Data section of Fig. 6.5. In particular, the channel is estimated at the beginning and the end of every frame, resulting in 100 channel estimations per transmission. In addition, the experiment is repeated 400 times for every SNR point. Lastly, analytical and simulation ABER curves are shown for SM in a Rician environment with and without the PIs given in (6.5).

The experimental results approximate the performance of the simulation results with PIs, as illustrated in Fig. 6.10. In addition, both the simulation and experimental results are closely approximated by the derived upper bound at low ABER. This result serves to validate theoretical work done in the field. In particular, the presented SNR is equivalent to the SNR on $h_{(1,1)}$. Furthermore, the large error between the experimental, simulation and analytical curves at high ABER can be attributed to a number of factors including incorrect frequency offset estimation, timing recovery errors, synchronisation problems, poor channel estimation and decoding. Notably, incorrect frequency offset estimation can result in a systematic error contributing significantly to the 30% error seen at low SNRs in the figure. As the SNR increases, however, frequency offset estimation, timing recovery and channel estimation improve, leading to a lower

ABER as shown in Fig. 6.10. Unfortunately, the acquired data does not result in a smooth performance curve. In particular, deviations from the general trend can be seen at SNRs values of 22 dB as well as 29 dB. These deviations may be caused by insufficient data at these points or changes in the channel environment. Nonetheless, if more experimental data is acquired, these deviations would be removed.

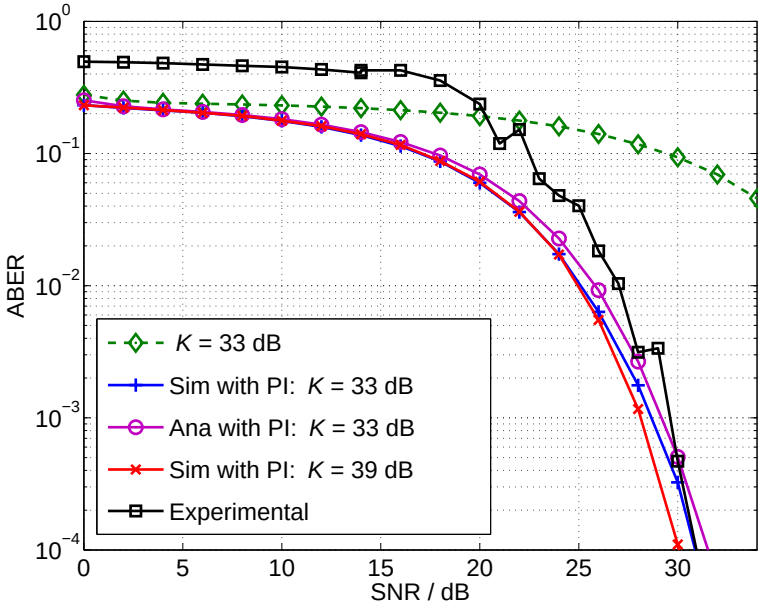

Figure 6.10: *ABER for SM in an experimental set-up with* 2 *transmit antennas,* 2 *receive antennas and a spectral efficiency of* $2\,\mathrm{bits/s/Hz}$*. The SNR is set as measured on* $h_{(1,1)}$ *with* $\alpha_{(1,1)} = 0\,\mathrm{dB}$*. The green diamond markers denote simulation results with no power imbalance (PI) between the links while the green dashed line is the analytical prediction. The remaining curves denote the simulation and analytical results where the black curve is denotes the experimental results.*

SM performs best in a rich scattering environment where the channel between each transmit and each receive antenna is unique. In particular, the larger the Euclidian distance between two received vectors is, the better the performance of SM becomes. Conversely, the more similar the channels are, the worse the ABER of SM is. However, the channel uniqueness can be the result of the scattering environment or PIs caused by hardware tolerances. To this extent, the analytical and simulation results presented in Fig. 6.10 show the poor performance of SM in a Rician environment with no PI between the various links. Fig. 6.10 also shows the analytical and simulation ABER for SM when PI are introduced. Indeed, the ABER of SM improves significantly when these PI are introduced as each channel becomes more separable from the remaining. This increases the Euclidian distance and improves performance.

The impact of this PI is clear when comparing the simulation results for a Rician fading environment with $K = 33$ dB and $K = 39$ dB. In particular, the ABER of the system reduces by around 1 dB at an ABER of 10^{-4} even when K is increased by 6 dB. This is because as K increases, the Rician distribution becomes more concatenated around the mean power and the PIs introduced by the hardware tolerances make each distribution more distinct. To this extent, the experimental results show that hardware imperfections and tolerances aid the performance of SM.

This work demonstrates that the hardware tolerances of practical communication systems are beneficial for the ABER performance of SM. This behaviour makes SM a viable candidate for future wireless networks.

6.6 Summary

In this chapter, the ABER performance of SM was validated experimentally for the first time in the world. In particular, the encoding and decoding algorithms were presented. The experimental set-up, equipment and channel conditions were then described in detail and the receiver operating curve was obtained in a practical testbed environment. In addition, the experimental results were compared to both simulation and analytical expectations. Indeed, it was shown that a Rician channel with different channel attenuations closely described the behaviour of SM in the physical environment. Furthermore, it was demonstrated that the different channel attenuations came from various hardware tolerances in both the transmitter and receiver RF chains. In fact, the induced power imbalances resulted in significant coding gains for the practical SM system relative to the theoretical ABER without such power imbalances. To this extent, SM performed as expected relative to the theoretical work when the power imbalances were introduced in the analytical model. This result validated the SM principles. The performance gains exhibited by SM in the practical implementation as a result of the hardware tolerances make SM a viable candidate for future wireless networks.

Chapter 7

Conclusions, Limitations and Further Research

7.1 Summary and Conclusions

The background for the undertaken research was introduced in Chapter 2. To this extent, a brief history of wireless communication systems was presented. The evolution of radio and mobile communication systems was then considered, starting from the earliest experiments by Hertz, Tesla and Marconi, to the implementation of the frequency reuse concept proposed by Bell Telephone Laboratories and widely accepted in the Global System for Mobile Communications (GSMC) networks. In addition, the growing global integration in terms of the 3^{rd} Generation Partnership Project (3GPP) and Long-Term Evolution Advanced (LTE-A) collaboration projects was presented. In particular, the demand for higher data rates was shown as a driving force for the development and deployment of multiple–input multiple–output (MIMO) systems. Furthermore, a basic description of the wireless channel was established and its influence on MIMO systems was discussed. Additionally, the operating principles of MIMO communications, along with the advantages and perceived disadvantages were elaborated. A possible solution to the perceived disadvantages was presented in the form of the spatial modulation (SM) concept. In particular, the advantages of SM relative to other MIMO techniques, along with its limitations, were examined. The chapter concluded with the motivation for the extensions of the SM concept and the need for its practical implementation.

In an attempt to remove the limitation on the number of transmit antennas, a novel and more versatile SM scheme, called fractional bit encoded spatial modulation (FBE–SM), was introduced in Chapter 3. The theory of modulus conversion was discussed and its application to SM was presented. To this extent, it allowed any SM wireless system to use an arbitrary number of antennas at the transmitter. On the one hand, numerical results showed that classic SM systems exhibited better performance in terms of the average bit error ratio (ABER) when compared to systems employing FBE–SM in an uncorrelated Rayleigh fading environment. On

the other hand, FBE–SM provided better performance when spatial correlation was introduced, despite suffering from error propagation. Various alternative techniques to FBE–SM, such as generalised spatial modulation (GSM), space-time block codes (STBC)–SM, and multiple active (MA)–SM were then discussed. In particular, the operating principles and advantages of each system were explored. Each alternative, however, required the activation of multiple transmit antennas. This introduced the problems of inter–channel interference (ICI), inter–antenna interference (IAI) and multiple radio frequency (RF) chains. By employing FBE–SM, one of the fundamental challenges to the practical deployment of SM was removed while retaining the essential advantages over other MIMO systems such as avoiding ICI, no IAI, the requirement for a single RF chain and better energy efficiency. To this extent, FBE–SM was shown as a viable candidate for the design of green and compact mobile devices employing SM.

The performance of SM in the interference limited scenario was investigated in Chapter 4. Two maximum likelihood (ML) detectors for use with SM were discussed. The first, interference-unaware detector, was defined and studied in the limit as the signal-to-interference-plus-noise-ratio (SINR) approached infinity. To this extent, a closed form solution for the upper bound of the system was provided and its performance in the Rayleigh fading environment was considered. In particular, the exact coding gains of SM using variable and constant amplitude modulation schemes relative to a SIMO system using quadrature amplitude modulation (QAM) in the noise limited scenario were defined. In fact, the interference-unaware detector was shown to reach an error floor depending on the SINR. In addition, the number of receive antennas was shown as a key component for the ABER performance of the system. Indeed, the addition of a single receive antenna resulted in greater coding gains than reducing the interference by more than 10 dB at high signal-to-noise-ratio (SNR). A second, interference-aware ML detector, was proposed and a closed form solution for the upper bound of the system was provided. In addition to avoiding the error floor present in the interference-unaware detector, the jointly optimal detector mimicked a noise limited scenario for the detection of all transmitted streams, *i.e.*, an arbitrarily small ABER could be obtained by any node for a sufficiently high SNR. Furthermore, the number of receive antennas was again shown to have a greater influence on the ABER performance of the system when compared with the number of transmit antennas. Although more computationally complex than the interference-unaware detector, the interference-aware detector guaranteed that the system does not reach an error floor. Lastly, the interference-aware detector enabled SM to perform better in terms of ABER than the complexity and cost equivalent multi-user MIMO system in an interference limited environment.

The application of SM in a dual-hop, non-cooperative scenario was considered in Chapter 5. To this extent, extra information bits were sent using the spatial constellation of SM which helped alleviate the multihop burden. In addition, dual-hop spatial modulation (Dh-SM) exhibited coding gains relative to the non-cooperative decode and forward (DF) system in a Rayleigh fading scenario by employing SM on the source to relay and relay to destination links. Furthermore, an upper bound for the source to destination ABER of Dh-SM was derived. The upper bound was shown to be asymptotically tight at low ABER. On the one hand, the coding gains of Dh-SM relative to DF increased as the number of transmit antennas was increased at the source or relay nodes. On the other hand, the coding gains also increased as more receive antennas were added at the relay or destination nodes. Indeed, it was demonstrated that SM could be implemented in a relaying scenario with tangible energy efficiency and coding gains relative to the non-cooperative DF algorithm. SM was also applied to a system with distributed relaying nodes. To this extent, it was shown that the source to destination ABER of distributed spatial modulation (DSM) was governed by the ABER of the node with the weakest SNR. To avoid bottlenecks, the number of receive antennas on each of the distributed nodes in DSM needed to be the same. If this was not the case, the worse performing link in terms of the ABER dominated the source to destination ABER. If the same source to relay and relay to destination SNR was assumed, Dh-SM exhibited a better performance than DSM because a single relay node removed two erroneous events which were possible when using multiple distributed relaying nodes. In addition, Dh-SM showed better energy efficiency by employing a single transmit RF chain at the single relaying node when compared to the multiple transmit RF chains required for the distributed nodes.

Finally, the ABER performance of SM was experimentally validated in Chapter 6. To this extent, the digital signal processing algorithms for the transmitter and receiver were discussed, the experimental setup and equipment were considered, and the empirical characteristics of the wireless channel were presented along with the equipment constraints. In particular, a Rician fading channel with different channel attenuations between each transmit to each receive antenna closely emulated the physical environment. Furthermore, the experimental ABER performance was compared to both simulation and analytical expectations. All three results were a close match and validated the expected theoretical performance of SM. Indeed, the power imbalances between the various links improved the ABER performance of SM. In addition, the power imbalances were not specifically design but were the results of hardware tolerances. To this extent, SM was shown to be particularly apt for practical implementation since hardware

tolerances are an inevitable part of real world systems.

Several aspects that constrained the deployment of SM in a practical scenario have been addressed in this thesis. The limitation on the number of transmit antennas was removed, the performance of SM in an interference limited scenario was considered, the possible extension and coding gains of applying SM in a relaying scenario were defined and SM was proven to be particularly suitable for deployment in a real world scenario. The energy efficiency of SM, along with other advantages over classical MIMO system, make SM a viable candidate for the next generation of wireless networks.

7.2 Limitations and Scope for Further Research

Despite the significant work done in SM and the extensions provided in this thesis, a number of fundamental limitations remain to be considered which constrain the deployment of SM in a practical system.

Along with much of the theoretical work in SM, much of the work in this thesis assumes full channel state information (CSI) at the receiver. Although this is not a practical assumption, the CSI may be obtained via rapid channel estimation at the receiver. Nonetheless, this would pose complexity constraints on the channel estimation algorithm as $N_r \times N_t$ number of channels must be estimated at each transmission instance. In some mobile scenarios, however, the channel may fluctuate so quickly that practical channel estimation becomes impossible. Indeed, initial results for systems with partial CSI are reported in [17], where the ABER performance of SM exhibits significant coding loss. To this extent, the development of low complexity, rapid and robust channel estimation algorithms is a key area of interest for the practical deployment of SM systems.

In addition to the channel estimation limitations, the detection complexity for the interference aware detector proposed in Chapter 4 is given as $\mathcal{O}\left(\left(MN_t\right)^{N_u}\right)$ which is proven to be NP-complete problem [112]. To this extent, the application of the sphere decoding (SD) techniques proposed in [16] to the interference aware detector may offer a possible solution and merit further investigation.

Another area of interest is the application of SM in an ultra wideband system. Narrowband SM systems consider only a single channel realisation as the channel signature. To this extent,

broadcasting a signal symbol over a wider bandwidth would make each spatial symbol more distinct. A wider bandwidth would also result in a larger Euclidean distance between the spatial symbols and would improve the ABER of the system. The open question is, whether the improved ABER performance justifies the loss in data rate if the bandwidth is used for multiple narrowband transmissions?

Although Dh-SM is shown to have better performance in terms of the ABER when compared to DSM, the performance of a system employing SM with cooperating distributed relay nodes may offer advantages in terms of energy efficiency and the ABER. For a start, the capacity analysis of a cooperative distributed relaying system shows the advantages of employing SM with respect to state-of-the-art solutions [122]. In particular, the spatial encoding process in SM lends itself to the creation and organisation of virtual antenna arrays from distributed nodes. Indeed, the SM principles may be used to avoid overhead in routing protocols and warrant investigation.

Furthermore, the practical implementation of SM in Chapter 6 exemplifies the important role of introducing power imbalances in a SM system. The slight power imbalances significantly improved the ABER of the experimental system. To this extent, opportunistic power allocation may be used to increase the Euclidean distance between the spatial constellation points and improve the ABER. This may be achieved by either providing the transmitter with CSI through feedback or designing the transmitter with inherent differences in the hardware of the RF chains. The optimal method for achieving these results is yet to be determined.

Along with the assumption of full CSI at the receiver, all work in the field considers that the transmitter is equipped with fast switching antennas. Although the experimental results mimic the possible performance of SM with a single RF chain, the hardware transmitter (PXIe–Tx) was equipped with multiple RF chains and the SM principles were maintained by ensuring that only one RF chain was active at any transmission instance. To this extent, fast switching antennas capable of emitting powerful signals are necessary to obtain the true performance of SM in terms of its energy efficiency and capacity bounds. This represents a key concept that must be addressed before SM can be implemented in a high rate practical deployment.

Lastly, the experimental results should be extended to evaluate the ABER of SM in different environments. To this extent, under the collaboration of the UK-China Bridges project, the physical channel should be replaced by a channel emulator. The new results would serve to

analyse the application of SM in a variety of practical scenarios and validate the theoretical predictions.

Appendix A

Additional Derivations for Interference Limited SM

A.1 Derivation of (4.32)

The first element to consider is ψ_1 which corresponds to $\sigma_z^2 = |x^{(\xi)}|^2 + |\hat{x}^{(\xi)}|^2$. For this, σ_z^2 is bound to two, which implies

$$\left(d_\nu^2 + d_{\hat{\nu}}^2\right) g_{\mathrm{QAM}} \leq 2, \tag{A.1}$$

where $\nu \in \{(1,1),(2,1),(3,1)\}$ and d_ν are the distances defined in Fig. A.1 and $g_{\mathrm{QAM}} = \frac{3}{2\left(M^{(\xi)}-1\right)}$. The normalising factor, g_{QAM}, is used to maintain unity power in the constellation and is given in [111]. There are only four possible combinations that satisfy (A.1). In particular:

- $\left(d_{(1,1)}^2 + d_{(1,1)}^2\right) g_{\mathrm{QAM}} = 0.4$, occurs $\left(M^{(\xi)}\right)^2/8 = 32$ times,
- $\left(d_{(1,1)}^2 + d_{(2,1)}^2\right) g_{\mathrm{QAM}} = 1.2$, occurs $\left(M^{(\xi)}\right)^2/4 = 64$ times,
- $\left(d_{(1,1)}^2 + d_{(3,1)}^2\right) g_{\mathrm{QAM}} = 2$, occurs $\left(M^{(\xi)}\right)^2/8 = 32$ times and,
- $\left(d_{(2,1)}^2 + d_{(2,1)}^2\right) g_{\mathrm{QAM}} = 2$, occurs $\left(M^{(\xi)}\right)^2/2 = 128$ times.

These combinations occur for every instance when $n_t \neq \hat{n}_t$. For a system with $N_t^{(\xi)}$ transmit antennas, there are $\binom{N_t^{(\xi)}}{2}$ unique pairings. This leads to

$$\psi_1 = \left((0.4/2)^{-N_r}32 + (1.2/2)^{-N_r}64 + 32 + 128\right)\binom{N_t^{(\xi)}}{2}. \tag{A.2}$$

Having established the derivation of ψ_1, ψ_2, defined as $\sigma_z^2 = |x^{(\xi)} - \hat{x}^{(\xi)}|^2$, must be obtained. Looking at Fig. A.1, there are additional combinations aside from the ones denoted. To this extent, $\sigma_z^2 = \min\{\sigma_z^2, 2\}$ serves to simplify the counting and sets many of them to 2. In particular, when $\sigma_z^2 = d_{(5,2)}^2$, then $\sigma_z^2 > 2$. In this case, σ_z^2 is bound to 2 and $d_{(4,2)}$ is the largest

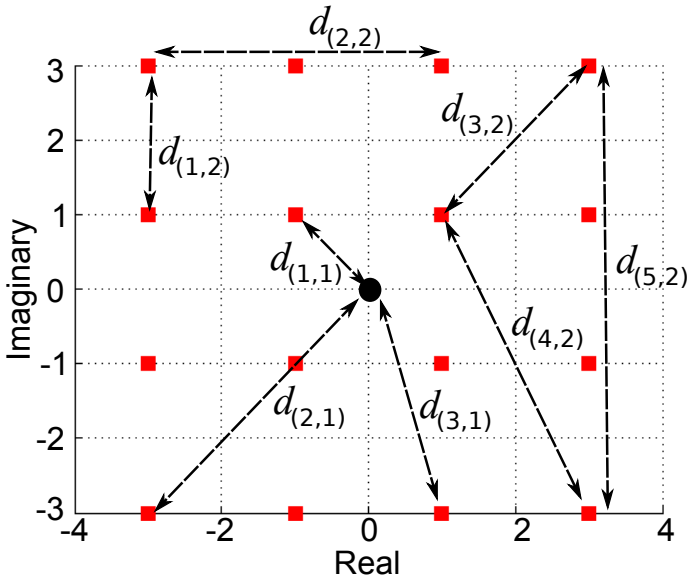

Figure A.1: *The red squares denote* 16*-QAM constellation points. The illustrated constellation is not normalised. The figure shows possible distance combinations between each of the constellation points and their distances to the origin in* 16*-QAM.*

distance that must be accounted for in the expectation analysis. This approach is applicable to larger constellation sizes and for a given constellation size of $M^{(\xi)}$:

- $d_{(1,2)}$ occurs a total of $D^{(1)} = 4\sqrt{M^{(\xi)}}\left(\sqrt{M^{(\xi)}} - 1\right)$ times,
- $d_{(2,2)}$ occurs a total of $D^{(2)} = 4\sqrt{M^{(\xi)}}\left(\sqrt{M^{(\xi)}} - 2\right)$ times,
- $d_{(3,2)}$ occurs a total of $D^{(3)} = 4\left(\sqrt{M^{(\xi)}} - 1\right)\left(\sqrt{M^{(\xi)}} - 1\right)$ times and,
- $d_{(4,2)}$ occurs a total of $D^{(4)} = 8\left(\sqrt{M^{(\xi)}} - 1\right)\left(\sqrt{M^{(\xi)}} - 2\right)$ times.

By looking at Fig. A.1, for $M^{(\xi)} = 16$:

- $d^2_{(1,2)}\, g_{\mathrm{QAM}} = 0.4$, occurs exactly 48 times,
- $d^2_{(2,2)}\, g_{\mathrm{QAM}} = 1.6$, occurs exactly 32 times,
- $d^2_{(3,2)}\, g_{\mathrm{QAM}} = 0.8$, occurs exactly 36 times, and
- $d^2_{(4,2)}\, g_{\mathrm{QAM}} = 2$, occurs exactly 48 times.

The combinations counted above are applicable for every transmit antenna. This implies that each count must be multiplied by $N_t^{(\xi)}$ which leads to

$$\psi_2 = \left((0.4/2)^{-N_r}48 + (1.6/2)^{-N_r}32 + (1.6/2)^{-N_r}36 + 48\right) N_t^{(\xi)}. \tag{A.3}$$

To arrive at a final solution, the bound on σ_z^2 is enforced and all other combination values are set to one, which results in

$$D_{\text{ones}} = \left(M^{(\xi)}N_t^{(\xi)}\right)^2 - \left(M^{(\xi)}\right)^2 \binom{N_t^{(\xi)}}{2} - \left(D^{(1)} + D^{(2)} + D^{(3)} + D^{(4)}\right)^2 N_t^{(\xi)},$$

which is the number of elements for which σ_z^2 was set to 2, *i.e.*, $\left(\sigma_z^2/2\right)^{-N_r} = 1$. Simple averaging leads to Ψ. To achieve this, merely normalise the sum of all combinations by $\left(M^{(\xi)}N_t^{(\xi)}\right)^2$ to account for the number of possible events,

$$\Psi = \frac{\psi_1 + \psi_2 + D_{\text{ones}}}{\left(M^{(\xi)}N_t^{(\xi)}\right)^2},$$

which, when simplified, becomes (4.32).

The asymptote of SM for $M^{(\xi)} = 16$ is compared to (4.34) when using (4.32) and (4.34) when not using (4.32). To this extent, Fig. A.2 exemplifies the accuracy and tightness of this approach.

A.2 Reaching (4.38) from (4.34) with (4.31) and (4.37)

Combining (4.34) with (4.31) results in

$$\begin{aligned} \lim_{\gamma\to\infty} \frac{\text{ABER}_{\xi}^{(\textbf{inter})}}{\gamma^{-N_r}} &= 4N_t^{(\xi)}\tbinom{2N_r-1}{N_r}2^{-(2N_r+1)}\,\frac{2N_t^{(\xi)}+2^{-N_r-1}-1}{2N_t^{(\xi)}} \\ &= \left(2N_t^{(\xi)} + (2^{-N_r-1}-1)\right)\tbinom{2N_r-1}{N_r}2^{-(2N_r)}. \end{aligned} \tag{A.4}$$

Restating (4.37) for convenience,

$$\lim_{\gamma\to\infty} \frac{\text{ABER}_{\text{QAM}}}{\gamma^{-N_r}} \leq \frac{4}{\log_2(\widetilde{M})}\left(1 - \frac{1}{\sqrt{\widetilde{M}}}\right)\left(\frac{3}{2(\widetilde{M}-1)}\right)^{-N_r}\binom{2N_r-1}{N_r}2^{-(2N_r)}.$$

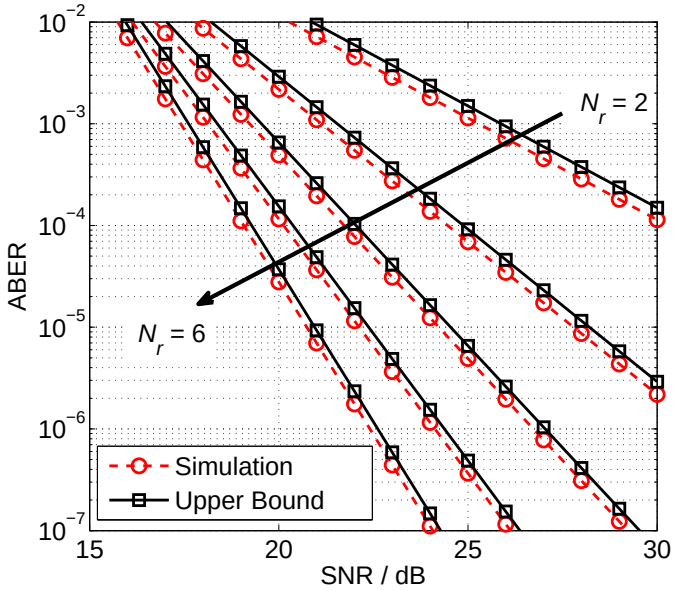

Figure A.2: *The dashed lines with circle markers denote the asymptote for the system if the expectation for* $\left(\sigma_z^2/2\right)^{-N_r}$ *is obtained via simulations. The solid lines with square markers denote the asymptote when* (4.32) *is used. Moving from the rightmost to the leftmost pairs of curves, each pair corresponds to an incremental increase in* N_r *from* 2 *to* 6*. The system is using two transmit antennas and has an overall spectral efficiency of* $5\,\mathrm{bits/s/Hz}$*.*

Taking the ratio of (A.4) over (4.37) results in (4.38) as

$$\lim_{\gamma\to\infty}\frac{\mathrm{ABER}_{\xi}^{(\mathbf{inter})}/\gamma^{-N_r}}{\mathrm{ABER}_{\mathrm{QAM}}/\gamma^{-N_r}}=\frac{\left(2N_t^{(\xi)}+2^{-N_r-1}-1\right)}{\left(\frac{2\left(4N_t^{(\xi)}-1\right)}{3}\right)^{N_r}\frac{4}{\log_2\left(4N_t^{(\xi)}\right)}\left(1-\frac{1}{\sqrt{4N_t^{(\xi)}}}\right)}.$$

A.3 Derivation of (4.43)

$$\begin{aligned}
&\Pr\{\mathbf{A}\neq\hat{\mathbf{A}}\}=\Pr\left\{||\mathbf{y}-\mathbf{A}||_{\mathrm{F}}^2>\left|\left|\mathbf{y}-\hat{\mathbf{A}}\right|\right|_{\mathrm{F}}^2\right\}\\
&=\Pr\left\{\sum_{r=1}^{N_r}\left[|y_r-A_r|^2\right]>\sum_{r=1}^{N_r}\left[\left|y_r-\hat{A}_r\right|^2\right]\right\}\\
&=\Pr\left\{\sum_{r=1}^{N_r}\left[2\Re\left\{\left(\hat{A}_r-A_r\right)\eta_r^*\right\}\right]>\sum_{r=1}^{N_r}\left[\left|A_r-\hat{A}_r\right|^2\right]\right\}\\
&\Rightarrow\eta_r^{\text{new}}\sim\mathcal{N}\left(\sum_{r=1}^{N_r}\left[2\Re\left\{(\hat{A}_r-A_r)^*\right\}\right],\sum_{r=1}^{N_r}\left[2N_o|\hat{A}_r-A_r|^2\right]\right),
\end{aligned}\tag{A.5}$$

where $\mathbf{A} = \frac{E_m}{2N_o} \sum_{u=1}^{N_u} \alpha_{(u)} \mathbf{h}_{n_t^{(u)}} x^{(u)}$ and $\hat{\mathbf{A}} = \frac{E_m}{2N_o} \sum_{u=1}^{N_u} \alpha_{(u)} \mathbf{h}_{\hat{n}_t^{(u)}} \hat{x}^{(u)}$.

If a Rayleigh fading channel is considered, then the closed form solution for $\mathrm{E}_{\mathcal{H}}\left[\mathrm{PEP}\left(\cdot\right)\right]$ in (4.42) can be derived by using [110, eq. 62]. To this extent, the argument within (4.43) can be represented as the summation of $2N_r$ squared Gaussian random variables, with zero mean and variance equal to 1, which means that they can be described by a central Chi-squared distribution with $2N_r$ degrees of freedom and a probability density function of

$$\tilde{\rho}_K(\kappa) = \frac{1}{2^{N_r}(N_r - 1)!} \kappa^{N_r - 1} \exp\left(-\kappa/2\right).$$

The result for $\mathrm{E}_{\mathcal{H}}\left[\mathrm{PEP}\left(\cdot\right)\right]$ is given as

$$\mathrm{E}_{\mathcal{H}}\left[\mathrm{PEP}\left(\cdot\right)\right] = f(\tilde{\beta})^{N_r} \sum_{r=0}^{N_r - 1} \binom{N_r - 1 + r}{r} \left(1 - f(\tilde{\beta})\right)^r, \tag{A.6}$$

such that $f(\tilde{\beta}) = \frac{1}{2}\left(1 - \sqrt{\frac{\tilde{\beta}}{1+\tilde{\beta}}}\right)$ and $\tilde{\beta} = \frac{E_m}{4N_o} \sum_{u=1}^{N_u} \alpha_{(u)}^2 \vartheta_{(u)}$.

Appendix B

Additional Derivations for Dh-SM

B.1 Derivation of (5.13)

The set of events that govern the conditional BER in (5.12) is considered. Specifically, **assuming that a '0' is transmitted by the source**, then the set of events that govern which relay is active is defined in Table B.1.

	R_0	R_1	Activation
$P_{C\|0}$	0	0	correct node
$P_{B\|0}$	0	1	both nodes
$P_{N\|0}$	1	0	no nodes
$P_{W\|0}$	1	1	wrong node

Table B.1: *Set of possible errors at the relays given a '0' was transmitted at the source*

Each event considered in Table B.1 is associated with a certain probability and is defined as:

- $P_{C|0}$ is the probability of correct detection at both relays and R_0 activates,
- $P_{B|0}$ is the probability of correct detection by R_0 and wrong detection by R_1 which results in both relays activating,
- $P_{N|0}$ is the probability of wrong detection by R_0 and correct detection by R_1 which results in no relays activating, and
- $P_{W|0}$ is the probability of wrong detection by R_0 and wrong detection by R_1 which results in the wrong relay activating.

Each probability can be expressed as a function of the instantaneous BER at both relays. This approach is permissible only when the probability of activating a particular relay is given as $(1 - \mathrm{BER}(\gamma))$ where $\mathrm{BER}(\gamma)$ is the instantaneous BER at a relay node experiencing an SNR

of γ. These probabilities are given as

$$\begin{aligned} P_{C|0} &= (1-\mathrm{BER}(\gamma_0))(1-\mathrm{BER}(\gamma_1)), \\ P_{B|0} &= (1-\mathrm{BER}(\gamma_0))\,\mathrm{BER}(\gamma_1), \\ P_{N|0} &= \mathrm{BER}(\gamma_0)\,(1-\mathrm{BER}(\gamma_1)), \\ P_{W|0} &= \mathrm{BER}(\gamma_0)\,\mathrm{BER}(\gamma_1), \end{aligned} \tag{B.1}$$

where γ_0 or γ_1 are the instantaneous SNRs of the source to R_0 link and the source to R_1 links, respectively, as shown in Fig. 5.8. The instantaneous BER for a 2-by-N_r space shift keying (SSK) system is exactly defined in (5.10).

Given (B.1),

$$\begin{aligned} \mathrm{BER}_{\mathrm{sd}|0} &= P_{C|0}\,\mathrm{BER}\left(\gamma_{0D}\right) \\ &+ P_{B|0}\,\mathrm{BER}_{0D/1D} \\ &+ P_{N|0}\,\mathrm{BER}\left(0\right) \\ &+ P_{W|0}\,\left[1-\mathrm{BER}\left(\gamma_{1D}\right)\right], \end{aligned} \tag{B.2}$$

where γ_{0D} and γ_{1D} are the instantaneous SNRs of the R_0 to the destination and R_1 to the destination links respectively, as given in Fig. 5.8. $\mathrm{BER}_{0D/1D}$ is the probability of detecting '1' at the destination when '0' was transmitted from the source and both relays are active. The given expressions in (B.2) are mutually exclusive.

Proceeding in a similar fashion, the set of events that govern which relay is active **given that a '1' is sent by the source** are shown in Table B.2.

	R_0	R_1	Activation
$P_{C\|1}$	1	1	correct node
$P_{B\|1}$	0	1	both nodes
$P_{N\|1}$	1	0	no nodes
$P_{W\|1}$	0	0	wrong node

Table B.2: *Set of possible errors at the relays given a '1' was transmitted at the source*

Each event considered in Table B.2 is again associated with a probability and is defined as:

- $P_{C|1}$ is the probability of correct detection at both relays and R_1 activates,
- $P_{B|1}$ is the probability of correct detection by R_1 and wrong detection by R_0 which results in both relays activating,

- $P_{N|1}$ is the probability of wrong detection by R_1 and correct detection by R_0 which results in no relays activating, and
- $P_{N|1}$ is the probability of wrong detection by R_1 and wrong detection by R_0 which results in the wrong relay activating.

Similarly to (B.2), the probabilities are defined as functions of the instantaneous BERs at the different relays,

$$\begin{aligned} P_{C|1} &= (1-\mathrm{BER}(\gamma_0))(1-\mathrm{BER}(\gamma_1)), \\ P_{B|1} &= \mathrm{BER}(\gamma_0)\,(1-\mathrm{BER}(\gamma_1)), \\ P_{N|1} &= (1-\mathrm{BER}(\gamma_0))\,\mathrm{BER}(\gamma_1)), \\ P_{W|1} &= \mathrm{BER}(\gamma_0)\,\mathrm{BER}(\gamma_1). \end{aligned} \tag{B.3}$$

Given (B.3),

$$\begin{aligned} \mathrm{BER}_{\mathrm{sd}|1} &= P_{C|1}\,\mathrm{BER}\left(\gamma_{1D}\right) \\ &+ P_{B|1}\,\mathrm{BER}_{1D/0D} \\ &+ P_{N|1}\,\mathrm{BER}\left(0\right) \\ &+ P_{W|1}\,\left[1-\mathrm{BER}\left(\gamma_{0D}\right)\right], \end{aligned} \tag{B.4}$$

where $\mathrm{BER}_{1D/0D}$ is the probability of detecting '0' at the destination when '1' was transmitted from the source and both relays are active.

It is apparent that $P_{C|0} = P_{C|1} = P_C$ and $P_{W|0} = P_{W|1} = P_W$. Furthermore, $P_{B|0} = P_{N|1}$ and $P_{B|1} = P_{N|0}$. The full source to destination BER can now be posed as

$$\begin{aligned} \mathrm{BER}_{\mathrm{sd}} &= \tfrac{1}{2}\left[\mathrm{BER}_{\mathrm{sd}|0} + \mathrm{BER}_{\mathrm{sd}|1}\right] \\ &= \tfrac{1}{2}\left[P_C\left(\mathrm{BER}(\gamma_{0D}) + \mathrm{BER}(\gamma_{1D})\right)\right] \\ &+ \tfrac{1}{2}\left[P_W\left(1-\mathrm{BER}(\gamma_{0D}) + 1 - \mathrm{BER}(\gamma_{1D})\right)\right] \\ &+ \tfrac{1}{2}\left[P_{B|0}\ \mathrm{BER}_{0D/1D}\right] \\ &+ \tfrac{1}{2}\left[P_{B|1}\ \mathrm{BER}_{1D/0D}\right]. \end{aligned} \tag{B.5}$$

Appendix C

List of Publications

This section contains a list of papers either accepted for publication, pending publication or submitted for publication.

C.1 Published

- **N. Serafimovski**, M. Di Renzo, S. Sinanović, R. Mesleh and H. Haas, "Fractional Bit Encoded Spatial Modulation (FBE–SM)," *IEEE Communications Letters*, vol.14, no.5, pp.429-431, May 2010.

- **N. Serafimovski**, S. Sinanović, M. Di Renzo and H. Haas, "Dual-Hop Spatial Modulation (Dh-SM)," *IEEE Vehicular Technology Conference (VTC Spring 2011)*, pp.1-5, 15-18 May 2011.

- **N. Serafimovski**, S. Sinanović, A. Younis, M. Di Renzo and H. Haas, "2-User Multiple Access Spatial Modulation," *IEEE GLOBECOM Workshops (GC Wkshps)*, pp.343-347, 5-9 Dec. 2011.

- A. Younis, **N. Serafimovski**, R. Mesleh and H. Haas, "Generalised Spatial Modulation," *Conference Record of the Forty Fourth Asilomar Conference on Signals, Systems and Computers (ASILOMAR)*, 2010 , pp.1498-1502, 7-10 Nov. 2010.

- S. Sinanović, **N. Serafimovski**, M. Di Renzo and H. Haas, "Secrecy Capacity of Space Keying with Two Antennas" *Proc. of IEEE Vehicular Technology Conference (VTC)* (to appear), pp. 1-5, 3-6 Sept. 2012.

- **N. Serafimovski**, S. Sinanović, M. Di Renzo and H. Haas, "Multiple Access Spatial Modulation," *EURASIP Journal on Wireless Communications and Networking Special Issue on MIMO Relays for Cooperative Wireless Networks*, 2012.

C.2 Accepted

- **N. Serafimovski**, A. Younis, R. Mesleh, P. Chambers, M. Di Renzo, C.-X. Wang, P. M. Grant, M. A. Beach and H. Haas, "Practical Implementation of Spatial Modulation," *IEEE Transactions on Vehicular Technology*, April. 2013

Appendix D

Selected Publications

This chapter contains all published work.

IEEE COMMUNICATIONS LETTERS, VOL. 14, NO. 5, MAY 2010

Fractional Bit Encoded Spatial Modulation (FBE–SM)

N. Serafimovski, M. Di Renzo, S. Sinanović, R. Y. Mesleh, and H. Haas

***Abstract*—In this Letter, we introduce fractional bit encoded (FBE)–spatial modulation (SM), which is a novel and more versatile SM scheme that allows the transmitter to be equipped with an arbitrary number of antennas. The solution is based on the theory of modulus conversion, and is especially useful for compact mobile devices where cost and space constraints pose fundamental limits on the achievable bit rate. Numerical results will show that FBE–SM can offer design flexibility and the desired trade–off in terms of attainable performance and capacity.**

***Index Terms*—Spatial modulation (SM), Multiple–input–multiple–output (MIMO) systems, modulus conversion.**

I. Introduction

THE aim of this Letter is to propose a method for overcoming the limitation on the number of transmit antennas in SM and allow the transmitter to be equipped with an arbitrary number of antennas. SM is a novel approach to multiple–input–multiple–output (MIMO) systems which entirely avoids inter–channel interference (ICI) and requires no synchronisation between the transmit antennas, while achieving a spatial multiplexing gain. This is performed by mapping a block of information bits into a constellation point in the signal and spatial domains [1]. In SM, the number k of information bits that are encoded in the spatial domain is directly related to the number M of transmit antennas, in particular $M = 2^k$. This means that the number of transmit antennas must be a power of two. We propose a solution to this limitation in SM which increases the granularity of the data encoding process in the spatial domain by using fractional bit encoding; the novel method is called FBE–SM.

When applied to SM, FBE relies on encoding each point in the spatial domain, *i.e.*, the antenna index, with, on average, a non–integer number of bits, while keeping unchanged the encoding process in the signal domain. This results in a more versatile system design allowing for a wider range of spectral efficiencies given restrictions on space and power consumption [1]. By using FBE–SM, a system can achieve otherwise unavailable data rates in the spatial domain. For example, it may not be possible to install 8 antennas in a small-scale portable device, while 5 or 6 might be feasible. In such a case, however, SM would use only 4 antennas [1]. FBE–SM is designed to address this exact problem.

The concept behind FBE is not new in modern communication systems. However, to the best of the authors' knowledge, this principle has never been applied to SM. For example, the application of FBE to a pulse amplitude modulation (PAM) communication system is reported in [5]. Two general methods for fractional bit transmission are described therein. The first approach is called *constellation switching* which alternates between the transmission of B and $B + 1$ bits per symbol to achieve the FBE over time. A notable downside of this approach is the inherent bit shift that results from incorrectly decoded symbols making it prone to error propagation effects. The second approach is called *modulus conversion* and is designed to minimise the error propagation effect that afflicts the performance of the constellation switching method [6]. In this Letter, we apply the theory of modulus conversion to SM and propose a system that can offer satisfactory performance for an arbitrary number of antennas at the transmitter.

The remainder of this Letter is organized as follows. In Section II, the theory of modulus conversion is briefly summarised. In Section III, the novel FBE–SM scheme is introduced. In Section IV, some numerical results are shown to analyse the performance of FBE–SM and compare it with conventional SM. Finally, Section V concludes the Letter.

II. Theory of Modulus Conversion

Modulus conversion achieves fractional bit rates by converting the incoming bitstream to numbers in an arithmetic base, or modulus, that is not a power of 2 [6]. In particular, the modulus converter operates as follows: i) blocks of SK bits are extracted from the incoming bitstream, where K is the desired fractional bit rate and S is a positive integer; ii) each block is then converted to S numbers of base L. The modulus is defined as the smallest integer number, L, such that $L \geq 2^K$.

In general, one may use the theory of modulus conversion to achieve an arbitrary fractional bit rate, *i.e.*, K could be a real number. In Section III, we will see that this is especially relevant when applying this method to SM. However, since both L and S are positive integer numbers it follows that the modulus converter can only handle rational bit rates, *i.e.*, $K \in \mathbb{Q}$. This problem can be circumvented by approximating any K, with $\tilde{K}$, given as the ratio of two positive and relatively prime integers p and q. In other words, the problem can be stated as finding the best rational approximation, $\tilde{K} = p/q$, to a real number K. A simple way to do that is to exploit the following inequality:

$$0 \leq nK - \lfloor nK \rfloor \leq 1 \Rightarrow 0 \leq K - \frac{\lfloor nK \rfloor}{n} \leq \frac{1}{n} \qquad (1)$$

where $\lfloor \cdot \rfloor$ denotes the floor function and n is an arbitrary and positive integer number.

From (1), it follows that $SK \cong S\tilde{K} = S(\lfloor nK \rfloor / n)$, which, according to the theory of modulus conversion, must be a positive integer. It is worth mentioning that, in general, $S \neq n$. In particular, although n and S could be arbitrarily chosen,

Manuscript received November 19, 2009. The associate editor coordinating the review of this letter and approving it for publication was J. Jalden.

N. Serafimovski, S. Sinanović, and H. Haas are with The University of Edinburgh, Edinburgh, EH9 3JL, UK (e-mail: {n.serafimovski, s.sinanovic, h.haas}@ed.ac.uk.).

M. Di Renzo is with L2S, UMR 8506 CNRS – SUPELEC – Univ Paris–Sud, 3 rue Joliot–Curie, 91192 Gif–sur–Yvette CEDEX, France (e-mail: marco.direnzo@lss.supelec.fr).

R. Y. Mesleh is with Jacobs University Bremen, 28759 Bremen, Germany (e-mail: r.mesleh@jacobs–university.de).

Digital Object Identifier 10.1109/LCOMM.2010.05.092270

the following guidelines can be considered for their optimal setting:

1) The larger n is, the smaller the approximation error $K - \tilde{K}$ is; this follows from (1).
2) The larger S is, the longer the decoding delay is: this follows from the operating principle of modulus conversion, which allows the receiver to decode the data only after receiving S base–L numbers.
3) The larger S is, the greater the vulnerability to error propagation within each block of bits (see Section IV).

Accordingly, for any given K, and provided that $S(\lfloor nK \rfloor / n)$ is a positive integer, n and S should be chosen as large and as small as possible, respectively.

III. Application of Modulus Conversion to SM

Let us now apply the theory of modulus conversion to SM and introduce the FBE–SM method. As mentioned in Section I, the motivation for the proposed scheme is to avoid fundamental constraints on the number of transmit antennas that can be used by classical SM systems. We emphasize that the proposed method applies to only the bit encoding in the spatial domain, while the encoding process in the signal domain is left unchanged. FBE–SM reduces to conventional SM [1] if the number of antennas is a power of 2.

A. FBE–SM: A Step–by–Step Description

The working principle of FBE–SM can be summarised in the following subsequent steps:

1) Determine the desired number of transmit antennas, M, according to the system constraints, *e.g.*, bit rate, cost, available space.
2) Set the modulus L in Section II equal to M, *i.e.*, $L = M$.
3) Compute the maximum spatial multiplexing gain offered by the system as $K = \log_2(M)$.
4) Choose the pair (S, n) such that $S(\lfloor nK \rfloor / n)$ is a positive integer number and following the design guidelines described in Section II, *i.e.*:
   - Optimize $\tilde{K} = \lfloor nK \rfloor / n$ such that it is as close as possible to K. This allows the system to approach the spatial multiplexing gain offered by the M transmit antennas. This is achieved, in general, for larger values of n.
   - Optimize S such that it is as small as possible: this reduces the decoding delay and, more importantly, minimises error propagation in the decoded bitstream.
5) Map each of the S base–M encoded numbers in the transmission block to a transmit antenna index in the range $[0, M-1]$.

The receiver will perform the reverse operation to recover the encoded data:

i) for each signaling interval, one of the algorithms in [1]–[3] is applied to detect the spatial and signal constellation points, ii) the spatial constellation points (the base–M encoded numbers) are grouped into blocks of S points each, and iii) each block is converted to the equivalent base–2 bitstream of $S(\lfloor nK \rfloor / n)$ bits each. At this point it should be noted that these are merely guidelines to achieve a balance between the best approximation of K and minimising the error propagation effects. The best rational approximation for any real number is obtained using continuous fractions [7] given the restriction on the available block size n.

B. FBE–SM: An Example

Let us consider a simple example with $M = 5$ without signal modulation: this is equivalent to considering the space shift keying (SSK) modulation method [3]. Thus, we have $K = 2.3219$. By choosing, *e.g.*, $(S, n) = (4, 4)$, we get $\tilde{K} = 2.25$, which closely approaches K and is greater than the spatial multiplexing gain offered by a system with $M = 4$. If, for instance, the block of $S\tilde{K}$ bits is equal to 110001011_2, then the modulus converter will return an $(S\tilde{K})_M$ block equal to 3040_5, where $(x)_b$ denotes the base–b representation of x. Then, the output of the modulus converter is mapped to a spatial constellation point. First, the antenna with index 3 transmits an energy signal, then the antenna with index 0 transmits the same signal, etc. The receiver will estimate each received antenna index by using an index–by–index detection algorithm according to [1]–[3]. After decoding the S antenna indexes, ideally with no errors, it will recover the original data stream as: $3040_5 = 110001011_2$.

In order to understand the effect of error propagation, let us consider that an error has occurred in the detection of the second antenna index. Let us assume that the decoded block is 3140_5. In this case, the decoded bitstream will be $3140_5 = 110100100_2$, which will result in 5 out of 9 bits in error. In particular, the error propagation effect in the last 4 digits is well evident in this case. This example highlights the important role played by S to limit the error propagation effect in the decoded bitstream for each incorrectly decoded base–M number in the received block. However, numerical results in Section IV will show that for moderately high signal–to–noise–ratios (SNRs) the performance degradation due to error propagation is not significant.

IV. Numerical Examples

The following system setup is considered: i) Each transmit antenna, when activated, transmits a 4–QAM (quadrature amplitude modulation) signal. ii) The channel is assumed to be Rayleigh distributed with uncorrelated fading among the wireless links. It is static and flat-fading for the duration of a transmission block. iii) The noise at the receiver input is assumed to be white complex Gaussian, with zero-mean and mutually independent samples. iv) The receiver is equipped with 4 antennas and uses a maximum–likelihood detector to jointly detecting spatial and signal constellation points [2].

Two performance metrics will be investigated: 1) the symbol–error–ratio (SER), which is defined as the average probability of incorrectly detecting a constellation and signal point [1], and 2) the bit–error–ratio (BER), which is defined as the average probability of incorrectly detecting a bit in the decoded bitstream [2]. This allows us to better highlight the effect of error propagation introduced by the FBE process.

In Fig. 1, we analyse the BER of FBE–SM for various combinations of (S, n) and $M = 5$ in order to substantiate the claims in Section II and Section III. We observe that the BER gets progressively worse for increasing values of S due

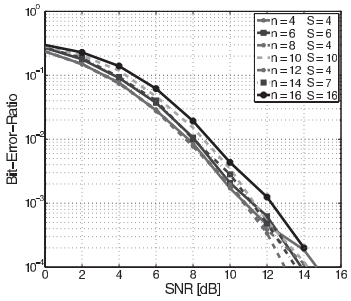

Fig. 1. BER of FBE–SM. Parametric study for different values of (S, n). Setup: i) $M = 5$, and ii) $K = 2.3219$bits/s/Hz.

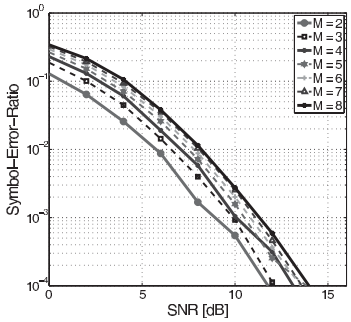

Fig. 2. SER of FBE–SM. Parametric study for different values of transmit antennas M. Setup: i) $S = 4$, and ii) $n = 4$.

to the error propagation effect discussed above. By comparing the best, $(S, n) = (4, 4)$, and the worst, $(S, n) = (16, 16)$, system setups shown in Fig. 1, we observe that the BER gets worse of approximately 1.5dB at a BER of 10^{-3}. However, this performance drop is compensated by a small increase, from 2.25 bits/s/Hz to 2.3125 bits/s/Hz, in the achievable bit rate which is an increase of less than 3%[1]. This example demonstrates the effects of error propagation and shows $S = 4$ and $\tilde{K} = 2.25$ as a better choice than $S = 16$ and $\tilde{K} = 2.3125$ resulting from jointly optimising the steps in Section III-A.

In Figs. 2 and 3, we show the SER and BER of FBE–SM for various antennas at the transmitter, respectively. If $M = 2,\ 4,\ 8$, the system reduces to conventional SM. As expected [3], in Fig. 2 we notice that the SER gets monotonically worse for increasing values of M. However, this translates to an increase in the system bit rate from 1 bit/s/Hz if $M = 2$ to 3 bits/s/Hz if $M = 8$. When looking into Fig. 3, we observe that the BER does not get worse monotonically for increasing M. For example, the system setups with $M = 5$, $M = 6$, and $M = 7$ offer a worse BER and a lower bit rate than the setup with $M = 8$. This is mainly due to the error propagation effect of the FBE process. However, we also notice that for high SNRs, the performance difference between the setups with $M = 5$, $M = 6$ and the setup with $M = 8$ is smaller. In particular, the 1.7dB difference seen at a BER of 10^{-1} between $M = 6$ and $M = 8$, reduces to only 0.7dB at a BER

[1]The bit rates are compared by considering only the number of transmit antennas since the modulation scheme in the signal domain is the same [1].

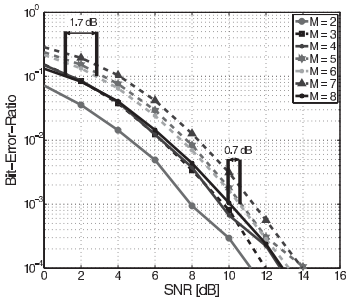

Fig. 3. BER of FBE–SM. Parametric study for different values of transmit antennas M. Setup: i) $S = 4$, and ii) $n = 4$.

of 10^{-3} as shown on Fig. 3. This is because error propagation is minimised for high SNRs. Even though the SM system with $M = 8$ offers a better bit rate, this solution may not be practical due to cost and physical space constraints. This is a typical case where the proposed FBE–SM scheme with $M = 5$ or $M = 6$ can be an effective solution for trading–off bit rate for performance, *e.g.*, with respect to the SM setup with $M = 4$. In this context, it has to be mentioned that the results for a large M are over–optimistic since no channel correlation is assumed. Naturally, if more antennas are fitted into a limited space, mutual coupling and correlation increases. In this Letter, we have not accounted for this effect as such investigation is beyond the scope of this work.

V. Conclusions

In this Letter, we have introduced a novel and more versatile SM scheme called FBE–SM. The method relies on the application of modulus conversion to achieve fractional bit rates, and allows any SM–MIMO wireless system to use an arbitrary number of antennas at the transmitter. Numerical results have also substantiated that the proposed method turns out to be a viable candidate to the design of compact mobile devices using SM, by offering the desired degrees of freedom for trading–off performance, achievable bit rates, and cost.

Acknowledgement

We greatfully acknowledge support from the Engineering and Physical Sciences Research Council (EP/G011788/1) for this work.

References

[1] R. Y. Mesleh, H. Haas, S. Sinanovic, C. W. Ahn, and S. Yun, "Spatial modulation," *IEEE Trans. Veh. Technol.*, vol. 57, no. 4, pp. 2228–2241, July 2008.

[2] J. Jeganathan, A. Ghrayeb, and L. Szczecinski, "Spatial modulation: optimal detection and performance analysis," *IEEE Commun. Lett.*, vol. 12, no. 8, pp. 545–547, Aug. 2008.

[3] J. Jeganathan, A. Ghrayeb, L. Szczecinski, and A. Ceron, "Space shift keying modulation for MIMO channels," *IEEE Trans. Wireless Commun.*, vol. 8, no. 7, pp. 3692–3703, July 2009.

[4] P. Wolniansky, G. Foschini, G. Golden, and R. Valenzuela, "V–BLAST: an architecture for realizing very high data rates over the rich–scattering wireless channel," in *Proc. IEEE Int. Symp. Signals, Systems, and Electronics*, pp. 295–300, Sep. 1998.

[5] W. L. Betts and K. D. Ko, "Fractional bit rate encoding in a pulse amplitude modulation communication system," U.S. Patent 6 993 067, Jan. 31, 2006.

[6] W. L. Betts, "Modulus converter for fractional rate encoding," U.S. Patent 5 103 227, Apr. 7, 1992.

[7] A. W. Paeth, Ed., *Graphics Gems V*. London: Academic Press, 1995.

Dual-hop Spatial Modulation (Dh-SM)

Nikola Serafimovski*, Sinan Sinanović*, Marco Di Renzo†, and Harald Haas*

*Institute for Digital Communications
Joint Research Institute for Signal and Image Processing
School of Engineering
The University of Edinburgh
EH9 3JL, Edinburgh, UK
{n.serafimovski, s.sinanovic, h.haas}@ed.ac.uk

†Laboratory of Signals and Systems (L2S),
French National Center for Scientific Research (CNRS)
École Supérieure d'Électricité (SUPÉLEC),
University of Paris–Sud XI (UPS)
3 rue Joliot–Curie, 91192 Gif–sur–Yvette (Paris), France
marco.direnzo@lss.supelec.fr

***Abstract*—In this paper, we introduce Dual-hop Spatial Modulation (Dh-SM). We look at the effect that Dh-SM has on the required signal to noise ratio (SNR) at the destination and how it can help alleviate the multi-hop burden. Initial bit-error-ratio (BER) results comparing the performance of Dh-SM with orthogonal decode-and-forward (DF) are presented where Dh-SM is shown to have up to a 10 dB SNR advantage.**

I. Introduction

Spatial modulation (SM) is a recently proposed approach to multiple–input–multiple–output (MIMO) systems which entirely avoids inter–channel interference (ICI) and requires no synchronisation between the transmit antennas, while achieving a spatial multiplexing gain [1]. This is performed by mapping a block of information bits into a constellation point in the signal and spatial domains [2]. In SM, the number of information bits, k, that are encoded in the spatial domain is directly related to the number of transmit antennas N_t; in particular $N_t = 2^k$. This means that the number of transmit antennas must be a power of two unless fractional bit encoding is used [3]. It should also be noted that SM is shown to outperform other MIMO schemes in terms of bit-error-ratio (BER) [2]. The presented work proposes the use of SM as a possible relaying technique.

The basic relaying problem can be reduced to the simple inability of a single transmitter to reach its intended target with the necessary signal to noise ratio (SNR) for a given spectral efficiency. There are several approaches to this problem. On one hand, orthogonal amplify-and-forward (AF) utilises the relay antenna as a simple amplifier. Any signal received by the relay at time instance t_1 is amplified and retransmitted at instance t_2 forming a non-regenerative system. On the other, the orthogonal decode-and-forward (DF) algorithm decodes the received signal at the relay, then re-encodes and retransmits this information establishing a regenerative system. Outage probabilities, mutual information calculations and transmit diversity bounds for AF and DF relaying are derived in [4] with end to end performance being considered in [5]. Taking into consideration the above relaying protocols, the use of SM is proposed to provide additional power and capacity gains over the non-cooperative AF and DF systems. In orthogonal AF and DF two time slots are needed for the relevant information to reach the destination node, effectively halving the source-destination spectral efficiency. Dual-hop Spatial Modulation (Dh-SM) can partially mitigate this effect. Dh-SM can utilise the spatial domain to transmit additional information bits, while maintaining a fixed signal constellation. Since the receiver decodes the channel used for the transmission, it can determine the transmitting antenna and, in so doing, decode the bits used to activate that particular antenna. This serves to increase the source to destination spectral efficiency and alleviate the multihop burden, as will be explained in Section II. Alternatively, since some of the data in SM is transmitted in the spatial domain, a lower order modulation scheme can be used for signal domain transmission which leads to a lower transmit power requirment. This is a unique advantage that Dh-SM has when compared to all other relaying systems and results in a decreased BER at the destination for the same transmit power, *i.e.* Dh-SM increases the coding gain of the system. Throughout this work we refer to the coding gain as the the difference between the SNR levels of two systems required to reach the same BER.

In [6–8], analytical bounds for the BER performance of SM are derived. Each work considers the channel and the signal symbol as a joint input variable and averages across the channel to achieve a closed form solution. We validate the results of this work with the union bound based approach originally presented in [9, Eq. (8)].

In the remainder of the paper we introduce the system model in Section II, provide the theoretical framework in Section III, show and discuss the numerical results in Section IV and conclude the paper in Section V.

II. System Model

In the following work we assume a three node scenario as shown in Fig. 1. While AF, DF and Dh-SM utilise a single transmit antenna at any instance, Dh-SM requires the transmitter to have multiple transmit antennas available. Since we seek to characterise the behaviour of SM in a dual-hop scenario, we compare its performance in terms of BER to non-cooperative DF. The source broadcasts a signal constellation symbol, x. The received signal is given by: $y_j = h_{ij}x + \eta$, where i is the index of the transmit and j is the index of the receive antenna, h_{ij} is the channel coefficient of the link between the active antenna i and the receiving antenna j. The additive white Gaussian noise (AWGN), η, is described by $\mathcal{N}(0, \sigma^2)$ with $\sigma^2 = \mathrm{E}_{\mathbf{x}}\left[|x|^2\right]/\bar{\gamma}_{ij}$ where $\bar{\gamma}_{ij}$ is the average SNR of the link between nodes i and j and $\mathrm{E}_{\mathbf{x}}[\cdot]$ is the expectation with respect to the set of signal constellation points. The estimated symbol at each receiving node in the

978-1-4244-8331-0/11/$26.00 ©2011 IEEE

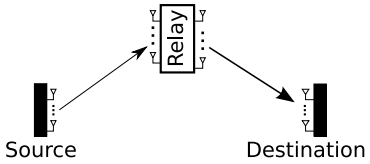

Fig. 1. Dual-hop spatial modulation

DF system using maximum-ratio-combining (MRC) is given by:

$$x_{\text{est}}^{\ell} = \frac{\left(\mathbf{h}_{k\ell}^{i}\right)^{\dagger} \bar{\mathbf{y}}_{k\ell}}{\left(\mathbf{h}_{k\ell}^{i}\right)^{\dagger} \mathbf{h}_{k\ell}^{i}} \tag{1}$$

$(\cdot)^{\dagger}$ denotes the complex conjugate and $\mathbf{h}_{k\ell}^{i} = \left[h_{i1} \dots h_{iN_r^{\ell}}\right]$ is a vector composed of the single tap channel coefficients from antenna i on the transmitting node k to the receiving node ℓ having N_r^{ℓ} number of receive antennas. The transmitting node is either the source, s, or the relay, r, while the receiving node is the relay or destination, d, *i.e.* $k \in \{\text{s, r}\}$ and $\ell \in \{\text{r, d}\}$. The vector $\bar{\mathbf{y}}_{k\ell}$ is comprised of the symbols at each receive antenna on node ℓ. Finally, x_{est}^{ℓ} is passed through a maximum likelihood (ML) detector to obtain the original bit sequence.

The basic idea of SM is to map blocks of information bits into two information carrying units [2]: i) a symbol, chosen from a complex signal–constellation diagram, and ii) a unique transmit–antenna, chosen from the set of transmit–antennas in the antenna–array, *i.e.* the spatial–constellation diagram. The working principle of SM is exemplified in Fig. 2.

Throughout this paper, we consider a ML decoder, which computes the Euclidean distance between the received signal $\bar{\mathbf{y}}_{k\ell}$ and the set of all possible received signals, selecting the closest one [6]:

$$(x_{\text{est}}, i_k) = \text{argmin} \left\{ \left|\left| \bar{\mathbf{y}}_{k\ell} - x_j \mathbf{h}_{k\ell}^{i} \right|\right|_{\text{F}}^{2} \right\}$$
$$x \in \mathcal{X} \qquad i \in \{1 \dots N_t^k\}$$

where the pair (x_{est}, i_k) is formed from the estimated symbol x_{est} emitted from antenna i on node k, x_j is the current symbol being evaluated from the set of possible constellation points $\mathcal{X}$, N_t^k is the number of available transmit antennas on node k and $||\cdot||_{\text{F}}$ is the Frobenius norm.

A. *Example*

Let us assume a basic system as shown in Fig. 1, where transmissions are carried out at 2 bits/s/Hz in the signal domain and only a single transmit antenna is active at the source and relay nodes. In orthogonal AF and DF two time slots are needed for the relevant information to reach the destination node, effectively halving the source-destination spectral efficiency to 1 bit/s/Hz. We now consider the system in Fig. 1 with a single source to relay transmit antenna and four relay to destination transmit antennas. In this case 2 bits can be sent in the spatial domain and 2 more in the signal domain on the relay to destination link. The use of SM on the relay to destination link enables the system to operate at 4 bits/s/Hz on that link. Since the system remains unchanged in the source to relay link, the source can transmit to the relay in the first two time slots a total of 4 bits. The relay can then transmit those 4 bits to the destination in the third slot by making use of the spatial domain. The use of Dh-SM results in 4 bits going from the source to the destination in three time slots and an end-to-end average spectral efficiency of 1.33 bits/s/Hz; a 33% improvement over standard AF and DF.

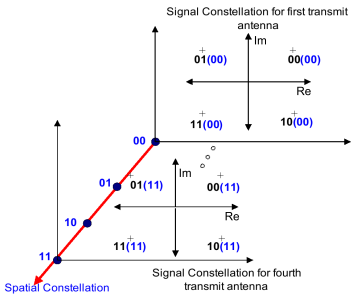

Fig. 2. If we wish to transmit four bits, the first two bits define the spatial–constellation point which identifies the active antenna, while the remaining two bits determine the signal–constellation point that is to be transmitted.

Alternatively, Dh-SM can be used to improve the bit-error-ratio of the system by transmitting a lower order modulation signal–symbol. We quantify the coding gains in Section IV-B.

III. Analytical Modelling

The scenario presented in Fig. 1 represents a well known orthogonal relaying system. A major distinction is the use of multiple transmit and receive antennas at the relay. The end-to-end performance of a two-hop wireless communication system with non-regenerative (AF) and regenerative (DF) relays over a Rayleigh-fading channel is presented in [5]. The authors develop a closed form expression for the average BER of AF given in terms of the system's moment generating function (MGF). The system performance in terms of outage probability and BER demonstrate that DF systems perform better than AF at both low and high average SNRs in a Rayleigh fading environment. For this reason, we limit our comparison and only look at Dh-SM's performance relative to DF. In this work we aim to show that the use of spatial modulation in a fixed relaying system, *i.e.* there is no node mobility, provides significant coding gains.

Starting from the system model presented in Section II, the signal undergoes two stages of decoding [10] and the bit error probability, for all dual–hop regenerative systems over independent channel SNRs, can readily be expressed as:

$$P_b(\bar{\gamma}_{\text{sd}}) = P_b(\bar{\gamma}_{\text{sr}}) + P_b(\bar{\gamma}_{\text{rd}}) - 2P_b(\bar{\gamma}_{\text{sr}})P_b(\bar{\gamma}_{\text{rd}}). \tag{2}$$

$P_b(\cdot)$ is the average BER of the link between nodes k and ℓ with an average SNR of $\bar{\gamma}_{k\ell}$. In a regenerative system, the overall bit error ratio is a function of the individual links. This means that if a system performs better in terms of BER on the individual links, it will also perform better for the dual–hop once we consider that both $P_b(\bar{\gamma}_{\text{sr}})$ and $P_b(\bar{\gamma}_{\text{rd}})$ must be less than $1/2$. To show this, we look at the directional derivative

of $P_b(\bar{\gamma}_{\text{sd}})$ with respect to $P_b(\bar{\gamma}_{\text{sr}})$ and $P_b(\bar{\gamma}_{\text{rd}})$. We define a unit vector $\vec{\mathbf{u}} = <\alpha, \beta>$ where α and β are non-negative coefficients defining the direction of the derivative.

$$\nabla_{\vec{\mathbf{u}}} P_b(\bar{\gamma}_{\text{sd}}) = \alpha\left(1 - 2P_b(\bar{\gamma}_{\text{rd}})\right) + \beta\left(1 - 2P_b(\bar{\gamma}_{\text{sr}})\right). \quad (3)$$

Looking at (3) we see that the function is monotonically increasing with respect to the individual error probabilities since $\{P_b(\bar{\gamma}_{\text{sr}}),\, P_b(\bar{\gamma}_{\text{rd}})\} \in [0,\, 1/2]$. We now look at the expressions for these error probabilities. It should be noted that since the overall system error depends solely on the error of the individual links, we proceed to analyse the error expressions for the arbitrary k to ℓ link.

The BER of an M quadrature amplitude modulation (QAM) across multiple fading channels is given in (4) where M is the size of the QAM constellation. The generalized expression for the average BER of a single link between nodes k and ℓ using QAM modulation and Gray coding is given by (4) [11].

$$P_b(E_{k\ell}) \cong A \sum_{b=1}^{\sqrt{M}/2} \frac{1}{\pi} \int_0^{\pi/2} M_{\gamma_{k\ell}}\left(\frac{c}{2\sin^2(\theta)}\right)^{N_r^\ell} d\theta \quad (4)$$

$$A = 4\left(\frac{\sqrt{M}-1}{\sqrt{M}\log_2(M)}\right) \qquad c = -\frac{3\log_2(M)(2b-1)^2}{M-1}$$

$M_\gamma(s)$ is the moment generating function of the fading channel. The moment generating functions for different channel fading models can be found in [11]. In particular, we look at a Rayleigh fading channel and $M_\gamma(s)$ is given by:

$$M_\gamma(s) = \frac{1}{1 + s\bar{\gamma}}$$

Similarly, because Dh-SM is in principle a DF system, its BER can be represented by (2), where the individual error probabilities are those of the individual SM links.

The BER of SM using the optimal detector can be bounded using union bound methods and is given as:

$$P_b(E_{k\ell}) \leq \mathrm{E}_{\mathbf{H}}\left[\sum_{\hat{x},\hat{n}_t} \text{PEP}\left(x,\, n_t,\, \hat{x},\, \hat{n}_t\right)\right] \quad (5)$$

where we define $\text{PEP}\left(x,\, n_t,\, \hat{x},\, \hat{n}_t\right)$ to be the pairwise error probability between the symbol x emitted from antenna n_t being detected as symbol $\hat{x}$ emitted by antenna $\hat{n}_t$. $\mathrm{E}_{\mathbf{H}}[\cdot]$ represents the expectation of the system with respect to the channel. Given this formulation, the symbol based union bound for (5) can be expressed as:

$$P_b(E_{k\ell}) \leq \sum_{x=1}^{M}\sum_{\hat{x}=1}^{M}\sum_{n_t=1}^{N_t^k}\sum_{\hat{n}_t=1}^{N_t^k} \frac{\text{PEP}_{k\ell}\left(x,\, n_t,\, \hat{x},\, \hat{n}_t\right)}{2\left(MN_t^k - 1\right)}. \quad (6)$$

In [9, Eq. (8)] the pairwise error probability conditioned on the channel between the two communicating nodes is given as:

$$\text{PEP}_{k\ell}\left(x,\, n_t,\, \hat{x},\, \hat{n}_t\right) = Q\left(\sqrt{\frac{\left|\left|\mathbf{h}_{k\ell}^{n_t}x - \mathbf{h}_{k\ell}^{\hat{n}_t}\hat{x}\right|\right|^2}{2\sigma^2}}\right) \quad (7)$$

where the symbol x is transmitted from antenna n_t.

Given this analytical modelling, we proceed to analyse the performance of Dh-SM and DF in terms of their BER.

IV. Numerical Analysis

The aim of this section is to compare the performance of Dh-SM with conventional relaying utilising M–QAM under a variety of conditions. In particular, the presented results depict the different behaviour of the system when: i) N_t^{s} is changed, ii) N_t^{r} is changed, iii) N_r^{r} is changed, iv) N_r^{d} is changed and, v) under different link SNRs. Our work begins by analysing the most constrained Dh-SM system where $N_t^{\text{s}} = 2, N_r^{\text{r}} = 2, N_t^{\text{r}} = 2$ and $N_r^{\text{d}} = 2$. We then adjust each parameter to see the effect it has on the system such that Fig. 6 shows the results for the least constrained system and the full advantages of Dh-SM are seen.

A. Simulation Setup

A frequency-flat Rayleigh fading channel with no correlation between the transmitting antennas and AWGN is assumed. MRC in combination with ML detection is used in the DF system, with the ML detector in [6] being used for Dh-SM. Perfect channel state information (CSI) is assumed at the receiving node, with no CSI at the transmitter. Only one of the available transmit antennas at the source and relay nodes of Dh-SM is active at any transmitting instance. Since part of the data is encoded in the spatial domain, Dh-SM uses a lower order modulation symbol but the energy per symbol is equivalent to that in the DF system.

B. Results

In the legend on each figure, $\text{An}(k, \ell)$ represents the analytical BER on the link between nodes k and ℓ, while $\text{Sim}(k, \ell)$ is the simulation result. To analytically describe the behaviour of DF we use (4), whereas (6) bounds the behaviour of Dh-SM.

We begin by looking at the effects of additional antennas at the transmitter. In particular, Fig. 3 shows that when the source to relay and relay to destination channel conditions are comparable, Dh-SM exhibits over a 2 dB coding gain over to DF. It should be noted that as any DF system, Dh-SM is susceptible to bottlenecks. In particular, the relay to destination link constraints the performance of Dh-SM and the addition of more transmit antennas at the source results in marginal gains. Indeed, having 4 transmit antennas at the source increases the advantage of Dh-SM to 2.4 dB and transmission using 32 transmit antennas results in 3.5 dB gains. The system is constrained by the BER of the relay to destination link. Hence, as a next step, we remove the bottleneck of the source to relay link by setting $N_t^{\text{s}} = 32$ and analyse the effects of the number of transmit antennas at the relay. Looking at Fig. 4, coding gains of 3.5 dB are achieved with only 2 transmit antennas at the relay. This advantage is increased to about 4 dB with 4 transmit antennas and reaches 5 dB when using 32 transmit antennas at the relay. In general, systems with more available antennas still exhibit better performance in terms of BER, although the coding gains achieved with every additional antenna are diminishing. It should be noted that while having 32 transmit antennas on a single node may not

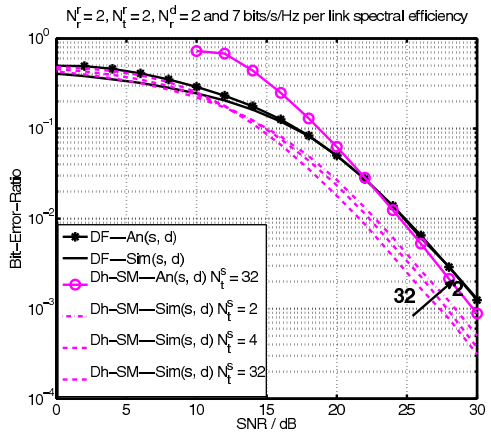

Fig. 3. Average bit error ratio when $\bar{\gamma}_{\text{sr}} = \bar{\gamma}_{\text{rd}}$ and the number of transmit antennas at the source is varied. The average source to destination spectral efficiency is 3.5 bits/s/Hz. The arrow on the figure indicates the progression of the curves going from $N_t^{\text{s}} = 32$ as the leftmost dashed curve to $N_t^{\text{s}} = 2$ as the rightmost dashed curve.

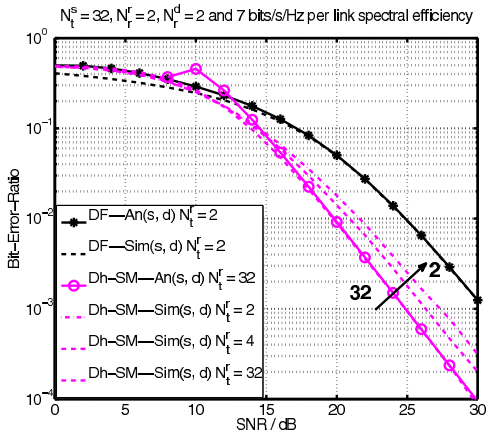

Fig. 4. Average bit error ratio when $\bar{\gamma}_{\text{sr}} = \bar{\gamma}_{\text{rd}}$ and the number of transmit antennas at the relay is varied. The average source to destination spectral efficiency is equal to 3.5 bits/s/Hz. The arrow on the figure indicates the progression of the curves going from $N_t^{\text{r}} = 32$ as the leftmost dashed curve to $N_t^{\text{r}} = 2$ as the rightmost dashed curve.

be realistic, this work provides a good basis for the expected performance of a distributed relaying scenario utilising SM where multiple transmit antennas would be available. It shows that such a system is expected to provide sufficient gains to motivate further work.

We now investigate the behaviour of Dh-SM with respect to the number of receive antennas. As Fig. 5 shows, Dh-SM performs better as more receive antennas are added to the system, irrespective of which node they are added to. Despite the coding gains observed, the system is still limited by its worse performing link in terms of the BER since the diversity

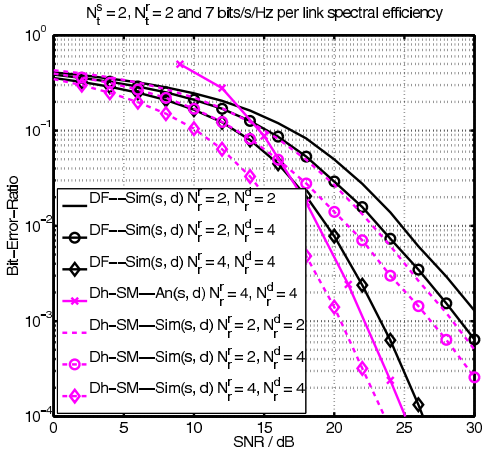

Fig. 5. Average bit error ratio when $\bar{\gamma}_{\text{sr}} = \bar{\gamma}_{\text{rd}}$ and the number of receive antennas at the relay and destination is varied. The average source to destination spectral efficiency is equal to 3.5 bits/s/Hz.

of the overall system is $\min\{N_r^{\text{r}}, N_r^{\text{d}}\}$. Looking at Fig. 5, we can see that Dh-SM has about 2.2 dB gain with respect DF when there are 2 receive antennas at both the relay and the destination. When there are 2 and 4 receive antennas at the relay and destination nodes respectively, Dh-SM has a 2.6 dB gain with respect to DF, *i.e.* the performance of Dh-SM improves by 0.4 dB with the addition of 2 receive antennas at the destination. Again, the small increase in the coding gain with an increase in the number of receive antennas at the destination is the result of a bottleneck created by having only 2 receive antennas at the relay. When there are 4 receive antennas at each of the nodes, Dh-SM exhibits about 3.3 dB better performance compared to DF. Similar to the effect of diminishing returns with every added transmit antenna, Dh-SM still exhibits better performance in terms of BER with the addition of more receive antennas, although the coding gains achieved diminish. It should be noted that these coding gains in Dh-SM are in addition to the diversity gains experienced by both, DF and Dh-SM, resulting from the increase in the number of receive antennas.

With the separate effects of the number of transmit and receive antennas analysed, Fig. 6 shows that Dh-SM can exhibit between 5 dB and 10 dB gains compared to DF when the number of receive antennas at both the relay and the destination is increased to 4 and $N_t^{\text{s}} = N_t^{\text{r}}$. These gains are larger than those presented in Fig. 3 and Fig. 4 since both links have more receive antennas. The greater number of receive antennas provides an increase in spatial diversity for both DF and Dh-SM with further coding gains for Dh-SM. The coding gains exhibited by Dh-SM are partially a result of the lower order signal–constellation symbols used in SM transmission. Additionally, the more receive antennas are available, the more distinguishable the transmit antennas become which helps to reduce the BER and increase the coding gain.

With the effect of the number of antennas analysed, Fig. 7

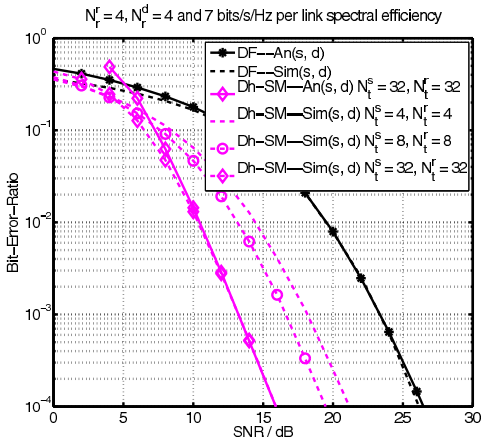

Fig. 6. Average bit error ratio when $\bar{\gamma}_{sr} = \bar{\gamma}_{rd}$ and the number of transmit antennas at the source and relay is varied. The average source to destination spectral efficiency is equal to 3.5 bits/s/Hz.

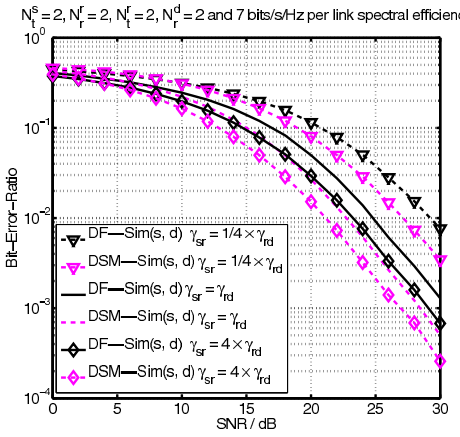

Fig. 7. The average source to destination spectral efficiency is equal to 3.5 bits/s/Hz and the channel gains are varied.

shows the effects of the varying link SNRs, *i.e.* $\bar{\gamma}_{sr} \neq \bar{\gamma}_{rd}$. Since Dh-SM relies on sequential detection, from Fig. 7 we can see that both, DF and Dh-SM, exhibit better performance when the average received SNR on the source to relay link is greater than the average received SNR on the relay to destination link. Nonetheless, the performance difference between the two systems remains the same regardless of $\bar{\gamma}_{sr}$ and $\bar{\gamma}_{rd}$. This means that the effects discussed above extend to arbitrary channel gain conditions and system geometry, provided that each node has the same transmit power.

V. Conclusion

In this work the application of SM in a dual-hop, non-cooperative scenario has been considered. The spatial domain of Dh-SM has been utilised to transmit extra information bits which help alleviate the multihop burden. Dh-SM has also been shown to provide coding gains by lowering the number of bits sent in the signal domain. The union bound method has been used to bound the BER behaviour of SM and provide a good estimate for the potential performance of Dh-SM.

It has been demonstrated that the application of SM in a relaying scenario results in better end–to–end system performance when compared to non-cooperative DF. The coding gain improved as the number of transmit antennas increased at either the source or relay nodes. Furthermore, the coding gain was also enhanced by more receive antennas added at either the relay or destination nodes. From this, it can be seen that Dh-SM has the potential to provide substantial spectral efficiency and coding gains in future wireless relay networks. Future work will focus on studying the application of SM in distributed relay networks.

Acknowledgement

We gratefully acknowledge support from the Engineering and Physical Sciences Research Council (EP/G011788/1) in the United Kingdom for this work. Professor Harald Haas acknowledges the Scottish Funding Council support of his position within the Edinburgh Research Partnership in Engineering and Mathematics between the University of Edinburgh and Heriot Watt University.

References

[1] R. Mesleh, H. Haas, Y. Lee, and S. Yun, "Interchannel Interference Avoidance in MIMO Transmission by Exploiting Spatial Information," in *Proc. of the 16th IEEE International Symposium on Personal, Indoor and Mobile Radio Communications (PIMRC)*, vol. 1, Berlin, Germany, 11-14 Sep. 2005, pp. 141–145.

[2] R. Mesleh, H. Haas, S. Sinanović, C. W. Ahn, and S. Yun, "Spatial modulation," *IEEE Trans. Veh. Technol.*, vol. 57, no. 4, pp. 2228 – 2241, July 2008.

[3] N. Serafimovski, M. D. Renzo, S. Sinanović, R. Y. Mesleh, and H. Haas, "Fractional Bit Encoded Spatial Modulation (FBE–SM)," *IEEE Commun. Lett.*, vol. 14, no. 5, pp. 429–431, May 2010.

[4] J. N. Laneman, D. N. C. Tse, and G. W. Wornell, "Cooperative Diversity in Wireless Networks: Efficient Protocols and Outage Behavior," *IEEE Trans. Inf. Theory*, vol. 50, no. 12, pp. 3062–3080, Dec. 2004.

[5] M. O. Hasna and M.-S. Alouini, "End-to-end performance of transmission systems with relays over rayleigh-fading channels," *IEEE Transactions on Wireless Communications*, vol. 2, no. 6, pp. 1126 – 1131, Nov. 2003.

[6] J. Jeganathan, A. Ghrayeb, and L. Szczecinski, "Spatial Modulation: Optimal Detection and Performance Analysis," *IEEE Commun. Lett.*, vol. 12, no. 8, pp. 545–547, 2008.

[7] T. Handte, A. Muller, and J. Speidel, "BER analysis and optimization of generalized spatial modulation in correlated fading channels," in *Vehicular Technology Conference Fall (VTC Fall-2009)*, Sep. 2009, pp. 1 –5.

[8] A. Younis, N. Serafimovski, R. Mesleh, and H. Haas, "Generalized Spatial Modulation," in *Asilomar Conference on Signals, Systems, and Computers*, Pacific Grove, CA, USA, 2010.

[9] M. D. Renzo and H. Haas, "Performance analysis of spacial modulation," in *5th International ICST Conference on Communications and Networking in China*, August 2010.

[10] R. M. Gagliardi, *Introduction to Communication Engineering*, 2, Ed. Wiley-Interscience, 1988.

[11] M. K. Simon and M. Alouini, *Digital Communication over Fading Channels*, 2nd ed., ser. Wiley series in telecommunications and signal processing. John Wiley & Sons, Inc., 2005, ISBN: 978-0-471-64953-3.

6th IEEE International Workshop on Heterogeneous, Multi-Hop, Wireless and Mobile Networks

2-User Multiple Access Spatial Modulation

Nikola Serafimovski*, Sinan Sinanović*, Abdelhamid Younis*, Marco Di Renzo†, and Harald Haas*

*Institute for Digital Communications
Joint Research Institute for Signal and Image Processing
School of Engineering
The University of Edinburgh
EH9 3JL, Edinburgh, UK
{n.serafimovski, s.sinanovic, a.younis, h.haas}@ed.ac.uk

†Laboratory of Signals and Systems (L2S),
French National Center for Scientific Research (CNRS)
École Supérieure d'Électricité (SUPÉLEC),
University of Paris–Sud XI (UPS)
3 rue Joliot–Curie, 91192 Gif–sur–Yvette (Paris), France
marco.direnzo@lss.supelec.fr

***Abstract*—Spatial modulation (SM) is a recently proposed approach to multiple–input–multiple–output (MIMO) systems which entirely avoids inter–channel interference (ICI) and requires no synchronisation between the transmit antennas, while achieving a spatial multiplexing gain. SM allows the system designer to freely trade off the number of transmit antennas with the signal constellation. Additionally, the number of transmit antennas is independent from the number of receive antennas which is an advantage over other multiplexing MIMO schemes. Most contributions thus far, however, have only addressed SM aspects for a point-to-point communication systems, *i.e.* the single-user scenario. In this work we seek to characterise the behaviour of SM in the interference limited scenario. The proposed maximum-likelihood (ML) detector can successfully decode incoming data from multiple sources in an interference limited scenario and does not suffer from the near-far problem.**

I. Introduction

Multiple-antenna systems are fast becoming a key technology for modern wireless systems. They offer improved error performance and higher data rates, at the expense of increased complexity and power consumption [1]. Spatial modulation (SM) is a recently proposed approach to multiple–input–multiple–output (MIMO) systems which entirely avoids inter–channel interference (ICI) and requires no synchronisation between the transmit antennas, while achieving a spatial multiplexing gain [2]. A spatial multiplexing gain is achieved by mapping a block of information bits into a constellation point in the signal and spatial domains [3]. In SM, the number of information bits, ℓ, encoded in the spatial domain can be related to the number of transmit antennas N_t as $N_t = 2^{\ell}$. This means that the number of transmit antennas must be a power of two unless fractional bit encoding is used [4]. Additionally, compared to other MIMO schemes, the spatial multiplexing gain *i.e.* the number of transmit antennas, is independent of the number of receive antennas. This offers the flexibility to trade off the number of transmit antennas with the modulation order in the signal domain to meet the desired data rate without regard for the number of receive antennas. It should also be noted that SM is shown to outperform other MIMO schemes in terms of bit-error-ratio (BER) [3].

A number of papers are available in the literature which are aimed at understanding and improving the performance of SM in various scenarios. Trellis coding on the transmit antenna is proposed in [5], a reduced complexity decoder is given in [6] and the performance of SM over a wide range of channels is presented in [7]. The optimal detector is known with and without channel state information at the receiver in [8–10]. The optimal power allocation problem for a 2 transmit with 1 receive antenna system is solved in closed form in [11] and the performance of SM in correlated fading channels is considered in [12]. Recent work has also shown that SM can be combined with space-time block codes to attain spectral efficiency gains [13]. SM has also been applied to relaying systems in [14] where it exhibits significant signal-to-noise-ratio (SNR) gains when compared to non-cooperative decode and forward.

Most contributions thus far, however, have only addressed SM aspects for a point-to-point communication systems, *i.e.* the single-user scenario. These scenarios include the application of SM in traditional orthogonal access systems such as frequency division multiple access (FDMA), time division multiple access (TDMA) or orthogonal frequency division multiple access (OFDMA) where co-channel interference is managed by ensuring orthogonal transmissions by all nodes in the system. A notable exception is given in [15], where the authors focus their analysis on a limited two user scenario employing only space-shift-keying (SSK). It should be noted, that SSK is similar to SM in that the antenna index is used for data transmission, but instead of a full signal-symbol only a reference signal is sent to enable channel estimation at the receiver.

In this work we seek to characterise the behaviour of SM in the interference limited scenario. In particular, we propose a maximum-likelihood (ML) detector which can successfully decode incoming data in the case of simultaneous transmission and does not suffer from the near-far problem, *i.e.* the detector can successfully decode data from a user with a lower signal-to-noise-ratio (SNR). The proposed jointly optimum multi-user detector minimises the BER for all users and does not suffer from the near-far problem.

The remainder of this work is organized as follows. In Section II, the system and channel models are introduced. In Section III, the performance of SM in the multiple access scenario is characterised and the analytical modelling for the multi-user detector is proposed. Section IV provides numerical and simulation results to substantiate the accuracy of the analytical framework developed. In Section V, we summarise and conclude the work.

978-1-4673-0040-7/11/$26.00 ©2011 IEEE

II. System Model

The basic idea of SM is to map blocks of information bits into two information carrying units [3]: i) a symbol, chosen from a complex signal–constellation diagram, and ii) a unique transmit–antenna, chosen from the set of transmit–antennas in the antenna–array, *i.e.* the spatial–constellation. The general SM constellation point is thus a combination of a signal-constellation point and a spatial-constellation point. The SM constellation diagram is presented in Fig. 1.

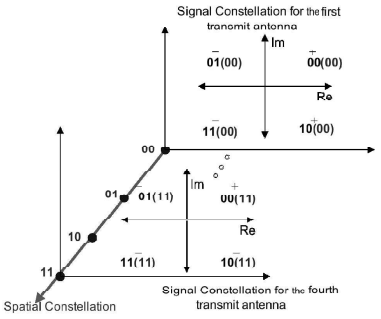

Fig. 1. A transmission of four bits is assumed. The first two bits from right to left define the spatial–constellation point identifying the active antenna, while the remaining two bits determine the signal–constellation point that will be transmitted. This scenario means that a single SM constellation point carries four information bits.

In the following work we assume a three node scenario as shown in Fig. 2 where we seek to characterise the behaviour of SM during simultaneous transmission *i.e.* in the presence of co-channel interference. We assume that the two transmit nodes, denoted as User1, node (U_1), and User2, node (U_2), in Fig. 2, transmit simultaneously to the receiver on the same time-frequency slot. Each node broadcasts a signal constellation symbol, x, from one of its available antennas.

The received signal is given by:

$$y_j = \sqrt{E_m \sigma^2_{(U_1)}}\, h_{i^{(U_1)}j} x^{(U_1)} + \sqrt{E_m \sigma^2_{(U_2)}}\, h_{k^{(U_2)}j} x^{(U_2)} + \eta \tag{1}$$

where:

- E_m is the average energy per symbol for both nodes,
- i and k are the indices of the transmit antennas from nodes 1 and 2 respectively,
- j is the index of the receive antenna from a total of N_r available,

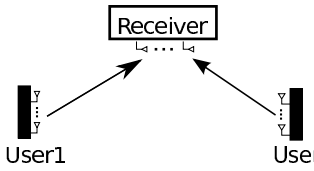

Fig. 2. Spatial modulation with simultaneous transmission. The receive cannot distinguish which is the desired and which is the interferencing user. Therefore, it must treat each users as its intended user.

- $\sigma^2_{(U_1)}$ and $\sigma^2_{(U_2)}$ are the channel attenuation coefficients on the U_1 to receiver and U_2 to receiver links in Fig. 2 respectively,
- $h_{i^{(U_1)}j}$ and $h_{k^{(U_2)}j}$ are the fast fading channel coefficients of the link between the active antennas (i, k) and the receiving antenna j, and
- η, is a complex normal random variable with zero mean and variance N_o, $\mathcal{CN}(0, N_o)$, and represents the additive white Gaussian noise (AWGN) at the receiver.

We note that all bold notations indicate vector notations. We now look at the analytical formulation of the system.

III. Analytical Modelling

In this section, we develop a ML detector for use in the presence of co-channel interference. The detector computes the Euclidean distance between the received vector signal $\bar{\mathbf{y}}$ and the set of all possible received signals, selecting the closest one. The mathematical formulation of the ML detector used in the system is given in (2). We note that this formulation is valid for any channel vectors and any transmitted symbols. In particular, if the channels are correlated *i.e.* non-orthogonal, then it will be more difficult for the receiver to distinguish the individual antennas used in the transmission, which will result in an increase of the BER.

Starting from the system model presented in Section II, the decoded pair $(x_{\text{est}}, n_t)^{(\xi)}$, formed from the estimated symbol x_{est} emitted from antenna n_t on node ξ, where $\xi \in \{(U_1), (U_2)\}$, is given by:

$$\begin{Bmatrix} (x_{\text{est}}, n_t)^{(U_1)}, \\ (x_{\text{est}}, n_t)^{(U_2)} \end{Bmatrix} = \underset{}{\text{argmin}} \left\{ \left\| \bar{\mathbf{y}} - \sum_{u \in \{(U_1),(U_2)\}} x^{(u)} \mathbf{h}_{n_t^{(u)}} \right\|^2_{\text{F}} \right\} \tag{2}$$

$$x^{(u)} \in \mathcal{X}^{(u)} \qquad n_t^{(u)} \in \{1 \dots N_t^{(u)}\}$$

$\mathcal{X}^{(u)}$ is the set of all possible signal constellation points for node u with $M^{(u)}$ number of elements, $N_t^{(u)}$ is the number of available transmit antennas on node u and $||\cdot||_{\text{F}}$ is the Frobenius norm.

From here we can use techniques base on the union bound to describe the behaviour of the interference aware SM detector in the high SNR regions. The union bound for the interference aware SM detector, which estimates the average bit-error-ratio (ABER) for node ξ, can be expressed as given in (3) where $\mathcal{N}_\xi(b, \hat{b}) = \mathcal{N}_\xi(n_t, \hat{n}_t) + \mathcal{N}_\xi(x, \hat{x})$. $\mathcal{N}_\xi(n_t, \hat{n}_t)$ denotes the Hamming distance between the binary representations of the antenna indices n_t and $\hat{n}_t$ on node ξ. Similarly, $\mathcal{N}_\xi(x, \hat{x})$ denotes the Hamming distance between the binary representations of the symbols x and $\hat{x}$ on node ξ.

We define PEP $\left(x^{(U_1),(U_2)}, n_t^{(U_1),(U_2)}, \hat{x}^{(U_1),(U_2)}, \hat{n}_t^{(U_1),(U_2)}\right)$ to be the pairwise error probability between the symbol $x^{(U_1),(U_2)}$ emitted from antennas $n_t^{(U_1),(U_2)}$ being detected as symbol $\hat{x}^{(U_1),(U_2)}$ emitted by antenna $\hat{n}_t^{(U_1),(U_2)}$. It should be noted that the pairs, $\left(x^{(U_1),(U_2)}, n_t^{(U_1),(U_2)}\right)$ and $\left(\hat{x}^{(U_1),(U_2)}, \hat{n}_t^{(U_1),(U_2)}\right)$, come from the set of

$$\text{ABER}_{\xi} \leq \sum_{\substack{x^{(U_1),(U_2)},\\ n_t^{(U_1),(U_2)}}}^{M^{(U_1)}N_t^{(U_1)}} \sum_{\substack{\hat{x}^{(U_1),(U_2)},\\ \hat{n}_t^{(U_1),(U_2)}}}^{M^{(U_2)}N_t^{(U_2)}} \frac{\mathcal{N}_{\xi}(b,\hat{b})}{\log_2\left(M^{(\xi)}N_t^{(\xi)}\right)} \frac{\text{E}_{\mathbf{H}}\left[\text{PEP}\left(x^{(U_1),(U_2)}, n_t^{(U_1),(U_2)}, \hat{x}^{(U_1),(U_2)}, \hat{n}_t^{(U_1),(U_2)}\right)\right]}{M^{(U_1)}N_t^{(U_1)}M^{(U_2)}N_t^{(U_2)}}. \quad (3)$$

$$\text{PEP}(\cdot) = Q\left(\sqrt{\frac{E_m}{2N_o}}\left|\left|\sigma_{(U_1)}\left(\mathbf{h}_{n_t^{(U_1)}}x^{(U_1)} - \mathbf{h}_{\hat{n}_t^{(U_1)}}\hat{x}^{(U_1)}\right) + \sigma_{(U_2)}\left(\mathbf{h}_{n_t^{(U_2)}}x^{(U_2)} - \mathbf{h}_{\hat{n}_t^{(U_2)}}x^{(U_2)}\right)\right|\right|^2\right) \quad (4)$$

all possible symbol-antenna pairs for both nodes, *i.e.* $\left(x^{(U_1),(U_2)}, n_t^{(U_1),(U_2)}\right) = \mathbf{h}_{n_t^{(U_1)}}x^{(U_1)} + \mathbf{h}_{n_t^{(U_2)}}x^{(U_2)}$ and $\left(\hat{x}^{(U_1),(U_2)}, \hat{n}_t^{(U_1),(U_2)}\right) = \mathbf{h}_{\hat{n}_t^{(U_1)}}\hat{x}^{(U_1)} + \mathbf{h}_{\hat{n}_t^{(U_2)}}\hat{x}^{(U_2)}$. $\text{E}_{\mathbf{H}}[\cdot]$ represents the expectation of the system with respect to the channel and $Q(\omega) = \frac{1}{\sqrt{2\pi}}\int_{\omega}^{\infty}\exp\left(-\frac{t}{2}\right)dt$.

The ABER for node ξ is shown in (3), where the pairwise error probability is given in (4). Due to space constraints, we omit the derivation of (4). We note that thus far no assumptions have been made as to the distribution of the channel.

If we consider a Rayleigh fading channel, then we can derive the closed form solution for $\text{E}_{\mathbf{H}}[\text{PEP}(\cdot)]$ in (3) by employing the solution to [16, eq. 62]. We note that by assuming a Rayleigh fading channel, the argument within (4) can be represented as the summation of $2N_r$ squared Gaussian random variables, with zero mean and variance equal to 1, which means that they can be described by a central Chi-squared distribution with $2N_r$ degrees of freedom and a probability density function of:

$$p_K(\kappa) = \frac{1}{2^{N_r}(N_r-1)!}\kappa^{N_r-1}\exp(-\kappa/2).$$

The result for $\text{E}_{\mathbf{H}}[\text{PEP}(\cdot)]$ is given as:

$$\text{E}_{\mathbf{H}}[\text{PEP}(\cdot)] = f(c)^{N_r}\sum_{r=0}^{N_r-1}\binom{N_r-1+r}{r}(1-f(c))^r \quad (5)$$

such that

$$f(c) = \frac{1}{2}\left(1-\sqrt{\frac{c}{1+c}}\right)$$

where

$$c = \frac{E_m}{4N_o}\sum_{u\in\{U_1,U_2\}}\sigma_{(u)}^2\lambda_{(u)} \quad (6)$$

which is a quarter of the received SNR at the receiver, and

$$\lambda_{(u)} = \begin{cases} \left(|x_{(u)}|^2 + |\hat{x}_{(u)}|^2\right) & n_t^{(u)} \neq \hat{n}_t^{(u)}, \\ \left(|x_{(u)} - \hat{x}_{(u)}|^2\right) & n_t^{(u)} = \hat{n}_t^{(u)}, \\ 0 & n_t^{(u)} = \hat{n}_t^{(u)} \text{ and } x_{(u)} = \hat{x}_{(u)}. \end{cases}$$

IV. Simulation Results and Discussion

In this section we aim to show that the interference aware detector proposed in (2) can successfully decode the incoming streams for the two users. Numerical results are shown which demonstrate that (3) provides a tight upper bound for the BER of the interference aware detector at high SNR. The aim of this work is to develop and test a viable multi-user detector for SM.

A. Simulation Setup

A frequency-flat Rayleigh fading channel with no correlation between the transmitting antennas and AWGN is assumed. Perfect channel state information (CSI) is assumed at the receiving node, with no CSI at the transmitter. Only one of the available transmit antennas for each node is active at any transmitting instance. In theory each user independently decides the number of transmit antennas and the symbol modulation it uses. For use in the simulation we assume each node has the same number of transmit antennas as well as the same spectral efficiency target. In each figure, for each user, there are three presented results: i) the simulation results for the interference aware detector, denoted by `Sim(User`ξ`)`, ii) the theoretical results from (3) using (5), denoted by `Analytical(User`ξ`)`, and iii) the single-user-lower-bound (SULB), denoted by `SULB(User`ξ`)`. We define SULB as the system performance in a single-user-single-receiver scenario where the system performance is determined purely by its SNR, defined as $\frac{E_m}{2N_o}$. The theory behind SULB is well developed in [7].

B. Results

Fig. 3 and Fig. 4 clearly demonstrate that the analytical model presented in (3) represents a tight upper bound for the system in the high SNR region. Additionally, we can see that the system with the lowest SNR has similar performance to that predicted by its SULB. It should be noted that this is not the case for the node with the better SNR. This difference in performance of the two systems can be explained by looking at the error contribution of each element from each node in the analytical prediction.

We define two sets, one for every pairwise possibility within a particular user, given by $\Omega^{(U_1)}$ in (7) for User1. We can similarly define the set $\Omega^{(U_2)}$ for User2. If we now consider (3) and (4) we see that the overall error for each user is inevitably influenced by the errors from the other user. However, since each element from $\Omega^{(U_1)}$ is associated with the full set of possible errors from $\Omega^{(U_2)}$, then all erroneous terms from $\Omega^{(U_1)}$ will 'carry' the full error from the terms in $\Omega^{(U_2)}$ and vice versa. This means that besides the pairwise error associated with the mis-detection of the antenna-symbol combination of User1 alone, the error term for User1 is increased by the pairwise error of User2 and vice versa, *i.e.* the overall error for node 1 has $\left[\left(\text{card}\left\{\Omega^{(U_1)}\right\} - M^{(U_1)}N_t^{(U_1)}\right)\text{card}\left\{\Omega^{(U_2)}\right\}\right]$ number of error terms where $\text{card}\{\cdot\}$ denotes the cardinality of a given set.

We further note that each pairwise error from the user with

the worse SNR makes a bigger contribution to the overall BER than the pairwise error from the node with the better SNR. This can be shown if we look at the Euclidean distance between the different pairwise errors. We classify a pairwise error if the Euclidean distance between the symbol-antenna pairs being tested is greater than zero. In particular, the greater the Euclidean distance becomes, the smaller the error from that term. From (4) it is clear that the pairwise error depends on the SNR as well as the Euclidean distance. It thus follows that given pairwise error terms with the same Euclidean distance, the worse the SNR is for each term, the greater the absolute pairwise error. Considering the above, it is clear that the node with the better channel gain never performs close to its SULB, while the node with the worse channel gain does perform near its SULB.

Fig. 3 and Fig. 4 demonstrate this behaviour. The gap in performance with respect to the SULB for the main contributor to the overall user error, *i.e.* the node with the lower SNR, effectively increases the BER of the node with the higher SNR. To further elaborate, we note that the difference between the simulation BER curves of the two nodes when $N_r = 2$ and $N_r = 3$ increases as more receive antennas are added. This can be explained if we consider that by increasing the number of receive antennas, the diversity of the system increases and the pairwise error terms for each node approach zero more rapidly. This mean that the absolute pairwise error contributed to the overall BER is less for each node. As a consequence, the node with the better channel gain *i.e.* the node with higher SNR, will perform closer to its SULB.

On the one hand, moving from Fig. 3 and Fig. 4 to Fig. 5, we notice that for a fixed spectral efficiency and a fixed number of transmit antennas, the addition of more receive antennas results in an increasing gap between the average analytical BER curves of the two nodes. In particular, a gap of around 4 dB between the performance of User1 and User2 with $N_r = 2$ is increased to around 7 dB when $N_r = 4$ and further increased to around 9 dB for $N_r = 8$. On the other hand, given that the two nodes experience a channel gain difference of 10 dB, we know that the interference aware detector cannot reach the performance of independent detection and the SULB for the node with the better SNR. Nonetheless, the gap between their respective BER curves tends toward the difference between the channel attenuations of the two users as N_r grows to infinity but can never reach it *i.e.* the gap tends towards 10 dB.

The addition of more transmit antennas at each of the nodes results in SNR gains for each node as can be seen when we compare Fig. 4 and Fig. 6. Interestingly, however, increasing the number of transmit antennas does not change the relative behaviour of the system, *i.e.* the SNR difference between the BER curves of the two nodes remains constant. This behaviour is expected when we consider that (5) is independent of N_t and heavily influenced by N_r. In particular, the BER of both nodes is dependent on the variance of the channel coefficients in (4) which follow a central chi-squared distribution with $2N_r$ degrees of freedom. This variance is defined in (6).

At this point it should be noted that while the proposed detector is jointly optimum for both nodes and does not suffer from the near-far problem, it needs full CSI from

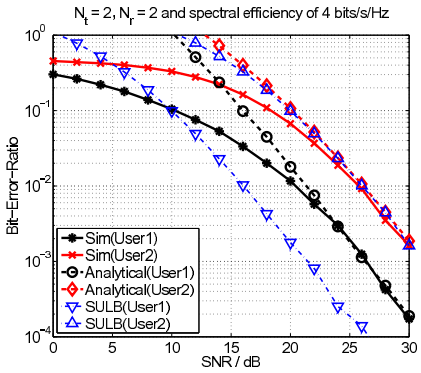

Fig. 3. BER for user 1 with $\sigma^2_{(U_1)} = 1$ and user 2 with $\sigma^2_{(U_2)} = 0.1$ using the interference aware detector.

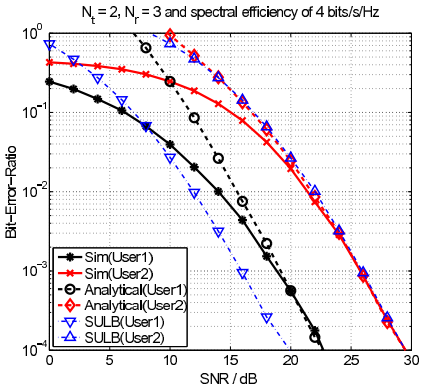

Fig. 4. BER for user 1 with $\sigma^2_{(U_1)} = 1$ and user 2 with $\sigma^2_{(U_2)} = 0.1$ using the interference aware detector.

all possible transmitting antennas to each receiving antenna. Additionally, finding the optimal solution is an exponentially complex problem, *i.e.* if we assume each node has the same number of transmit antennas and uses the same signal constellation, then the multi user ML detector has $\mathcal{O}\left((MN_t)^{N_u}\right)$ computational complexity which is proven to be NP-complete [17]. Fortunately, recent work on sphere detection algorithms may be used to alleviate this computational cost [18].

V. Conclusion

In this work the performance of SM with simultaneous transmission was analysed. A ML detector for SM in the interference limited scenario was proposed. Its performance over uncorrelated Rayleigh fading channels was studied and a closed form solution for the upper bound of the system was provided. Numerical results verified that the proposed analysis was fairly accurate for the high SNR regions. On the one hand, increasing the number of transmit antennas at each of the nodes from 2 to 4 resulted in SNR gains of around 2 dB. This measure did not, however, have any effect on the

$$\Omega^{(U_1)} = \{(\mathbf{h_1}x_1, \mathbf{h_1}x_1), (\mathbf{h_1}x_1, \mathbf{h_2}x_2), \ldots, (\mathbf{h_1}x_1, \mathbf{h_{N_t}}x_M),\ (\mathbf{h_2}x_1, \mathbf{h_1}x_1), \ldots, (\mathbf{h_{N_t}}x_M, \mathbf{h_{N_t}}x_M)\} \quad (7)$$

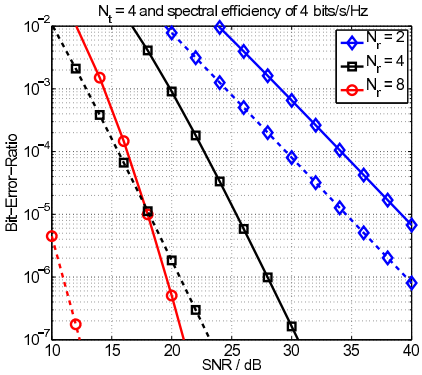

Fig. 5. BER for user 1 with $\sigma^2_{(U_1)} = 1$ and user 2 with $\sigma^2_{(U_2)} = 0.1$. Solid lines denote the performance of user 2 with a varying number of receive antennas while dashed lines denote the performance of user 1 with a varying number of receive antennas.

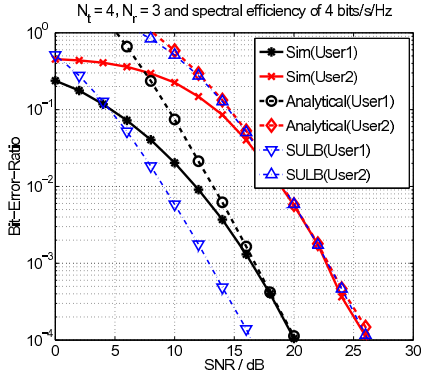

Fig. 6. BER for user 1 with $\sigma^2_{(U_1)} = 1$ and user 2 with $\sigma^2_{(U_2)} = 0.1$ using the interference aware detector.

relative coding gain between the BER curves of the two nodes *i.e.* the two nodes improved their performance by the same amount. On the other hand, increasing the number of receive antennas increased the diversity of the system and decreased the error contribution of each node, thus increasing the SNR gap between the BER curves of the two nodes.

The generalization of this work to a system with an arbitrary number of nodes, along with further investigation on the performance of SM in an interference limited scenario will be considered in the future.

Acknowledgement

We gratefully acknowledge support from the Engineering and Physical Sciences Research Council (EP/G011788/1) in the United Kingdom for this work. Professor Harald Haas acknowledges the Scottish Funding Council support of his position within the Edinburgh Research Partnership in Engineering and Mathematics between the University of Edinburgh and Heriot Watt University. Nikola Serafimovski would like to acknowledge Harald Burchardt for his advice.

References

[1] J. Mietzner, R. Schober, L. Lampe, W. H. Gerstacker, and P. A. Hoeher, "Multiple-antenna techniques for wireless communications - a comprehensive literature survey," *Communications Surveys Tutorials, IEEE*, vol. 11, no. 2, pp. 87 –105, 2009.

[2] R. Mesleh, H. Haas, Y. Lee, and S. Yun, "Interchannel Interference Avoidance in MIMO Transmission by Exploiting Spatial Information," in *Proc. of the 16th IEEE International Symposium on Personal, Indoor and Mobile Radio Communications (PIMRC)*, vol. 1, Berlin, Germany, 11-14 Sep. 2005, pp. 141–145.

[3] R. Mesleh, H. Haas, S. Sinanović, C. W. Ahn, and S. Yun, "Spatial Modulation," *IEEE Trans. Veh. Technol.*, vol. 57, no. 4, pp. 2228 – 2241, July 2008.

[4] N. Serafimovski, M. Di Renzo, S. Sinanović, R. Y. Mesleh, and H. Haas, "Fractional Bit Encoded Spatial Modulation (FBE–SM)," *IEEE Commun. Lett.*, vol. 14, no. 5, pp. 429–431, May 2010.

[5] R. Mesleh, M. Di Renzo, H. Haas, and P. M. Grant, "Trellis Coded Spatial Modulation," *IEEE Trans. on Wireless Commun.*, vol. 9, no. 7, pp. 2349–2361, July 2010.

[6] A. Younis, R. Mesleh, H. Haas, and P. Grant, "Reduced Complexity Sphere Decoder for Spatial Modulation Detection Receivers," in *2010 IEEE Global Telecommunications Conference GLOBECOM 2010*, Miami, USA, 2010, pp. 1 –5.

[7] M. Di Renzo and H. Haas, "Performance analysis of spatial modulation," in *5th International ICST Conference on Communications and Networking in China*, August 2010.

[8] J. Jeganathan, A. Ghrayeb, and L. Szczecinski, "Spatial Modulation: Optimal Detection and Performance Analysis," *IEEE Commun. Lett.*, vol. 12, no. 8, pp. 545–547, 2008.

[9] S. U. Hwang, S. Jeon, S. Lee, and J. Seo, "Soft-Output ML Detector for Spatial Modulation OFDM Systems," *IEICE Electronics Express*, vol. 6, no. 19, pp. 1426–1431, Oct. 2009.

[10] M. Di Renzo and H. Haas, "Spatial modulation with partial-csi at the receiver: optimal detector and performance evaluation," in *Proceedings of the 33rd IEEE conference on Sarnoff*, ser. Sarnoff'10. Piscataway, NJ, USA: IEEE Press, 2010, pp. 58–63. [Online]. Available: http://portal.acm.org/citation.cfm?id=1843486.1843498

[11] ——, "Improving the performance of space shift keying (SSK) modulation via opportunistic power allocation," *Communications Letters, IEEE*, vol. 14, no. 6, pp. 500 –502, 2010.

[12] T. Handte, A. Muller, and J. Speidel, "BER analysis and optimization of generalized spatial modulation in correlated fading channels," in *Vehicular Technology Conference Fall (VTC Fall-2009)*, Sep. 2009, pp. 1 –5.

[13] E. Basar, U. Aygolu, E. Panayirci, and V. H. Poor, "Space-time block coded spatial modulation," *Communications, IEEE Transactions on*, vol. 59, no. 3, pp. 823 –832, 2011.

[14] N. Serafimovski, S. Sinanovic, M. Di Renzo, and H. Haas, "Dual-hop Spatial Modulation (Dh-SM)," in *IEEE 73rd Vehicular Technology Conference: VTC2011-Spring*, Budapest, Hungary, May 2011.

[15] M. Di Renzo and H. Haas, "On the performance of ssk modulation over multiple-access rayleigh fading channels," in *GLOBECOM 2010, 2010 IEEE Global Telecommunications Conference*, dec. 2010, pp. 1 –6.

[16] M.-S. Alouini and A. Goldsmith, "A Unified Approach for Calculating Error Rates Of Linearly Modulated Signals over Generalized Fading Channels," *IEEE Transactions on Communications*, vol. 47, no. 9, pp. 1324–1334, 1999.

[17] S. Verdu, "Computational complexity of optimum multiuser detection," *Algorithmica*, vol. 4, pp. 303–312, 1989, 10.1007/BF01553893. [Online]. Available: http://dx.doi.org/10.1007/BF01553893

[18] A. Younis, M. Di Renzo, R. Mesleh, and H. Haas, "Sphere Decoding for Spatial Modulation," in *IEEE International Conference on Communications (IEEE ICC 2011)*, Kyoto, Japan, 5–9 Jun. 2011.

Generalised Spatial Modulation

Abdelhamid Younis*, Nikola Serafimovski*, Raed Mesleh‡ and Harald Haas*‡
*Institute for Digital Communications, Joint Research Institute for Signal and Image Processing, The University of Edinburgh, Edinburgh EH9 3JL, UK, Email: {a.younis & n.serafimovski & h.haas}@ed.ac.uk
‡University of Tabuk, Electrical Engineering Department, P.O.Box: 741, 71491 Tabuk, Saudi Arabia, Email: raed.mesleh@ieee.org

***Abstract*—In this paper, a generalised technique for spatial modulation (SM) is presented. Generalised spatial modulation (GSM) overcomes in a novel fashion the constraint in SM that the number of transmit antennas has to be a power of two. In GSM, a block of information bits is mapped to a constellation symbol and a spatial symbol. The spatial symbol is a combination of transmit antennas activated at each instance. The actual combination of active transmit antennas depends on the random incoming data stream. This is unlike SM where only a single transmit antenna is activated at each instance. GSM increases the overall spectral efficiency by base–two logarithm of the number of antenna combinations. This reduces the number of transmit antennas needed for the same spectral efficiency. The performance of GSM is analysed in this paper, and an upper bound on the bit–error–ratio (BER) performance is derived. In addition, an algorithm to optimise the antenna combination selection is proposed. Finally, the performance of GSM is validated through Monte Carlo simulations. The results are compared with traditional SM. It is shown that for the same spectral efficiency GSM performs nearly the same as SM, but with a significant reduction in the number of transmit antennas.**

***Index Terms*—Spatial modulation, generalised spatial modulation, MIMO.**

I. Introduction

Multiple-input multiple-output (MIMO) systems offer a significant increase in spectral efficiency, in comparison to single antenna systems [1]. An example is the Vertical Bell Labs layered space-time (V-BLAST) architecture [2], where the spectral efficiency increases linearly with the number of transmit antennas. However, transmitting from all antennas at the same time, on the same frequency, causes inter-channel interference (ICI) at the receiver.

Spatial Modulation (SM) is a spatial multiplexing MIMO technique that is proposed in [3] to increase the spectral efficiency and to overcome inter–channel interference (ICI). This is attained by activating only a single transmit antenna at each instance to transmit a certain data symbol, where the active antenna index and the data sent depend on the incoming random data bits. Thereby, an overall increase in the spectral efficiency by base–two logarithm of the number of transmit antennas is achieved. Note that, the number of transmit antennas must be a power of two. A detector that jointly estimates the active antenna index and the sent data symbol is required at the receiver side. The optimal SM decoder is proposed in [4] and SM combined with trellis-coded modulation (TCM) is recently proposed in [5]. Furthermore, space shift keying (SSK) with partial channel state information is presented in [6], and a general framework for performance analysis of SSK for multiple input single output (MISO) systems over correlated Nakagami-m fading channels is shown in [7]. It is shown in [3]–[5] that ICI avoidance results in better BER performance and a significant reduction in detection complexity, as compared to V-BLAST, for instance. However, the logarithmic increase in spectral efficiency and the requirement that the number of antennas must be a power of two would require large number of antennas.

Fractional bit encoded spatial modulation (FBE-SM) is proposed in [8] to overcome the limitation in the number of transmit antennas. FBE-SM is based on the theory of modulus conversion and allows an arbitrary number of transmit antennas. However, the system suffers from error propagation.

An alternative approach to limit the number of transmit antennas is proposed in this paper. Generalised spatial modulation (GSM) activates more than one transmit antenna at a time to simultaneously transmit a data symbol. In GSM the transmitted information is conveyed in the activated combination of transmit antennas and the transmitted symbol from a signal constellation. As a result, the number of transmit antennas required to achieve a certain spectral efficiency is reduced by more than a half in GSM as compared to SM, and generalised space shift keying modulation (GSSK) proposed in [9]. Transmitting the same data symbol from more than one antenna at a time, retains the key advantage of SM, which is the complete avoidance of ICI at the receiver. Moreover, GSM offers spatial diversity gains and increases the reliability of the wireless channel, by providing replicas of the transmitted signal to the receiver [10]. Nonetheless, the activated transmit antennas must be synchronised to avoid inter-symbol interference (ISI). At the receiver, a maximum likelihood (ML) detection algorithm is considered to estimate the activated combination of transmit antennas and the transmitted constellation symbol.

A tight analytical upper bound for the BER performance of GSM is derived in this paper and analytical results are validated through Monte Carlo simulation results. Moreover, GSM performance is shown to be very close to the performance of SM but with major reduction in the required number of transmit antennas.

The remainder of this paper is organised as follows: Section II presents GSM system model and the optimal detection technique. Section III presents the analytical BER derivation for GSM and proposes the selection process for the optimal antenna combinations. The receiver complexity is discussed in

978-1-4244-9721-8/10/$26.00 ©2010 IEEE

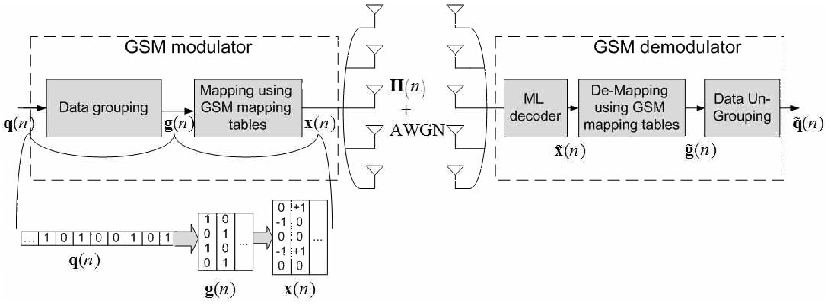

Fig. 1. Generalised spatial modulation system model. At each instance, four bits are transmitted. Three bits are encoded in the indices of the combination of transmit antennas and one bit is conveyed in the signal domain using BPSK modulation.

section IV. Monte Carlo Simulation results are presented in Section V, and the paper is concluded in Section VI.

II. GSM System Model

GSM uses more than one transmit antenna to send the same complex symbol. Hence, a set of antenna combinations can be formed, and used as spatial constellation points. The number of possible antenna combinations is $N_c' = \binom{N_t}{N_u}$, where N_t is the number of transmit antennas and N_u is the number of active antennas at each instance. However, the number of antenna combinations that can be considered for transmission must be a power of two. Therefore, only $N_c = 2^{m_\ell}$ combinations, can be used, where $m_\ell = \lfloor \log_2 \binom{N_t}{N_u} \rfloor$, and $\lfloor \cdot \rfloor$ is the floor operation.

The GSM system model is depicted in Fig. 1 and an example of data mapping and transmission for two instances is also shown. The incoming data bits are mapped to a spatial symbol and a data symbol according to the mapping table shown in Table I. The mapping procedure maps the first m_ℓ bits to the antenna combinations, and the remaining bits (m_s) are modulated using M-QAM modulation, where $M = 2^{m_s}$. In the example, $N_t = 5$ and $N_u = 2$ are assumed. The resultant antenna combinations are listed in Table I. For instance, the data bits to be transmitted at the first instance in Fig. 1 $\mathbf{g}(n) = \begin{bmatrix} 0 & 1 & 0 & 1 \end{bmatrix}$ are mapped to $\mathbf{x}(n) = \begin{bmatrix} +1 & 0 & 0 & +1 & 0 \end{bmatrix}$. Each column vector of $\mathbf{x}(n)$ is transmitted at a specific instance from the existing five transmit antennas where only two antennas are activated at any given time. If SM is used instead with the same modulation order, the number of transmit antennas must be increased to eight to maintain the same spectral efficiency. In general, the number of bits that can be transmitted using GSM is given by,

$$m = m_\ell + m_s = \left\lfloor \log_2 \binom{N_t}{N_u} \right\rfloor + \log_2 M \qquad (1)$$

The GSM modulated signal is transmitted over an $N_r \times N_t$ MIMO Rayleigh flat fading wireless channel, $\mathbf{H}$, and, thus, the entries of $\mathbf{H}$ are modeled as complex independent and identically distributed (i.i.d.) Gaussian random variables with zero–mean and unit–variance, where N_r is the number of receive antennas.

TABLE I
GSM Mapping Table for $N_t = 5$, $N_u = 2$ and BPSK Modulation, where $(\cdot,\cdot)$ indicates the indices of the active antennas

Grouped Bits	Antenna Combination (ℓ)	Symbol (s)
0000	(1,2)	-1
0001	(1,2)	+1
0010	(1,3)	-1
0011	(1,3)	+1
0100	(1,4)	-1
0101	(1,4)	+1
0110	(1,5)	-1
0111	(1,5)	+1
1000	(2,3)	-1
1001	(2,3)	+1
1010	(2,4)	-1
1011	(2,4)	+1
1100	(3,5)	-1
1101	(3,5)	+1
1110	(4,5)	-1
1111	(4,5)	+1

The received signal at any given time is,

$$\mathbf{y} = \mathbf{h}'_\ell s + \mathbf{v} \qquad (2)$$

where $s \in M$-QAM is the transmitted symbol, from the antenna combination $\ell = (\ell_1, \ell_2, \ldots, \ell_{N_u}) \in \Phi$, ℓ_n indicates the index of the n-th antenna in the antenna combination ℓ, and Φ is the set of used antenna combinations. An optimal algorithm for the selection of Φ is proposed in next section. Furthermore the vector $\mathbf{h}'_\ell = \sum_{n=1}^{N_u} \mathbf{h}_{\ell_n}$ contains the summation of the active antennas channel vectors, and $\mathbf{h}_{\ell_n}$ is the channel vector from the active transmit antenna ℓ_n to all receive antennas. $\mathbf{v}$ is an AWGN vector with zero–mean and variance σ_n^2 per dimension at the receiver input.

At the receiver, the spatial symbol and the data symbol are jointly decoded using the ML principle, as follows,

$$\begin{aligned} [\tilde{\ell}, \tilde{s}] &= \arg\max_{\ell,s} p_{\mathbf{y}}(\mathbf{y}|\mathbf{x}, \mathbf{H}) \\ &= \arg\min_{\ell,s} \sum_{i=1}^{N_r} |y_i - h'_{\ell,i} s|^2 \end{aligned} \qquad (3)$$

where,

$$p_{\mathbf{y}}(\mathbf{y}|s,\ell,\mathbf{H}) = \frac{1}{(\pi\sigma_n^2)^{N_t}} \exp\left(-\frac{\|\mathbf{y}-\mathbf{h}'_\ell s\|_{\mathrm{F}}^2}{\sigma_n^2}\right) \quad (4)$$

is the probability density function (PDF) of $\mathbf{y}$ conditional on s, ℓ and $\mathbf{H}$, $\|\cdot\|_{\mathrm{F}}^2$ is the Frobenius norm.

III. Analytical derivation and optimal combination selection

A. Analytical BER calculation of GSM

The analytical performance of GSM is estimated using the well-known union bounding technique [11]. The average BER in GSM is,

$$\Pr_{\text{e,bit}} \leq \mathrm{E}_{\mathbf{x}}\left[\sum_{\tilde{\ell},\tilde{s}} \frac{N\left(x_{\ell,s}, x_{\tilde{\ell},\tilde{s}}\right)\Pr\left(x_{\ell,s} \to x_{\tilde{\ell},\tilde{s}}\right)}{2^m}\right] \quad (5)$$

where $x_{\ell,s}$ indicates the symbol s transmitted from the antenna combination ℓ, $N\left(x_{\ell,s}, x_{\tilde{\ell},\tilde{s}}\right)$ is the number of bits in error between $x_{\ell,s}$ and $x_{\tilde{\ell},\tilde{s}}$, and $\Pr\left(x_{\ell,s} \to x_{\tilde{\ell},\tilde{s}}\right)$ denotes the probability of deciding on $x_{\tilde{\ell},\tilde{s}}$ given that $x_{\ell,s}$ is transmitted.

The probability $\Pr\left(x_{\ell,s} \to x_{\tilde{\ell},\tilde{s}}\right)$ can be computed by using (3) as follows,

$$\Pr\left(x_{\ell,s} \to x_{\tilde{\ell},\tilde{s}}\right) = \Pr\left(\sum_{i=1}^{N_r} |D_i(\ell,s)|^2 > \sum_{i=1}^{N_r} \left|D_i(\tilde{\ell},\tilde{s})\right|^2\right) \quad (6)$$

where

$$D_i(\ell,s) = y_i - h'_{\ell,i}s, \quad (7)$$

and,

$$y_i = v_i + h'_{\ell,i}s, \quad (8)$$

where $v_i \sim \mathcal{CN}(0,\sigma_n^2)$. Substituting (8) into (7) result in,

$$D_i(\ell,s) = v_i \quad (9)$$

and

$$D_i(\tilde{\ell},\tilde{s}) = v_i + h'_{\ell,i}s - h'_{\tilde{\ell},i}\tilde{s} \quad (10)$$

Hence, $D_i(\ell,s) \sim \mathcal{CN}(0,\sigma_n^2)$, $D_i(\tilde{\ell},\tilde{s}) \sim \mathcal{CN}(0,\sigma^2_{D_{\tilde{\ell},\tilde{s}}})$, and,

$$\begin{aligned}\sigma^2_{D_{\tilde{\ell},\tilde{s}}} &= \sigma_n^2 + \left(|s|^2 + |\tilde{s}|^2\right) d(\ell,\tilde{\ell}) + |s-\tilde{s}|^2\left(N_u - d(\ell,\tilde{\ell})\right) \\ &= \sigma_n^2 + 2\mathrm{Re}\{s\tilde{s}^*\} d(\ell,\tilde{\ell}) + |s-\tilde{s}|^2 N_u \end{aligned} \quad (11)$$

where $\mathrm{Re}(\cdot)$ is the real part of a complex variable and $d(\ell,\tilde{\ell})$ is the number of elements where ℓ and $\tilde{\ell}$ differ from each other.

Let,

$$\kappa_{D_{\ell,s}} = \sum_{i=1}^{N_r}\left|\frac{D_i(\ell,s)}{\sigma_n/\sqrt{2}}\right|^2 \quad (12)$$

and

$$\kappa_{D_{\tilde{\ell},\tilde{s}}} = \sum_{i=1}^{N_r}\left|\frac{D_i(\tilde{\ell},\tilde{s})}{\sigma_{D_{\tilde{\ell},\tilde{s}}}/\sqrt{2}}\right|^2 \quad (13)$$

be the summation of N_r squared complex Gaussian random variables, with zero mean and variance equal to 1, *i.e.* $\kappa_{D_{\ell,s}}$ and $\kappa_{D_{\tilde{\ell},\tilde{s}}}$ are a central chi–squared random variables with $2N_r$ degrees of freedom [11].

Substituting (12) and (13) in (6) gives,

$$\begin{aligned}\Pr\left(x_{\ell,s} \to x_{\tilde{\ell},\tilde{s}}\right) &= \Pr\left(\frac{\sigma_n^2}{2}\kappa_{D_{\ell,s}} > \frac{\sigma^2_{D_{\tilde{\ell},\tilde{s}}}}{2}\kappa_{D_{\tilde{\ell},\tilde{s}}}\right) \\ &= \Pr\left(\frac{\kappa_{D_{\tilde{\ell},\tilde{s}}}}{\kappa_{D_{\ell,s}}} < \frac{\sigma_n^2}{\sigma^2_{D_{\tilde{\ell},\tilde{s}}}}\right) \end{aligned} \quad (14)$$

Both $\kappa_{D_{\tilde{\ell},\tilde{s}}}$ and $\kappa_{D_{\ell,s}}$ are chi–square distributed random variables and have the same degree of freedom. Let,

$$\varphi = \frac{\kappa_{D_{\tilde{\ell},\tilde{s}}}}{\kappa_{D_{\ell,s}}} \quad (15)$$

which follows an F–distribution with degrees of freedom $\varsigma_1 = \varsigma_2 = 2N_r$. Substituting (15) in (14),

$$\begin{aligned}\Pr\left(x_{\ell,s} \to x_{\tilde{\ell},\tilde{s}}\right) &= \Pr\left(\varphi < \frac{\sigma_n^2}{\sigma^2_{D_{\tilde{\ell},\tilde{s}}}}\right) \\ &= F_\varphi\left(\frac{\sigma_n^2}{\sigma^2_{D_{\tilde{\ell},\tilde{s}}}}\right). \end{aligned} \quad (16)$$

$F_\varphi(\cdot)$ is the cumulative distribution function (CDF) of the F–distributed random variable given by,

$$F_\varphi(x) = I_{\frac{\varsigma_1 x}{\varsigma_1 x + \varsigma_2}}(\varsigma_1/2, \varsigma_2/2), \quad (17)$$

where $I_x(a,b)$ is the regularised incomplete beta function given by,

$$I_x(a,b) = \frac{B(x;a,b)}{B(a,b)} = \frac{1}{B(a,b)}\int_0^x t^{(a-1)}(1-t)^{(b-1)}\,dt \quad (18)$$

with

$$B(a,b) = \int_0^1 t^{(a-1)}(1-t)^{(b-1)}\,dt \quad (19)$$

From (16) and (17) it follows that,

$$\Pr\left(x_{\ell,s} \to x_{\tilde{\ell},\tilde{s}}\right) = I_{\frac{\sigma_n^2}{\sigma_n^2+\sigma^2_{D_{\tilde{\ell},\tilde{s}}}}}(N_r, N_r) \quad (20)$$

Substituting (20) in (5) yields,

$$\begin{aligned}\Pr_{\text{e,bit}} &\leq \mathrm{E}_{\mathbf{x}}\left[\sum_{\tilde{\ell},\tilde{s}} \frac{N\left(x_{\ell,s}, x_{\tilde{\ell},\tilde{s}}\right) I_{\frac{\sigma_n^2}{\sigma_n^2+\sigma^2_{D_{\tilde{\ell},\tilde{s}}}}}(N_r,N_r)}{2^m}\right] \\ &\leq \sum_{\ell,s}\sum_{\tilde{\ell},\tilde{s}} \frac{N\left(x_{\ell,s}, x_{\tilde{\ell},\tilde{s}}\right) I_{\frac{\sigma_n^2}{\sigma_n^2+\sigma^2_{D_{\tilde{\ell},\tilde{s}}}}}(N_r,N_r)}{2^{2m}} \end{aligned} \quad (21)$$

It is shown later in section V, that (21) gives a tight approximation to the GSM BER performance.

B. Optimal set of antenna combinations selection

The optimal antenna combination Φ_{opt} is found by minimising the average BER given in (21).

$$\tilde{\Gamma}_{\text{opt}} = \arg\min_{\Gamma} \Pr_{\text{c,bit}} \tag{22}$$

where Γ is the set of parameters (N_t, N_u, Φ).

From (21), it can be noted that only $N(x_{\ell,s}, x_{\tilde{\ell},\tilde{s}})$ and $\sigma^2_{D_{\tilde{\ell},\tilde{s}}}$ depend on Γ. Moreover, it can be found that the relation between I and $\sigma^2_{D_{\tilde{\ell},\tilde{s}}}$ is,

$$I_{\frac{\sigma^2_{\tilde{n}}}{\sigma^2_n + \sigma^2_{D_{\tilde{\ell},\tilde{s}}}}}(N_r, N_r) \propto \frac{1}{\sigma^2_{D_{\tilde{\ell},\tilde{s}}}} \tag{23}$$

Hence, the optimisation in (22) can be simplified to,

$$\tilde{\Gamma}_{\text{opt}} = \arg\min_{\Gamma} \sum_{\ell,s} \sum_{\tilde{\ell},\tilde{s}} \frac{N\left(x_{\ell,s}, x_{\tilde{\ell},\tilde{s}}\right)}{\sigma^2_{D_{\tilde{\ell},\tilde{s}}}} \tag{24}$$

Fig. 2 shows GSM BER performance using (21) for different set of parameters (Γ), where $m = 5$ and $N_r = 8$. On the one hand, it can be seen from Fig. 2 that the larger N_t is, the better the performance. On the other hand, as it will be shown in the next section, increasing N_t increases the complexity. Furthermore, increasing N_u increases the possibility of having the same antenna in different antenna combinations, which will reduce $d(\ell, \tilde{\ell})$, and consequently degrades GSM performance.

To further elaborate on this, it can be seen from Fig. 2 that there is an optimum number of transmit antennas. Generally a low number of transmit antennas (*e.g.* $N_t = 4$) results in a worse performance. However, increasing the number of transmit antennas does not necessarily improve the performance. For example, the performance of GSM with $N_t = 5$ is better than with $N_t = 6, 7$ or 8.

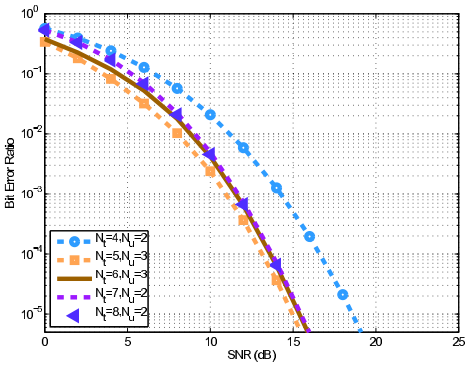

Fig. 2. GSM BER bounds for different Γ

Another interesting observation in Fig. 2 is that a different set of parameters might give very similar performance. In other words, there might not be a unique solution for the optimisation problem in (24) which provides useful flexibility for choosing Γ.

IV. Receiver Complexity

In this section the receiver complexity for GSM is compared to the complexity of the SM optimal decoder given in [4, eq. (4)], using the number of complex operations needed at the receiver. A complex operation is a complex multiplication or addition.

The optimum SM receiver is given by,

$$[\tilde{\ell}_{\text{SM}}, \tilde{s}_{\text{SM}}] = \arg\min_{\ell,s} ||\mathbf{g}_{\ell s}||^2 - 2\text{Re}\{\mathbf{y}^H \mathbf{g}_{\ell s}\} \tag{25}$$

where $\mathbf{g}_{\ell s} = \mathbf{h}_{\ell} s$. The complexity of SM optimal decoder in (25) is equal to $N_t M(3N_r + 1)$, where the first term $||\mathbf{g}_{\ell s}||^2$ needs $N_r + 1$ complex operations, and the second term $\mathbf{y}^H \mathbf{g}_{\ell s}$ needs $2N_r$ complex operations, giving a total of $3N_r + 1$ complex operations to compute the equation $(||\mathbf{g}_{\ell s}||^2 - 2\text{Re}\{\mathbf{y}^H \mathbf{g}_{\ell s}\})$, which is evaluated $N_t M$ times.

The GSM receiver has a complexity of $N_r N_c M(N_u + 2)$ complex operations, where the squared euclidean distance $|y_i - h'_{\ell,i} s|^2$ needs $N_u + 2$ complex operations, which is calculated $N_r N_c M$ times. Note that $h'_{\ell,i}$ requires a $N_u - 1$ complex summations.

The ratio of GSM receiver complexity to the complexity of SM optimal decoder for the same m_ℓ is,

$$R = \frac{N_r N_C M(N_u + 2)}{N_t M(3N_r + 1)} = \frac{N_r(N_u + 2)}{3N_r + 1} \tag{26}$$

where $N_t = N_c = 2^{m_\ell}$. This is plotted in Fig. 3 for $N_r = 8$. It can be seen that the complexity of GSM increases with the increase of N_u, but this increase is compensated by the substantial reduction in the number of transmit antennas.

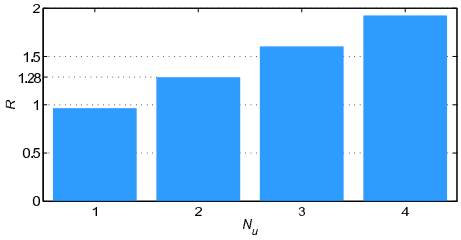

Fig. 3. The ratio of GSM receiver complexity to the complexity of SM optimal decoder

For example, let $m = 6$ bis/s/Hz, $M = 4$ and $N_r = 8$. GSM would have $\sim 28\%$ increase in complexity in comparison to SM, when $N_u = 2$. However, the number of transmit antennas required by GSM is less than half the number of transmit antennas required for SM, where $N_t = 7$ for GSM, and $N_t = 16$ for SM.

Another observation which can be made from Fig. 3 is that for $N_u = 1$ the complexity of GSM is less than the complexity of SM. This is because, the GSM ML receiver proposed here

is less complex than the SM optimal decoder. Note that, GSM with only one active antenna resembles traditional SM.

V. Simulation Results

In the following, Monte Carlo simulation results for at least 10^6 channel realisations are considered in order to compare the performance of GSM with the performance of SM. In the analysis, two different set of parameters (Γ) are considered, to achieve a spectral efficiency of $m = 6$ bits/s/Hz, using $M = 4$ and $M = 8$ QAM and $N_r = 4$.

The BER performance versus signal to noise ratio (SNR) for $M = 4$ is depicted in Fig. 4, where for GSM $N_t = 7$ and $N_u = 2$ and for SM $N_t = 16$. The performance of GSM is nearly identical to the performance of SM. The better performance of SM is mainly due to the higher probability of error when detecting two active antennas instead of only one. However, SM requires more than twice the number of transmit antennas to achieve the same spectral efficiency as compared to GSM. The result also validates the derived analytical bound and shows that, indeed, it is very tight.

The results for $M = 8$ are depicted in Fig. 5 where $N_t = 5$ and $N_u = 2$ are considered for GSM and $N_t = 8$ for SM. Again, GSM and SM have nearly the same performance, with a slightly better performance of SM at high SNR.

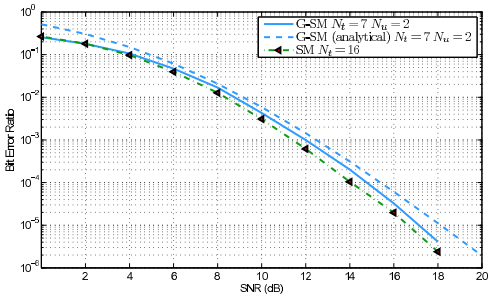

Fig. 4. BER performance versus SNR, for M=4

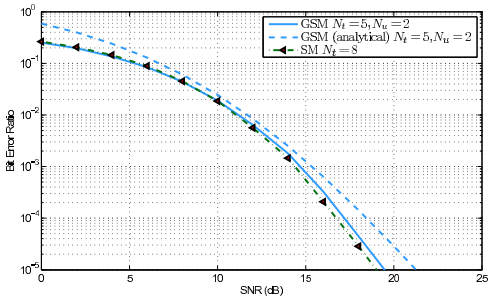

Fig. 5. BER performance versus SNR, for M=8

VI. Summary and Conclusions

In this paper SM was generalised by sending the same symbol from more than one transmit antenna at a time. Hence, SM is no longer limited to a number of transmit antennas which strictly has to follow a power of two. Instead an arbitrary number of transmit antennas can be used. Moreover, higher spectral efficiency can be achieved with a much lower number of transmit antennas, as compared to SM. These, enhancements are achieved at the cost of a slight increase in the complexity. This complexity increase depends on the number of active antennas. The smaller the number of active transmit antennas the less the complexity increase. In general, however, the increase in complexity is outweighed by the significant reduction in the number of transmit antennas. In this context, it is important to highlight that the BER performance of SM and GSM are almost identical. Moreover, GSM retains one of the key advantages of SM, namely that ICI is avoided while spatial multiplexing gains are obtained. Furthermore, this paper proposed a novel receiver based on the ML principle to determine the complete information bits, *i.e.*, the antenna combination used and the transmitted complex symbol. In addition, an algorithm to optimise the selection of the set of antenna combinations, was proposed. Finally, the analytical BER performance for GSM was derived, along with its complexity.

References

[1] E. Telatar, "Capacity of Multi-Antenna Gaussian Channels," *European Transaction on Telecommunication*, vol. 10, no. 6, pp. 585–595, November / December 1999.

[2] G. J. Foschini, "Layered Space-Time Architecture for Wireless Communication in a Fading Environment when Using Multi-Element Antennas," *Bell Labs Technical Journal*, vol. 1, no. 2, pp. 41–59, 1996.

[3] R. Mesleh, H. Haas, S. Sinanović, C. W. Ahn, and S. Yun, "Spatial modulation," *IEEE Trans. Veh. Technol.*, vol. 57, no. 4, pp. 2228 – 2241, July 2008.

[4] J. Jeganathan, A. Ghrayeb, and L. Szczecinski, "Spatial Modulation: Optimal Detection and Performance Analysis," *IEEE Commun. Lett.*, vol. 12, no. 8, pp. 545–547, 2008.

[5] R. Mesleh, M. Di Renzo, H. Haas, and P. M. Grant, "Trellis Coded Spatial Modulation," *IEEE Trans. on Wireless Commun.*, vol. 9, no. 7, pp. 2349–2361, July 2010.

[6] M. Di Renzo and H. Haas, "Space shift keying (ssk) modulation with partial channel state information: Optimal detector and performance analysis over fading channels," *IEEE Trans. on Commun.*, vol. 58, no. 11, pp. 3196 –3210, 2010.

[7] ——, "A general framework for performance analysis of space shift keying (ssk) modulation for miso correlated nakagami-m fading channels," *IEEE Trans. on Commun.*, vol. 58, no. 9, pp. 2590 –2603, 2010.

[8] N. Serafimovski, M. D. Renzo, S. Sinanović, R. Y. Mesleh, and H. Haas, "Fractional Bit Encoded Spatial Modulation (FBE–SM)," *IEEE Commun. Lett.*, vol. 14, no. 5, pp. 429–431, May 2010.

[9] J. Jeganathan, A. Ghrayeb, and L. Szczecinski, "Generalized space shift keying modulation for MIMO channels," in *Proc. IEEE 19th International Symposium on Personal, Indoor and Mobile Radio Communications PIMRC 2008*, Cannes, France, 15–18 September 2008, pp. 1–5.

[10] V. Tarokh, N. Seshadri, and A. Calderbank, "Space-Time Codes for High Data Rate Wireless Communication: Performance Criterion and Code Construction," *IEEE Trans. on Inform. Theory*, vol. 44, no. 2, pp. 744–765, 1998.

[11] J. G. Proakis, *Digital Communications*, 4th ed., ser. McGraw-Hill Series in Electrical and Computer Engineering, S. W. Director, Ed. McGraw-Hill Higher Education, December 2000.

Secrecy Capacity of Space Keying with Two Antennas

Sinan Sinanovic*, Nikola Serafimovski*, Marco Di Renzo† and Harald Haas*

*Institute for Digital Communications
Joint Research Institute for Signal and Image Processing
School of Engineering
The University of Edinburgh
EH9 3JL, Edinburgh, UK
{s.sinanovic, h.haas}@ed.ac.uk

†French National Centre for Scientific Research (CNRS)
Laboratory for Signals and Systems (LSS)
École Supérieure d'Électricité (SUPELEC)
3 rue Joliot-Curie, 91192 Gif-sur-Yvette (Paris), France
marco.direnzo@lss.supelec.fr

***Abstract*—Spatial modulation (SM) and space shift keying (SSK) use only *one* out of several transmit antennas *at a time* to transmit data via an antenna index. In such a system, the information is encoded by exploiting channel randomness *i.e.* the fact that channels between different transmit and receive antennas are random. This difference is used to distinguish among the transmit antennas. While SSK uses only antenna index to transmit data, SM also uses ordinary signal modulation. In wireless secrecy systems, one of the key performance measures is secrecy capacity. It specifies the rate at which the transmitter can communicates on the main link to the desired receiver while this information cannot be decoded by the eavesdropper. We investigate SM and SSK in the context of wireless secrecy capacity when the underlying modulation and the difference between the legitimate and eavesdropper signal to noise ratios (SNRs) are varied.**

I. Introduction

A novel multiple transmitting antenna system, termed spatial modulation (SM), has been developed in [1]. The key concept is that *only one* of several transmit antennas is active at any one time. This approach is used to convey information. For example, in the case of four transmit antennas, the fact that a specific antenna is active carries two bits, in addition to the bits transmitted by the signal itself. While the rate of this system increases only logarithmically with the number of transmit antennas, its simplicity offers an interesting complexity–rate tradeoff. In [2], the SM optimum detector has been developed. A special case, termed spatial shift keying (SSK) where *only* antenna indices are used to transmit bits, has been studied in [3].

In this paper, we study SM and SSK systems in the context of secure wireless communications. The basic setting in physical layer security in wireless systems can be described as follows. In the main link, the transmitter communicates to the intended receiver, while the eavesdropper tries to decode this information. One of the important goals is to determine the rate at which the main link can be used in such a way that the eavesdropper cannot successfully decode the same information. In classical secrecy communication, a Gaussian wiretap channel has been studied where secrecy capacity is shown to be the difference between the main and eavesdropper channel capacities when the former is greater than the latter and zero otherwise [4], [5].

In recent years, multiple-input multiple-output systems [6]–[8] and the effects of fading [9] on secrecy capacity have been studied. In this paper, we study how randomness, due to the fading of the wireless channel, can help distinguish among different transmit antennas in the context of secrecy capacity. The part of the data bits which is transmitted via the antenna index is called the spatial component of the capacity of SM. This spatial components of the capacity of SM and the capacity of SSK are studied in the context of secure communication. This concept of using a specific transmit antenna and detection of its index at the receiver in order to transmit data is termed *spatial keying*. In SM case, it offers higher rate than the SISO system with the same signal constellation size. Spatial keying also has lower rate but also less complexity than the usual multiple transmit antenna techniques which require antenna synchronisation and complex receiver for decoding the parallel streams which interfere with each other. This paper's contribution is in quantifying SM and SSK secrecy capacities under varying constellation sizes and various SNR differences between the main and eavesdropper's link.

The paper is organised as follows. In Section II, we briefly explain spatial encoding of the data. Section III explains spatial detection. In Section IV, we review symmetric channel capacity results. Section V introduces wireless secrecy concepts. In Section VII, we provide simulation results. Finally, Section VIII summarises key findings and concludes the paper with suggestions for future work.

II. Spatial Encoding of Data

A. Spatial Modulation

SM uses only one out of several transmit antennas (per channel use) to convey information in two different ways. Part of the transmitted message is encoded in the antenna number. In other words, the fact that a specific antenna is active is utilised to transmit bits. This idea relies on the ability of the receiver to distinguish between the antennas since the randomness of wireless channels associated with each transmit-receive antenna pair generally provides different channels. In simulations, it is assumed that channel coefficients are Rayleigh distributed. The remaining part of the message is encoded in a usual manner, via the signal constellation. Bits

encoded in the antenna index form the *spatial symbol* while conventional modulation bits form the *radiated symbol*.

The SM system model has N_{T} transmit and N_{R} receive antennas. The underlying signal constellation is of size M. Since $\log_2(M)$ bits are transmitted via conventional modulation and $\log_2(N_{\mathrm{T}})$ bits are transmitted via the antenna index, then one channel use corresponds to $\log_2(N_{\mathrm{T}})+\log_2(M)$ total transmitted bits. A sequence of data bits of length $\log_2(N_{\mathrm{T}})+\log_2(M)$ is mapped to a vector $\mathbf{x}$ of length N_{T} which is to be transmitted. Vector $\mathbf{x}$ satisfies the unity power constraint: $\mathrm{E}[\mathbf{x}^H\mathbf{x}]=1$. The channel is represented with the matrix $\mathbf{H}$ of size N_{R} by N_{T}, while the noise is expressed as a vector $\mathbf{n}$ of length N_{R}. $\mathbf{H}$ and $\mathbf{n}$ contain independent and identically distributed components with zero mean, unity variance complex Gaussian distribution, $\mathcal{CN}(0,1)$. The received signal $\mathbf{y}$ can then be written as $\mathbf{y}=\sqrt{\gamma}\mathbf{H}\mathbf{x}+\mathbf{n}$, where γ is the average received signal-to-noise ratio (SNR) at each receiving antenna. When vector $\mathbf{x}$ specifies activated antenna at position i from which the m^{th} constellation symbol is sent, it is denoted as $\mathbf{x}_{im}$ and the constellation symbol is denoted by x_m. Therefore, the received signal can be written as $\mathbf{y}=\sqrt{\gamma}\mathbf{h}_i x_m+\mathbf{n}$ where $\mathbf{h}_i$ denotes the i^{th} column of $\mathbf{H}$.

B. Space Shift Keying

One can view SSK as a special case of SM since there are no bits transmitted via the conventional modulation symbol x_m but only via the antenna index i since $x_m=1$ always holds. Equivalently, the fact that the only non-zero entry in vector $\mathbf{x}$ is at the i^{th} position is used to transmit information. Notation $\mathbf{x}_i$ is used to denote i^{th} active antenna. The received signal $\mathbf{y}$ can initially be expressed as $\mathbf{y}=\sqrt{\gamma}\mathbf{H}\mathbf{x}+\mathbf{n}$. The received signal can be more succinctly written as $\mathbf{y}=\sqrt{\gamma}\mathbf{h}_i+\mathbf{n}$. In other words, the transmitted symbol determines which column of $\mathbf{H}$ is used. SSK relies on a unique channel which can be recognised at the receiver in order to decode the information bits. One can therefore view the columns of $\mathbf{H}$ as random constellation points of SSK modulation. For example, if two antennas are available at the transmitter, activating either antenna can transmit one bit.

We note that *generalised* SSK and SM have been developed in [10] where more than one antenna can be active and where antenna locations are still used to encode the data but this approach is outside of the scope of the current work.

III. Spatial Detection

A. Optimal SM Detection

The maximum likelihood (ML) detector for SM jointly detects the antenna index $\hat{i}$ and conventional modulation symbol $\hat{m}$ in the following manner [2]:

$$\begin{aligned}[\hat{i},\hat{m}] &= \arg\max_{i,m} p_{\mathbf{Y}}(\mathbf{y}|\mathbf{x}_{im},\mathbf{H})\\ &= \arg\min_{i,m} \sqrt{\gamma}||\mathbf{g}_{im}||_{\mathrm{F}}^2-2\mathrm{Re}\{\mathbf{y}^{\mathrm{H}}\mathbf{g}_{im}\}\end{aligned}$$

where $||\cdot||_{\mathrm{F}}$ denotes the Frobenius norm, $\mathbf{g}_{im}=\mathbf{h}_i x_m$, $1\le i\le N_{\mathrm{T}}$, $1\le m\le M$ and $p_{\mathbf{Y}}(\mathbf{y}|\mathbf{x}_{im},\mathbf{H})=\pi^{-N_{\mathrm{R}}}\exp\left(-||\mathbf{y}-\sqrt{\rho}\mathbf{H}\mathbf{x}_{im}||_{\mathrm{F}}^2\right)$ is the probability density function (pdf) of $\mathbf{y}$ conditioned on $\mathbf{x}_{im}$ and $\mathbf{H}$. Knowledge of the channel $\mathbf{H}$ can be acquired by transmitting the known training sequence since the channel is assumed to be quasi-static, as in [9]. On the one hand, there is no closed form solution for the error performance of ML detector in SM [11]. The union bound approach provides a relatively tight upper bound but only for relatively large SNRs [11]. On the other hand, simulation will be used to compute the error probability of antenna detection, which is denoted by p_{SM}. This error can then be used in conjunction with results from Section IV to ascertain the capacity of the spatial component of SM.

B. Optimal SSK Detection

The ML detector for SSK detects the antenna index $\hat{i}$ used at the transmitter in a manner similar to SM [3]:

$$\begin{aligned}\hat{i} &= \arg\max_{i} p_{\mathbf{Y}}(\mathbf{y}|\mathbf{x}_i,\mathbf{H})\\ &= \arg\min_{i} \sqrt{\gamma}||\mathbf{h}_i||_{\mathrm{F}}^2-2\mathrm{Re}\{\mathbf{y}^{\mathrm{H}}\mathbf{h}_i\}\end{aligned}$$

where $p_{\mathbf{Y}}(\mathbf{y}|\mathbf{x}_i,\mathbf{H})=\pi^{-N_{\mathrm{R}}}\exp\left(-||\mathbf{y}-\sqrt{\rho}\mathbf{H}\mathbf{x}_i||_{\mathrm{F}}^2\right)$ is the pdf of $\mathbf{y}$ conditioned on $\mathbf{x}_i$ and $\mathbf{H}$.

As in SM case, there is no known closed form solution for the error performance of ML detector in SSK setting and the union bound approach provides relatively tight upper bound only for large SNRs [3]. Simulations are therefore used to compute the error probability of antenna detection, denoted by p_{SSK}. However, in a simple case when $N_{\mathrm{T}}=2$ and $N_{\mathrm{R}}=1$, p_{SSK} is known in closed form [12]:

$$p_{\mathrm{SSK}}=\frac{1}{2}\left(1-\sqrt{\frac{\gamma}{2+\gamma}}\right). \tag{1}$$

IV. Symmetric Channel

In a binary symmetric channel (BSC), there are two inputs which are correctly received at the output with probability $1-p$ and incorrectly with probability p. The capacity of this channel is

$$C_{\mathrm{BSC}}=1-H(p)\text{ bits per channel use,} \tag{2}$$

where $H(p)$ denotes the binary entropy function: $H(p)=-p\log_2(p)-(1-p)\log_2(1-p)$, [13]. The capacity is achieved for equally likely inputs. We can use the BSC approach to evaluate the capacity of the spatial component of SM and the SSK capacity with two transmitting antennas by noting that their error probabilities of antenna detection, p_{SM} and p_{SSK}, can replace p in the BSC in (2). In particular, the capacity of the spatial component of SM in the case of $N_{\mathrm{T}}=2$ can be expressed as

$$C_{\mathrm{SM}}=1-H(p_{\mathrm{SM}}), \tag{3}$$

while the capacity of the SSK when $N_{\mathrm{T}}=2$ can be expressed as

$$C_{\mathrm{SSK}}=1-H(p_{\mathrm{SSK}}). \tag{4}$$

More generally, let us consider the transmission matrix where the w^{th} row and the z^{th} column denote the conditional probability $p(z|w)$ such that z is received when w is sent. Then, if the rows of the channel transition matrix are

permutations of each other and the columns are permutations of each other, the channel is called *symmetric* and its capacity is given as

$$C_{\mathrm{SYM}} = \log_2 |\mathcal{Z}| - H(\text{row of transition matrix}). \quad (5)$$

where the cardinality of the output set $\mathcal{Z}$ is denoted as $|\mathcal{Z}|$. The entropy $H(W)$ of a discrete random variable W with alphabet $\mathcal{W}$ is defined as $H(W) = -\sum_{w\in\mathcal{W}} p(w)\log_2(p(w))$ where the probability mass function $p(w) = \Pr\{W = w\}$. The symmetric channel can be used to evaluate the capacity of the spatial component of SM by using the fact that $|\mathcal{Z}| = N_{\mathrm{T}}$, assuming that the channels from different transmit antennas are identically distributed and noting that the row of the transition matrix has one entry. This entry denotes the probability of correctly detecting the transmit antenna, equal to $1-p_{\mathrm{SM}}$ and all other equal to $p_{\mathrm{SM}}/(N_{\mathrm{T}}-1)$, given that the confusion between any two antennas is assumed to be equally likely. Similarly, the SSK capacity can be computed by having one entry of the row of the transition matrix equal to $1-p_{\mathrm{SSK}}$ and the rest equal to $p_{\mathrm{SSK}}/(N_{\mathrm{T}}-1)$ by assuming again that the confusion between any two antennas is equally likely.

V. Wireless Secrecy Model

A. Model

In order to study secrecy capacity, we consider a situation where a user Alice transmits a message to the legitimate receiver Bob on the legitimate channel (L). The third party Eve, who is able to eavesdrop Alice's signals, is also present and its channel is denoted by subscript (E), as shown in Fig. 1. The message is communicated via $\mathbf{x}$ over a quasi-static Rayleigh fading channel on the legitimate channel

$$\mathbf{y}_L = \sqrt{\gamma_L}\mathbf{H}_L\mathbf{x} + \mathbf{n}_L \quad (6)$$

where $\mathbf{y}_L$ denotes received signal at the intended receiver, γ_L denotes SNR at the legitimate receiver, $\mathbf{H}_L$ denotes the fading coefficients and $\mathbf{n}_L$ denotes circularly symmetric complex Gaussian noise. Knowledge of the channel $\mathbf{H}_L$ can be acquired by transmitting the known training sequence. Eve receives the signal as

$$\mathbf{y}_E = \sqrt{\gamma_E}\mathbf{H}_E\mathbf{x} + \mathbf{n}_E \quad (7)$$

where $\mathbf{y}_E$ denotes the received signal at the eavesdropper, γ_E denotes SNR at the eavesdropper, $\mathbf{H}_E$ denotes the independently faded coefficients and $\mathbf{n}_E$ denotes circularly symmetric complex Gaussian noise. It is assumed that Eve knows its quasi-static channel since it will be used repeatedly.

VI. Secrecy Capacity

In this section, secrecy capacity of SSK and the spatial component of SM are characterised in a semi-analytical fashion. First, we state the secrecy capacity of the BSC. This result is then applied to SSK and SM by using the antenna detection error probabilities, which are obtained via simulation, in the expressions for the secrecy capacity of the BSC.

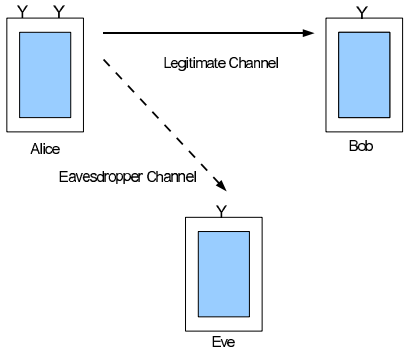

Fig. 1. Secrecy model showing legitimate user Alice with two transmit antennas and legitimate receiver Bob and eavesdropper Eve with one receiving antenna.

A. Secrecy Capacity of BSC

The secrecy capacity can be described as the maximum rate at which Alice can send information on the legitimate channel to Bob such that the rate at which eavesdropper Eve receives this information is arbitrarily small. Secrecy capacity therefore quantifies the number of bits which can be sent from Alice to Bob in secret. Let us consider BSC between Alice and Bob with the crossover probability(*i.e.* error probability) p_L and the BSC between Alice and Eve with the crossover probability p_E. It is assumed that the two BSCs are independent. Without loss of generality, it can be assumed that $p_L \leq 1/2$ and $p_E \leq 1/2$. We can now express the secrecy capacity of BSC as follows [5], [14]

$$C_s(p_L, p_E) = \begin{cases} H(p_E) - H(p_L) & \text{if } p_E > p_L, \\ 0 & \text{otherwise} \end{cases} \quad (8)$$

In other words, non-zero secrecy capacity is only possible if the crossover probability on the channel between Alice and Eve is higher than the crossover probability on the channel between Alice and Bob. We note that the secrecy capacity can also be expressed as the difference of two BSC capacities, see (8), with crossover probabilities equal to p_L and p_E. Existence of the feedback channel changes the secrecy capacity result significantly, as shown in [15], but this is outside of the scope of this paper.

B. Secrecy Capacities of SSK and Spatial Component of SM

Let $p_{L,\mathrm{SM}}$ and $p_{E,\mathrm{SM}}$ denote error probabilities of antenna detection at the legitimate receiver and eavesdropper in the SM context. Based on (8), in the case of two transmit antennas, the secrecy capacity of the spatial component of SM can be written as

$$C_{s,\mathrm{SM}}(p_{L,\mathrm{SM}}, p_{E,\mathrm{SM}}) = H(p_{E,\mathrm{SM}}) - H(p_{L,\mathrm{SM}}) \quad (9)$$

if $p_{E,\mathrm{SM}} > p_{L,\mathrm{SM}}$. Otherwise, secrecy capacity of the spatial component of SM is equal to 0. The secrecy capacity of SSK can be expressed as

$$C_{s,\mathrm{SSK}}(p_{L,\mathrm{SSK}}, p_{E,\mathrm{SSK}}) = H(p_{E,\mathrm{SSK}}) - H(p_{L,\mathrm{SSK}}) \quad (10)$$

if $p_{E,\mathrm{SSK}} > p_{L,\mathrm{SSK}}$. Otherwise, the SSK secrecy capacity is equal to 0.

VII. Simulation Results

In this section, we quantify secrecy capacities of the spatial component of SM and SSK by employing the semi-analytical approach. Simulations of communication with optimal SM and SSK detectors are performed in order to obtain their respective error probabilities of antenna detection, p_{SM} and p_{SSK} for different values of SNR since union bound values for error probability are precise only for high SNR. The SNR value is varied at the legitimate receiver to obtain a range of error probabilities of antenna detection $p_{L,\mathrm{SM}}$ and $p_{L,\mathrm{SSK}}$ while the eavesdropper's SNR is kept fixed to provide corresponding $p_{E,\mathrm{SM}}$ and $p_{E,\mathrm{SSK}}$. The secrecy capacity of the spatial component of SM is computed by using (9) and the secrecy capacity of SSK by using (10). The results are plotted to show secrecy capacity versus SNR on the legitimate channel while SNR at the eavesdropper is kept at some fixed value for a particular scenario.

We first start by plotting error probabilities of antenna detection in SSK and SM for a varying size of the signal constellation M for a system with N_{T}=2 and N_{R}=1 in Fig. 2. For $M = 2$, binary phase shift keying (BPSK) is used, while for the other values of M quadrature amplitude (QAM) modulation is employed. We first note that the SSK theoretical

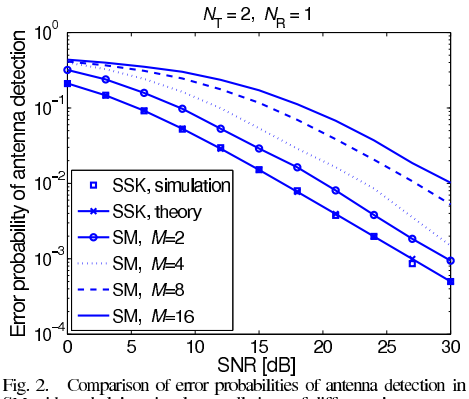

Fig. 2. Comparison of error probabilities of antenna detection in SSK and SM with underlying signal constellations of different sizes.

result in (1) agrees with the simulation. As expected, SSK has the best error performance since the receiver only has to detect the antenna index as opposed to SM where both the antenna index *and* the underlying signal constellation symbol have to be detected. Furthermore, as the size of the constellation increases, the error performance predictably worsens since the constellation points move closer to each other. We also note that, for larger SNR values, the slopes of the error curves are the same: they are equal to -1 since a tenfold decrease of error corresponds to an SNR increase of 10 dB when N_{R}=1. The gap between the error curves is due to the difference in the underlying constellation sizes: as constellations grow, the necessary SNR to achieve the same error probability also grows. Based on the fact that SSK has superior error performance over the spatial component of SM for all constellation sizes, *i.e.* $p_{\mathrm{SSK}}<p_{\mathrm{SM}}$ at a given SNR, one might suspect that SSK would have better secrecy capacity than SM. We show next, however, that this is not necessarily the case.

We start the characterisation of the secrecy capacity by considering the case of N_{T}=2 and N_{R}=1 with SNR at the eavesdropper being fixed at 0 dB, while the SNR at the legitimate link varies, as shown in Fig. 3. SM secrecy capacity

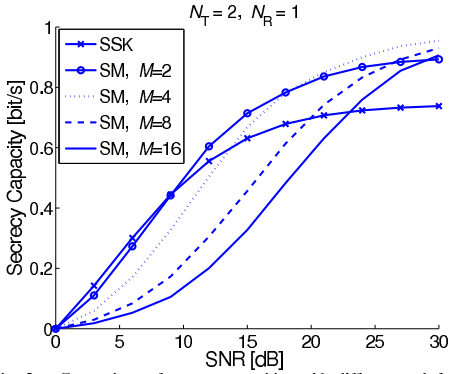

Fig. 3. Comparison of secrecy capacities with different underlying signal constellations with varying legitimate SNR and Eve's SNR equal to 0 dB.

decreases, except for high SNRs, as the constellation size increases. While SSK provides larger secrecy capacity than the SM variants at lower SNRs, SM secrecy capacities for all M overtake SSK secrecy capacity for sufficiently high SNRs. This, somewhat counterintuitive, result can be understood by considering the secrecy capacity as the SNR on the legitimate link increases to infinity. It is easily seen that p_L tends to zero as SNR on the legitimate link goes to infinity. Since the BSC secrecy capacity is expressed as the difference of two binary entropies evaluated at p_E and p_L, as in (8), we have that $C_s(0, p_E)=H(p_E)$ in the limit. In the case of SSK, secrecy capacity is asymptotically given by

$$C_{s,\mathrm{SSK}}(0, p_{E,\mathrm{SSK}})=H(p_{E,\mathrm{SSK}}), \tag{11}$$

while in the case of SM, it is

$$C_{s,\mathrm{SM}}(0, p_{E,\mathrm{SM}})=H(p_{E,\mathrm{SM}}). \tag{12}$$

Since, as discussed earlier, $p_{E,\mathrm{SM}}>p_{E,\mathrm{SSK}}$, it follows that $H(p_{E,\mathrm{SM}})>H(p_{E,\mathrm{SSK}})$ because the binary entropy is an increasing function for crossover probabilities less than a half. Therefore, it becomes clear that, as the SNR on the legitimate channel tends to infinity, secrecy capacity of the spatial component of SM becomes larger than the SSK secrecy capacity. Paradoxically, the main reason for SM outperforming SSK in terms of secrecy capacity is that SM *underperforms* in terms of the error probability of antenna detection. This phenomenon also explains why, for a large SNR, SM performs better for large M than for small M.

We next study the changes in secrecy capacity when Eve's SNR is equal to 12 dB. Fig. 4 shows that secrecy capacities are lower than the counterparts in Fig. 3. Naturally, the secrecy

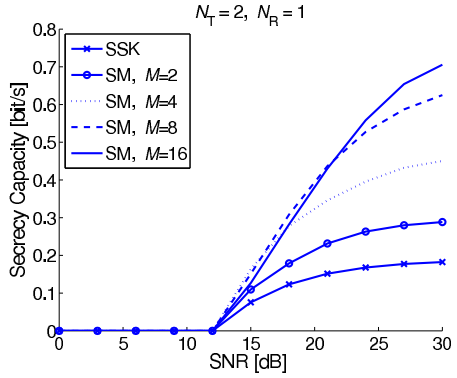

Fig. 4. Comparison of secrecy capacities with different underlying signal constellations with varying legitimate SNR and Eve's SNR equal to 12 dB.

capacity is equal to zero when the legitimate receiver's SNR is below 12 dB. At higher SNRs, it can be seen that SM with the highest M, M=16, outperforms other schemes. This is due to the asymptotic behaviour of the secrecy capacity when SNR tends to infinity, as discussed earlier in the section.

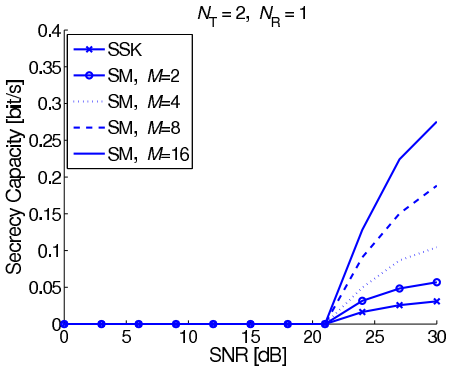

Fig. 5. Comparison of secrecy capacities with different underlying signal constellations with varying legitimate SNR and Eve's SNR equal to 21 dB.

Finally, we observe the changes in the secrecy capacity when Eve's SNR is equal to 21 dB. Fig. 5 shows that the secrecy capacities are even lower than the corresponding values in Fig. 3 and 4. This is to be expected since the gap between Bob's and Eve's SNRs is smaller and, consequently, the difference between their capacities is also smaller. At high SNRs, the advantage of larger M becomes even more apparent in this case compared to the previous two cases shown in Fig. 3 and 4.

VIII. Summary and Conclusions

We have explored secrecy capacity of the spatial component of SM and SSK systems. We have shown that the effect of constellation size depends on the values of the legitimate and eavesdropper's SNRs. For low eavesdropper's SNR, smaller constellations perform better than larger ones for most of the SNR range, while for the high eavesdropper's SNR, larger constellations provide larger secrecy capacities. As the gap between the eavesdropper's and legitimate receiver's SNRs is reduced, the secrecy capacity is significantly reduced for SM and SSK. Furthermore, while SSK secrecy capacity may be expected to perform better due to the lack of conventional modulation and its smaller error of antenna detection, it actually performs worse than the secrecy capacity of the spatial component of SM at high SNR precisely due to the smaller error probability. Future work will seek to tighten probability of error obtained via union bound so that it can be used for fully analytical computation of SM and SSK capacity. Furthermore, effects of varying the number of transmit and receive antennas on secrecy capacity will be explored.

Acknowledgment

Professor Haas acknowledges the Scottish Funding Council support of his position within the Edinburgh Research Partnership in Engineering and Mathematics between the University of Edinburgh and Heriot Watt University. We gratefully acknowledge support from the Engineering and Physical Sciences Research Council (EP/G011788/1) in the United Kingdom for this work.

References

[1] R. Mesleh, H. Haas, S. Sinanović, C. W. Ahn, and S. Yun, "Spatial Modulation," *IEEE Trans. Veh. Technol.*, vol. 57, no. 4, pp. 2228 – 2241, July 2008.

[2] J. Jeganathan, A. Ghrayeb, and L. Szczecinski, "Spatial Modulation: Optimal Detection and Performance Analysis," *IEEE Commun. Lett.*, vol. 12, no. 8, pp. 545–547, 2008.

[3] J. Jeganathan, A. Ghrayeb, L. Szczecinski, and A. Ceron, "Space Shift Keying Modulation for MIMO Channels," *IEEE Transaction on Wireless Communications*, vol. 8, no. 7, pp. 3692–3703, Jul. 2009.

[4] A. Wyner, "The Wire-tap Channel," *Bell. Syst. Tech. J.*, vol. 54, pp. 1355–1387, 1975.

[5] I. Csiszár and J. Körner, "Broadcast channels with confidential messages," *IEEE Trans. Inf. Theory*, vol. 24, no. 3, pp. 339–348, 1978.

[6] A. Khisti and G. W. Wornell, "Secure Transmission With Multiple Antennas I: The MISOME Wiretap Channel," *IEEE Trans. Inf. Theory*, vol. 56, no. 7, pp. 3088–3104.

[7] F. Oggier and B. Hassibi, "The Secrecy Capacity of the MIMO Wiretap Channel," in *IEEE International Symposium on Information Theory*, Toronto, ON, 2008, pp. 524–528.

[8] Z. Li, W. Trappe, and R. Yates, "Secret Communication Via Multi-Antenna Transmission," in *41st Annual Conference on Information Sciences and Systems, CISS '07.*, Baltimore, MD, 2007, pp. 905–910.

[9] J. Barros and M. R. D. Rodrigues, "Secrecy Capacity of Wireless Channels," in *IEEE International Symposium on Information Theory*, Seattle, WA, 2006, pp. 356–360.

[10] A. Younis, N. Serafimovski, R. Mesleh, and H. Haas, "Generalized Spatial Modulation," in *Asilomar Conference on Signals, Systems, and Computers*, Pacific Grove, CA, USA, 2010.

[11] M. Di Renzo and H. Haas, "Performance Analysis of Spatial Modulation," in *5th International ICST Conference on Communications and Networking in China*, Aug. 2010.

[12] ——, "Performance Comparison of Different Spatial Modulation Schemes in Correlated Fading Channels," in *Proc. of International Conference on Communications*, May 2010.

[13] T. M. Cover and J. A. Thomas, *Elements of Information Theory*, 1st ed., ser. Wiley Series in Telecommunications, D. L. Schilling, Ed. John Wiley & Sons, Sep. 1991.

[14] U. M. Maurer, "Secret Key Agreement by Public Discussion from Common Information," *IEEE Transactions on Information Theory*, vol. 39, no. 3, pp. 733–742, May 1993.

[15] L. Lai, H. Elgamal, and V. Poor, "The Wiretap Channel With Feedback: Encryption Over the Channel," *IEEE Transactions on Information Theory*, vol. 54, pp. 5059–5067, 2008.

EURASIP Journal on Wireless Communications and Networking

SpringerOpen

This Provisional PDF corresponds to the article as it appeared upon acceptance. Fully formatted PDF and full text (HTML) versions will be made available soon.

Multiple access spatial modulation

EURASIP Journal on Wireless Communications and Networking 2012, **2012**:299 doi:10.1186/1687-1499-2012-299

Nikola Serafimovski (n.serafimovski@ed.ac.uk)
Sinan Sinanovic (s.sinanovic@ed.ac.uk)
Marco Di Renzo (marco.direnzo@lss.supelec.fr)
Harald Haas (h.haas@ed.ac.uk)

ISSN 1687-1499

Article type Research

Submission date 26 March 2012

Acceptance date 4 September 2012

Publication date 19 September 2012

Article URL http://jwcn.eurasipjournals.com/content/2012/1/299

Multiple access spatial modulation

Nikola Serafimovski[1]*
*Corresponding author
Email: n.serafimovski@ed.ac.uk

Sinan Sinanović[1]
Email: s.sinanovic@ed.ac.uk

Marco Di Renzo[2]
Email: marco.direnzo@lss.supelec.fr

Harald Haas[1]
Email: h.haas@ed.ac.uk

[1]Institute for Digital Communications, Joint Research Institute for Signal and Image Processing, School of Engineering, The University of Edinburgh, Edinburgh EH9 3JL, UK

[2]Laboratory of Signals and Systems (L2S), French National Center for Scientific Research (CNRS), L'Ecole Supérieure d'Électricité (SUPÉLEC), University of Paris–Sud XI (UPS), 3 rue Joliot-Curie, 91192 Gif-sur-Yvette (Paris), France

Abstract

In this study, we seek to characterise the behaviour of Spatial modulation (SM) in the multiple access scenario. By only activating a single transmit antenna for any transmission, SM entirely avoids inter-channel interference, requires no synchronisation between the transmit antennas and a single radio frequency chain at the transmitter. Most contributions thus far have only addressed aspects of SM for a point-to-point communication system. We propose a maximum-likelihood (ML) detector which can successfully decode incoming data from multiple simultaneous transmissions and does not suffer from the near-far problem. We analyse the performance of the interference-unaware and interference-aware detectors. We look at the behaviour of SM as the signal-to-interference-plus-noise ratio goes to infinity and compare it to the complexity and cost equivalent single-input-multiple-output (SIMO) system. Two systems are considered to be equivalent in terms of complexity if their respective detection algorithms are of the same order in $\mathcal{O}(\cdot)$ notation. Simulation results show that the interference-aware SM detector performs better than the complexity equivalent multi-user ML-SIMO detector by at least 3 dB at an average bit-error-ratio of 10^{-3}.

Introduction

Multiple-antenna systems are fast becoming a key technology for modern wireless systems. They offer improved error performance and higher data rates, at the expense of increased complexity and power consumption [1]. Spatial modulation (SM) is a recently proposed approach to multiple–input–multiple–output (MIMO) systems which entirely avoids inter-channel interference, requires no synchronisation between the transmit antennas and achieves a spatial multiplexing gain [2]. This is performed by mapping a block of information bits into a constellation point in the signal and

spatial domains [3]. In SM, the number of information bits, ℓ, that are encoded in the spatial domain can be related to the number of transmit antennas N_t as $N_t = 2^{\ell}$. This means that the number of transmit antennas must be a power of two unless fractional bit encoding [4] or generalised SM [5] are used. SM offers an intrinsic flexibility to trade off the number of transmit antennas with the modulation order in the signal domain to meet the desired data rate. It should be noted that SM is shown to outperform other point-to-point MIMO schemes in terms of average bit-error-ratio (ABER) [3].

In the single user scenario, only a single transmit antenna is active at any instance, this avoids the need for complicated interference cancellation algorithms at the SM receiver. In addition, unlike other MIMO schemes, the number of receive antennas is independent of the number of transmit antennas. Several articles are available in literature which are aimed at understanding and improving the performance of SM in various scenarios, e.g., [6–8]. The study in [6] seeks to improve the ABER performance of SM by introducing trellis coding on the transmitting antennas. The study in [9] shows that the detector complexity of SM is independent of the number of transmit antennas. The optimal detector is known with and without channel state information at the receiver in [10–12]. The optimal power allocation problem for a two-transmit with one receive antenna system is solved in closed form in [13] and the performance of SM in correlated fading channels is considered in [14, 15]. Recent work has also shown that SM can be combined with space–time block codes to attain spectral efficiency gains [16] by exploiting transmit-side diversity. At this point, it is worth noting that if we choose to use only the spatial constellation of SM to transmit information, then SM is reduced to space-shift-keying (SSK) as proposed in [17]. To this extent, we note that all presented work can be extended to SSK without loss of generality.

MIMO techniques can also be used in relaying networks to improve the diversity, provide multiplexing gains and aid in interference cancellation. To this extent, the orthogonal decode and forward (DF) algorithm decodes the received signal at the relay, then re-encodes and retransmits this information, establishing a regenerative system. Outage probabilities, mutual information calculations and transmit diversity bounds for orthogonal amplify and forward (AF) and DF relaying are derived in [18] with the end-to-end performance being considered in [19] where DF is shown to perform better in terms of the ABER when compared to AF. However, the ABER of regenerative systems depends on the ABER on the individual links. In particular, since SM is shown to outperform other spatial multiplexing techniques on a single link, the application of SM to relaying systems is also shown to provide significant signal-to-noise ratio (SNR) gains when compared to orthogonal DF [20]. Nonetheless, these results are only applicable in a noise-limited relaying system. The deployment of relaying systems around the cell edges, however, may result in interference-limited systems. Therefore, to enable the deployment of SM in a relaying scenario, the ABER performance of SM on a single link must also be assessed in the interference-limited environment.

Most contributions thus far, however, have only addressed SM aspects for point-to-point communication systems, i.e. the single user scenario. Notable exceptions are given in [21, 22], where the authors focus their analysis on scenarios employing SSK. The aim of this study is to characterise the behaviour of SM in the multi-user, interference-limited scenario and compare it to the *complexity and cost equivalent* multi-user MIMO system. We emphasise that SM requires only a single radio frequency (RF) chain at the transmit side since only one is active at any particular instance. Requiring only a single RF chain at the transmitter means that multi-user SM is not comparable in terms of cost to the more complicated spatial-multiplexing multi-user systems analysed in [23–26].

Furthermore, the study in [27] shows that the most energy consuming part of a wireless base station is the power amplifiers and consequently RF chains associated with each transmitter. The study in [28] demonstrates that the power requirements of a base station increase linearly with the number of RF

chains added. In addition to higher power consumption, multiple RF chains imply higher manufacturing costs and inter-antenna synchronisation problems. To this extent, SM is an optimal system for utilising the advantages of multiple transmit antennas while still maintaining a single RF chain for Green communications. The aggregate power usage in a system employing SM is significantly lower than a system employing classical MIMO techniques. Furthermore, the lower detection complexity for SM reduces mobile station power usage, enabling a longer battery life for the mobile terminal [9]. Understanding the performance of SM in a multi-user system is necessary to assess its suitability for practical deployment scenarios. In this context, it is of interest if the particular structure of the SM encoding scheme can be exploited to devise novel multi-user detection techniques.

In this study, we first characterise the performance of a single user detector as applied in an interference-limited scenario, i.e. we analyse a ML interference-unaware optimal receiver. We then propose an ML detector which can successfully decode incoming data in the multi-user scenario and is not interference limited, i.e. an interference-aware detector which can successfully decode data from several nodes. For each detector, we develop an analytical framework to support simulation results and closed form solutions are provided to compute the ABER over identical and independently distributed (i.i.d.) Rayleigh fading channels.

The remainder of this article is organised as follows. In the "System model" section, the system and channel models are introduced. In the "Analytical modelling and receiver design" section, the performance of SM in the multiple access scenario is characterised and the analytical modelling for the multi-user detector is proposed. The "Simulation results and discussion" section provides simulation results to substantiate the accuracy of the developed analytical framework. In the "Summary and conclusions" section, we summarise and conclude this study.

System model

The basic idea of SM is to map blocks of information bits onto two information carrying units [3]: (i) a symbol, chosen from a complex signal-constellation diagram, and (ii) a unique transmit-antenna, chosen from the set of transmit-antennas in an antenna-array, i.e. the spatial-constellation. Jointly, the spatial and signal constellation symbols form a single SM constellation symbol. If, for example, we wish to transmit a total of 4 bits/s/Hz using SM with four available transmit antennas; then the first 2 bits would define the spatial-constellation point identifying the active antenna, while the remaining 2 bits would determine the signal-constellation point that will be transmitted.

In the following work, we assume multiple nodes/users, as shown in Figure 1. A total of N_u transmit nodes, denoted as $\{1, \ldots, \xi, \ldots N_u\}$, broadcast simultaneously on the same time-frequency slot to a single receiver. Each node broadcasts a signal constellation symbol, $x^{(u)}$, from one of its available antennas.

Figure 1 Multi-user SM system setup. Nodes $1, \ldots, \xi, \ldots N_u$ broadcast simultaneously to the receiver on the same time-frequency resource block. Each solid line represents the active transmit antenna on each node to every receiving antenna. Each dashed line represents the inactive channel from every transmit antenna at a particular node to every receiving antenna

The received signal at antenna r is given by

$$y_r = \sum_{u=1}^{N_u} \left[\sqrt{E_m \alpha_{(u)}^2}\, h_{n_t^{(u)},r} x^{(u)} \right] + \eta_r, \tag{1}$$

where E_m is the average transmit energy per symbol, $n_t^{(u)}$ is the index of the active transmit antenna from a total of $N_t^{(u)}$ available on node u, r is the index of the receive antenna from a total of N_r available on the receiving node, $\alpha_{(u)}^2$ is the power of the channel attenuation coefficients between all receive antennas and all transmit antennas on the link between node u and the receiver, $h_{n_t^{(u)},r}$ is the fast fading channel coefficient between the active transmit antenna n_t on node u and the receiving antenna r, $x^{(u)}$ is the signal constellation symbol transmitted from the set of all possible signal constellation points, $\mathcal{X}^{(u)}$, for node u and η_r, is additive white Gaussian noise (AWGN), defined as a complex normally random variable with zero mean and variance N_o, $\mathcal{CN}(0, N_o)$.

Throughout the study $\mathrm{E}_{\mathbf{X}}[|x|^2] = 1$, meaning the average power in the signal constellation $\mathcal{X}^{(u)}$ is normalised to one for all u. To avoid repetitive definitions of symbols, we note that symbols denoted with $\hat{\cdot}$ are simply an element of the same set as the symbol without $\hat{\cdot}$, i.e. $\hat{x}$ comes from the same set as x. Furthermore, all bold letters are vectors. If we set the signal constellation to be only a single constellation point, where N_t is chosen such that $\log_2(N_t)$ equals the spectral efficiency, then all presented work can directly be applied to any system employing SSK by simply replacing $x^{(u)} = 1$.

Analytical modelling and receiver design

We analyse the ML detector for use in the multiple access scenario. The detector computes the Euclidean distance between the received vector signal, $\mathbf{y}$, and the set of all possible received signals, selecting the closest one.

Interference-unaware detection

Starting from the system model presented in the "System model" section, the decoded pair $(x_{\text{est}}, n_t)^{(\xi)}$, formed from the estimated symbol x_{est} emitted from antenna n_t on node ξ is given by

$$(x_{\text{est}}, n_t)^{(\xi)} = \operatorname{argmin} \left\{ \left\| \mathbf{y} - \sqrt{E_m \alpha_{(\xi)}^2}\, x^{(\xi)} \mathbf{h}_{n_t^{(\xi)}} \right\|_{\mathrm{F}}^2 \right\}, \tag{2}$$

$$x_{\text{est}}^{(\xi)} \in \mathcal{X}^{(\xi)}, \qquad n_t^{(\xi)} \in \{1 \ldots N_t^{(\xi)}\}, \qquad \mathbf{h}_{n_t^{(\xi)}} = \left[h_{n_t^{(\xi)},1} \ldots h_{n_t^{(\xi)},N_r} \right],$$

where $N_t^{(\xi)}$ is the number of available transmit antennas on node ξ, $||\cdot||_{\mathrm{F}}$ is the Frobenius norm and $\mathcal{X}^{(\xi)}$ has a total of $M^{(\xi)}$ constellation points. We note that u represents the index of a general node in the system, and ξ is the index of the desired node whose data stream is being decoded.

We can use union bound techniques to describe the behaviour of the interference-unaware SM detector in the high SNR regions. From here, we proceed to characterise the behaviour of the

interference-unaware detector by defining

$$\begin{aligned} \mathbf{A} &= \sqrt{E_m \alpha_{(\xi)}^2}\, \mathbf{h}_{n_t^{(\xi)}} x^{(\xi)}, \\ \mathbf{B} &= \sum_{u \neq \xi = 1}^{N_u} \sqrt{E_m \alpha_{(u)}^2}\, \mathbf{h}_{n_t^{(u)}} x^{(u)}, \end{aligned} \tag{3}$$

such that

$$\begin{aligned} A_r &= \sqrt{E_m \alpha_{(\xi)}^2}\, h_{n_t^{(\xi)},r} x^{(\xi)}, \quad \text{and} \\ B_r &= \sum_{u \neq \xi = 1}^{N_u} \sqrt{E_m \alpha_{(u)}^2}\, h_{n_t^{(u)},r} x^{(u)}, \end{aligned}$$

define the symbols at the receive antenna r. With this, we can pose $\mathbf{y} = \mathbf{A} + \mathbf{B} + \boldsymbol{\eta}$. The pairwise error probability (PEP) can now be derived as

$$\begin{aligned} &\Pr\{\mathbf{A} \neq \hat{\mathbf{A}} | \mathbf{B}\} = \Pr\left\{ ||\mathbf{y} - \mathbf{A}||_{\mathrm{F}}^2 > \left|\left|\mathbf{y} - \hat{\mathbf{A}}\right|\right|_{\mathrm{F}}^2 \right\} \\ &= \Pr\left\{ \sum_{r=1}^{N_r} \left[|y_r - A_r|^2 \right] > \sum_{r=1}^{N_r} \left[\left| y_r - \hat{A}_r \right|^2 \right] \right\} \\ &= \Pr\left\{ \sum_{r=1}^{N_r} \left[2\Re\left\{ \left(\hat{A}_r - A_r \right) (B_r + \eta_r)^* \right\} \right] > \sum_{r=1}^{N_r} \left[\left| A_r - \hat{A}_r \right|^2 \right] \right\} \\ &\Rightarrow \eta_r^{\text{new}} \sim \mathcal{N}\left(\sum_{r=1}^{N_r} \left[2\Re\left\{ (\hat{A}_r - A_r) B_r^* \right\} \right], \sum_{r=1}^{N_r} \left[2N_o |\hat{A}_r - A_r|^2 \right] \right), \end{aligned} \tag{4}$$

where $(\cdot)^*$ represents the complex conjugate, η_r^{new} is the distribution of the PEP defined by $\mathcal{N}(\mu, \sigma^2)$ which represents the normal distribution with mean μ and variance σ^2. Knowing that η_r^{new} is the only remaining random variable with a known distribution, enables us to define the PEP in (4) using the Q-function. Considering η_r^{new} and (4), we can see that the PEP can be defined as

$$\Pr\{\mathbf{A} \neq \hat{\mathbf{A}} | \mathbf{B}\} = Q\left(\frac{\sum_{r=1}^{N_r} \left[\left| A_r - \hat{A}_r \right|^2 - 2\Re\left\{ \left(\hat{A}_r - A_r \right) B_r^* \right\} \right]}{\sqrt{\sum_{r=1}^{N_r} \left[2N_o \left| A_r - \hat{A}_r \right|^2 \right]}} \right), \tag{5}$$

where $Q(\omega) = \frac{1}{\sqrt{2\pi}} \int_{\omega}^{\infty} \exp\left(-\frac{t^2}{2}\right) \mathrm{dt}$ defines the Q-function. It should be noted that this PEP is valid for all channel fading statistics. We can further simplify it if we assume that the fast fading channel statistics of each element of $\mathbf{B}$ are Rayleigh distributed, i.e. $h_{n_t^{(u)},r} \sim \mathcal{CN}(0,1)$ and $\mathbf{h}_{n_t^{(u)}}$ has N_r number of elements. To this end, we define

$$\Omega_P = \left|\left|\mathbf{A} - \hat{\mathbf{A}}\right|\right|_{\mathrm{F}}^2, \quad \Omega_I = 2\Re\left\{ (\hat{\mathbf{A}} - \mathbf{A}) \mathbf{B}^* \right\}, \quad \Omega_N = \sqrt{2N_o \Omega_P}, \tag{6}$$

where we can see that

$$\Omega_I \sim \mathcal{N}\left(0, 2E_m |x_{\mathbf{B}}|^2 \Omega_P\right), \tag{7}$$

such that $|x_{\mathbf{B}}|^2 = \sum_{u \neq \xi = 1}^{N_u} \alpha_{(u)}^2 |x^{(u)}|^2$ and define $\sigma_I^2 = 2E_m |x_{\mathbf{B}}|^2 \Omega_P$. We can remove the channel effects of $\mathbf{B}$ from the expression by taking the expectation of (5) across the fading channel $\mathbf{h}_{\mathbf{B}}$, such that

$$\begin{aligned}\Pr\{\mathbf{A}\neq\hat{\mathbf{A}}\} &= \mathrm{E}_{\mathbf{h_B}}\Big[\Pr\{\mathbf{A}\neq\hat{\mathbf{A}}|\mathbf{h_B}\}\Big],\\ \Pr\{\mathbf{A}\neq\hat{\mathbf{A}}\} &= \mathrm{E}_{\mathbf{h_B}}\left[Q\left(\tfrac{\Omega_P-\Omega_I}{\Omega_N}\right)\right],\\ &= \mathrm{E}_{\mathbf{h_B}}\left[Q\left(\tfrac{\Omega_P}{\Omega_N}-\tfrac{\sigma_I}{\Omega_N}\hat{\Omega}_I\right)\right],\end{aligned} \tag{8}$$

where $\hat{\Omega}_I \sim \mathcal{N}(0,1)$ and $\mathrm{E}_{\mathbf{h}}[\cdot]$ represents the expectation of the system with respect to the fast fading channel **h**. From here, we can apply ([29], eq. 3.66) which results in

$$\Pr\{\mathbf{A}\neq\hat{\mathbf{A}}\} = Q\left(\frac{\Omega_P}{\sqrt{\Omega_N^2+\sigma_I^2}}\right). \tag{9}$$

After some analytical manipulations we obtain (10)

$$\Pr\{\mathbf{A}\neq\hat{\mathbf{A}}\} = Q\left(\sqrt{\gamma_{\mathbf{I}}\left\|\mathbf{h}_{n_t^{(\xi)}}x^{(\xi)}-\mathbf{h}_{\hat{n}_t^{(\xi)}}\hat{x}^{(\xi)}\right\|_{\mathrm{F}}^2}\right), \tag{10}$$

where

$$\gamma_{\mathbf{I}} = \frac{1}{2}\frac{E_m\alpha_{(\xi)}^2}{N_o+E_m\sum\limits_{u\neq\xi=1}^{N_u}\alpha_{(u)}^2\,|x^{(u)}|^2}, \tag{11}$$

represents half of the signal-to-interference-plus-noise ratio (SINR) between node ξ and the receiver. Throughout the study, we average only across the fast fading channel statistics. As (11) shows, $\gamma_{\mathbf{I}}$ is still dependent on the magnitude of the modulated signal symbols of the interfering nodes, $|x^{(u)}|$. This means that all expressions using $\gamma_{\mathbf{I}}$ maintain their conditioning on the modulated signal symbols of the interfering nodes.

Given this formulation, we can now define the ABER of the single-user detector using the union bounding techniques in the presence of interference as

$$\mathrm{ABER}_{\xi}^{(\mathbf{inter})} \leq \sum_{\substack{x^{(\xi)},\,n_t^{(\xi)},\\ \hat{x}^{(\xi)},\,\hat{n}_t^{(\xi)}}}^{M^{(\xi)}N_t^{(\xi)}} \underbrace{\sum\sum\cdots\sum}_{(N_u-1)\text{ summations}} \frac{d_{\xi}(b,\hat{b})}{\log_2\left(M^{(\xi)}N_t^{(\xi)}\right)}\frac{\mathrm{E}_{\mathbf{h_A}}\Big[\Pr\{\mathbf{A}\neq\hat{\mathbf{A}}\}\Big]}{M^{(\xi)}N_t^{(\xi)}}\left[\prod_{u\neq\xi=1}^{N_u}\frac{1}{M^{(u)}}\right], \tag{12}$$

where the uth summation from the (N_u-1) summations above is defined for all $x^{(u)}\in\mathcal{X}^{(u)}$ and $u\neq\xi$ with $M^{(\xi)}$ being the cardinality of $\mathcal{X}^{(\xi)}$. The symbol $\sum_{\substack{x^{(\xi)},\,n_t^{(\xi)},\\ \hat{x}^{(\xi)},\,\hat{n}_t^{(\xi)}}}^{M^{(\xi)}N_t^{(\xi)}}$ is defined as a fourfold summation, two for all $x^{(\xi)}, \hat{x}^{(\xi)}\in\mathcal{X}^{(\xi)}$ and two for the indices $n_t^{(\xi)}, \hat{n}_t^{(\xi)}\in\left[1,\ldots,N_t^{(\xi)}\right]$. In addition, $d_{\xi}(b,\hat{b}) = d_{\xi}(n_t,\hat{n}_t) + d_{\xi}(x,\hat{x})$, where $d_{\xi}(\cdot,\hat{\cdot})$ denotes the Hamming distance between the binary representations any two symbols coming from the same set for node ξ.

As with the interfering nodes, we assume that the desired node's fast fading follows a Rayleigh distribution. To obtain the average PEP, we define $z_r = h_{n_t^{(\xi)},r} x_{(\xi)} - h_{\hat{n}_t^{(\xi)},r} \hat{x}_{(\xi)}$, with a variance of

$$\sigma_z^2 = \begin{cases} \left(|x^{(\xi)}|^2 + |\hat{x}^{(\xi)}|^2\right) & n_t^{(\xi)} \neq \hat{n}_t^{(\xi)}, \\ \left(|x^{(\xi)} - \hat{x}^{(\xi)}|^2\right) & n_t^{(\xi)} = \hat{n}_t^{(\xi)}, \\ 0 & n_t^{(\xi)} = \hat{n}_t^{(\xi)} \text{ and } x^{(\xi)} = \hat{x}^{(\xi)}, \end{cases} \tag{13}$$

where σ_z^2 is the variance of SM using a variable amplitude modulation scheme. In particular, it is the variance per receive antenna of the argument inside the Q-function in (10). We define the random variable

$$\kappa = \frac{\|\mathbf{z}\|_{\mathrm{F}}^2}{\gamma_1 \sigma_z^2/2} = \sum_{r=1}^{N_r} \left| \frac{z_r}{\gamma_1 \sigma_z/\sqrt{2}} \right|^2, \tag{14}$$

which has a central Chi-squared distribution with $2N_r$ degrees of freedom given as

$$\tilde{\rho}_K(\kappa) = \frac{1}{2^{N_r}(N_r-1)!} \kappa^{N_r-1} e^{-\kappa/2} \tag{15}$$

where $(\cdot)!$ represents the factorial function. We can now pose

$$\mathrm{E}_{\mathbf{h}_\mathbf{A}}\left[\Pr\{\mathbf{A} \neq \hat{\mathbf{A}}\}\right] = \frac{(1/2)^{N_r}}{(N_r-1)!} \int_0^\infty e^{-\kappa/2} \kappa^{N_r-1} Q\left(\sqrt{\frac{\gamma_1 \sigma_z^2}{2}\kappa}\right) \mathrm{d}\kappa. \tag{16}$$

By direct inspection, we can now apply the solution to ([30], eq. 62) and obtain

$$\mathrm{E}_{\mathbf{h}_\mathbf{A}}\left[\Pr\{\mathbf{A} \neq \hat{\mathbf{A}}\}\right] = f(\beta)^{N_r} \sum_{r=0}^{N_r-1} \binom{N_r-1+r}{r} (1-f(\beta))^r, \tag{17}$$

where

$$f(\beta) = \frac{1}{2}\left(1 - \sqrt{\frac{\beta}{1+\beta}}\right), \tag{18}$$

and

$$\beta = \frac{\gamma_1 \sigma_z^2}{2}. \tag{19}$$

We note that (12) presents an analytical bound for a system employing quadrature-amplitude-modulation (QAM). If we choose to use constant-amplitude modulation such as phase-shift-keying (PSK), then for a fixed channel realisation, we define $a = h_{n_t^{(\xi)},r}$, $b = x_{(\xi)}$, and pose

$$z_r^{\mathrm{PSK}} = |a| e^{j \arg(a)} |b| e^{j \arg(b)} - \left|\hat{a}\right| e^{j \arg(\hat{a})} |\hat{b}| e^{j \arg(\hat{b})}, \tag{20}$$

where $\arg(\cdot)$ represents the phase of a complex symbol. We realise that the amplitude of all constellation points is unity and thus

$$z_r^{\mathrm{PSK}} = |a| e^{j(\arg(a) + \arg(b))} - |\hat{a}| e^{j\left(\arg(\hat{a}) + \arg(\hat{b})\right)}. \tag{21}$$

From the definition of z_r^{PSK}, it is clear that its variance is defined as

$$\sigma_{z^{\mathrm{PSK}}}^2 = \begin{cases} 2 & \text{if } n_t^{(\xi)} \neq \hat{n}_t^{(\xi)} \text{ or } \arg\left(x_{(\xi)}\right) \neq \arg\left(\hat{x}_{(\xi)}\right), \\ 0 & \text{if } n_t^{(\xi)} = \hat{n}_t^{(\xi)} \text{ and } \arg\left(x_{(\xi)}\right) = \arg\left(\hat{x}_{(\xi)}\right). \end{cases} \tag{22}$$

In this case, (12) reduces to

$$\text{ABER}_{\xi}^{(\text{PSK-inter})} \leq \sum_{n_t=1}^{N_t^{(\xi)}} \sum_{\hat{n}_t=1}^{N_t^{(\xi)}} \frac{d_{\xi}(b,\hat{b})}{\log_2\left(M^{(\xi)}N_t^{(\xi)}\right)} \frac{\text{E}_{\mathbf{h_A}}^{\text{PSK}}\left[\Pr\{\mathbf{A}\neq\hat{\mathbf{A}}\}\right]}{M^{(\xi)}N_t^{(\xi)}}, \tag{23}$$

where

$$\text{E}_{\mathbf{h_A}}^{\text{PSK}}\left[\Pr\{\mathbf{A}\neq\hat{\mathbf{A}}\}\right] = f\left(\beta^{\text{PSK}}\right)^{N_r} \sum_{r=0}^{N_r-1} \binom{N_r-1+r}{r} \left(1-f\left(\beta^{\text{PSK}}\right)\right)^r, \tag{24}$$

such that

$$\beta^{\text{PSK}} = \gamma_{\mathbf{I}}^{\text{PSK}} = \frac{1}{2} \frac{E_m\alpha_{(\xi)}^2}{N_o + 2E_m \sum_{u\neq\xi=1}^{N_u} \alpha_{(u)}^2}. \tag{25}$$

The average power carried by any signal-symbol constellation in (12) is 1. Nonetheless, a variable amplitude modulation scheme means that the instantaneous SINR changes. The instantaneous SINR must strictly be defined to study the asymptotic behaviour of the system. This is necessary because the instantaneous SINR is an argument of the PEP which is defined using the Q-function. To obtain the ABER, the PEP must be averaged across all channel realisations and all signal-symbol constellations. A closed-form expression for the asymptotic behaviour of (12) and (13) is therefore difficult to obtain. However, we note that (22) and (23) are special cases of (12) and (13) which enable a simpler theoretical analysis of the asymptotic behaviour of the system as the SINR grows to infinity. Simulation results in the "Simulation results and discussion" section show that the asymptotic bounds derived for SM using a constant amplitude modulation scheme are also valid for SM using 4-QAM. In addition, it is shown that for the point-to-point single user scenario, SM using PSK may have a better ABER performance than SM using QAM depending on the number of available transmit antennas [31]. We now proceed with the asymptotic analysis of this system.

Asymptotic analysis of an interference-unaware detector

In this section, we investigate some asymptotic cases to highlight trends in SM at high SNR. Simulations in the "Simulation results and discussion" section show that the presented results are asymptotically tight in the high SNR region. We first define $\text{SNR}_{\xi} = E_m\alpha_{(\xi)}^2/(2N_o)$ and $\text{SIR}_{\xi} = \frac{\alpha_{(\xi)}^2}{\sum_{u\neq\xi=1}^{N_u} \alpha_{(u)}^2 |x^{(u)}|^2}$. With these definitions, we look at three systems, the asymptotic performance of SM and SIMO in the noise-limited scenario and the asymptotic performance of SM in the interference-limited scenario.

$\text{SNR}_{\xi} \gg 1$ and SINR $\approx$ SNR (noise-limited scenario)

This is the classic single user scenario where multiple access interference can be neglected, and high-SNR analysis for the probe link can be considered. We look at (12), where in the limit $\gamma_{\mathbf{I}} \approx \gamma = E_m\alpha_{(\xi)}^2/(2N_o)$. Since interference can be neglected,

$$\lim_{\gamma\to\infty} \text{ABER}_{\xi}^{(\textbf{inter})} = \lim_{\gamma\to\infty} \sum_{\substack{x^{(\xi)},n_t^{(\xi)},\\ \hat{x}^{(\xi)},\hat{n}_t^{(\xi)}}}^{M^{(\xi)}N_t^{(\xi)}} \frac{d_{\xi}(b,\hat{b})}{\log_2\left(M^{(\xi)}N_t^{(\xi)}\right)} \frac{\text{E}_{\mathbf{h_A}}\left[\Pr\{\mathbf{A}\neq\hat{\mathbf{A}}\}\right]}{M^{(\xi)}N_t^{(\xi)}}. \tag{26}$$

To simplify (26), the limit in (17) and (24) can be tackled by considering a Taylor expansion with two terms of (18) and obtain

$$\begin{aligned} f(\beta) &= \frac{1}{2}\left(1-\sqrt{\frac{\beta}{1+\beta}}\right) \Rightarrow \text{Taylor expansion} \\ f(\beta) &\approx \frac{1}{2}\left(\frac{1}{2(\beta+1)}\right) = 2^{-2}(\beta+1)^{-1}. \end{aligned} \tag{27}$$

We realise that the average symbol-error-ratio (ASER) for SM is defined similar to the ABER and can be posed as

$$\text{ASER}_{\xi}^{(\textbf{inter})} \leq \sum_{\substack{x^{(\xi)}, n_t^{(\xi)}, \\ \hat{x}^{(\xi)}, \hat{n}_t^{(\xi)}}}^{M^{(\xi)}N_t^{(\xi)}} \frac{\text{E}_{\mathbf{h}_\text{A}}\left[\Pr\{\mathbf{A} \neq \hat{\mathbf{A}}\}\right]}{M^{(\xi)}N_t^{(\xi)}}. \tag{28}$$

From here, we know that $\text{ABER}_{\xi}^{(\textbf{inter})} \leq \text{ASER}_{\xi}^{(\textbf{inter})}/2$. In particular, this is a close approximation for ABER of SM, since the fast fading channel coefficients effectively make the SM constellation completely random at the receiver. This negates any benefits from advanced bit-to-symbol mappings such as Gray coding. In effect, the detector will create a long binary sequence which has at most 50% bit-errors within the erroneous symbol sequence, i.e. the ABER is bounded to be at most 1/2 of the ASER. The tightness of this bound can be seen in the "Simulation results and discussion" section. This step eliminates the dependence on the Hamming distance between the various SM symbols, which permits us to pose

$$\lim_{\gamma\to\infty} \frac{\text{ABER}_{\xi}^{(\textbf{inter})}}{\gamma_1^{-N_r}} = \lim_{\gamma\to\infty} \binom{2N_r-1}{N_r} 2^{-2N_r} \frac{M^{(\xi)}N_t^{(\xi)}}{2} \text{E}_{x,n_t,\hat{x},\hat{n}_t}\left[\left(\frac{\sigma_z^2}{2}\right)^{-N_r}\right], \tag{29}$$

where

$$\text{E}_{x,n_t,\hat{x},\hat{n}_t}\left[\left(\frac{\sigma_z^2}{2}\right)^{-N_r}\right] \tag{30}$$

is the expectation of $\left(\frac{\sigma_z^2}{2}\right)^{-N_r}$ across the various possibilities of σ_z^2 for $x, n_t, \hat{x}$ and $\hat{n}_t$. We are not aware of a closed form solution to the more generic expression for (30) given a variable-amplitude modulation. However, we can upper bound (30) by setting $\sigma_z^2 = \min\left(\sigma_z^2, 2\right)$. In particular, the general form of σ_z^2 is defined by the underlying SM signal-symbol constellation size, $M^{(\xi)}$. To this extent, expressions for σ_z^2 are defined using the upper bound for square QAM constellation sizes. A summary of the derivation of (32) is provided in Appendix.

When $M^{(\xi)} = 4$, then

$$\Psi = \text{E}_{n_t,x,\hat{n}_t,\hat{x}}\left[\left(\frac{\sigma_z^2}{2}\right)^{-N_r}\right] \leq \frac{4N_t^{(\xi)} + \left(2^{-N_r}-2\right)}{4N_t^{(\xi)}}. \tag{31}$$

When $M^{(\xi)} = 16$, then

$$\Psi = \text{E}_{n_t,x,\hat{n}_t,\hat{x}}\left[\left(\frac{\sigma_z^2}{2}\right)^{-N_r}\right] \leq \frac{\psi_1+\psi_2}{(16N_t^{(\xi)})^2}, \tag{32}$$

where

$$\begin{aligned} \psi_1 &= \left(16(0.2)^{-N_r} + 32(0.6)^{-N_r} + 208\right)\left(N_t^{(\xi)}\right)^2, \\ \psi_2 &= \left(32(0.2)^{-N_r} + 36(0.4)^{-N_r} - 32(0.6)^{-N_r} + 32(0.8)^{-N_r} - 84\right)N_t^{(\xi)}. \end{aligned} \tag{33}$$

With this in mind, the closed form of the limit is defined as

$$\lim_{\gamma\to\infty}\frac{\mathrm{ABER}_{\xi}^{(\mathbf{inter})}}{\gamma^{-N_r}} = M^{(\xi)}N_t^{(\xi)}\binom{2N_r-1}{N_r}2^{-(2N_r+1)}\Psi. \tag{34}$$

At this point, the work can be simplified by considering a constant-amplitude modulation scheme such as PSK where $\sigma^2_{\tilde{z}_{\mathrm{PSK}}}$ is either 2 or 0 as shown in (22), then the expression in (30) is unity which simplifies further analysis. In such a scenario, however, the study in [31] shows that SM using PSK cannot always guarantee a better performance than SM using QAM. In particular, the authors of [31] demonstrate that there is a crossing point where the ABER of SM using PSK improves over SM using QAM. Nonetheless, there are two conclusions that we can drawn from this limit: (i) the system error increases with the product of the spatial constellation size, $N_t^{(\xi)}$, and symbol constellation size, $M^{(\xi)}$, (ii) the system error decreases exponentially with the addition of each received antenna, i.e. the diversity order is equal to N_r. In addition, we quantify the coding gains with respect to the number of receive antennas as $\binom{2N_r-1}{N_r}2^{-(2N_r+1)}$. This is apparent considering

$$\binom{2N_r-1}{N_r} < \binom{2N_r}{N_r} \ll \sum_{r=0}^{2N_r}\binom{2N_r}{r} = 2^{2N_r} < 2^{2N_r+1}. \tag{35}$$

In general, it can be shown that as $N_r \to \infty$, the inverse of (35) tends to zero and is always less than 1. Since the inverse of (35) is always less than 1, the addition of an extra receive antenna implies a smaller ratio, which means a lower ABER and hence coding gains for the system.

SIMO system utilising QAM (noise-limited scenario)

To quantify the SNR difference between SM and SIMO using QAM, we need to look at the ABER performance of a SIMO system using QAM in the asymptote. We use ([32], eq. 9.23) which provides a closed form solution for the ASER of a SIMO system using QAM with i.i.d. inputs, i.e. no correlation between the receive antennas. To begin the asymptotic analysis, ([32], eq. 9.23) is tightly upper bounded by

$$\mathrm{ASER}_{\mathrm{QAM}} \leq 4\left(1-\frac{1}{\sqrt{\widetilde{M}}}\right)f(\gamma_{\mathrm{QAM}})^{N_r}\sum_{r=0}^{N_r-1}\binom{N_r-1+r}{r}\left(1-f(\gamma_{\mathrm{QAM}})\right)^r, \tag{36}$$

where $\gamma_{\mathrm{QAM}} = \frac{3}{2(\widetilde{M}-1)}\gamma$. The interested reader is invited to look at the work in [32] for more details in obtaining (36). We can now pose $\mathrm{ASER}_{\mathrm{QAM}}/\log_2(\widetilde{M}) \approx \mathrm{ABER}_{\mathrm{QAM}}$ provided Gray mapping is used ([32], eq. 8.7), where $\widetilde{M} = M^{(\xi)}N_t^{(\xi)}$.

Using (27) and evaluating (36) in the limit as γ tends to infinity, it reduces to

$$\lim_{\gamma\to\infty}\frac{\mathrm{ABER}_{\mathrm{QAM}}}{\gamma^{-(N_r)}} \leq \frac{4}{\log_2(\widetilde{M})}\left(1-\frac{1}{\sqrt{\widetilde{M}}}\right)\left(\frac{3}{2(\widetilde{M}-1)}\right)^{-N_r}\binom{2N_r-1}{N_r}2^{-(2N_r)}. \tag{37}$$

If we look at the ratio of (34) with (31) to (37) then, after some analytical manipulations shown in the

"Reaching (38) from (34) with (31) and (37)" section in the Appendix, we can pose

$$\lim_{\gamma\to\infty}\frac{\mathrm{ABER}_{\xi}^{(\mathbf{inter})}/\gamma^{-N_r}}{\mathrm{ABER}_{\mathrm{QAM}}/\gamma^{-N_r}}=\frac{\left(2N_t^{(\xi)}+2^{-N_r-1}-1\right)}{\left(\frac{2\left(4N_t^{(\xi)}-1\right)}{3}\right)^{N_r}\frac{4}{\log_2\left(4N_t^{(\xi)}\right)}\left(1-\frac{1}{\sqrt{4N_t^{(\xi)}}}\right)}, \tag{38}$$

for $M^{(\xi)}=4$. If we equate the right-hand side of (38) to 1, then the expression cannot be solved in closed form. However, since N_r and $N_t^{(\xi)}$ are natural numbers we can readily evaluate (38). When evaluating (38), if the result is greater than 1, then SIMO transmission using only QAM is better than using SM. If the result is less than 1, then transmission using SM performs better than transmission using only QAM. The results for $N_t^{(\xi)}=2^q$ where $q\in\{1,\ldots,6\}$ and $N_r\in\{1,2,3\}$ are presented in Table 1, which shows that SM is always better if $N_r\geq 2$. In addition, the ratio of the two, as given in Table 1, exactly quantifies the minimum coding gain of SM relative to QAM for the same spectral efficiency of $\log_2\left(M^{(\xi)}N_t^{(\xi)}\right)$ in a noise-limited scenario, given $M^{(\xi)}=4$.

Table 1 Relative coding gains of SM using 4-QAM compared to SIMO using $\widetilde{M}$-QAM

N_r	$N_t^{(\xi)}=2^1$	$N_t^{(\xi)}=2^2$	$N_t^{(\xi)}=2^3$	$N_t^{(\xi)}=2^4$	$N_t^{(\xi)}=2^5$	$N_t^{(\xi)}=2^6$
1	1.6	1.9	2.3	2.6	2.9	3.2
2	0.67	0.38	0.22	0.12	0.068	0.038
3	0.28	0.075	0.021	0.0057	0.0016	$4.4(10^{-4})$

Proceeding in a similar manner as for (38), we pose the general ratio of the relative coding gains achieved by SM, using a variable-amplitude modulation, over a SIMO system using QAM as

$$\lim_{\gamma\to\infty}\frac{\mathrm{ABER}_{\xi}^{(\mathbf{inter})}/\gamma^{-(N_r)}}{\mathrm{ABER}_{\mathrm{QAM}}/\gamma^{-(N_r)}}=\frac{\widetilde{M}\Psi}{\left(\frac{2(\widetilde{M}-1)}{3}\right)^{N_r}\frac{2}{\log_2(\widetilde{M})}\left(1-\frac{1}{\sqrt{\widetilde{M}}}\right)}, \tag{39}$$

where Ψ must be defined for the desired SM signal constellation size, $M^{(\xi)}$. The exact ratios as given in Table 1 will vary depending on $M^{(\xi)}$, but the trend (SM outperforming SIMO) will remain, as can be seen in Table 2 for $M^{(\xi)}=16$, i.e. the values in the last two rows of the tables are smaller than one.

Table 2 Relative coding gains of SM using 16-QAM compared to SIMO using $\widetilde{M}$-QAM

N_r	$N_t^{(\xi)}=2^1$	$N_t^{(\xi)}=2^2$	$N_t^{(\xi)}=2^3$	$N_t^{(\xi)}=2^4$	$N_t^{(\xi)}=2^5$	$N_t^{(\xi)}=2^6$
1	3.8359	3.8724	4.0859	4.4031	4.7832	5.2024
2	0.2551	0.1121	0.0542	0.0278	0.0147	0.0079
3	0.0245	0.0050	0.0011	0.0003	0.0001	$2.0\left(10^{-5}\right)$

Similarly, using a constant-amplitude modulation scheme such as PSK, we realise that the only difference is that Ψ will be unity in (39). Implementing this change means removing the dependence on the signal constellation size for SM and resulting in a single table of values for (39), as given in Table 3.

Table 3 Relative coding gains of SM using PSK compared to SIMO using $\widetilde{M}$-QAM

N_r	$\widetilde{M}=2^2$	$\widetilde{M}=2^3$	$\widetilde{M}=2^4$	$\widetilde{M}=2^5$	$\widetilde{M}=2^6$	$\widetilde{M}=2^7$
1	2	1.9889	2.1333	2.3511	2.6122	2.9022
2	0.5000	0.2131	0.1067	0.0569	0.0311	0.0171
3	0.1250	0.0228	0.0053	0.0014	$3.7\left(10^{-4}\right)$	$1.0\left(10^{-4}\right)$

From Tables 1, 2, and 3, we can conclude that a single-input-single-output system using QAM performs better than SM using QAM or PSK, i.e. the values in the first row of each table are greater than 1. These results are applicable only to SM which means that at least 1 bit must be sent via the signal-symbol.

SIR*$_\xi \gg 1$ *and SINR* $\approx$ *SIR*$_\xi$ *(interference-limited scenario)

In this case, we neglect the AWGN in the channel and realise that the SIR_ξ is the dominant term dictating the ABER performance of the system. Looking at the expression for the SIR, we realise that $\gamma_{\mathbf{I}}$ is a function of the signal-symbol amplitude for all users and their respective channel attenuations. Thus, we cannot simply extract $\gamma_{\mathbf{I}}$ from (34). In particular, in the expression for $\gamma_{\mathbf{I}}$ in (11), $|x_{(u)}|$ may be greater than 1, which would increase the interference from the remaining users. Due to the complexity of the expressions, further asymptotic study of the interference-limited scenario for SM will be constrained to using a constant-amplitude modulation scheme such as PSK. SM using PSK is shown to perform better than SM using QAM in certain cases [31]. For SM using PSK,

$$\gamma_{\mathbf{I}}^{\mathrm{PSK}} \approx \frac{\alpha_{(\xi)}^2}{2\sum_{u\neq\xi=1}^{N_u} \alpha_{(u)}^2}, \tag{40}$$

in the interference-limited scenario. We see that the limit of the ABER tends to (34) with a slight, but very important distinction: the system reaches an error floor. This is to be expected when the receiver is interference-unaware. If $\gamma_{\mathbf{I}}$ or $\gamma_{\mathbf{I}}^{\mathrm{PSK}}$ are not large enough, i.e. the channel attenuations of the various nodes are similar, then this study presents an upper bound for the ABER of the system since (34) still defines the behaviour of the system in the limit. There are three consequences that should be considered similar to the noise-limited scenario analysed above: (i) the system error performance improves when more receive antennas are added at the receiver, (ii) the system error performance worsens as more SM constellation points are added, as either $N_t^{(\xi)}$ or $M^{(\xi)}$ is increased and (iii) the detector will fail to decode any data emitted from a node whose desired signal is weaker than the interfering signal. Although analytical work for SM using QAM becomes intractable, numerical results demonstrate that SM using a variable-amplitude modulation performs in a similar fashion to SM using PSK and leads to the same conclusions. In the remainder of this study, we show that the near–far problem is completely mitigated by applying a jointly optimal ML detector for SM in an interference-limited scenario. In other words, all incoming streams will be decoded and, in particular, the error performance of the system will tend to zero as AWGN approaches zero, despite any interference.

Interference-aware detection

Starting from the system model presented in the "System model" section, the decoded pair $(x_{\mathrm{est}}, n_t)^{(\xi)}$, formed from the estimated symbol x_{est} emitted from antenna n_t on node ξ is given by

$$\begin{Bmatrix} (x,n_t)^{(1)}, \\ \vdots \\ (x,n_t)^{(\xi)}, \\ \vdots \\ (x,n_t)^{(N_u)}, \end{Bmatrix} = \operatorname{argmin} \left\{ \left\| \mathbf{y} - \sum_{u=1}^{N_u} x^{(u)} \mathbf{h}_{n_t^{(u)}} \right\|_{\mathrm{F}}^2 \right\}, \tag{41}$$

$$x^{(u)} \in \mathcal{X}^{(u)} \qquad \text{and} \qquad n_t^{(u)} \in \{1,\ldots,N_t^{(u)}\}.$$

Similar to the work in the "Interference-unaware detection" section, the union bound technique is used to describe the behaviour of the interference-aware SM detector in the high SNR regions. The main difference between the two detectors comes from the computation of the PEP between the possible received symbols. The union bound for the interference-aware SM detector, which estimates the ABER for node ξ, can be expressed as

$$\mathrm{ABER}_{\xi} \leq \sum_{\substack{x^{(1)}, n_t^{(1)}, \\ \hat{x}^{(1)}, \hat{n}_t^{(1)}}}^{M^{(1)}N_t^{(1)}} \cdots \sum_{\substack{x^{(N_u)}, n_t^{(N_u)}, \\ \hat{x}^{(N_u)}, \hat{n}_t^{(N_u)}}}^{M^{(N_u)}N_t^{(N_u)}} \frac{d_{\xi}(b,\hat{b})}{\log_2\left(M^{(\xi)}N_t^{(\xi)}\right)} \frac{\mathrm{E}_{\mathbf{H}}\left[\mathrm{PEP}\left(x^{(\Omega)}, n_t^{(\Omega)}, \hat{x}^{(\Omega)}, \hat{n}_t^{(\Omega)}\right)\right]}{\prod_{u=1}^{N_u} M^{(u)}N_t^{(u)}}. \tag{42}$$

The pairs, $\left(x^{(\Omega)}, n_t^{(\Omega)}\right)$ and $\left(\hat{x}^{(\Omega)}, \hat{n}_t^{(\Omega)}\right)$, come from the set of all possible symbol-antenna pairings for all nodes, i.e. they independently take values from the set of all possible spatial and signal constellation points, Ω. We define $\mathrm{PEP}\left(x^{(\Omega)}, n_t^{(\Omega)}, \hat{x}^{(\Omega)}, \hat{n}_t^{(\Omega)}\right)$ to be the PEP between the symbol $x^{(\Omega)}$ emitted from antenna $n_t^{(\Omega)}$ being detected as symbol $\hat{x}^{(\Omega)}$ emitted by antenna $\hat{n}_t^{(\Omega)}$.

Similar to the analytical derivation of (4) in the "Interference-unaware detection" section, the ABER for node ξ is shown in (42), where the PEP is given as

$$\mathrm{PEP}\left(x^{(\Omega)}, n_t^{(\Omega)}, \hat{x}^{(\Omega)}, \hat{n}_t^{(\Omega)}\right) = Q\left(\sqrt{\frac{E_m}{2N_o}\left\|\sum_{u=1}^{N_u}\alpha_{(u)}\left(\mathbf{h}_{n_t^{(u)}}x^{(u)} - \mathbf{h}_{\hat{n}_t^{(u)}}\hat{x}^{(u)}\right)\right\|_{\mathrm{F}}^2}\right). \tag{43}$$

A more detailed derivation of (43) is given in the "Derivation of (43)" section in the Appendix. We note that thus far no assumptions have been made as to the channel distribution. Considering Rayleigh fading channels for all links in the system, we can derive the closed form solution for $\mathrm{E}_{\mathbf{H}}[\mathrm{PEP}(\cdot)]$ in (42) in the same manner as shown in the "Interference-unaware detection" section with (16) and (17) such that

$$\beta = \frac{E_m}{4N_o}\sum_{u=1}^{N_u}\alpha_{(u)}^2\vartheta_{(u)} \tag{44}$$

and

$$\vartheta_{(u)} = \begin{cases} \left(|x_{(u)}|^2 + |\hat{x}_{(u)}|^2\right) & n_t^{(u)} \neq \hat{n}_t^{(u)}, \\ \left(|x_{(u)} - \hat{x}_{(u)}|^2\right) & n_t^{(u)} = \hat{n}_t^{(u)}, \\ 0 & n_t^{(u)} = \hat{n}_t^{(u)} \text{ and } x_{(u)} = \hat{x}_{(u)}. \end{cases} \tag{45}$$

Note that (42) presents an analytical treatment of the most general case of SM using variable amplitude modulation for the signal symbol. Given this, the system using the interference-aware detector behaves in a similar fashion to the noise-limited system, in that for an arbitrarily high SNR, each user can achieve an arbitrarily low ABER. It should be pointed out that due to the simultaneous detection process, the users with the best SNR will not be able to achieve their single-user-lower-bound (SULB). The exact effect of the additional nodes/users is further discussed in the "Simulation results and discussion" section.

Simulation results and discussion

In this section, we aim to show the performance of the interference-unaware and interference-aware detectors proposed in (2) and (41). In particular, we aim to show that (41) can successfully decode the incoming streams for all nodes. Numerical results demonstrate that (12) and (42) provide tight upper bounds for the ABER of the detectors at high SNR in the interference-limited scenario. Furthermore, we demonstrate that the interference-aware detector for SM performs better than the ML detector for a multi-user SIMO system using QAM.

The proposed interference-aware detector is jointly optimal for all nodes and does not suffer from the near–far problem, but it needs full channel state information (CSI) from all possible transmitting antennas to each receiving antenna. In addition, finding the optimal solution is an exponentially complex problem. Assuming each node has the same number of transmit antennas, N_t, and uses the same signal constellation with M points, then the interference-aware ML detector proposed has $\mathcal{O}\left((MN_t)^{N_u}\right)$ computational complexity which is proven to be NP-complete [33].

To justify our $\mathcal{O}(\cdot)$ complexity, we point to the key difference between SM and other multi-user MIMO schemes, the signal and spatial domains combine to form a single SM symbol. The constellation size, i.e. the spectral efficiency of any SM system, depends on the multiplication of the number of available transmit antennas and the signal-symbol constellation used, MN_t. This is in stark contrast to other MIMO systems where each spatial branch is used to increase the diversity or multiplexing gains. In such a system, if each transmit antenna is used for multiplexing gains, the system has a maximum spectral efficiency of M^{N_t}. From here, the detection complexity of a single user SM system is given by $\mathcal{O}\left(MN_t\right)$, while the detection complexity of a single user MIMO system used for multiplexing gains is given by $\mathcal{O}\left(M^{N_t}\right)$. In this case, the two systems have different spectral efficiencies. Alternatively, if the two systems operate at the same spectral efficiency, then their complexities will be of the same $\mathcal{O}$ order, but the cost, in terms of RF chains and power consumption would not be. The aim of this study is to characterise the behaviour of SM in the multi-user, interference-limited scenario and compare it to the *complexity and cost equivalent* multi-user MIMO system. As discussed in the "Introduction" section and given the complexity expressions for the single user MIMO system and the single user SM system, it is apparent that the only valid *complexity and cost equivalent* comparison is to compare multi-user SM with multi-user SIMO. The optimal ML detector for the interference-aware SIMO system has $\mathcal{O}\left(\left(\widetilde{M}\right)^{N_u}\right)$ computational complexity, where $\widetilde{M} = MN_t$ from the "SIMO system utilising QAM (noise-limited scenario)" section, making it comparable to the interference-aware SM detector. Recent work on sphere detection algorithms may be used to alleviate this computational cost [9]. Despite the generality of our results, we restrict our simulation results to two and three node scenarios for the sake of conciseness.

Simulation setup

A frequency-flat Rayleigh fading channel with no correlation between the transmitting antennas and AWGN is assumed. Perfect CSI is assumed at the receiving node, with no CSI at the transmitter. Only one of the available transmit antennas for each node is active at any transmitting instance. In theory, each node independently decides the number of transmit antennas, and, by extension, the signal-symbol modulation it uses. In the simulation each node has the same number of transmit antennas as well as the same spectral efficiency target. In each of the figures, there are three sets of results presented: (i) the simulation results for the multi-user detector for each node, denoted by $\texttt{Sim}\left(\mathrm{N}_{(\xi)}\right)$, (ii) the theoretical results from (12) or (42) for the node of interest and (iii) the SULB, denoted by $\texttt{SULB}\left(\mathrm{N}_{(\xi)}\right)$. We define the asymptotically tight SULB as the system performance in a

noise-limited scenario given in (26) which is governed purely by its SNR, defined as E_m/N_o. It should be noted that in Figures 2, 3 and 4 in addition to (26), ASER/2, i.e. (28) divided by 2, is presented and overlaps (26); both are denoted as $\texttt{SULB}(\mathrm{N}_{(\xi)})$ in Figures 2, 3 and 4. This serves to justify the use of (28) in our asymptotic analysis in the "Asymptotic analysis of an interference-unaware detector" section. In addition, (26) is based on the union bound technique and, in some results, $\texttt{SULB}(\mathrm{N}_{(\xi)})$ is above 1, which is impossible for a real system. In this regard, the SULB is a lower bound on the analytical performance of each system only at low ABER. To help illustrate the difference in the behaviour of the two detectors, the channel attenuations, $\alpha^2_{(u)}$, are set in 10-dB intervals. In general, $\alpha^2_{(u)}$ may be any real number. Throughout the results, QAM modulation is used for the signal-symbol modulation in SM with the notable exception of Figure 2, where PSK modulation is used to illustrate the accuracy of work done in the "Asymptotic analysis of an interference-unaware detector" section.

Figure 2 $N_t^{(u)} = 4, N_r = 1$ **and a spectral efficiency of 4 bits/s/Hz.** ABER for node 1 using the interference-unaware detector with $\alpha^2_{(1)} = 1$ and node 2 with a varying $\alpha^2_{(2)}$. Dashed lines denote simulation results for node 1 while solid lines denote the analytical upper bound. Since the analytical bound is asymptotically tight, at low ABER the dashed and solid lines overlap. Each constant value dashed-dot line with '+' markers corresponds to the asymptote derived in (34) using (40) for the different values of $\alpha^2_{(2)}$

Figure 3 $N_t^{(u)} = 4, N_r = 2$ **and a spectral efficiency of 4 bits/s/Hz.** ABER for node 1 using the interference-unaware detector with $\alpha^2_{(1)} = 1$ and node 2 with a varying $\alpha^2_{(2)}$. Dashed lines denote simulation results for node 1 while solid lines denote the analytical upper bound. Since the analytical bound is asymptotically tight, at low ABER the dashed and solid lines overlap

Figure 4 $N_t^{(u)} = 4, N_r = 3$ **and a spectral efficiency of 4 bits/s/Hz.** ABER for node 1 using the interference-unaware detector with $\alpha^2_{(1)} = 1$ and node 2 with a varying $\alpha^2_{(2)}$. Dashed lines denote simulation results for node 1 while solid lines denote the analytical upper bound. Since the analytical bound is asymptotically tight, at low ABER the dashed and solid lines overlap

Results for interference-unaware detection

Asymptotic results in the "Asymptotic analysis of an interference-unaware detector" section, in particular (34) using QPSK for the signal-symbol modulation are verified in Figure 2. In this case, Ψ is strictly defined by (22). The horizontal lines in Figure 2 represent (34) for varying values of $\alpha^2_{(u)}$ using QPSK modulation. From Figure 3, 4 and 5, where QAM is used for the signal-symbol modulation, the developed analytical framework is accurate in all the presented instances. By moving from Figure 3 to Figure 3, where an additional receive antenna is added, the analytical model presented in (12) is a tight upper bound on the system in the high SINR region. As the channel attenuations for the interfering nodes increase, the detector approaches SULB. Similar to the effects observed in Figures 2 and 3, Figure 4 shows how the tightness of the bound improves as the number of receive antennas increases. In all instances where the interference-unaware detector is used, the node with the strongest SNR dominates the detection. The bit streams of all other nodes are not decoded. Since the SINR does not change, all other nodes remain below the effective noise floor at the receiver. This is apparent by looking at the simulation results for $N_{(2)}$ and $N_{(3)}$ in Figure 2, 3 and 4. By looking at the presented results, we conclude that (34) tightens as the system approaches its ideal transmission and the mass of the complex Gaussian distributions around each SM constellation point concentrates around the mean. This is achieved by decreasing the interference in the system or by increasing the number of receive antennas.

Figure 5 $N_t^{(u)} = 4$, a varying N_r and a spectral efficiency of 4 bits/s/Hz. ABER for node 1 using the interference-unaware detector with $\alpha_{(1)}^2 = 1$, node 2 with $\alpha_{(2)}^2 = 0.1$ and node 3 with $\alpha_{(3)}^2 = 0.01$. All presented curves are for node 1 unless otherwise stated in the legend. Dashed lines denote simulation results for node 1 while solid lines denote the analytical upper bound. We note that the addition of more receive antennas reduces the ABER and hence closes the gap between the analytical and simulation results

Figure 4 shows that the increase in diversity resulting from the addition of only a single receive antenna significantly influences the system performance. The addition of the receive antenna increases the Euclidean distance between the received and hypothesis vectors, which results in a lower ABER. Comparing Figure 2 with Figure 3 and similarly Figure 3 with Figure 4 where the number of receive antennas is increased in each figure, showing how the addition of a single receive antenna is equivalent to lowering the interference $\left(\alpha_{(u)}^2\right)$ by more than 10 dB. In fact, the effect of each receive antenna is more pronounced as the imbalance between the desired and interfering links increases. By looking at the results for $\alpha_{(2)}^2 = 10^{-2}$ in Figure 2, the results for $\alpha_{(2)}^2 = 10^{-2}$ in Figure 3, and the results for $\alpha_{(2)}^2 = 10^{-2}$ in Figure 4 at an SNR of 40 dB, we see the error rate of the simulation and analytical prediction moving from 2×10^{-1} in Figure 2, to 4×10^{-3} in Figure 3, to 9×10^{-5} in Figure 4. This ABER decrease shows how the number of receive antennas dominates the performance of SM in general, and particularly in an interference limited scenario. Figure 5 demonstrates that the findings can be extended even in the presence of two interfering nodes.

From the presented results it is clear that when the interference-unaware detector is used, the system ABER plateaus at the derived limits, irrespective of the transmit power being used. As discussed in the "Interference-unaware detection" section, and as work in [20] has shown, the ABER improves when the number of transmit or receive antennas is increased, i.e. the system achieves coding gains.

Results for interference-aware detection

In Figure 6 we see the performance of the jointly optimal interference-aware ML detector for a two user scenario. Figure 6 clearly demonstrates that the analytical model presented in (42) represents an asymptotically tight upper bound for the system in the high SNR region. The node with the worse channel attenuation performs close to its SULB. This is not the case for the node with the better channel.

Figure 6 $N_t^{(u)} = 2, N_r = 3$ and a spectral efficiency of 4 bits/s/Hz. ABER using the interference-aware detector for node 1 with $\alpha_{(1)}^2 = 1$ and node 2 with $\alpha_{(2)}^2 = 0.1$. $\texttt{Ana}(\ \mathrm{N}_{(u)}\ )$ denotes the analytical upper bound for node u. Since the analytical bound is asymptotically tight, at low ABER the dashed and solid lines overlap

To understand this, we can think of the multi-user ML detector as employing interference cancellation for the node with the worse channel attenuation. If the interfering user is sufficiently powerful, then the primary source of errors for the weakest node is the background AWGN rather than the randomness caused by the interfering signal [29]. All users that have good channel conditions can be considered as strong interferers, so when they are removed, the weakest nodes obtain performance closer to their SULB, i.e. the interference-aware detector is akin to strong interference cancellation for the weakest node. On the contrary, for the nodes with better channel conditions, the primary source of errors is the randomness caused by the interfering signal rather than the background AWGN, which is why the nodes with better channel conditions never perform near their SULB.

The addition of more transmit antennas at each of the nodes results in coding gains for each node as can be seen when Figures 6 and 7 are compared. The reduction in ABER as the number of transmit antennas increases is explained by realising that as the number of transmit antennas increases, the average variance σ_z^2 increases. As σ_z^2 increases, it leads to a larger Euclidean distance in (10) and (43). The Euclidean distance is increased because there are more cases where the variance is the summation of the individual symbol constellation points, rather than the difference, i.e. $n_t^{(\xi)} = \hat{n}_t^{(\xi)}$ occurs less frequently. Effectively, more transmit antennas mean that the transmit vectors are spread in a larger Euclidean space. This effect can only be observed when the same spectral efficiency is maintained. In particular, a 2-dB coding gain is apparent when comparing Figures 6 and 7 at an ABER of 10^{-4}. However, increasing the number of transmit antennas does not change the relative behaviour of the system, i.e. the SNR difference between the ABER curves of the two nodes remains constant. This behaviour is expected when we consider that (17) is independent of N_t and influenced only by N_r.

Figure 7 $N_t^{(u)} = 2, N_r = 3$ **and a spectral efficiency of 4 bits/s/Hz.** ABER using the interference-aware detector for node 1 with $\alpha_{(1)}^2 = 1$ and node 2 with $\alpha_{(2)}^2 = 0.1$. `Ana(` $N_{(u)}$ `)` denotes the analytical upper bound for node u. Since the analytical bound is asymptotically tight, at low ABER the dashed and solid lines overlap

Figure 8 shows the performance of the system when the number of receive antennas is increased. On the one hand, moving from Figure 7 to 8, for a fixed spectral efficiency and a fixed number of transmit antennas, the addition of more receive antennas results in an increasing gap between the analytical ABER curves of the two nodes. In particular, a gap of 4 dB between the performance of nodes 1 and 2 with $N_r = 2$ is increased to around 7 dB when $N_r = 4$ and further increased to 9 dB for $N_r = 8$. On the other hand, given that the two nodes experience a channel gain difference of 10 dB, we know that the interference-aware detector cannot reach the performance of independent detection and the SULB for the node with the better channel attenuation. Nonetheless, the gap between their respective ABER curves tends toward the difference between their respective channel attenuation as N_r grows.

Figure 8 $N_t^{(u)} = 4$**, a varying** N_r **and a spectral efficiency of 4 bits/s/Hz.** ABER using the interference-aware detector for node 1 with $\alpha_{(1)}^2 = 1$ and node 2 with $\alpha_{(2)}^2 = 0.1$. Dashed lines denote the performance of node 1 with a varying number of receive antennas while solid lines denote the performance of node 2 with a varying number of receive antennas

These trends can also be observed if we look at the progression of the ABER curves in Figures 9 and 10. Figures 9 and 10 show the system performance of three users and varying N_r. Similar to the two user scenario, as N_r increases, for the three user case, each user performs better and slowly closes the gap to its SULB. As expected, the addition of more nodes increases the interference and pushes the performance of each node further from its SULB, noticeable when comparing Figures 7 and 10 for node 2.

Figure 9 $N_t^{(u)} = 4, N_r = 1$ **and a spectral efficiency of 4 bits/s/Hz.** ABER for node 1 with $\alpha_{(1)}^2 = 1$, node 2 with $\alpha_{(2)}^2 = 0.1$ and node 3 with $\alpha_{(3)}^2 = 0.01$. `Ana(` $N_{(u)}$ `)` denotes the analytical upper bound for node u. Since the analytical bound is asymptotically tight, at low ABER the dashed and solid lines overlap

Figure 10 $N_t^{(u)} = 4, N_r = 3$ **and a spectral efficiency of 4 bits/s/Hz.** ABER for node 1 with $\alpha_{(1)}^2 = 1$, node 2 with $\alpha_{(2)}^2 = 0.1$ and node 3 with $\alpha_{(3)}^2 = 0.01$. `Ana( N(u) )` denotes the analytical upper bound for node u. The analytical bound is again shown to be asymptotically tight at low ABER

Lastly, Figure 11 demonstrates that in the multiple access interference-limited scenario, by using the interference-aware detector, SM performs better than the complexity and cost equivalent ML detector for the multi-user SIMO system. Specifically, SM exhibits an approximately 3 dB better performance in terms of SNR at an ABER of 10^{-4} for each user. The relatively constant coding gain is the result of the similar detection used for both systems. While multi-user SM and multi-user SIMO may be comparable in terms of detector complexity and the number of transmit and receive RF chains required, each SM node requires multiple transmit antenna elements. The multiple transmit antennas mean that the SM constellation points are spread in a larger Euclidean space and thus have lower error probability.

Figure 11 $N_t^{(u)} = 4, N_r = 3$ **and a spectral efficiency of 4 bits/s/Hz.** ABER of multi-user SM and multi-user SIMO using interference-aware detectors with node 1 experiencing channel attenuation of $\alpha_{(1)}^2 = 1$, node 2 with $\alpha_{(2)}^2 = 0.1$ and node 3 with $\alpha_{(3)}^2 = 0.01$

Summary and conclusions

In this study, the performance of SM in the multiple access, interference-limited scenario was investigated. Two ML detectors for use with SM were discussed.

The interference-unaware detector was defined and studied in the limit as the SNR approached infinity. Its performance over uncorrelated Rayleigh fading channels was studied and a closed form solution for the upper bound of the system was provided. It was shown that this detector inevitably reaches an error floor which is dependent on the system SINR. The exact level was defined as a function and concrete examples were provided. It was shown that the increase in the number of receive antennas has a greater impact on the asymptotic performance of the system compared to reducing the interference in the system. The addition of a single receive antenna resulted in greater SNR gains than reducing the interference, $\alpha_{(u)}^2$, by more than 10 dB at high SNR. This implies that the number of receive antennas dominates the performance of SM in general, and particularly in an interference-limited scenario.

The interference-aware ML detector for SM was proposed. As with the interference-unaware detector, its performance over uncorrelated Rayleigh fading channels was studied and a closed form solution for the upper bound of the system was provided. In addition to avoiding the error floor present in the interference-unaware detector, the jointly optimal detector results in a noise-limited scenario for the detection of all transmitted streams, i.e. an arbitrarily small ABER can be obtained by any user for a sufficiently high SNR. On the one hand, for the same spectral efficiency, increasing the number of transmit antennas at each of the nodes from 2 to 4 resulted in SNR gains of around 2 dB. This measure did not, however, have any effect on the coding gain difference between the ABER curves. On the other hand, increasing the number of receive antennas increased the diversity of the system. This, increased the coding gain difference between the ABER curves of the nodes because the receiver could distinguish the channels more easily and better mitigate interference. The impact on the diversity and coding gains further shows the importance of the number of receive antennas in any SM system. A limiting factor, as with all ML detectors, is the complexity. In addition, the receiver must have channel knowledge from all transmitting nodes. These two limitations constrain the application of this detector to the uplink scenario. The interference-aware detector enabled SM to perform better in terms of

ABER than the complexity and cost equivalent multi-user SIMO system in an interference-limited environment.

This study demonstrated that in order to effectively apply SM in an interference-limited scenario, the number of receive antennas should be maximised. Although more computationally complex than the interference-unaware detector, the interference-aware detector can guarantee that the system does not reach an error floor.

Acknowledgement

We gratefully acknowledge the support from the Engineering and Physical Sciences Research Council (EP/G011788/1) in the United Kingdom for this study.

Appendix

Derivation of (32)

We begin by considering $\widetilde{\psi_1}$ which corresponds to $\sigma_z^2 = |x^{(\xi)}|^2 + |\hat{x}^{(\xi)}|^2$. For this event, we seek to bound σ_z^2 to two which implies that we should consider

$$\left(d_\epsilon^2 + d_{\hat{\epsilon}}^2\right) g_{\text{QAM}} \leq 2 \tag{46}$$

where $\epsilon \in \{(1,1),(2,1),(3,1)\}$ and d_ϵ are the distances defined in Figure 12 and $g_{\text{QAM}} = \frac{3}{2\left(M^{(\xi)}-1\right)}$. We introduce the normalising factor g_{QAM}, given in [32], to maintain unity power in our constellation. We see that there are only four possible combinations that satisfy (46). In particular

- $\left(d_{(1,1)}^2 + d_{(1,1)}^2\right) g_{\text{QAM}} = 0.4$, occurs $\left(M^{(\xi)}\right)^2/8 = 32$ times,
- $\left(d_{(1,1)}^2 + d_{(2,1)}^2\right) g_{\text{QAM}} = 1.2$, occurs $\left(M^{(\xi)}\right)^2/4 = 64$ times,
- $\left(d_{(1,1)}^2 + d_{(3,1)}^2\right) g_{\text{QAM}} = 2$, occurs $\left(M^{(\xi)}\right)^2/8 = 32$ times and
- $\left(d_{(2,1)}^2 + d_{(2,1)}^2\right) g_{\text{QAM}} = 2$, occurs $\left(M^{(\xi)}\right)^2/2 = 128$ times.

Figure 12 The red squares denote 16-QAM constellation points. In this image, the constellation is not normalised. The figure shows possible distance combinations between each of the constellation points and their distances to the origin

We know that these combinations occur for every instance when $n_t \neq \hat{n}_t$. For a system with $N_t^{(\xi)}$ transmit antennas, we have $\binom{N_t^{(\xi)}}{2}$ unique pairings. This leads to

$$\widetilde{\psi_1} = \left((0.4/2)^{-N_r}32 + (1.2/2)^{-N_r}64 + 32 + 128\right)\binom{N_t^{(\xi)}}{2}. \tag{47}$$

Having established the derivation of $\widetilde{\psi_1}$, we turn our attention to $\widetilde{\psi_2}$ which corresponds to $\sigma_z^2 = |x^{(\xi)} - \hat{x}^{(\xi)}|^2$. If we look at Figure 12, we see there are additional combinations aside from the

ones denoted. To this extent, our bound, $\sigma_z^2 = \min\{\sigma_z^2, 2\}$, serves to simplify the counting and set many of them to 2. In particular, we see that when $\sigma_z^2 = d_{(5,2)}^2$, then $\sigma_z^2 > 2$. In this case, we bound σ_z^2 to 2 and realise that $d_{(4,2)}$ is the largest distance that we must account for in our expectation analysis. We note that our approach is applicable to larger constellation sizes and, after some careful counting, we see that in general for a given constellation size of $M^{(\xi)}$ we have that

- $d_{(1,2)}$ occurs a total of $D^{(1)} = 4\sqrt{M^{(\xi)}}\left(\sqrt{M^{(\xi)}} - 1\right)$ times,
- $d_{(2,2)}$ occurs a total of $D^{(2)} = 4\sqrt{M^{(\xi)}}\left(\sqrt{M^{(\xi)}} - 2\right)$ times,
- $d_{(3,2)}$ occurs a total of $D^{(3)} = 4\left(\sqrt{M^{(\xi)}} - 1\right)\left(\sqrt{M^{(\xi)}} - 1\right)$ times and,
- $d_{(4,2)}$ occurs a total of $D^{(4)} = 8\left(\sqrt{M^{(\xi)}} - 1\right)\left(\sqrt{M^{(\xi)}} - 2\right)$ times.

By looking at Figure 12, we can easily see that for $M^{(\xi)} = 16$:

- $d_{(1,2)}^2\, g_{\text{QAM}} = 0.4$, occurs exactly 48 times,
- $d_{(2,2)}^2\, g_{\text{QAM}} = 1.6$, occurs exactly 32 times,
- $d_{(3,2)}^2\, g_{\text{QAM}} = 0.8$, occurs exactly 36 times and
- $d_{(4,2)}^2\, g_{\text{QAM}} = 2$, occurs exactly 48 times.

We realise that the combinations counted above are applicable for every transmit antenna. This implies that we must multiply each count by $N_t^{(\xi)}$ which leads to

$$\widetilde{\psi_2} = \left((0.4/2)^{-N_r}48 + (1.6/2)^{-N_r}32 + (1.6/2)^{-N_r}36 + 48\right)N_t^{(\xi)}. \tag{48}$$

To arrive at a final solution, we set all other combination values to g_{QAM} as we enforce our bound on σ_z^2 giving

$$D_{\text{ones}} = \left(M^{(\xi)}N_t^{(\xi)}\right)^2 - \left(M^{(\xi)}\right)^2\binom{N_t^{(\xi)}}{2} - \left(D^{(1)} + D^{(2)} + D^{(3)} + D^{(4)}\right)^2 N_t^{(\xi)}$$

which is the number of elements for which σ_z^2 was set to 2, i.e. $\left(\sigma_z^2/2\right)^{-N_r} = 1$. We now average and arrive at Ψ. To achieve this, we merely normalise our sum by $\left(M^{(\xi)}N_t^{(\xi)}\right)^2$ to account for the number of possible events, resulting in

$$\Psi = \frac{\widetilde{\psi_1} + \widetilde{\psi_2} + D_{\text{ones}}}{\left(M^{(\xi)}N_t^{(\xi)}\right)^2}$$

which when simplified becomes (32).

In Figure 13 we compare the asymptote of SM, given by (34), in the noise-limited scenario for $M^{(\xi)} = 16$ with and without using (32). Figure 13 exemplifies the accuracy and tightness of our approach.

Figure 13 The dashed lines with circle markers denote the asymptote for the system if the expectation for $\left(\sigma_z^2/2\right)^{-N_r}$ is obtained via simulations. The solid lines with square markers denote the asymptote when (32) is used. Moving from the rightmost to the leftmost pairs of curves, each pair corresponds to an incremental increase in N_r from 2 to 6. The system is using two transmit antennas and has an overall spectral efficiency of 5 bits/s/Hz

Reaching (38) **from** (34) **with** (31) **and** (37)

Combining (34) with (31) results in

$$\begin{aligned}\lim_{\gamma_{\mathbf{I}}\to\infty} \frac{\mathrm{ABER}_{\xi}^{(\mathbf{inter})}}{\gamma_{\mathbf{I}}^{-N_r}} &= 4N_t^{(\xi)}\binom{2N_r-1}{N_r}2^{-(2N_r+1)}\,\frac{2N_t^{(\xi)}+2^{-N_r-1}-1}{2N_t^{(\xi)}} \\ &= \left(2N_t^{(\xi)}+(2^{-N_r-1}-1)\right)\binom{2N_r-1}{N_r}2^{-(2N_r)}.\end{aligned} \tag{49}$$

Restating (37) for convenience, we have

$$\lim_{\gamma\to\infty}\frac{\mathrm{ABER}_{\mathrm{QAM}}}{\gamma^{-N_r}} \le \frac{4}{\log_2(\widetilde{M})}\left(1-\frac{1}{\sqrt{\widetilde{M}}}\right)\left(\frac{3}{2(\widetilde{M}-1)}\right)^{-N_r}\binom{2N_r-1}{N_r}2^{-(2N_r)}.$$

Taking the ratio of (49) over (37) gives (38) as

$$\lim_{\gamma\to\infty}\frac{\mathrm{ABER}_{\xi}^{(\mathbf{inter})}/\gamma^{-N_r}}{\mathrm{ABER}_{\mathrm{QAM}}/\gamma^{-N_r}} = \frac{\left(2N_t^{(\xi)}+2^{-N_r-1}-1\right)}{\left(\frac{2\left(4N_t^{(\xi)}-1\right)}{3}\right)^{N_r}\frac{4}{\log_2\left(4N_t^{(\xi)}\right)}\left(1-\frac{1}{\sqrt{4N_t^{(\xi)}}}\right)}.$$

Derivation of (43)

$$\begin{aligned}&\Pr\{\mathbf{A}\neq\hat{\mathbf{A}}\} = \Pr\left\{||\mathbf{y}-\mathbf{A}||_{\mathrm{F}}^2 > \left\|\mathbf{y}-\hat{\mathbf{A}}\right\|_{\mathrm{F}}^2\right\} \\ &= \Pr\left\{\sum_{r=1}^{N_r}\left[|y_r-A_r|^2\right] > \sum_{r=1}^{N_r}\left[\left|y_r-\hat{A}_r\right|^2\right]\right\} \\ &= \Pr\left\{\sum_{r=1}^{N_r}\left[2\Re\left\{\left(\hat{A}_r-A_r\right)\eta^*\right\}\right] > \sum_{r=1}^{N_r}\left[\left|A_r-\hat{A}_r\right|^2\right]\right\} \\ &\Rightarrow \eta_r^{\mathrm{new}} \sim \mathcal{N}\left(\sum_{r=1}^{N_r}\left[2\Re\left\{(\hat{A}_r-A_r)^*\right\}\right], \sum_{r=1}^{N_r}\left[2N_o|\hat{A}_r-A_r|^2\right]\right),\end{aligned} \tag{50}$$

where $\mathbf{A} = \frac{E_m}{2N_o}\sum_{u=1}^{N_u}\alpha_{(u)}\mathbf{h}_{n_t^{(u)}}x^{(u)}$ and $\hat{\mathbf{A}} = \frac{E_m}{2N_o}\sum_{u=1}^{N_u}\alpha_{(u)}\mathbf{h}_{\hat{n}_t^{(u)}}\hat{x}^{(u)}$.

If we consider a Rayleigh fading channel, then we can derive the closed form solution for $\mathrm{E}_{\mathbf{H}}\left[\mathrm{PEP}\left(\cdot\right)\right]$ in (42) by using ([30], eq. 62). We note that by assuming a Rayleigh fading channel, the argument within (43) can be represented as the summation of $2N_r$ squared Gaussian random variables, with zero mean and variance equal to 1, which means that they can be described by a central Chi-squared

distribution with $2N_r$ degrees of freedom and a probability density function of

$$\tilde{\rho}_K(\kappa) = \frac{1}{2^{N_r}(N_r-1)!}\kappa^{N_r-1}\exp(-\kappa/2).$$

The result for $\mathrm{E}_{\mathbf{H}}[\mathrm{PEP}(\cdot)]$ is given as

$$\mathrm{E}_{\mathbf{H}}[\mathrm{PEP}(\cdot)] = f(\tilde{\beta})^{N_r}\sum_{r=0}^{N_r-1}\binom{N_r-1+r}{r}\left(1-f(\tilde{\beta})\right)^r \tag{51}$$

such that $f(\tilde{\beta}) = \frac{1}{2}\left(1-\sqrt{\frac{\tilde{\beta}}{1+\tilde{\beta}}}\right)$ and $\tilde{\beta} = \frac{E_m}{4N_o}\sum_{u=1}^{N_u}\alpha_{(u)}^2\vartheta_{(u)}$.

Competing interests

The authors declare that they have no competing interests.

References

1. J Mietzner, R Schober, L Lampe, WH Gerstacker, PA Hoeher, Multiple-antenna techniques for wireless communications—a comprehensive literature survey. IEEE Commun. Surv. Tutor. **11**(2), 87–105 (2009)
2. R Mesleh, H Haas, Y Lee, S Yun, Interchannel interference avoidance in MIMO transmission by exploiting spatial information, in *Proc. of the 16th IEEE International Symposium on Personal, Indoor and Mobile Radio Communications (PIMRC)*, vol. 1, Berlin, Germany, 11–14 September 2005, pp. 141–145
3. R Mesleh, H Haas, S Sinanović, CW Ahn, S Yun, Spatial modulation. IEEE Trans. Veh. Technol. **57**(4), 2228–2241 (2008)
4. N Serafimovski, M Di Renzo, S Sinanović, RY Mesleh, H Haas, Fractional bit encoded spatial modulation (FBE–SM). IEEE Commun. Lett. **14**(5), 429–431 (2010)
5. A Younis, N Serafimovski, R Mesleh, H Haas, Generalized spatial modulation, in *Asilomar Conference on Signals, Systems, and Computers*, Pacific Grove, CA, USA, November 2010
6. R Mesleh, M Di Renzo, H Haas, PM Grant, Trellis coded spatial modulation. IEEE Trans. Wirel. Commun. **9**(7), 2349–2361 (2010)
7. A Younis, R Mesleh, H Haas, PM Grant, Reduced complexity sphere decoder for spatial modulation detection receivers, in *2010 IEEE Global Telecommunications Conference (GLOBECOM 2010)*, Miami, Florida, USA. December 2010, pp. 1–5
8. MD Renzo, H Haas, Performance analysis of spatial modulation, in *International ICST Conference on Communications and Networking in China (CHINACOM)*, Beijing, China. August 2010, pp. 1–7
9. A Younis, M Di Renzo, R Mesleh, H Haas, Sphere decoding for spatial modulation, in *Proc. of IEEE International Conference on Communications (IEEE ICC 2011)*, Kyoto, Japan, 5–9 June 2011, pp. 1–6

10. J Jeganathan, A Ghrayeb, L Szczecinski, Spatial modulation: optimal detection and performance analysis. IEEE Commun. Lett. **12**(8), 545–547 (2008)

11. SU Hwang, S Jeon, S Lee, J Seo, Soft-output ML detector for spatial modulation OFDM systems. IEICE Electron. Exp. **6**(19), 1426–1431 (2009)

12. M Di Renzo, H Haas, Spatial modulation with partial-CSI at the receiver: optimal detector and performance evaluation, in *Proceedings of the 33rd IEEE conference on Sarnoff* (IEEE Press, Piscataway, NJ, USA, 2010), pp. 58–63, http://portal.acm.org/citation.cfm?id=1843486.1843498

13. M Di Renzo, H Haas, Improving the performance of Ssace shift keying (SSK) modulation via opportunistic power allocation. IEEE Commun. Lett. **14**(6), 500–502 (2010)

14. T Handte, A Muller, J Speidel, BER analysis and optimization of generalized spatial modulation in correlated fading channels, in *Vehicular Technology Conference Fall (VTC Fall-2009)*, September 2009, pp. 1–5

15. MD Renzo, H Haas, Bit error probability of SM-MIMO over generalized fading channels. IEEE Trans. Veh. Technol. **61**(3), 1124–1144 (2012)

16. E Basar, U Aygolu, E Panayirci, VH Poor, Space-time block coded spatial modulation. IEEE Trans. Commun. **59**(3), 823–832 (2011)

17. J Jeganathan, A Ghrayeb, L Szczecinski, A Ceron, Space shift keying modulation for MIMO channels. IEEE Trans. Wirel. Commun. **8**(7), 3692–3703 (2009)

18. JN Laneman, DNC Tse, GW Wornell, Cooperative diversity in wireless networks: efficient protocols and outage behavior. IEEE Trans. Inf. Theory **50**(12), 3062–3080 (2004)

19. MO Hasna, M-S Alouini, End-to-end performance of transmission systems with relays over Rayleigh-fading channels. IEEE Trans. Wirel. Commun. **2**(6), 1126–1131 (2003)

20. N Serafimovski, S Sinanovic, M Di Renzo, H Haas, Dual-hop spatial modulation (Dh-SM), in *Proc. of the Vehicular Technology Conference (VTC Spring)*, Budapest, Hungary, IEEE, 15–18 May 2011, pp. 1–5

21. M Di Renzo, H Haas, On the performance of SSK modulation over multiple-access Rayleigh fading channels, in *IEEE Global Telecommunications Conference (GLOBECOM)*, Miami, Florida, USA. December 2010, pp. 1–6

22. M Di Renzo, H Haas, Bit error probability of space-shift keying MIMO over multiple-access independent fading channels. IEEE Trans. Veh. Technol. **60**(8), 3694–3711 (2011)

23. J Duplicy, B Badic, R Balraj, R Ghaffar, P Horvth, FKR Knopp, IZ Kovacs, HT Nguyen, D Tandur, G Vivier, MU-MIMO in LTE systems. EURASIP J. Wirel. Commun. Netw. **2011**, 13 (2011)

24. JG Andrews, W Choi, RW Heath Jr., Overcoming interference in spatial multiplexing MIMO cellular networks. IEEE Wirel. Commun. Mag. **14**(6), 95–104 (2007)

25. D Gesbert, M Kountouris, RW Heath, C byoung Chae, T Salzer, From single user to multiuser communications: shifting the MIMO paradigm. IEEE Signal Process. Mag. **24**, 36–46 (2007)

26. CW Tan, AR Calderbank, Multiuser detection of alamouti signals. IEEE Trans. Commun. **57**, 2080–2089 (2009), http://dl.acm.org/citation.cfm?id=1651065.1651094

27. G Auer, V Gianni, I Godor, P Skillermark, M Olsson, M Imran, M Gonzalez, C Desset, O Blume, A Fehske, How much energy is needed to run a wireless network? IEEE Wirel. Commun. **11**, 40-49 (2011)

28. C Desset, B Debaillie, V Giannini, A Fehske, G Auer, H Holtkamp, W Wajda, D Sabella, F Richter, MJ Gonzalez, H Klessig, I Godor, M Olsson, MA Imran, A Ambrosy, O Blume, Flexible power modeling of LTE base stations, in *IEEE Wireless Communications and Networking Conference (WCNC)*, Paris, France. April 2012, pp. 2858–2862

29. S Verdu, *Multiuser Detection* (Cambridge University Press, Cambridge, MA, 1998)

30. M-S Alouini, A Goldsmith, A unified approach for calculating error rates of linearly modulated signals over generalized fading channels. IEEE Trans. Commun. **47**(9), 1324–1334 (1999)

31. M Di Renzo, H Haas, Bit error probability of spatial modulation (SMï£¡) MIMO over generalized fading channels. IEEE Trans. Veh. Technol. **61**, 1124–1144 (2012)

32. MK Simon, M Alouini, *Digital Communication over Fading Channels*, 2nd edn. Wiley Series in Telecommunications and Signal Processing (John Wiley & Sons, Inc., NEw York, 2005), ISBN: 978-0-471-64953-3

33. S Verdu, Computational complexity of optimum multiuser detection. Algorithmica **4**, 303–312 (1989), doi:10.1007/BF01553893.

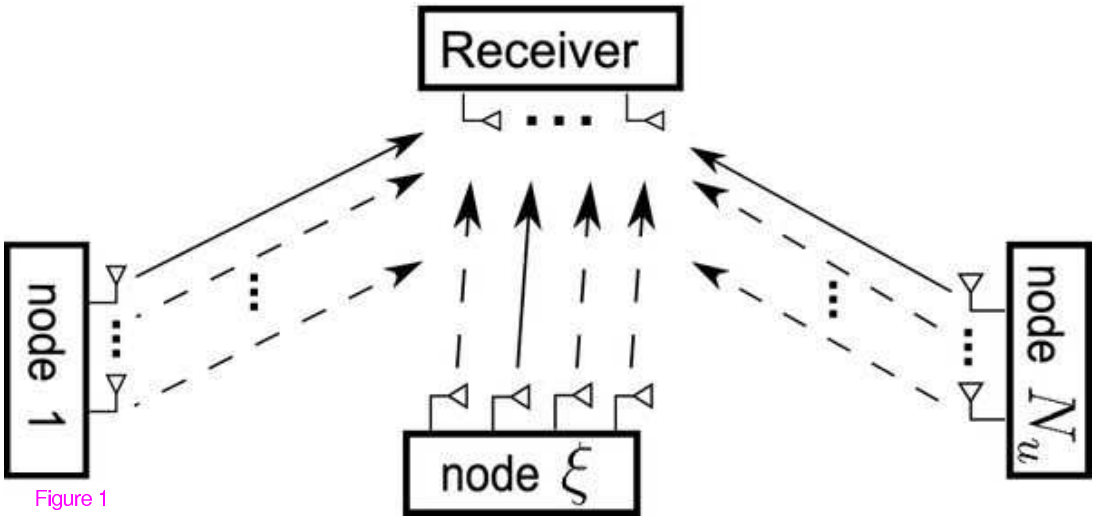

Figure 1

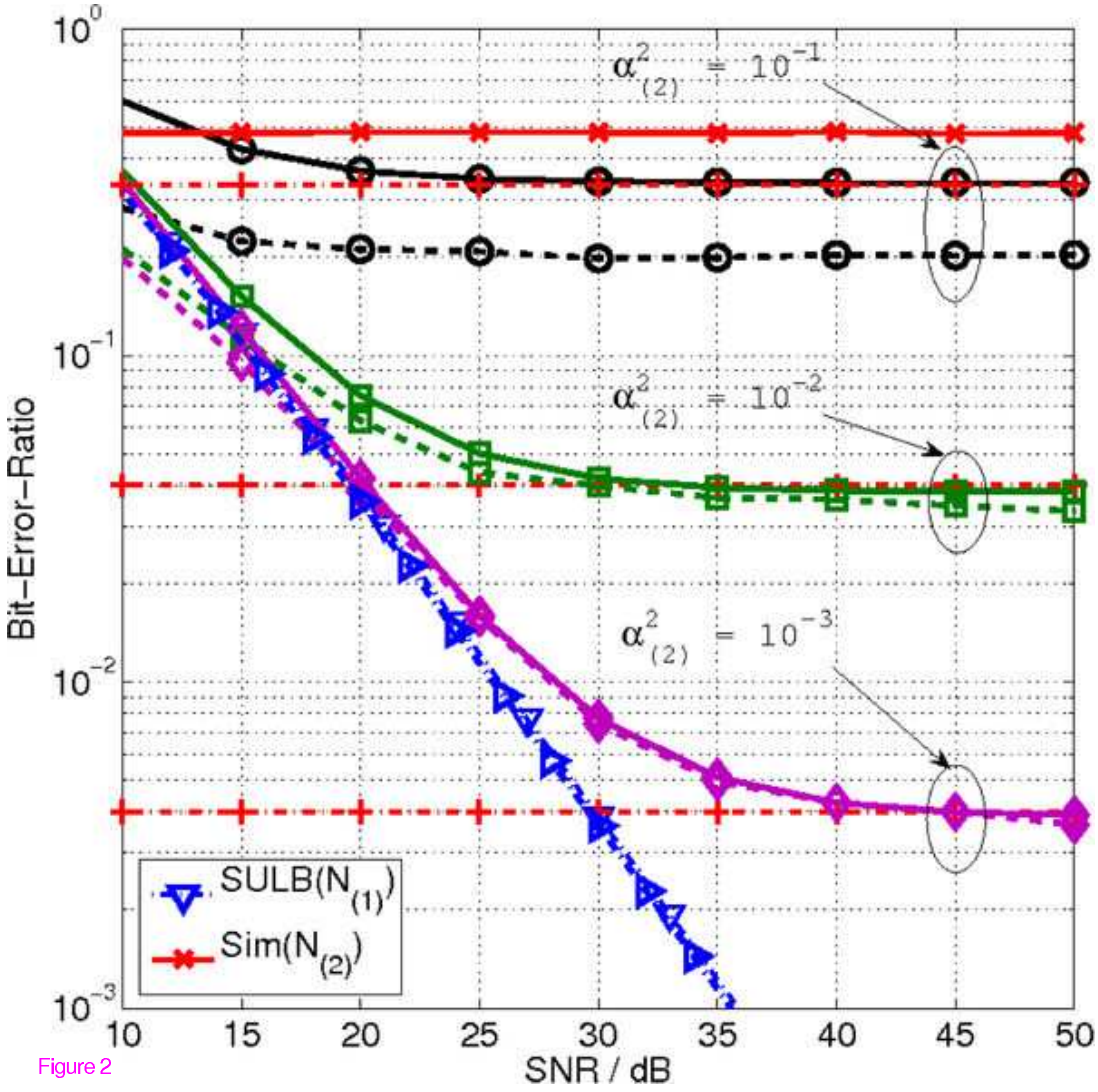
10^0
10^{-1}
10^{-2}
10^{-3}
Bit−Error−Ratio
10
15
20
25
30
35
40
45
50
SNR / dB
$\alpha^2_{(2)} = 10^{-1}$
$\alpha^2_{(2)} = 10^{-2}$
$\alpha^2_{(2)} = 10^{-3}$
SULB($N_{(1)}$)
Sim($N_{(2)}$)

Figure 2

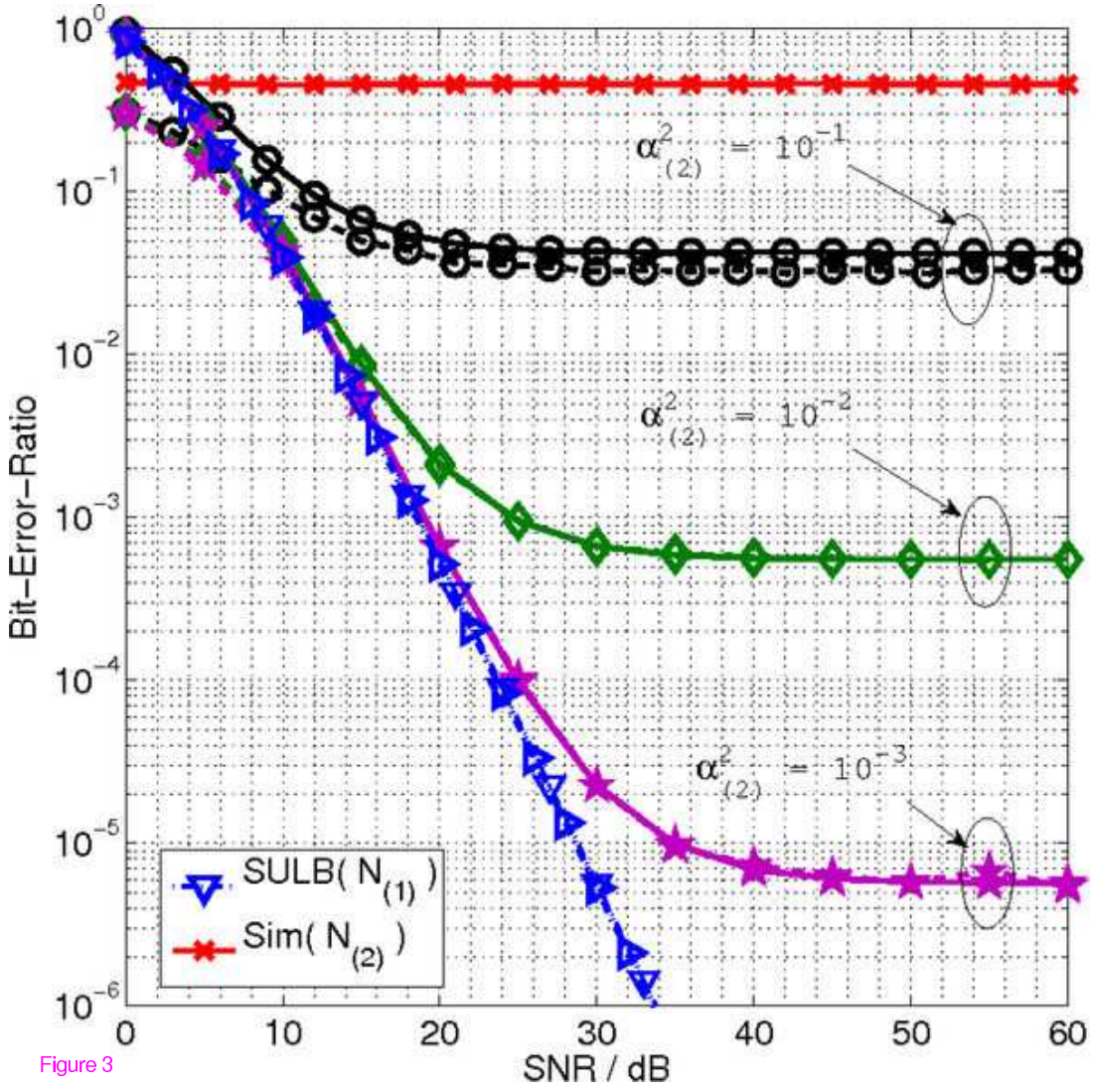
Bit–Error–Ratio
SNR / dB
$\alpha^2_{(2)} = 10^{-1}$
$\alpha^2_{(2)} = 10^{-2}$
$\alpha^2_{(2)} = 10^{-3}$
SULB($N_{(1)}$)
Sim($N_{(2)}$)

Figure 3

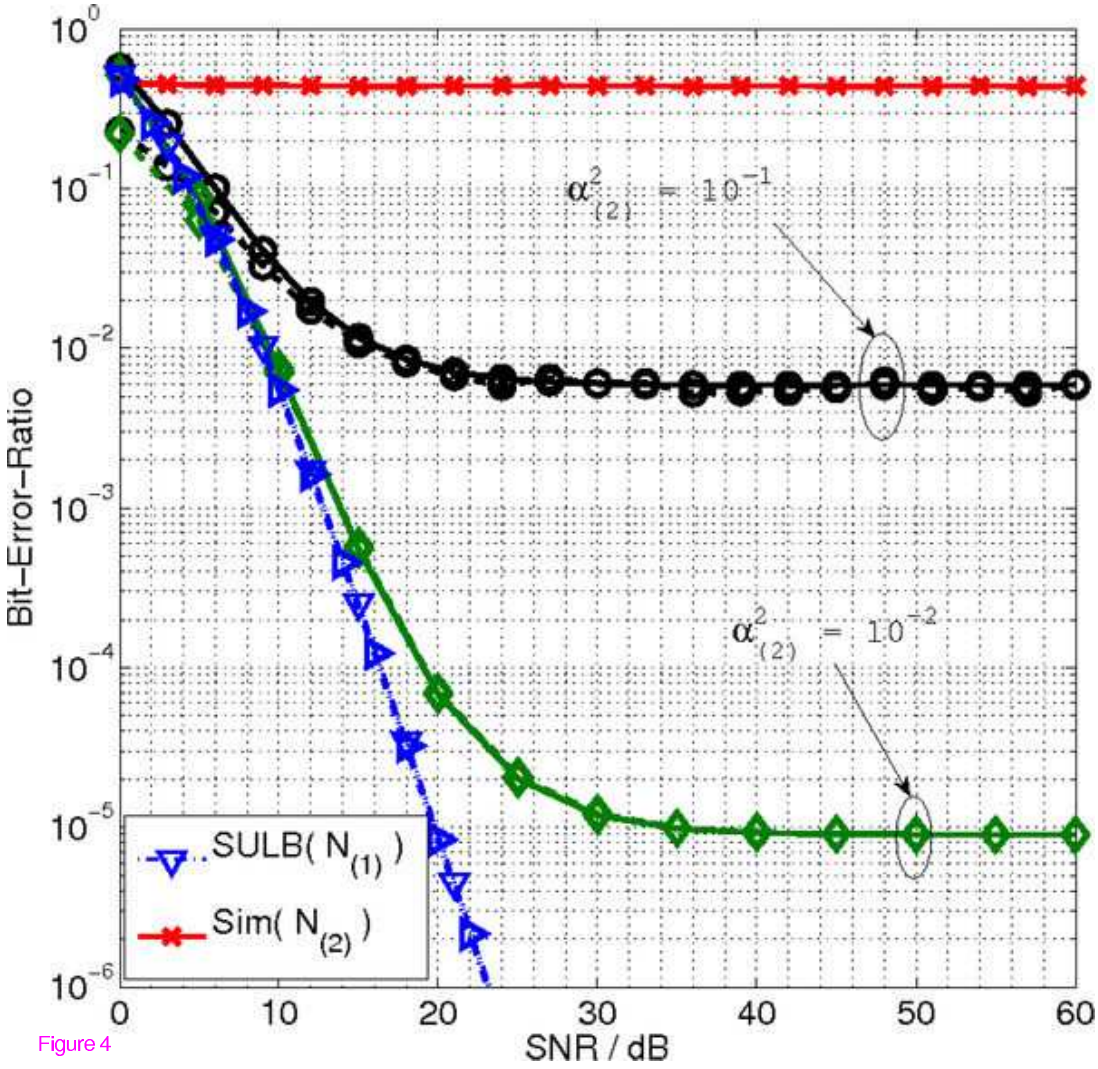
Bit–Error–Ratio
SNR / dB
$\alpha^2_{(2)} = 10^{-1}$
$\alpha^2_{(2)} = 10^{-2}$
SULB($N_{(1)}$)
Sim($N_{(2)}$)
10^0
10^{-1}
10^{-2}
10^{-3}
10^{-4}
10^{-5}
10^{-6}
0
10
20
30
40
50
60

Figure 4

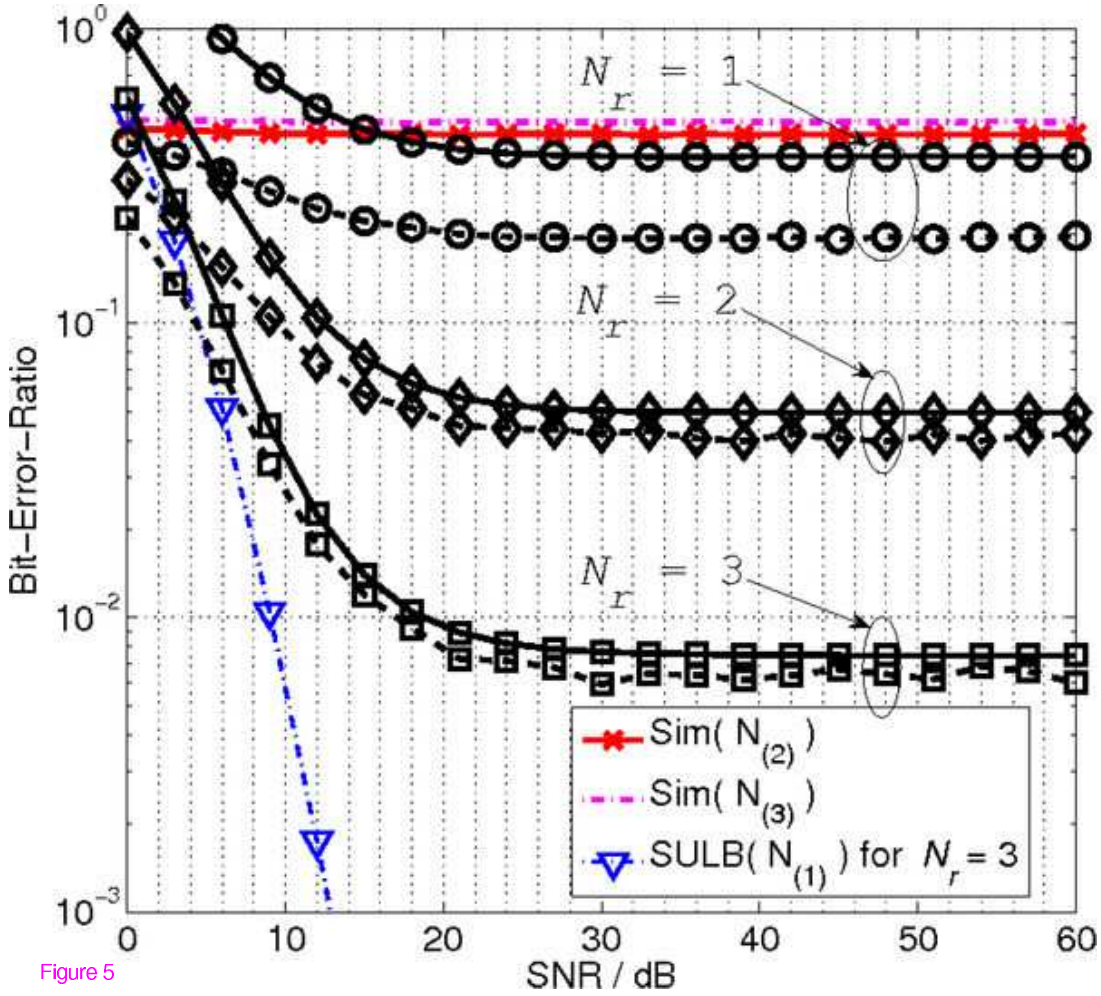

Figure 5

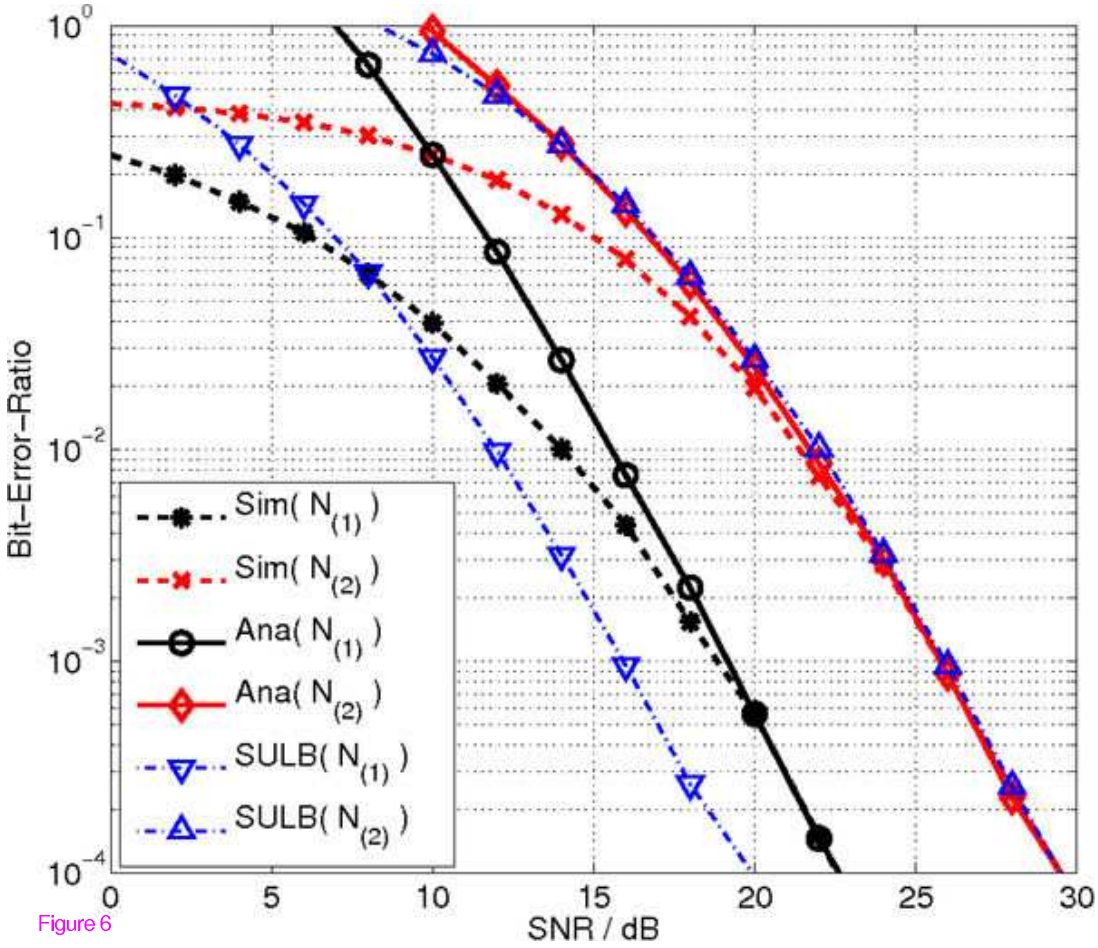
Bit–Error–Ratio
SNR / dB
Sim(N(1))
Sim(N(2))
Ana(N(1))
Ana(N(2))
SULB(N(1))
SULB(N(2))

Figure 6

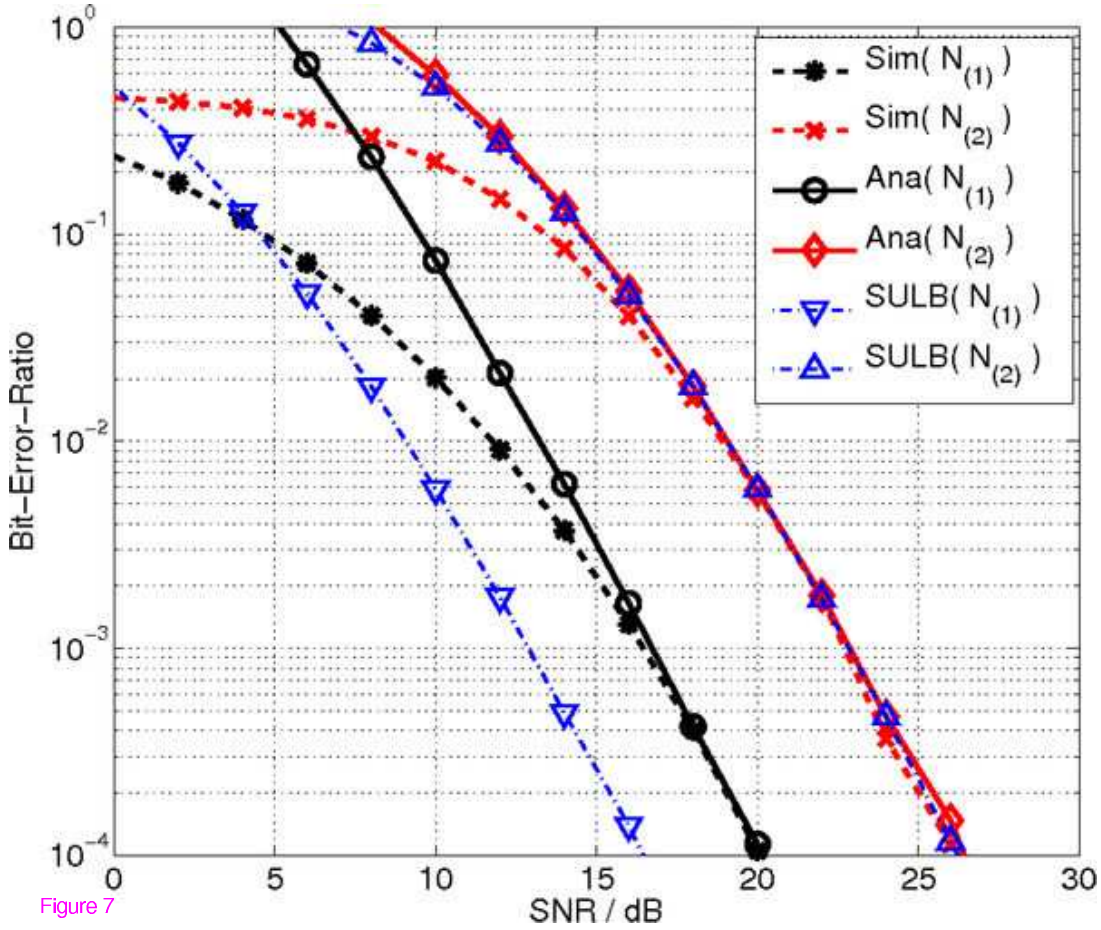
Bit−Error−Ratio
SNR / dB
Sim(N(1))
Sim(N(2))
Ana(N(1))
Ana(N(2))
SULB(N(1))
SULB(N(2))

Figure 7

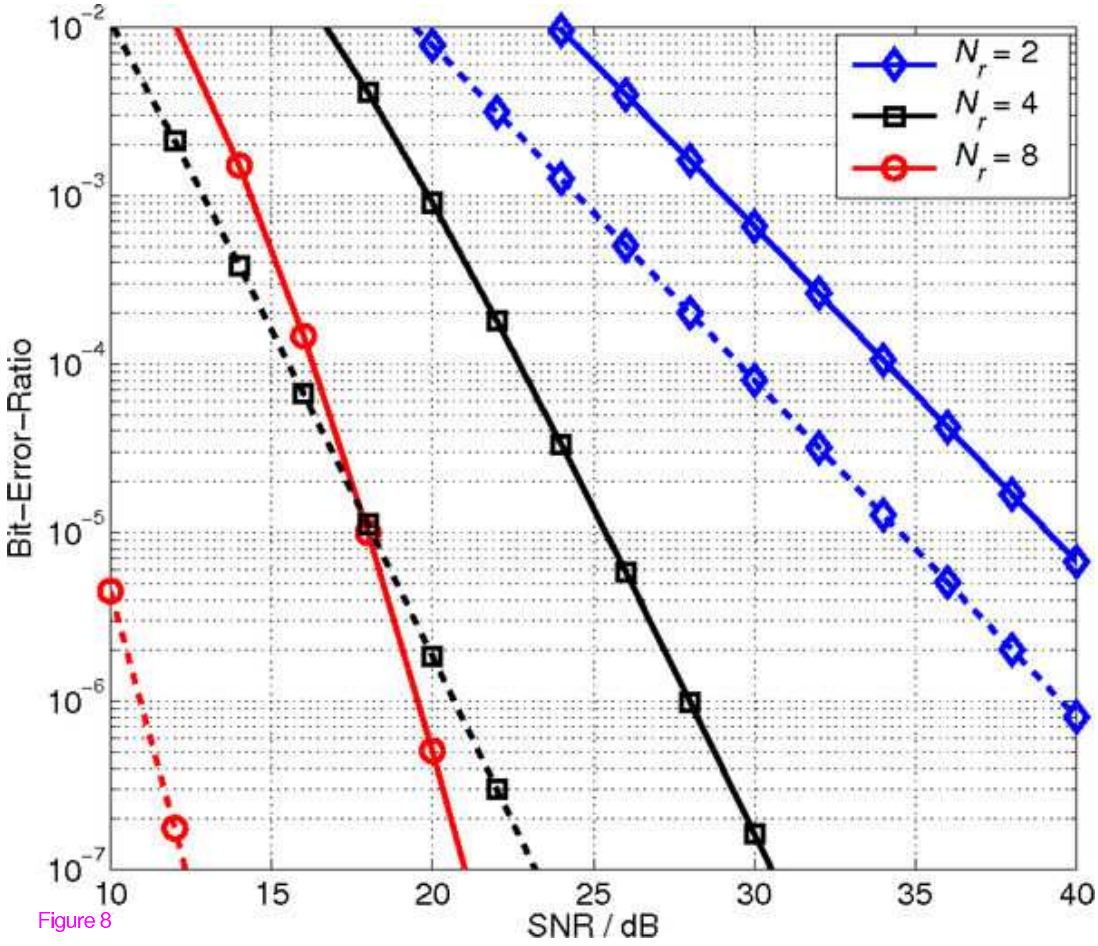
Bit–Error–Ratio
SNR / dB
$N_r = 2$
$N_r = 4$
$N_r = 8$
10^{-2}
10^{-3}
10^{-4}
10^{-5}
10^{-6}
10^{-7}
10
15
20
25
30
35
40

Figure 8

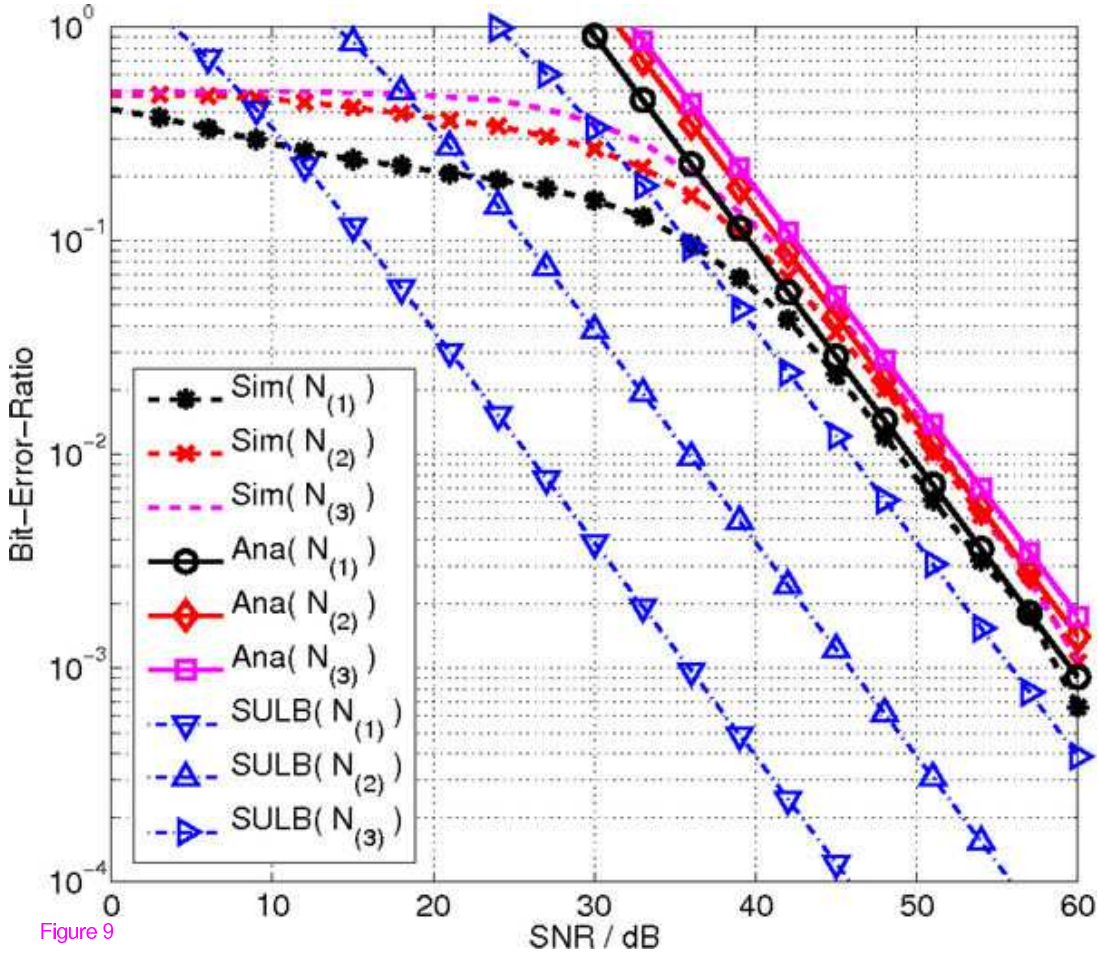
Bit−Error−Ratio
SNR / dB
Sim(N(1))
Sim(N(2))
Sim(N(3))
Ana(N(1))
Ana(N(2))
Ana(N(3))
SULB(N(1))
SULB(N(2))
SULB(N(3))

Figure 9

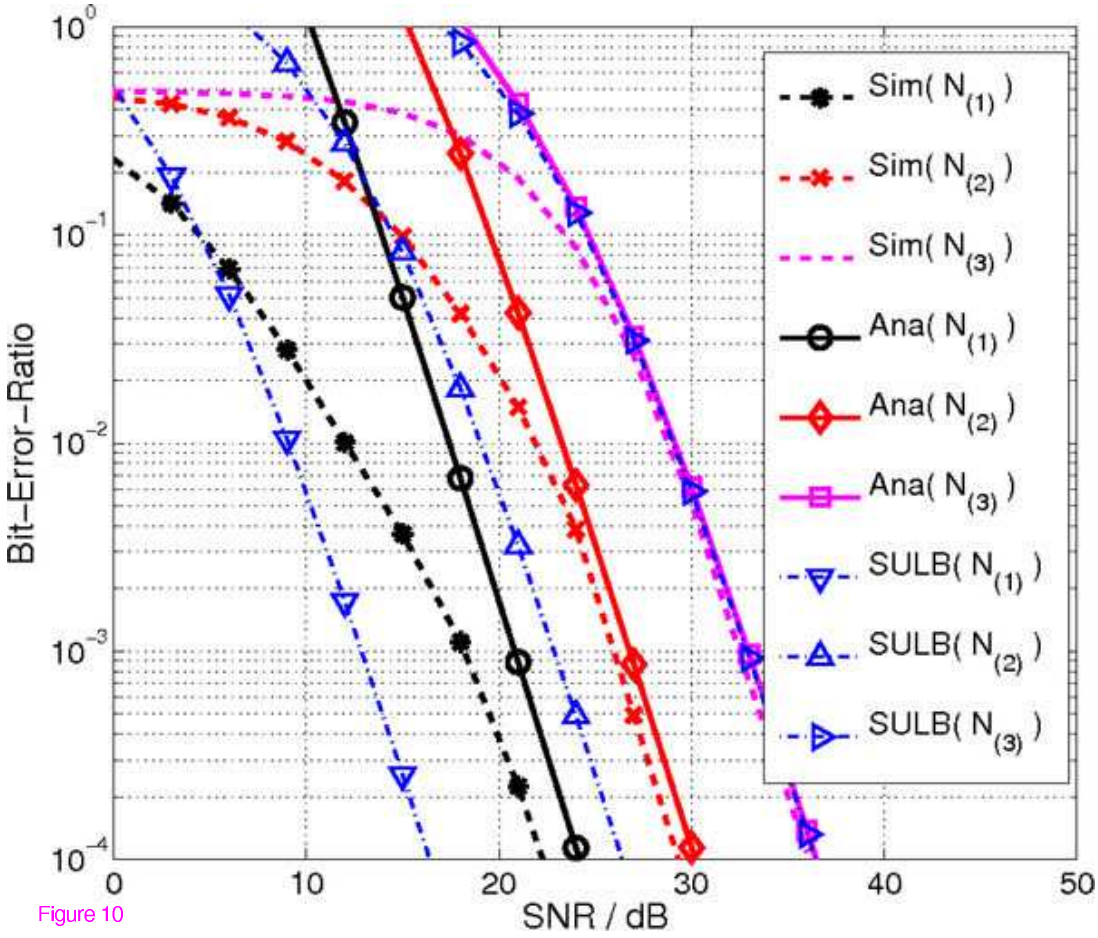
Bit–Error–Ratio
SNR / dB
Sim(N(1))
Sim(N(2))
Sim(N(3))
Ana(N(1))
Ana(N(2))
Ana(N(3))
SULB(N(1))
SULB(N(2))
SULB(N(3))

Figure 10

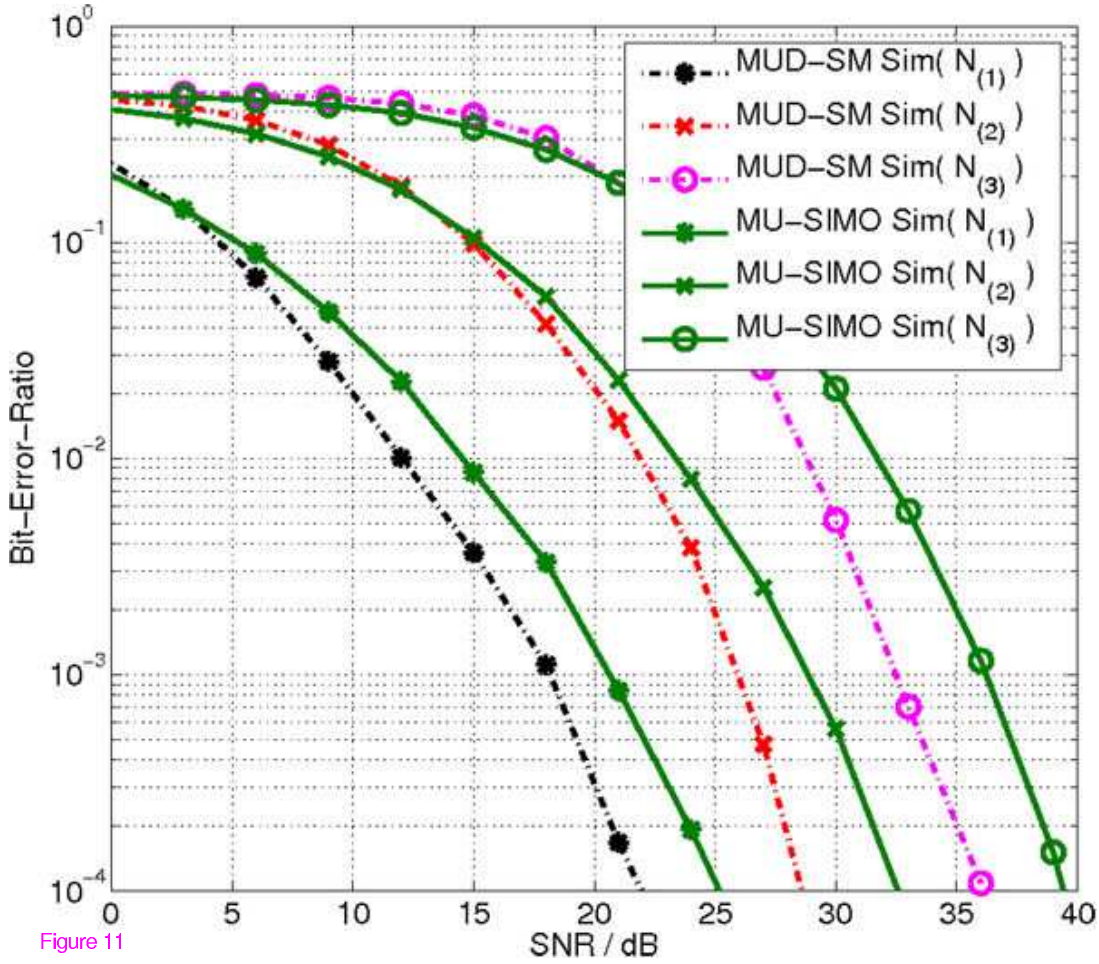
MUD–SM Sim(N(1))
MUD–SM Sim(N(2))
MUD–SM Sim(N(3))
MU–SIMO Sim(N(1))
MU–SIMO Sim(N(2))
MU–SIMO Sim(N(3))
Bit–Error–Ratio
SNR / dB
10^0
10^-1
10^-2
10^-3
10^-4
0
5
10
15
20
25
30
35
40

Figure 11

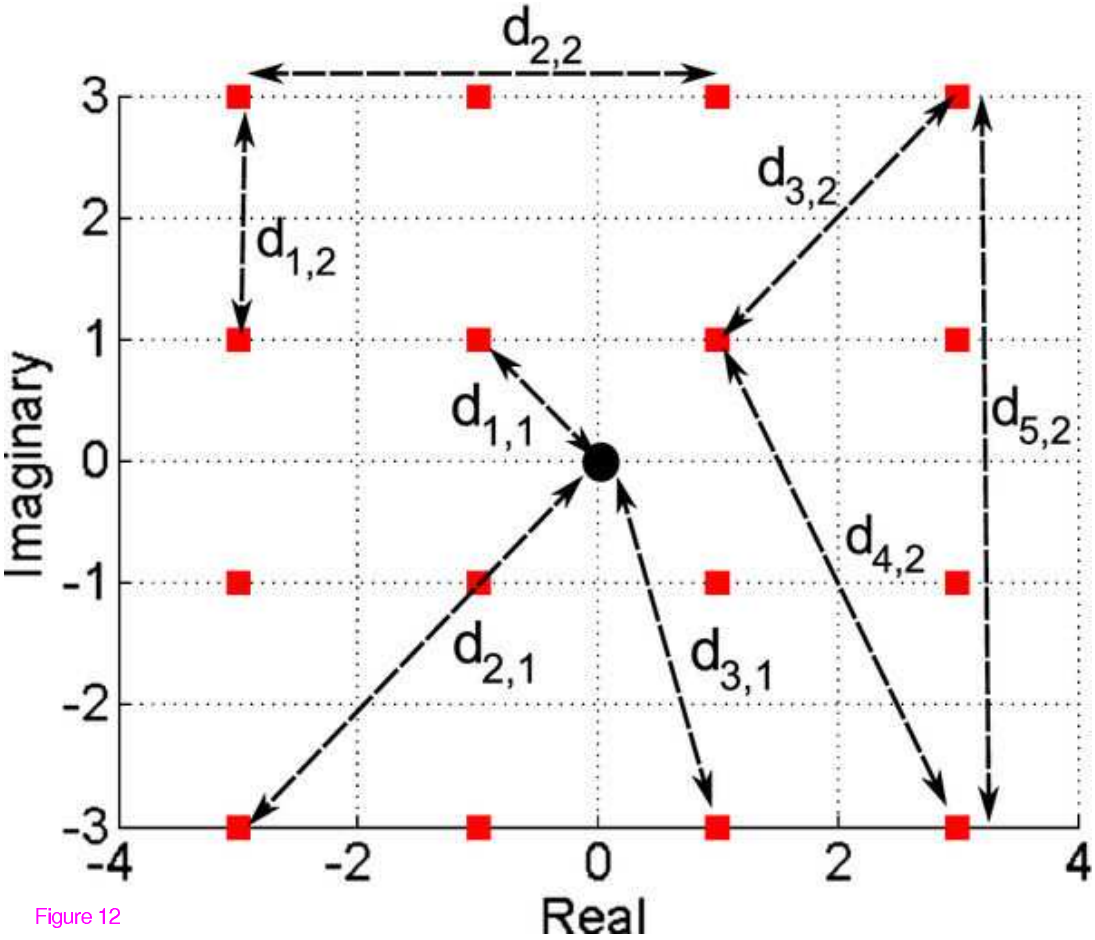

Figure 12

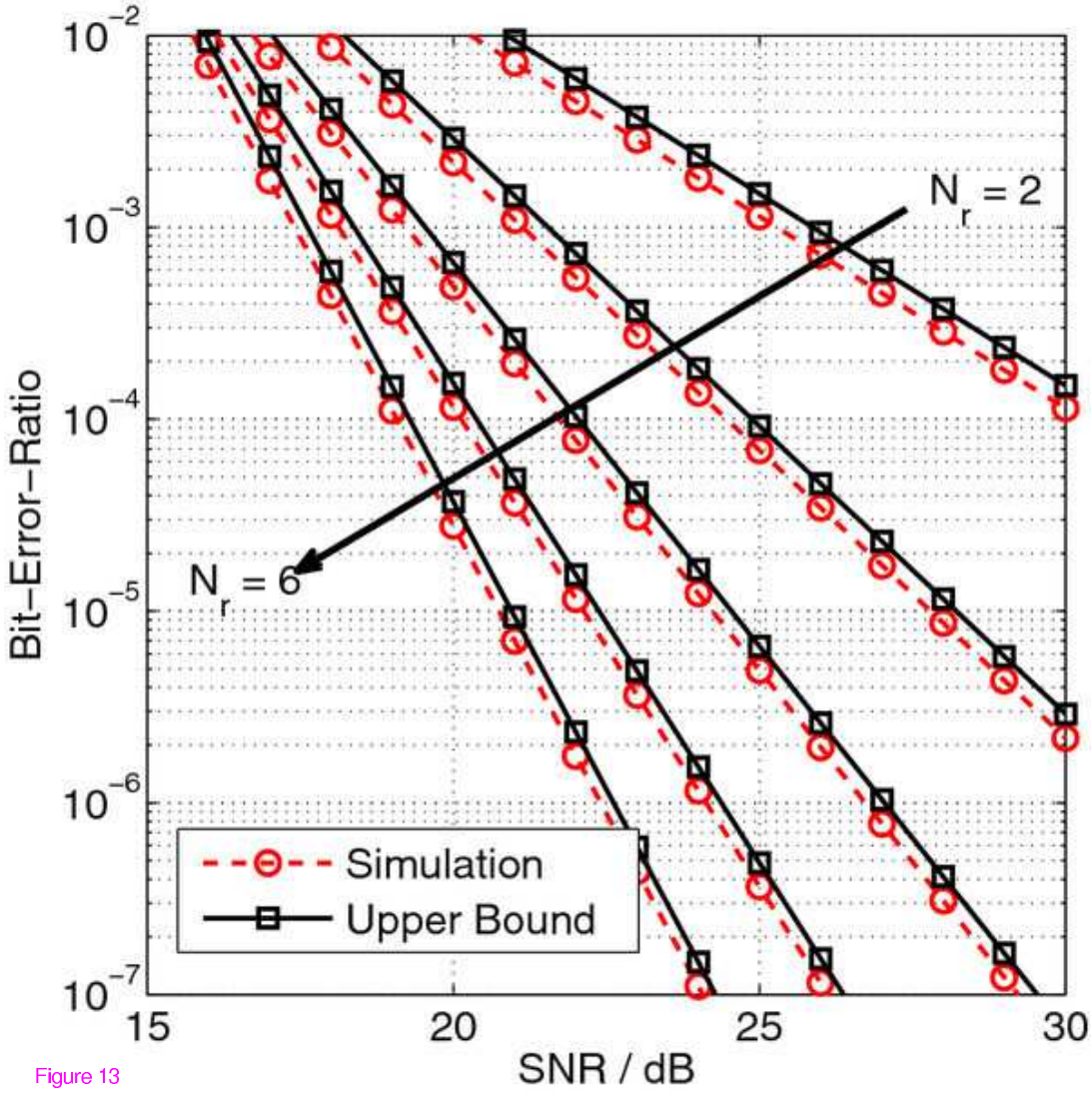
Bit−Error−Ratio
SNR / dB
10^{-2}
10^{-3}
10^{-4}
10^{-5}
10^{-6}
10^{-7}
15
20
25
30
$N_r = 2$
$N_r = 6$
Simulation
Upper Bound

Figure 13

Bibliography

[1] Cisco visual networking index. Global mobile data traffic forecast update, 2010-2015. [Online]. Available: http://www.cisco.com/en/US/solutions/collateral/ns341/ns525/ns537/ns705/ns827/white_paper_c11-520862.html

[2] C. Shannon, "A Mathematical Theory of Communication," *Bell System Technical Journal*, vol. 27, pp. 379–423 & 623–656, Jul. & Oct. 1948.

[3] OFCOM, "The Communications Market 2008," OFCOM, Tech. Rep. 4 Telecoms, August 2009. [Online]. Available: http://www.ofcom.org.uk/research/cm/cmr09/CMRMain_4.pdf

[4] ——. (2012) Spectrum Information. Independent regulator and competition authority for the UK communications industries (Ofcom). [Online]. Available: http://stakeholders.ofcom.org.uk/spectrum/spectrum-information/

[5] OFCOM, "Public Fixed Wireless Access - 3.4 GHz Auction ," 2009. [Online]. Available: http://www.ofcom.org.uk/static/archive/ra/topics/pfwa/3-4ghz/3-4-index.htm

[6] OFCOM. (2012) Spectrum Usage Rights. Independent regulator and competition authority for the UK communications industries (Ofcom). [Online]. Available: http://stakeholders.ofcom.org.uk/consultations/sur/

[7] L. Brandenburg and A. Wyner, "Capacity of the Gaussian Channel with Memory: The Multivariate Case," Bell Systems, Tech. Rep., June 1974.

[8] A. J. Paulraj and T. Kailath, USA Patent 5 345 599, 1994.

[9] G. J. Foschini, "Layered Space-Time Architecture for Wireless Communication in a Fading Environment when Using Multi-Element Antennas," *Bell Labs Technical Journal*, vol. 1, no. 2, pp. 41–59, 1996.

[10] P. Wolniansky, G. Foschini, G. Golden, and R. Valenzuela, "V-BLAST: an Architecture for Realizing very High Data Rates over the Rich-Scattering Wireless Channel," in *Unino Radio-Scientifique Internationale (URSI) Intern. Symp. on Signals, Systems, and Electronics (ISSSE)*, Sep. 29–Oct. 2, 1998, pp. 295–300.

[11] G. D. Golden, G. J. Foschini, R. A. Valenzuela, and P. W. Wolniansky, "Detection Algorithm and Initial Laboratory Results using V-BLAST SpaceTime Communication Architecture," in *Electronics Letters*, 1999.

[12] G. Auer, V. Gianni, I. Godor, P. Skillermark, M. Olsson, M. Imran, M. Gonzalez, C. Desset, O. Blume, and A. Fehske, "How Much Energy is Needed to Run a Wireless Network?" *IEEE Wireless Communications*, Oct. 2011.

[13] C. Desset, B. Debaillie, V. Giannini, A. Fehske, G. Auer, H. Holtkamp, W. Wajda, D. Sabella, F. Richter, M. J. Gonzalez, H. Klessig, I. Godor, M. Olsson, M. A. Imran, A. Ambrosy, and O. Blume, "Flexible Power Modeling of LTE Base Stations," in *IEEE Wireless Communications and Networking Conference (WCNC)*, Apr. 2012, pp. 2858 –2862.

[14] H. Haas, E. Costa, and E. Schulz, "Increasing Spectral Efficiency by Data Multiplexing using Antenna Arrays," in *Proc. of the 13th IEEE International Symposium on Personal, Indoor and Mobile Radio Communications (PIMRC)*, vol. 2, Sep. 2002, pp. 610–613.

[15] R. Mesleh, H. Haas, S. Sinanović, C. W. Ahn, and S. Yun, "Spatial Modulation," *IEEE Transactions on Vehicular Technology*, vol. 57, no. 4, pp. 2228 – 2241, Jul. 2008.

[16] A. Younis, M. Di Renzo, R. Mesleh, and H. Haas, "Sphere Decoding for Spatial Modulation," in *Proc. of IEEE International Conference on Communications (ICC 2011)*, Kyoto, Japan, 5–9 Jun. 2011, pp. 1 –6.

[17] M. Di Renzo and H. Haas, "Spatial Modulation with Partial-CSI at the Receiver: Optimal Detector and Performance Evaluation," in *IEEE Sarnoff Symposium*, april 2010, pp. 1 –6.

[18] ——, "Bit Error Probability of Space Modulation over Nakagami-m Fading: Asymptotic Analysis," *IEEE Communications Letters*, vol. 15, no. 10, pp. 1026 –1028, Oct. 2011.

[19] The Franklin Institute. The Case Files: Nikola Tesla. [Online]. Available: http://www.fi.edu/learn/case-files/tesla/

[20] G. Marconi, "Improvements in Transmitting Electrical impulses and Signals, and in Apparatus therefor," British Patent 12 039, Mar., 1897.

[21] C. Shannon, "Communication in the Presence of Noise," in *Proc. of the IRE*, vol. 37, no. 1, Jan. 1949, pp. 10–21.

[22] D. H. Ring, "Mobile Telephony - Wide Area Coverage," Bell Telephone Laboratories, Tech. Rep. 20564, Dec. 1947.

[23] A. E. Joel, "Mobile Communication System," USA Patent 3 663 762, May, 1972.

[24] S. Sesia, I. Toufik, and M. Baker, *LTE - The UMTS Long Term Evolution: From Theory to Practice*, 1st ed., S. Sesia, I. Toufik, and M. Baker, Eds. Wiley, 2009.

[25] A. J. Viterbi and R. Padovani, "Implications of Mobile Cellular CDMA," *IEEE Communications Magazine*, vol. 30, no. 12, pp. 38–41, Dec. 1992.

[26] J. D. Gibson, *The Mobile Communications Handbook*, J. D. Gibson, Ed. Springer/IEEE Press/CRC Press, Jun. 1996.

[27] R. Kohno, "Spatial and Temporal Filtering for Co-channel Interference in CDMA," in *Proc. of the International Symposium on Spread Spectrum Techniques and Applications (ISSSTA)*, vol. 1. Oulu, Finland: IEEE, Jul. 4–6, 1994, pp. 51–60.

[28] ——, "Spatial and temporal communication theory using adaptive antenna array," *IEEE Personal Communications [see also IEEE Wireless Communications]*, vol. 5, no. 1, pp. 28–35, Feb. 1998.

[29] A. S. Macedo and E. S. Sousa, "Antenna-Sector Time-Division Multiple Access for Broadband Indoor Wireless Systems," *IEEE Journal on Selected Areas in Communications*, vol. 16, no. 6, pp. 937–952, Aug. 1998.

[30] D. Astely, E. Dahlman, A. Furuskar, Y. Jading, M. Lindstrom, and S. Parkvall, "LTE: The Evolution of Mobile Broadband," *IEEE Communications Magazine*, vol. 47, no. 4, pp. 44–51, 2009.

[31] Motorola Inc., "Driving 4G: WiMAX & LTE," Motorola Inc., positioning paper, Retrieved Feb. 19, 2009, from http://www.motorola.com, 2007.

[32] BROADCOM Corporation, "802.11n: Next-Generation Wireless LAN Technology," White paper, BROADCOM Corporation, Tech. Rep., Apr. 2006, retrieved Aug. 4, 2006 http://www.broadcom.com/docs/WLAN/802-11n-WP100-R.pdf.

[33] R. B. Ertel, P. Cardieri, K. W. Sowerby, T. S. Rappaport, and J. H. Reed, "Overview of Spatial Channel Models for Antenna Array Communication Systems," *IEEE Personal Communications [see also IEEE Wireless Communications]*, vol. 5, no. 1, pp. 10–22, Feb. 1998.

[34] D. Gesbert, H. Bolcskei, D. Gore, and A. Paulraj, "Outdoor MIMO Wireless Channels: Models and Performance Prediction," *IEEE Transactions on Communications*, vol. 50, no. 12, pp. 1926–1934, Dec. 2002.

[35] T. S. Rappaport, *Wireless Communications: Principles and Practice*, 2nd ed. Prentice Hall PTR, 2002.

[36] D. P. McNamara, "Characterisation and Investigation of Multiple-Input-Multiple-Output Wireless Communication Channels," Ph.D. dissertation, University of Bristol, 2003.

[37] J. Mietzner, R. Schober, L. Lampe, W. H. Gerstacker, and P. A. Hoeher, "Multiple-Antenna Techniques for Wireless Communications - A Comprehensive Literature Survey," *IEEE Communications Surveys Tutorials*, vol. 11, no. 2, pp. 87 –105, 2009.

[38] V. Tarokh, H. Jafarkhani, and A. R. Calderbank, "Space-Time Block Coding for Wireless Communications: Performance Results," *IEEE Journal on Selected Areas in Communications*, vol. 17, no. 3, pp. 451–460, Mar. 1999.

[39] H. El Gamal, "On the Robustness of Space-Time Coding," *IEEE Transactions on Signal Processing*, vol. 50, no. 10, pp. 2417–2428, Oct. 2002.

[40] H. Jafarkhani, *Space-Time Coding: Theory and Practice*. Cambridge University Press, 2005.

[41] S. M. Alamouti, "A Simple Transmit Diversity Technique for Wireless Communications," *IEEE Journal on Selected Areas in Communications*, vol. 16, no. 8, pp. 1451–1458, Oct. 1998.

[42] R. Mesleh, "Spatial Modulation: A Spatial Multiplexing Technique for Efficient Wireless Data Transmission," Ph.D. dissertation, Jacobs University, Bremen, Germany, Jun. 2007.

[43] G. H. Golub and C. F. van Loan, *Matrix Computations*. The John Hopkins University Press, 1996.

[44] M. Bazdresch, J. Cortez, and D. Torres, "Bit-Error Rate Evaluation of V-BLAST Receivers Using Limited-Precision QR Decomposition," in *Proc. 3rd International Conference on Electrical and Electronics Engineering*, 2006, pp. 1–4.

[45] Agilent Technologies, "E4438C-419 Signal Studio for 3GPP W-CDMA HSPA Online Documentation." [Online]. Available: http://wireless.agilent.com/wireless/helpfiles/opt419/opt419.htm

[46] S. Catreux, P. Driessen, and L. Greenstein, "Simulation Results for an Interference-Limited Multiple-Input Multiple-Output Cellular System," *IEEE Communications Letters*, vol. 4, no. 11, pp. 334–336, Nov. 2000.

[47] M. Chiani, M. Win, and A. Zanella, "On the Capacity of Spatially Correlated MIMO Rayleigh-Fading Channels," *IEEE Transactions on Information Theory*, vol. 49, no. 10, pp. 2363–2371, Oct. 2003.

[48] I. Ku, C.-X. Wang, J. Thompson, and P. Grant, "Impact of Receiver Interference Cancellation Techniques on the Base Station Power Consumption in MIMO Systems with Inter-Cell Interference," in *IEEE International Symposium on Personal Indoor and Mobile Radio Communications (PIMRC)*, Sep. 2011, pp. 1798 –1802.

[49] Y. Yang and B. Jiao, "Information-Guided Channel-Hopping for High Data Rate Wireless Communication," *IEEE Communications Letters*, vol. 12, no. 4, pp. 225 –227, Apr. 2008.

[50] Y. A. Chau and S.-H. Yu, "Space Modulation on Wireless Fading Channels," in *IEEE Vehicular Technology Conference (VTC Fall 2001)*, vol. 3, 7–11 Oct. 2001, pp. 1668–1671.

[51] S. Ganesan, R. Mesleh, H. Haas, C. W. Ahn, and S. Yun, "On the Performance of Spatial Modulation OFDM," in *Asilomar Conference on Signals, Systems, and Computers*, Pacific Grove, CA, USA, 29 Oct. - 1 Nov. 2006, pp. 1825–1829.

[52] J. Jeganathan, A. Ghrayeb, and L. Szczecinski, "Spatial Modulation: Optimal Detection and Performance Analysis," *IEEE Communications Letters*, vol. 12, no. 8, pp. 545–547, 2008.

[53] M. D. Renzo and H. Haas, "Performance analysis of Spatial Modulation," in *International ICST Conference on Communications and Networking in China (CHINACOM),*, Aug. 2010, pp. 1 –7.

[54] E. Basar, U. Aygolu, E. Panayirci, and H. V. Poor, "Performance of Spatial Modulation in the Presence of Channel Estimation Errors," *IEEE Communications Letters*, vol. 16, no. 2, pp. 176 –179, Feb. 2012.

[55] M. D. Renzo and H. Haas, "Bit Error Probability of SM-MIMO Over Generalized Fading Channels," *IEEE Transactions on Vehicular Technology*, vol. 61, no. 3, pp. 1124 –1144, Mar. 2012.

[56] R. Mesleh, I. Stefan, H. Haas, and P. Grant, "On the Performance of Trellis Coded Spatial Modulation," in *ITG International Workshop on Smart Antennas (WSA'09)*, Berlin, Germany, Feb. 16–19 2009. [Online]. Available: http://www.mk.tu-berlin.de/wsa2009/

[57] R. Mesleh, M. Di Renzo, H. Haas, and P. M. Grant, "Trellis Coded Spatial Modulation," *IEEE Transactions on Wireless Communications*, vol. 9, no. 7, pp. 2349–2361, Jul. 2010.

[58] E. Basar, U. Aygolu, E. Panayirci, and H. V. Poor, "New Trellis Code Design for Spatial Modulation," *IEEE Transactions on Wireless Communications*, vol. 10, pp. 2670 – 2680, Aug. 2011.

[59] A. Younis, R. Mesleh, H. Haas, and P. M. Grant, "Reduced Complexity Sphere Decoder for Spatial Modulation Detection Receivers," in *2010 IEEE Global Telecommunications Conference (GLOBECOM 2010)*, Dec. 2010, pp. 1 –5.

[60] R. Mesleh, S. Gansean, and H. Haas, "Impact of Channel Imperfections on Spatial Modulation OFDM," in *IEEE 18th International Symposium on Personal, Indoor and Mobile Radio Communications (PIMRC)*, Athens, Greece, Mar. 2007, pp. 1–5.

[61] S. U. Hwang, S. Jeon, S. Lee, and J. Seo, "Soft-Output ML Detector for Spatial Modulation OFDM Systems," *IEICE Electronics Express*, vol. 6, no. 19, pp. 1426–1431, Oct. 2009.

[62] J. Jeganathan, A. Ghrayeb, and L. Szczecinski, "Generalized Space Shift Keying Modulation for MIMO Channels," in *Proc. IEEE 19th International Symposium on Personal, Indoor and Mobile Radio Communications PIMRC 2008*, Cannes, France, 15–18 Sep. 2008, pp. 1–5.

[63] J. Jeganathan, A. Ghrayeb, L. Szczecinski, and A. Ceron, "Space Shift Keying Modulation for MIMO Channels," *IEEE Transaction on Wireless Communications*, vol. 8, no. 7, pp. 3692–3703, Jul. 2009.

[64] M. Di Renzo and H. Haas, "Space Shift Keying (SSK) Modulation with Partial Channel State Information: Optimal Detector and Performance Analysis over Fading Channels," *IEEE Transactions on Communications*, vol. 58, no. 11, pp. 3196 –3210, Nov. 2010.

[65] M. Di Renzo, D. De Leonardis, F. Graziosi, and H. Haas, "On the Performance of Space Shift Keying (SSK) Modulation with Imperfect Channel Knowledge," in *IEEE Proc. of the Global Telecommunications Conference (GLOBECOM)*, Houston, Texas, USA, Dec. 5–9, 2011, pp. 1–6.

[66] M. Di Renzo and H. Haas, "A General Framework for Performance Analysis of Space Shift Keying (SSK) Modulation for MISO Correlated Nakagami-m Fading Channels," *IEEE Transactions on Communications*, vol. 58, no. 9, pp. 2590 –2603, Sep. 2010.

[67] S. Sinanović, N. Serafimovski, M. D. Renzo, and H. Haas, "Secrecy Capacity of Space Keying with Two Antennas," in *IEEE Proc. of the Vehicular Technology Conference (VTC)*, Québec City, Canada, Sep. 3–6, 2012, pp. 1–5, (to appear).

[68] M. Di Renzo and H. Haas, "Improving the Performance of Space Shift Keying (SSK) Modulation via Opportunistic Power Allocation," *IEEE Communications Letters*, vol. 14, no. 6, pp. 500 –502, 2010.

[69] M. Di Renzo and H. Haas, "Performance Comparison of Different Spatial Modulation Schemes in Correlated Fading Channels," in *IEEE International Conference on Communications (ICC)*, May 2010.

[70] M. D. Renzo, D. D. Leonardis, F. Graziosi, and H. Haas, "Space Shift Keying (SSK) MIMO with Practical Channel Estimates," *IEEE Transactions on Communications*, vol. 60, no. 4, pp. 998 –1012, Apr. 2012.

[71] S. Sugiura, S. Chen, and L. Hanzo, "A Unified MIMO Architecture Subsuming Space Shift Keying, OSTBC, BLAST and LDC," in *IEEE Vehicular Technology Conference Fall (VTC 2010-Fall)*, Sept. 2010, pp. 1 –5.

[72] ——, "Generalized Space-Time Shift Keying Designed for Flexible Diversity-, Multiplexing- and Complexity-Tradeoffs," *IEEE Transactions on Wireless Communications*, vol. 10, no. 4, pp. 1144 –1153, Apr. 2011.

[73] D. Yang, C. Xu, L.-L. Yang, and L. Hanzo, "Transmit-Diversity-Assisted Space-Shift Keying for Colocated and Distributed/Cooperative MIMO Elements," *IEEE Transactions on Vehicular Technology*, vol. 60, no. 6, pp. 2864 –2869, Jul. 2011.

[74] R. Mesleh, R. Mehmood, H. Elgala, and H. Haas, "Indoor MIMO Optical Wireless Communication Using Spatial Modulation," in *IEEE International Conference on Communications (ICC)*, Cape Town, South Africa, May 22–27 2010, pp. 1–5.

[75] T. Fath, H. Haas, Marco Di Renzo, and R. Mesleh, "Spatial Modulation Applied to Optical Wireless Communications in Indoor LOS Environments," in *IEEE Proc. of the Global Communications Conference (GLOBECOM)*, Houston, Texas, USA, 5–9 Dec. 2011, pp. 1–5, 5 pages.

[76] R. Mesleh, H. Elgala, and H. Haas, "Optical Spatial Modulation," *IEEE/OSA Journal of Optical Communications and Networking*, vol. 3, no. 3, pp. 234–244, Mar. 2011, ISSN: 1943-0620.

[77] T. Fath, J. Klaue, and H. Haas, "Coded Spatial Modulation applied to Optical Wireless Communications in Indoor Environments," in *IEEE Proc. of the Wireless Communications and Networking Conference (WCNC)*. Paris, France: IEEE, Apr. 1–4 2012, pp. 1000 – 1004.

[78] E. Poves, W. Popoola, H. Haas, J. Thompson, and D. Cárdenas, "Experimental results on the performance of Optical Spatial Modulation," in *Proc. of the IEEE Vehicular Technology Conference (IEEE VTC Fall)*. Quebec City, Canada: IEEE, Sep. 3–6 2012.

[79] M. Di Renzo, H. Haas, and P. M. Grant, "Spatial Modulation for Multiple-Antenna Wireless Systems: A Survey," *IEEE Communications Magazine*, vol. 49, no. 11, pp. 182–191, Nov. 2011.

[80] J. N. Laneman, D. N. C. Tse, and G. W. Wornell, "Cooperative Diversity in Wireless Networks: Efficient Protocols and Outage Behavior," *IEEE Transactions on Information Theory*, vol. 50, no. 12, pp. 3062–3080, Dec. 2004.

[81] M. O. Hasna and M.-S. Alouini, "End-to-end Performance of Transmission Systems with Relays over Rayleigh-fading Channels," *IEEE Transactions on Wireless Communications*, vol. 2, no. 6, pp. 1126 – 1131, Nov. 2003.

[82] W. L. Betts and K. D. Ko, "Fractional Bit Rate Encoding in a Pulse Amplitude Modulation Communication System," Jan. 2006.

[83] W. L. Betts, "Modulus Converter for Fractional Rate Encoding," 1992.

[84] B. Masnick and J. Wolf, "On Linear Unequal Error Protection Codes," *IEEE Transactions on Information Theory*, vol. 13, no. 4, pp. 600 –607, Oct. 1967.

[85] S. Borade, B. Nakiboglu, and L. Zheng, "Some Fundamental Limits of Unequal Error Protection," in *IEEE International Symposium on Information Theory*, Jul. 2008, pp. 2222 –2226.

[86] A. W. Paeth, Ed., *Graphics Gems V*. 24-28 Oval Road, London NW1 7DX, United Kingdom: Academic Press, 1995.

[87] M. I. Irshid and I. S. Salous, "Bit Error Probability for Coherent M-ary PSK systems," *IEEE Transactions on Communications*, vol. 39, no. 3, pp. 349 –352, Mar. 1991.

[88] S. Haykin, *Communication Systems*, 4th ed. Wiley,, 2000.

[89] T. Handte, A. Muller, and J. Speidel, "BER Analysis and Optimization of Generalized Spatial Modulation in Correlated Fading Channels," in *Vehicular Technology Conference Fall (VTC Fall-2009)*, Sep. 2009, pp. 1 –5.

[90] J. P. Kermoal, L. Schumacher, K. I. Pedersen, P. E. Mogensen, and F. Frederiksen, "A Stochastic MIMO Radio Channel Model with Experimental Validation," *IEEE Journal on Selected Areas in Communications*, vol. 20, no. 6, pp. 1211 – 1226, Aug. 2002.

[91] A. Forenza, D. Love, and R. Heath Jr., "A Low Complexity Algorithm to Simulate the Spatial Covariance Matrix for Clustered MIMO Channel Models," in *IEEE Vehicular Technology Conference (VTC Fall 2004)*, vol. 2, Los Angeles, CA, USA, 17-19 May 2004, pp. 889–893.

[92] A. V. Zelst and J. S. Hammerschmidt, "A Single Coefficient Spatial Correlation Model for Multiple-Input Multiple-Output (MIMO) Radio Channels," in *27th General Assembly of the International Union of Radio Science (URSI)*, 2002, pp. 1–4.

[93] V. Erceg et al., *TGn Channel Models*, IEEE P802.11 Wireless LANs, IEEE Std. IEEE 802.11-03/940r4, May 10, 2004. Retrieved Jan. 12, 2007 from http://www.nari.ee.ethz.ch/ dsbaum/11-03-0940-04-000n-tgn-channel-models.pdf.

[94] 3rd Generation Partnership Project (3GPP), Technical Specification Group Radio Access Network, *Spatial Channel Model for Multiple-Input Multiple Output (MIMO) simulations (Release 6)*, 3GPP TR 25.996 V 6.1.0(2003-09), 3GPP Std., 2003. Retrieved Sep. 1, 2006 from www.3gpp.org/specs/.

[95] P. D. Teal, T. D. Abhayapala, and R. A. Kennedy, "Spatial Correlation for General Distributions of Scatterers," *IEEE Signal Processing Letters*, vol. 9, no. 10, pp. 305 –308, Oct. 2002.

[96] F. Quitin, C. Oestges, F. Horlin, and P. D. Doncker, "Multipolarized MIMO Channel Characteristics: Analytical Study and Experimental Results," *IEEE Transactions on Antennas and Propagation*, vol. 57, no. 9, pp. 2739 –2745, 2009.

[97] Y. Yang and S. Aissa, "Bit-Padding Information Guided Channel Hopping," *IEEE Communications Letters*, vol. 15, no. 2, pp. 163 –165, Feb. 2011.

[98] A. Younis, N. Serafimovski, R. Mesleh, and H. Haas, "Generalized Spatial Modulation," in *Asilomar Conference on Signals, Systems, and Computers*, Pacific Grove, CA, USA, Nov. 2010.

[99] E. Basar, U. Aygolu, E. Panayirci, and V. H. Poor, "Space-Time Block Coded Spatial Modulation," *IEEE Transactions on Communications*, vol. 59, no. 3, pp. 823 –832, Mar. 2011.

[100] J. Wang, S. Jia, and J. Song, "Signal Vector Based Detection Scheme for Spatial Modulation," *IEEE Communications Letters*, vol. 16, no. 1, pp. 19 –21, Jan. 2012.

[101] D. Tse and P. Viswanath, *Fundamentals of Wireless Communication*. Cambridge University Press, 2005.

[102] D. Wilcox, E. Tsakalaki, A. Kortun, T. Ratnarajah, C. B. Papadias, and M. Sellathurai, "On Spatial Domain Cognitive Radio Using Single-Radio Parasitic Antenna Arrays," in *IEEE Journal on Selected Areas in Communications*, vol. 31, no. 3, March 2013, pp. 571 – 580.

[103] M. Di Renzo and H. Haas, "On the Performance of SSK Modulation over Multiple-Access Rayleigh Fading Channels," in *IEEE Global Telecommunications Conference (GLOBECOM)*, Dec. 2010, pp. 1 –6.

[104] ——, "Bit Error Probability of Space-Shift Keying MIMO Over Multiple-Access Independent Fading Channels," *IEEE Transactions on Vehicular Technology*, vol. 60, no. 8, pp. 3694 –3711, Oct. 2011.

[105] J. Duplicy, B. Badic, R. Balraj, R. Ghaffar, P. Horvth, F. K. R. Knopp, I. Z. Kovacs, H. T. Nguyen, D. Tandur, and G. Vivier, "MU-MIMO in LTE Systems," *EURASIP Journal on Wireless Communications and Networking*, p. 13, 2011.

[106] J. G. Andrews, W. Choi, and R. W. Heath Jr., "Overcoming Interference in Spatial Multiplexing MIMO Cellular Networks," *IEEE Wireless Communications Magazine*, vol. 14, no. 6, pp. 95–104, Dec. 2007.

[107] D. Gesbert, M. Kountouris, R. W. Heath, C. byoung Chae, and T. Salzer, "From Single user to Multiuser Communications: Shifting the MIMO paradigm," in *IEEE Signal Processing Magazine*, 2007.

[108] C. W. Tan and A. R. Calderbank, "Multiuser Detection of Alamouti Signals," *IEEE Transactions on Communications*, vol. 57, pp. 2080–2089, Jul. 2009. [Online]. Available: http://dl.acm.org/citation.cfm?id=1651065.1651094

[109] S. Verdu, *Multiuser Detection*. Cambridge University Press, 1998.

[110] M.-S. Alouini and A. Goldsmith, "A Unified Approach for Calculating Error Rates Of Linearly Modulated Signals over Generalized Fading Channels," *IEEE Transactions on Communications*, vol. 47, no. 9, pp. 1324–1334, 1999.

[111] M. K. Simon and M. Alouini, *Digital Communication over Fading Channels*, 2nd ed., ser. Wiley series in telecommunications and signal processing. John Wiley & Sons, Inc., 2005, ISBN: 978-0-471-64953-3.

[112] S. Verdu, "Computational Complexity of Optimum Multiuser Detection," *Algorithmica*, vol. 4, pp. 303–312, 1989, 10.1007/BF01553893. [Online]. Available: http://dx.doi.org/10.1007/BF01553893

[113] A. Host-Madsen and J. Zhang, "Capacity Bounds and Power Allocation for Wireless Relay Channels," *IEEE Transactions on Information Theory*, vol. 51, no. 6, pp. 2020–2040, 2005.

[114] K. Azarian, "Outage Limited Cooperative Channels: Protocols and Analysis," Ph.D. dissertation, Graduate School of The Ohio State University, 2006.

[115] K. Azarian, H. El Gamal, and P. Schniter, "On the Optimality of the ARQ-DDF Protocol," *IEEE Transactions on Information Theory*, vol. 54, no. 4, pp. 1718–1724, Apr. 2008.

[116] R. M. Gagliardi, *Introduction to Communication Engineering*, 2, Ed. Wiley-Interscience, 1988.

[117] J. L. Massey, "Optimum Frame Synchronization," *IEEE Transactions on Communications*, vol. 20, pp. 115–119, 1972.

[118] H. Xuefei and C. Jie, "Implementation Frame Synchronization for MIMO-OFDM System with ZCZ-codes," in *IEEE International Symposium on Microwave, Antenna, Propagation and EMC Technologies for Wireless Communications (MAPE)*, vol. 1, Aug. 2005, pp. 241 – 244 Vol. 1.

[119] J.-J. van de Beek, M. Sandell, M. Isaksson, and P. Ola Borjesson, "Low-complex Frame Synchronization in OFDM Systems," in *IEEE International Conference on Universal Personal Communications*, Nov. 1995, pp. 982 –986.

[120] National Instruments, *NI PXIe-5622 Specifications*, 2011, 16-Bit IF Digitizer with Onboard Signal Processing.

[121] M. Oerder and H. Meyr, "Digital Filter and Square Timing Recovery," *IEEE Transactions on Communications*, vol. 36, no. 5, pp. 605 –612, May 1988.

[122] Y. Yang, "Information-Guided Relay Selection for High Throughput in Half-Duplex Relay Channels," in *IEEE Global Telecommunications Conference (GLOBECOM)*, Dec. 2009, pp. 1 –5.